Electrodynamics of correlated electron materials

D. N. Basov

Department of Physics, University of California San Diego, La Jolla, California 92093-0319, USA

Richard D. Averitt

Department of Physics, Boston University, Boston, Massachusetts 02215, USA

Dirk van der Marel

Département de Physique de la Matière Condensée, Université de Genève, CH-1211 Genève 4, Switzerland

Martin Dressel

1. Physikalisches Institut, Universität Stuttgart, Pfaffenwaldring 57, 70550 Stuttgart, Germany

Kristjan Haule

Department of Physics, Rutgers University, Piscataway, New Jersey 08854, USA

(Received 4 September 2009; published 2 June 2011)

Studies of the electromagnetic response of various classes of correlated electron materials including transition-metal oxides, organic and molecular conductors, intermetallic compounds with d and f electrons, as well as magnetic semiconductors are reviewed. Optical inquiry into correlations in all these diverse systems is enabled by experimental access to the fundamental characteristics of an ensemble of electrons including their self-energy and kinetic energy. Steady-state spectroscopy carried out over a broad range of frequencies from microwaves to UV light and fast optics time-resolved techniques provides complimentary prospectives on correlations. Because the theoretical understanding of strong correlations is still evolving, the review is focused on the analysis of the universal trends that are emerging out of a large body of experimental data augmented where possible with insights from numerical studies.

DOI: 10.1103/RevModPhys.83.471 PACS numbers: 71.27.+a, 71.30.+h, 74.25.Gz, 78.20.−e

CONTENTS

I. INTRODUCTION

In their report on the Conference on the Conduction of Electricity in Solids held in Bristol in July 1937, Peierls and Mott wrote "Considerable surprise was expressed by several speakers that in crystals such as NiO in which the *d* band of the metal atoms were incomplete, the potential barriers between the atoms should be high enough to reduce the conductivity by such an enormous factor as 10^{10}" (Mott and Peierls, 1937). The "surprise" was quite understandable. The quantum mechanical description of electrons in solids— the band theory, developed in the late 1920s (Bethe, 1928; Sommerfeld, 1928; Bloch, 1929)—offered a straightforward account for distinctions between insulators and metals. Furthermore, the band theory has elucidated why interactions between 10^{23} cm^{-3} electrons in simple metals can be readily neglected, thus validating inferences of free electron models. According to the band theory NiO (along with many other transition-metal oxides) are expected to be metals in conflict with experimental findings. The term "Mott insulator" was later coined to identify a class of solids violating the above fundamental expectations of band theory. Peierls and Mott continued their seminal 1937 report by stating that "a rather drastic modification of the present electron theory of metals would be necessary in order to take these facts into account" and proposed that such a modification must include Coulomb interactions between the electrons. Arguably, it was this brief paper that has launched systematic studies of interactions and correlations of electrons in solids. Ever since, the quest to fully understand correlated electrons has remained in the vanguard of condensed matter physics. More recent investigations showed that strong interactions are not specific to transition-metal oxides. A variety of *d*- and *f*-electron intermetallic compounds as well as a number of π-electron organic conductors also revealed correlations. In this review we attempt to analyze the rich physics of correlated electrons probed by optical methods focusing on common attributes revealed by diverse materials.

Central to the problem of strong correlations is an interplay between the itineracy of electrons in solids originating from wave function hybridization and localizing effects often rooted in electron-electron repulsion (Millis, 2004). Information on this interplay is encoded in experimental observables registering the electron motion in solids under the influence of the electric field. For that reason experimental and theoretical studies of the electromagnetic response are indispensable for the exploration of correlations. In Mott insulators Coulomb repulsion dominates over all other processes and blocks electron motion at low temperatures and energies. This behavior is readily detected in optical spectra revealing an energy gap in absorption. If a conducting state is induced in a Mott insulator by changes of temperature and/or doping, then optical experiments uncover stark departures from conventional free electron behavior.

Of particular interest is the kinetic energy K of mobile electrons that can be experimentally determined from the sum rule analysis of optical data (see Sec. II.D) and theoretically from band-structure calculations. As a rule, experimental results for itinerant electronic systems are in good agreement with the band-structure findings leading to $K_{exp}/K_{band} \simeq 1$ in simple metals (see Fig. 1). However, in correlated systems, strong Coulomb interaction which has spin and orbital components (Slater, 1929) impedes the motion of electrons, leading to the breakdown of the simple single-particle picture of transport. Thus, interactions compete with itinerancy of electrons favoring their localization and specifically suppress the K_{exp}/K_{band} value below unity (see Fig. 1). This latter aspect of correlated systems appears to be quite generic and in fact can be used as a working definition of correlated electron materials. Correlation effects are believed to be at the heart of many yet unsolved enigmas of contemporary physics including high-T_c superconductivity (see Sec. V.A.1), the metal-insulator transition (see Sec. IV), electronic phase separation (see Sec. IV.F), and quantum criticality (see Sec. III.E).

Optical methods are emerging as a primary probe of correlations. Apart from monitoring the kinetic energy, experimental studies of the electromagnetic response over a broad energy range (see Sec. II.A) allow one to examine all essential energy scales in solids associated with both elementary excitations and collective modes (see Sec. III). Complementary to this are insights inferred from time-domain measurements allowing one to directly investigate

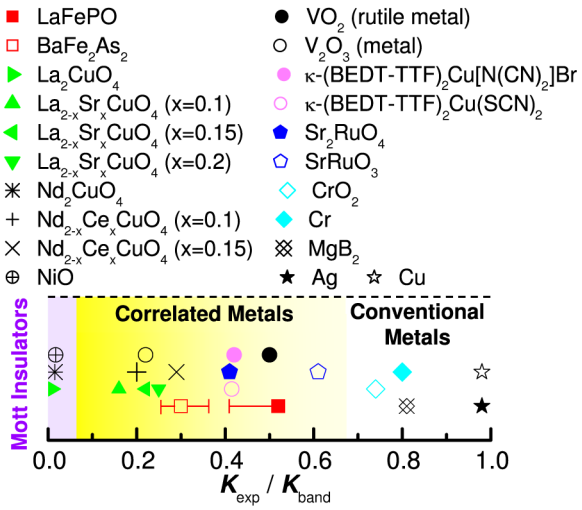

FIG. 1 (color online). The ratio of the experimental kinetic energy and the kinetic energy from band theory K_{exp}/K_{band} for various classes of correlated metals and also for conventional metals. The data points are offset in the vertical direction for clarity. From Qazilbash, Hamlin *et al.*, 2009.

dynamical properties of correlated matter (see Sec. IV). For these reasons, optical studies have immensely advanced the physics of some of the most fascinating many-body phenomena in correlated electron systems.

More importantly, spectroscopic results provide an experimental foundation for tests of theoretical models. The complexity of the problem of correlated electrons poses difficulties for the theoretical analysis of many of their properties. Significant progress was recently achieved by computational techniques including the dynamical mean-field theory (DMFT) offering in many cases an accurate perspective on the observed behavior (see Sec. II.F). The ability of the DMFT formalism to produce characteristics that can be directly compared to spectroscopic observables is particularly relevant to the main topic of this review.

In Fig. 2 we schematically show possible approaches toward an optical probe of interactions. It is instructive to start this discussion with a reference to Fermi liquids (FL) (left panels), where the role of interactions is reduced to mild corrections of susceptibilities of the free electron gas (Mahan, 2000). The complex optical conductivity $\tilde{\sigma}(\omega) = \sigma_1(\omega) + i\sigma_2(\omega)$ of FL quasiparticles residing in a partially filled parabolic band is adequately described by the Drude model

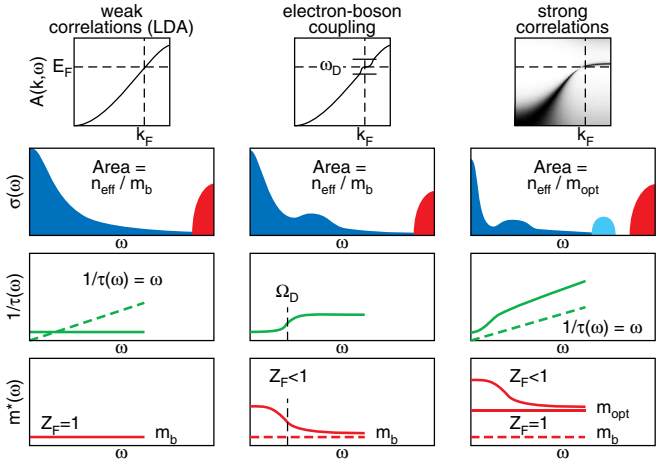

FIG. 2 (color online). Schematic diagram revealing complimentary approaches to probing electronic correlations using IR and optical methods. Top panels show the momentum-resolved spectral function in a noninteracting metal (left), weakly interacting system (middle), and strongly correlated system (right). Characteristic forms of the real part of the conductivity $\sigma_1(\omega)$, the frequency-dependent scattering rate $1/\tau(\omega)$, and effective mass $m^*(\omega)$ are displayed. The Drude intraband contribution to the conductivity (the low energy shaded area in the second row) develops a "sideband" in a system with strong electron-boson coupling. The corresponding enhancement of $m^*(\omega)$ at energies below a characteristic bosonic mode Ω_0 can be registered through the extended Drude analysis (see Sec. II.C). The magnitude of $m^*(\omega \to 0)$ is related to the quasiparticle renormalization amplitude Z introduced in Sec. II.C. In a strongly correlated system (right panels) the oscillator strength of the entire intraband contribution is suppressed with the spectral-weight transfer to the energy scale of the order of U. The strength of this effect can be quantified through the ratio of $K_{\rm exp}/K_b$ as in Fig. 1 or equivalently through the ratio of optical and band mass $m_b/m_{\rm opt}$. Quite commonly this renormalization effect and strong electron-boson interaction act in concert yielding further enhancement of m^* over the $m_{\rm opt}$ at $\omega < \Omega_0$.

(see Sub. II.A for the definition of the complex conductivity). The model prescribes the Lorentzian form of the real part of the conductivity associated with the intraband processes (Drude, 1900; Dressel and Grüner, 2002; Dressel and Scheffler, 2006):

$$\tilde{\sigma}(\omega) = \frac{N_{\rm eff} e^2 \tau_D}{m_b} \frac{1}{1 - i\omega\tau_D} = \frac{\sigma_{\rm dc}}{1 - i\omega\tau_D}, \tag{1}$$

where e is the electronic charge, $N_{\rm eff}$ is the relevant density, and m_b is the band mass of the carriers which is generally different from the free electron mass m_e, $1/\tau_D$ is the scattering rate, and $\sigma_{\rm dc}$ is the dc conductivity. In dirty metals impurities dominate and the scattering rate $1/\tau_D$ is independent of frequency, thus obscuring the quadratic form of $1/\tau(\omega)$ that is expected for electron-electron scattering of a Fermi liquid.[1] Nevertheless, this latter behavior of $1/\tau(\omega)$ has been confirmed at least for two elemental metals (Cr and γ-Ce) through optical experiments (van der Eb *et al.*, 2001; Basov *et al.*, 2002) using the so-called extended Drude analysis (see Sec. II.A). Another characteristic feature of Fermi liquids in the context of infrared data is that the relaxation rate of quasiparticles at finite energies is smaller than their energy: $1/\tau(\omega) < \omega$ (at temperature $T \to 0$). The contribution of interband transitions is also shown in Fig. 2 [right-hand-side peak in $\sigma(\omega)$] and is usually adequately described through band-structure calculations. The band-structure results also accurately predict the electronic kinetic energy of a Fermi liquid that is proportional to the area under the intraband Drude contribution to the conductivity spectra (see Sec. II.D).

One of the best understood examples of interactions is the Eliashberg theory of the electron-boson coupling (Carbotte, 1990). Interactions with a bosonic mode at Ω_0 modify the dispersion of electronic states near the Fermi energy E_F (top panel in the middle row of Fig. 2). The spectra of $1/\tau(\omega)$ reveal a threshold near Ω_0 reflecting an enhancement of the probability of scattering processes at $\omega > \Omega_0$. The spectral form of $\sigma_1(\omega)$ is modified as well, revealing the development of a "side band" in $\sigma_1(\omega)$ at $\omega > \Omega_0$. However, the total spectral weight including the coherent Drude-like structure and side bands is nearly unaltered compared to a noninteracting system, and these small changes are usually neglected. Thus, electron-boson interaction alone does not modify $K_{\rm exp}$ with respect to $K_{\rm band}$. Importantly, characteristic features of the bosonic spectrum can be extracted from the optical data (Farnworth and Timusk, 1974). Various analysis protocols employed for this extraction are reviewed in Sec. III.F. Coupling to other excitations, including magnetic resonances, also leads to the formation of sidebands that in a complex system may form a broad incoherent background in $\sigma_1(\omega)$.

The right panels in Fig. 2 exemplify the characteristic electronic dispersion and typical forms of the optical functions for a correlated metal. Strong broadening of the dispersion away from E_F indicates that the concept of weakly damped Landau quasiparticles may not be applicable to many correlated systems over the entire energy range. An optical counterpart of the broadened dispersion are the large

[1] See, for example, Abrikosov *et al.* (1963), Pines and Nozières (1966), and Ashcroft and Mermin (1976).

values of $1/\tau(\omega)$. Finally, the low-energy spectral weight is significantly reduced compared to band-structure expectations leading to $K_{\rm exp}/K_{\rm band}$ that is substantially less than unity. Suppression of the coherent Drude conductivity implies the transfer of electronic spectral weight to energies of the order of intrasite Coulomb energy U and/or the energy scale of interband transitions. These effects are routinely found in doped Mott insulators, for example (see Sec. V), as well as in other classes of correlated materials.[2]

It is instructive to discuss dynamical properties of correlated electron systems in terms of the effective mass which in general is a tensor m_k. For a general dispersion ϵ_k, the mass is defined as $m_k^{-1} = (1/\hbar^2)\partial^2\epsilon_k/\partial k^2$, which reduces to a constant for free electrons with a parabolic dispersion. Deviations of m_k from the free electron mass in simple metals are adequately described by band-structure calculations yielding m_b. This quantity is frequency independent (bottom left frame in Fig. 2) and enters the Drude equation for the complex conductivity Eq. (1). Electron-boson interaction leads to the enhancement of the effective mass compared to the band mass m_b at $\omega < \Omega_0$ as $m^*(\omega) = m_b[1 + \lambda(\omega)]$, quantifying the strength of the interaction λ (middle panel in the bottom row). The frequency dependence of $m^*(\omega)$ can be evaluated from the effective Drude analysis of the optical constants. Strong electron-electron interaction can radically alter the entire dispersion so that $m_{\rm opt}$ is significantly enhanced over m_b (right bottom panel). An equivalent statement is that $K_{\rm exp}$ is reduced compared to $K_{\rm band}$ (see also Fig. 1). Additionally, electron-boson interactions may be operational in concert with the correlations in modifying the dispersion at $\omega < \Omega_0$. In this latter case one finds the behavior schematically sketched in the bottom right panel of Fig. 2 with the thick line.

Because multiple interactions play equally prominent roles in correlated systems, the resulting many-body state reveals a delicate balance between localizing and delocalizing trends. This balance can be easily disturbed by minute changes in the chemical composition, temperature, applied pressure, and electric and/or magnetic field. Thus, correlated electron systems are prone to abrupt changes of properties under applied stimuli and reveal a myriad of phase transitions (see Secs. III and V). Quite commonly, it is energetically favorable for correlated materials to form spatially nonuniform electronic and/or magnetic states occurring on diverse length scales from atomic to mesoscopic. Real space inhomogeneities are difficult to investigate using optical techniques because of the fairly coarse spatial resolution imposed by the diffraction limit. Nevertheless, methods of near-field subdiffractional optics are appropriate for the task (see Sec. V.B.1).

Our main objective in this review is to give a snapshot of recent developments in the studies of electrodynamics of correlated electron matter focusing primarily on works published over the last decade. Introductory sections of this article are followed by the discussion of excitations and collective effects (Sec. III) and metal-insulator transition physics (Sec. IV) exemplifying through optical properties these essential aspects of correlated electron phenomena. The second half of this review is arranged by specific classes of correlated systems for the convenience of readers seeking a brief representation of optical effects in a particular type of correlated compounds. Given the abundant literature on the subject, this review is bound to be incomplete in terms of both topics covered and references cited. We conclude this account by outlining unresolved issues.

II. EXPERIMENTAL PROBES AND THEORETICAL BACKGROUND

A. Steady-state spectroscopy

Optical spectroscopy carried out in the frequency domain from 1 meV to 10 eV has played a key role in establishing the present physical picture of semiconductors and Fermi-liquid metals (Dressel and Grüner, 2002; Burch *et al.*, 2008) and has immensely contributed to uncovering exotic properties of correlated materials (Imada *et al.*, 1998; Degiorgi, 1999; Millis, 2004; Basov and Timusk, 2005). Spectroscopic measurements in the frequency domain allow one to evaluate the optical constants of materials that are introduced in the context of materials parameters in Maxwell's equations. The optical conductivity is the linear response function relating the current j to the applied electric field E: $j(\omega) = \sigma(\omega)E(\omega)$. Another commonly employed notation is that of the complex dielectric function $\tilde{\epsilon}(\omega) = \epsilon_1(\omega) + i\epsilon_2(\omega)$. The real and imaginary parts of these two sets of optical constants are related by $\sigma_1(\omega) = (\omega/4\pi)\epsilon_2(\omega)$ and $\sigma_2(\omega) = -(\omega/4\pi)[\epsilon_1(\omega) - 1]$.[3] Absorption mechanisms associated with various excitations and collective modes in solids (Fig. 3) give rise to additive contributions to spectra of $\sigma_1(\omega)$ and thus can be directly revealed through optical experiments. In anisotropic materials the complex optical constants acquire a tensor form. For instance, time reversal symmetry breaking by an applied magnetic field introduces nondiagonal components to these tensors implying interesting polarization effects (Zvezdin and Kotov, 1997). In the vast majority of optics literature it is assumed that the magnetic permeability of a material $\mu = 1$ with the exception of magnetic resonances usually occurring in microwave and very far-infrared frequencies.[4]

The complex optical constants can be inferred from one or several complementary procedures (Dressel and Grüner, 2002): (i) a combination of reflectance $R(\omega)$ and transmission

[2]In transition-metal oxides the magnitude of the on-site Coulomb repulsion can be both smaller or larger than the energy scale of interband transitions (Zaanen *et al.*, 1985). In organic conductors the hierarchy of energy scales is consistent with a sketch in Fig. 2.

[3]In general higher-energy contributions from interband transitions $\epsilon_b(\omega)$ (''bound charge'' polarizability) are present apart from the quasifree electrons that are summarized in ϵ_∞ replacing the factor 1 in this expression of $\sigma_2(\omega)$. The static bound charge polarizability is defined as the zero-frequency limit of $\epsilon_b(\omega)$, i.e., $\epsilon_\infty = \epsilon_b(0)$.

[4]This common assertion has recently been challenged by the notion of ''infrared and optical magnetism'' (Yen *et al.*, 2004; Padilla *et al.*, 2006; Shalaev, 2007) realized primarily in lithographically prepared metamaterial structures but also in bulk colossal magnetoresistance manganites (Pimenov *et al.*, 2005; Pimenov *et al.*, 2007). For inhomogeneous media, however, spatial dispersion becomes relevant that in general mixes electric and magnetic components (Agranovich and Ginzburg, 1984).

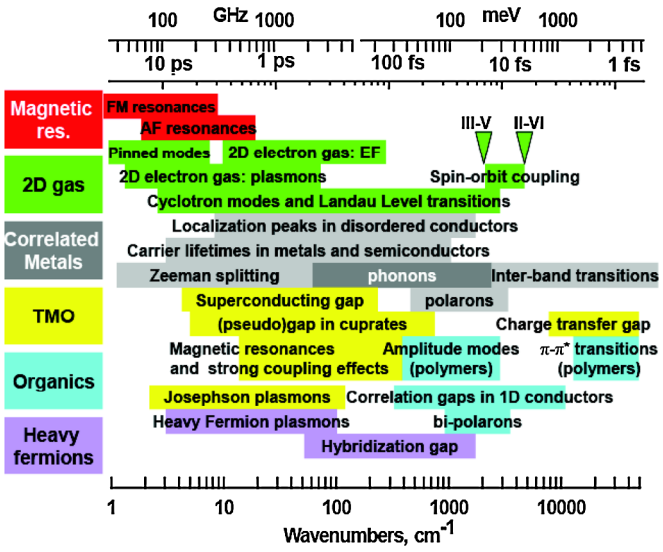

FIG. 3 (color online). Schematic representation of characteristic energy scales in correlated electron systems. These different processes give additive contributions to the dissipative parts of optical constants. TMO: transition-metal oxides.

$T(\omega)$ spectra obtained for transparent materials can be used to extract the dielectric function through analytic expressions; (ii) Kramers-Kronig analysis of $R(\omega)$ for opaque systems or of $T(\omega)$ for transparent systems; (iii) ellipsometric coefficients ψ and Δ for either transparent or opaque materials can be used to determine the dielectric function through analytic expressions[5]; (iv) various interferometric approaches, in particular, Mach-Zehnder interferometry; and (v) THz time-domain spectroscopy directly yields optical constants. These experimental techniques have been extensively applied to correlated matter. The extension of ''optical'' data to the microwave region is often desirable especially for superconductors and heavy electron materials that show interesting properties below 1 meV (see Sec. IV).

B. Pump-probe spectroscopy

Ultrafast optical spectroscopy provides the possibility to temporally resolve phenomena in correlated electron matter at the fundamental time scales of atomic and electronic motion. Subpicosecond temporal resolution combined with spectral selectivity enables detailed studies of electronic, spin, and lattice dynamics, and, crucially, the coupling between these degrees of freedom. In this sense, ultrafast optical spectroscopy complements time-integrated optical spectroscopy and offers unique possibilities to investigate correlated electron materials. This includes, as examples, phenomena such as electron-phonon coupling, charge-density-wave dynamics, condensate recovery, and quasiparticle formation.

In time-resolved optical experiments, a pump pulse photoexcites a sample initiating a dynamical response that is monitored with a time delayed probe pulse. Experiments on correlated electron materials fall into two categories as determined by the photoexcitation fluence (Hilton *et al.*, 2006). In the low-fluence regime ($\lesssim 100\ \mu\mathrm{J/cm^2}$) it is desirable to perturb the sample as gently as possible to minimize the temperature increase. Examples of low-fluence experiments discussed below include condensate dynamics in conventional and high-temperature superconductors (Secs. III.G and V.A.1, respectively), spin-lattice relaxation in manganites (Sec. V.C), and electron-phonon coupling in heavy fermions (Sec. V.B.2). At the other extreme are high-fluence nonperturbative experiments, where goals include photoinducing phase transitions or creating nonthermally accessible metastable states having a well-defined order parameter.[6] This is an emerging area of research that is quite unique to ultrafast optical spectroscopy. The coupling and interplay of correlated electron materials are of considerable interest in these high-fluence experiments as discussed in more detail in Sec. IV.E on photoinduced phase transitions and Sec. V.B.2 on the vanadates.

Low- and high-fluence time-resolved experiments have been made possible by phenomenal advances in ultrashort optical pulse technology during the past 15 years which have enabled the generation and detection of subpicosecond pulses from the far-infrared through the visible and into the x-ray region of the electromagnetic spectrum (Kobayashi *et al.*, 2005). Formally, ultrafast optical spectroscopy is a nonlinear optical technique. In the low-fluence regime, pump-probe experiments can be described in terms of the third-order nonlinear susceptibility. However, more insight is often obtained by considering ultrafast optical spectroscopy as a modulation spectroscopy where the self-referencing probe beam measures the induced change in reflectivity $\Delta R/R$ or transmission $\Delta T/T$ (Cardona, 1969; Sun *et al.*, 1993). This provides an important connection with time-integrated optical spectroscopy, where the experimentally measured reflectivity and the extracted dielectric response are the starting point to interpret and analyze the results of measurements. Further, this is applicable to high-fluence experiments from the perspective of temporally resolving spectral-weight transfer (see Sec. II.D). In femtosecond experiments, the dynamics can be interpreted using

$$\frac{\Delta R}{R}(t) = \frac{\partial \ln(R)}{\partial \epsilon_1}\Delta\epsilon_1(t) + \frac{\partial \ln(R)}{\partial \epsilon_2}\Delta\epsilon_2(t), \tag{2}$$

where R is the reflectivity, and $\Delta\epsilon_1$, $\Delta\epsilon_2$ are the induced changes in the real and imaginary parts of the dielectric function, respectively (Sun *et al.*, 1993). Insights into the electronic properties obtained from time-integrated measurements of $\epsilon_1 + i\epsilon_2$ (or the complex conductivity $\sigma_1 + i\sigma_2$) serve as a useful starting point in understanding the quasiparticle dynamics measured using time-resolved techniques. Further, the development of time-gated detection techniques has enabled direct measurement of the electric field which, in turn, permits the determination of the temporal evolution of

[5]This is straightforward only in the case of isotropic bulk materials; in the case of anisotropic materials or films some models have to be assumed.

[6]See, for example, Averitt and Taylor (2002), Nasu (2004), Hilton *et al.* (2006), Kuwata-Gonokami and Koshihara (2006), Kaindl and Averitt (2007), and Yonemitsu and Nasu (2008).

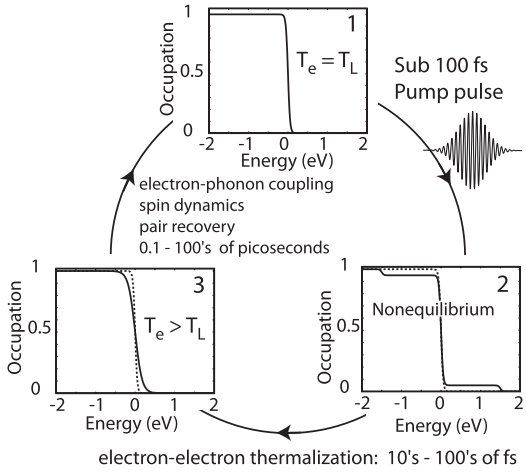

FIG. 4. Schematic description of dynamics in condensed matter probed with femtosecond spectroscopy. Prior to photoexcitation (1) the electrons, lattice, and spins are in thermal equilibrium. Photoexcitation creates (2) a nonthermal electron distribution. The initial relaxation proceeds primarily through electron-electron thermalization. Following thermalization, the electrons have excess energy which is transferred to other degrees of freedom on characteristic time scales ranging from ~1 ps for electron-phonon relaxation to tens of picoseconds for processes such as pair recovery across a gap. From Averitt and Taylor, 2002.

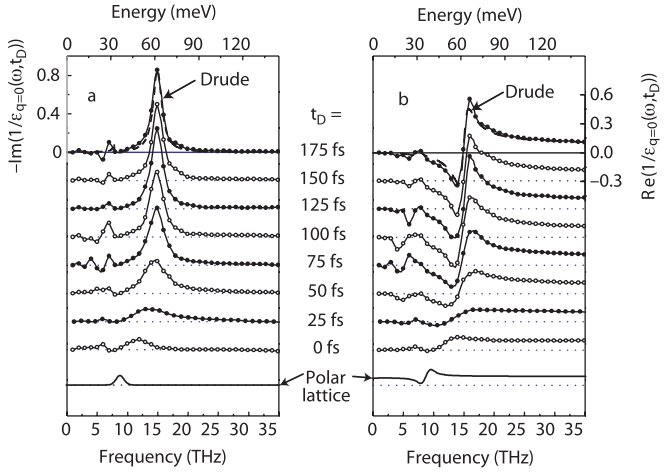

FIG. 5 (color online). Quasiparticle formation in GaAs at room temperature following excitation with 10 fs, 1.55 eV pulses. The dynamic loss function is plotted as a function of frequency at various delays following photoexcitation. The response evolves to a coherent Drude response on a time scale of 175 fs as dressed quasiparticles are formed from an initially uncorrelated state at zero delay. From Huber *et al.*, 2001.

$\sigma_1 + i\sigma_2$ over the useful spectral bandwidth of the probe pulse.[7]

The foundation for ultrafast experiments on correlated electron materials (at any fluence) is based on efforts during the past 25 years in understanding quasiparticle dynamics in semiconductors and metals.[8] In ultrafast optical experiments, an incident pump pulse perturbs (or prepares) a sample on a sub-100 fs time scale. This induced change is probed with a second ultrashort pulse that, depending on the wavelength and experimental setup, measures pump-induced changes in the reflectivity, transmission, or conductivity. In the majority of experimental studies in condensed matter to date, the pump pulse creates a nonthermal electron distribution [see Fig. 4 (1 → 2)] fast enough that, to first order, there is no coupling to other degrees of freedom. During the first 100 fs, the nonthermal (and potentially coherent) distribution relaxes primarily by electron-electron scattering [see Fig. 4 (2 → 3)] (Allen, 1987; Fann *et al.*, 1992; Sun *et al.*, 1993; Groeneveld *et al.*, 1995). Subsequently, the excited Fermi-Dirac distribution thermalizes through coupling to the other degrees of freedom (3 → 1).

There are, of course, important aspects that Fig. 4 does not capture. Of particular importance are coherence effects where the impulsive nature of the initial photoexcitation leads to a phase-coherent collective response (Shah, 1999). This can include coherent phonons or magnons (Thomsen *et al.*, 1986; Dekorsy *et al.*, 1996; Koopmans *et al.*, 2005; Talbayev *et al.*, 2005). However, even in the coherent limit, the results can often be interpreted as a dynamic modulation of the optical conductivity tensor, although the connection with Raman scattering is important for certain experiments (Merlin, 1997; Misochko, 2001).

For an example that embodies what is possible with ultrafast optical spectroscopy, we consider recent results on the formation of quasiparticles following above band-gap photoexcitation in undoped GaAs (Huber *et al.*, 2001).[9] The experimental results are shown in Fig. 5, where spectra of the dynamic loss function $1/\tilde{\epsilon}(\omega, \tau_D)$ are plotted at various delays τ_D between the optical-pump and THz-probe pulses. The imaginary part of $1/\tilde{\epsilon}(\omega, \tau_D)$ is plotted in Fig. 5(a) and the real part in Fig. 5(b). This is a particularly useful form to display the data as it highlights what this experiment is actually measuring, namely, the evolution of particle interactions from a bare Coulomb potential V_q to a screened interaction potential $W_q(\omega, \tau_D)$, where q is the momentum exchange between two particles during a collision.

In essence, V_q becomes renormalized by the longitudinal dielectric function leading to a retarded response associated with the polarization cloud about the carriers. This is a many-body resonance at the plasma frequency, where the loss function peaks at the plasma frequency with a width corresponding to the scattering rate. Thus, the results of Fig. 5 show the evolution from an uncorrelated plasma to a many-

[7]See Averitt and Taylor (2002), Kaindl and Averitt (2007), and references therein for details.

[8]See, for example, Allen (1987), Sun *et al.* (1993), Groeneveld *et al.* (1995), Beaurepaire *et al.* (1996), Shah (1999), Chemla and Shah (2001), and Axt and Kuhn (2004).

[9]These results provide a striking example of the onset of correlation following photoexcitation. In this experiment, pulses with 1.55 eV photon energy and ~10 fs duration excited an electron-hole plasma at a density of 10^{18} cm^{-3}. Monitoring the dynamics requires probe pulses with sufficient temporal resolution and with a spectral bandwidth extending beyond 160 meV. This was achieved using a scheme based on difference-frequency generation in GaSe combined with ultrabroadband free-space electro-optic sampling (Huber *et al.*, 2001).

body state with a well-defined collective plasmon excitation. This is evident in Fig. 5(a) where, prior to photoexcitation, there is a well-defined peak at 36 meV corresponding to polar optical phonons. Following photoexcitation, a broad resonance appears at higher energies that evolves on a 100 fs time scale into a narrow plasma resonance centered at 60 meV. The response is described by the Drude model only at late delay times. These results are consistent with quantum kinetic theories describing nonequilibrium Coulomb scattering (Huber *et al.*, 2001).

In wide-band materials, it is possible to consider the dynamics largely in terms of the band structure, where photoexcitation leads to changes in band occupation followed by subsequent relaxation processes. The example in Fig. 5 is along these lines highlighting the dynamical evolution of low-energy spectral weight following photoexcitation of carriers across the band gap. In many ways, this can be considered as a model example of measurements in correlated electron materials in that it is the dynamical evolution of spectral weight (even if only over a narrow spectral range) that is monitored. The situation can be considerably more complicated in correlated materials starting with the fact that the electronic structure varies with occupancy. Thus, an excitation pulse can initiate a sequence of dynamical events quite different in comparison to the relaxation of a nonthermal electron distribution in a rigid band. For example, a change in orbital occupancy upon photoexcitation can near instantaneously relax the need for a coherent lattice distortion (e.g., cooperative Jahn-Teller effect in the manganites) (Tokura, 2000; Polli *et al.*, 2007), thereby launching a coherent lattice excitation that will in turn couple to other degrees of freedom. More generally, a delicate balance between various degrees of freedom occurs. Consequently, many such materials teeter on the edge of stability and exhibit gigantic susceptibilities to small external perturbations (Dagotto, 2003; 2005). Short optical pulses can play an important role as the external perturbation yielding a powerful tool to investigate dynamical interactions which determine the macroscopic response. Many examples will be encountered in the following sections.

The results presented in Fig. 5 represent the state of the art of what is currently feasible in terms of both experiment and theory of ultrafast optical spectroscopy as applied to condensed matter. The challenge is to utilize such experimental tools to investigate more complicated materials. This includes, as discussed in more detail below, the cuprates, manganites, heavy fermions, organics, and others. Interesting experimental insights have been obtained, but there is a need for theoretical studies focused on interpreting the results of time-resolved measurements. While theoretical studies on dynamics in wide-band semiconductors and heterostructures are relatively mature (Axt and Kuhn, 2004), to date, there have been relatively few theoretical studies on dynamics in correlated electron materials.[10] As described in this review, DMFT is a promising approach to analyze time-domain optical experiments and recently a DMFT study along these lines was published (Eckstein and Kollar, 2008).

C. Theoretical background

In an optical experiment a current is induced in the solid by the electric (proportional to $\partial\mathbf{A}/\partial\mathbf{t}$, where $\mathbf{A}$ is the vector potential) and magnetic ($\mathbf{B}$) components of the electromagnetic field (Cohen-Tannoudji, 2004). The coupling in leading order of $\mathbf{A}$ and $\mathbf{B}$ is

$$H^i = \frac{e}{2mc}[\mathbf{A}(\mathbf{r})\cdot\mathbf{p} + \mathbf{p}\cdot\mathbf{A}(\mathbf{r})] - \frac{e\hbar g}{2mc}\mathbf{B}(\mathbf{r})\cdot\mathbf{S}. \tag{3}$$

The $\mathbf{A}\cdot\mathbf{p}$ term of the interaction couples the angular momentum of the photon ($\hbar$) to the orbital degree of freedom of the electron, leaving the spin unaffected. The $\mathbf{B}\cdot\mathbf{S}$ term couples the photon angular momentum to the spin of the electron. In the absence of spin-orbit coupling these two couplings lead to the electric and magnetic dipole selection rules, respectively. Spin-orbit coupling relaxes these rules, which provides a channel for optically induced spin-flip processes through the $\mathbf{A}\cdot\mathbf{p}$ term. Since this coupling contributes typically $1/\alpha^2$ times the oscillator strength from the $\mathbf{B}\cdot\mathbf{S}$ term, the latter coupling is usually neglected; here $\alpha = e^2/\hbar c = 1/137$ is the fine-structure constant. The optical conductivity is then computed by the linear response theory (Mahan, 2000)

$$\tilde{\sigma}^{\mu\nu}_{\mathbf{q}}(\omega) = \frac{ie^2n}{m\omega}\delta_{\mu\nu} + \frac{1}{i\omega}\chi_{\mu\nu}(\mathbf{q},\omega+i\delta), \tag{4}$$

where

$$\chi_{\mu\nu}(\mathbf{q},i\omega_n) = \int_0^{1/T} e^{i\omega_n\tau}\langle j^p_{\mu,\mathbf{q}}(\tau)j^p_{\nu,-\mathbf{q}}(0)\rangle d\tau \tag{5}$$

is the current-current correlation function, and j^p is the paramagnetic current density $\mathbf{j}^p(x) = -(ie/2m)\sum_\sigma[\psi^\dagger_\sigma(x)\nabla\psi_\sigma(x) - (\nabla\psi^\dagger_\sigma(x))\psi_\sigma(x)]$. T is temperature. Calculation of the current-current correlation function Eq. (5) requires the full solution of the many-body problem. Usually Eq. (5) is then expressed in terms of the one-particle Green's function $G_{\mathbf{k}}(\omega)$, the two-particle vertex function $\Gamma(\mathbf{k}\nu,\mathbf{q}\omega)$, and electron velocities $v^{\mathbf{k}\mu}$ by

$$\begin{aligned}\chi_{\mu\nu}(\mathbf{q},i\omega_n) = -e^2T\sum_{\mathbf{k}\nu_m}\mathrm{Tr}[&G_{\mathbf{k}-\mathbf{q}/2}(i\nu_m - i\omega_n)v^{\mathbf{k}\nu}\\ &\times G_{\mathbf{k}+\mathbf{q}/2}(i\nu_m)v^{\mathbf{k}\mu} + G_{\mathbf{k}-\mathbf{q}/2}(i\nu_m - i\omega_n)\\ &\times\Gamma(\mathbf{k}\nu_m,\mathbf{q}\omega_n)G_{\mathbf{k}+\mathbf{q}/2}(i\nu_m)v^{\mathbf{k}\mu}],\end{aligned} \tag{6}$$

as diagrammatically shown in Fig. 6. All three quantities are matrices in the band index, i.e., $v^{\mathbf{k}\mu}_{ij}$, $G_{\mathbf{k},ij}$, and $\Gamma(\mathbf{k},\mathbf{q})_{ij}$. The velocities are $v^{\mathbf{k}\mu}_{ij} = -(i/m)\langle\psi_{\mathbf{k}i}|\nabla_\mu|\psi_{\mathbf{k}j}\rangle$, where $\psi_{\mathbf{k}i}(\mathbf{r})$ are a set of one-particle basis functions.

Within a single-band approximation, the Green's function $G_{\mathbf{k}}(\omega)$, the spectral function of electronic excitations $A_{\mathbf{k}}(\omega)$, and electronic self-energy $\Sigma_{\mathbf{k}}(\omega)$ are related by

$$A_{\mathbf{k}}(\omega) = -\frac{1}{\pi}\mathrm{Im}G_{\mathbf{k}}(\omega) = -\frac{1}{\pi}\mathrm{Im}\frac{1}{\omega - \epsilon_{\mathbf{k}} - \Sigma_{\mathbf{k}}(\omega)}. \tag{7}$$

[10]See, for example, Takahashi *et al.* (2002), Ahn *et al.* (2004), Carbotte and Schachinger (2004), Howell *et al.* (2004), and Unterhinninghofen *et al.* (2008).

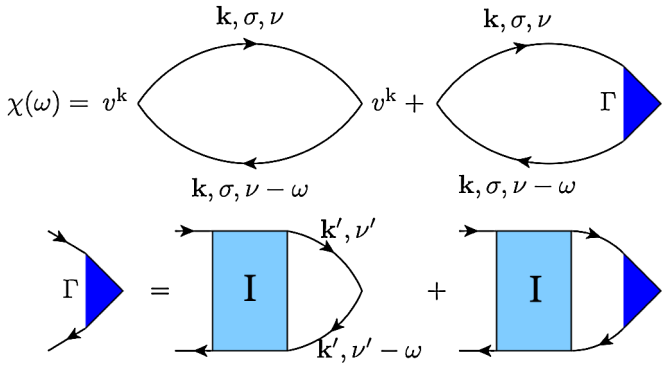

FIG. 6 (color online). Diagrammatic representation of the current-current correlation function and the Bethe-Salpeter equation for the vertex correction to the optical conductivity.

The self-energy $\Sigma_{\mathbf{k}}(\omega)$ in Eq. (7) contains information on all possible interactions of an electron with all other electrons in the system and the lattice. In the absence of interactions the spectral function is merely a δ peak at $\omega = \epsilon_{\mathbf{k}}$, whereas $\mathrm{Re}\Sigma_{\mathbf{k}}(\omega) = \mathrm{Im}\Sigma_{\mathbf{k}}(\omega) = 0$. Interactions have a twofold effect on the spectral function. First, the energy is shifted with respect to the noninteracting case by the amount proportional to $\mathrm{Re}\Sigma_{\mathbf{k}}(\omega)$. Second, the spectral function acquires a Lorentzian form with the width given by $\mathrm{Im}\Sigma_{\mathbf{k}}(\omega)$. The corresponding states are referred to as dressed states or quasiparticle states. The spectral function and the complex self-energy are both experimentally accessible through photoemission measurements (Damascelli *et al.*, 2003).

Finally, the two-particle vertex function $\Gamma(\mathbf{k}, \mathbf{q})$ (dark triangles in Fig. 6) can be computed from the fully irreducible two-particle vertex function $I(\mathbf{k}\mathbf{k}'; \mathbf{q})$ (light squares in Fig. 6) through the Bethe-Salpeter equation depicted in the second line of Fig. 6. A consequence of this vertex is that an electron-hole pair can form a bound neutral particle, i.e., an exciton. In wide-band insulators such as rock salts (Philipp and Ehrenreich, 1963), semiconductors (Klingshirn, 1995), or organic materials (Agranovich, 2009), the exciton binding energies form a Rydberg series below the band gap of unbound electron-hole pairs. In transition-metal compounds the interaction is often strong enough to bind an electron-hole pair on a single atomic site (see Sec. III.B).

D. Sum rules

The response functions including optical constants of materials obey numerous sum rules (Kubo, 1957). The most frequently used sum rule is the f-sum rule for the real part of the optical conductivity $\sigma_1(\omega)$:

$$\int_0^\infty \sigma_1(\omega)d\omega = \frac{\pi n e^2}{2m_e}. \tag{8}$$

This expression relates the integral of the dissipative part of the optical conductivity to the density of particles participating in optical absorption and their bare mass. The optical conductivity of a solid is dominated by the electronic response, and therefore an integration of the data using Eq. (8) can be compared to the total number of electrons including both core and valence electrons.

A special role is played by the following sum rule for the optical conductivity of a single-band system governed by a Hamiltonian H:

$$\int_0^\infty \sigma_1(\omega)d\omega = -\frac{\pi e^2}{2\hbar^2}\langle K\rangle. \tag{9}$$

Here $K = \delta^2 H/\delta A^2$ and the brackets $\langle\cdots\rangle$ denote the thermal average. In a tight binding model, K is the kinetic energy (Maldague, 1977; Baeriswyl *et al.*, 1987):

$$K = -4/N\sum_{\mathbf{k}} \frac{d^2\epsilon_{\mathbf{k}}}{dk_x^2} n_{\mathbf{k}}, \tag{10}$$

where $n_{\mathbf{k}}$ is the electron momentum distribution function. Since K must accommodate the entire free-carrier response (i.e., the Drude peak and all sidebands due to interactions), one has to extend the integration to an energy above the free-carrier response while still below the interband transitions. Kinetic energy [Eq. (10)] quantifies the oscillator strength of intraband transitions that can be equivalently characterized with the plasma frequency $\omega_p^2 = ne^2/m_b$ in weakly interacting systems or ne^2/m_{opt} in a strongly interacting material, where correlations renormalize the entire dispersion so that $m_{\mathrm{opt}} > m_b$ and $K_{\mathrm{exp}}/K_{\mathrm{band}} < 1$.

Devreese *et al.* (1977) obtained the following "partial sum rules" for electrons occupying a band with a k-independent mass m_b coupled to phonons causing band mass m_b to increase to the renormalized value m^* at energies below the phonon frequencies:

$$\int_0^\infty \sigma_{\mathrm{Drude}}(\omega)d\omega = \frac{\pi n_{\mathrm{eff}} e^2}{2m^*}, \tag{11}$$

$$\int_0^\infty \sigma_{\mathrm{intra}}(\omega)d\omega = \frac{\pi n_{\mathrm{eff}} e^2}{2m_b}, \tag{12}$$

where $\sigma_{\mathrm{Drude}}(\omega)$ is the narrow Drude peak alone, whereas $\sigma_{\mathrm{intra}}(\omega)$ is the complete intraband contribution involving both the Drude peak and sidebands resulting from electron-phonon coupling (middle panels of Fig. 2). A caveat: As pointed out in many correlated electron materials the entire dispersion is modified by correlations leading to a suppression of the total intraband spectral weight (Qazilbash, Hamlin *et al.*, 2009). This implies that m_b in Eq. (12) has to be replaced with higher optical mass m_{opt} and electron-boson mass renormalization is also executed with respect to m_{opt}, not m_b. Following Maldague (1977) it is customary to define the following effective spectral weight $N_{\mathrm{eff}}(\omega)$:

$$N_{\mathrm{eff}}(\omega) = \frac{2m_e}{\pi e^2}\int_0^\omega \sigma_1(\omega')d\omega', \tag{13}$$

which has the meaning of the effective number of electrons contributing to electromagnetic absorption at frequencies below ω.

Of special significance for superconductors is the Ferrell-Glover-Tinkham (FGT) sum rule (Tinkham, 1996):

$$\frac{\rho_s}{8} = \int_{0+}^\infty d\omega[\sigma_1(\omega, T > T_c) - \sigma_1(\omega, T < T_c)]. \tag{14}$$

This equation relates the spectral weight "missing" from the real part of the conductivity upon transition to the

superconducting state to the superfluid density ρ_s which is proportional to the density of superconducting pairs n_s and inversely related to their effective mass m^* as $\rho_s = 4\pi n_s e^2/m^*$. Often, for practical reasons, the integration is limited to the free-carrier response. Validity of the FGT sum rule in this restricted sense requires that the electronic kinetic energy is unchanged below T_c (see Sec. V.A.1 which discusses sum rule anomalies in high-T_c cuprates). The superfluid density is of fundamental importance for the electrodynamics of superconductors. The sum rule [Eq. (14)] allows one to evaluate all three diagonal components of the superfluid density in anisotropic superconductors such as cuprates.[11]

Experimental access to the quasiparticle kinetic energy is one important virtue of optical probes of correlations. An analysis of the one-dimensional Hubbard Hamiltonian is particularly instructive in this regard (Baeriswyl *et al.*, 1986). Exact results obtained for a half-filled band reveal that the electronic kinetic energy is monotonically reduced with the increase of the on-site repulsion U and tends to zero as $K \propto 1/U$. This result, along with the analysis of the spectral weight within the two-dimensional Hubbard model (Millis and Coppersmith, 1990), reinforces the notion that K_{exp} reported in Fig. 1 can be used as a quantitative measure of correlation effects.

Equation (9) is derived for a hypothetical single-band system where the kinetic energy may depend on temperature T, magnetic field B, or other external stimuli. Strong variations of the electronic spectral weight commonly found in correlated electron systems upon changes of temperature T or magnetic field B may signal interesting kinetic energy effects. Consider, for example, a $\sigma_1(\omega)$ data set collected for a conducting system over the spectral range that is at least of the order of the width of the electronic band W, where the Fermi energy resides. The kinetic energy interpretation of Eq. (9) applied to such a data set is highly plausible. Quite commonly, one finds that the sum rule results in this case are temperature dependent (Molegraaf *et al.*, 2002; Ortolani *et al.*, 2005). The only source of such a temperature dependence in a noninteracting system pertains to thermal smearing of the Fermi-Dirac distribution function leading to fairly weak effects scaling as T^2/W (Benfatto *et al.*, 2005; Benfatto, Carbotte, and Marsiglio, 2006). In correlated electron systems this temperature dependence can become much more pronounced. This latter issue has been explicitly addressed within the framework of several scenarios of interacting electrons.[12] We pause here to strike a note of caution and stress that apart from intrinsic origins the variation of the electronic spectral weight may be caused by ambiguities with the choice of cutoff for integration of experimental spectra (Benfatto and Sharapov, 2006; Norman *et al.*, 2007). Indeed, in many realistic materials including transition-metal oxides intraband and interband contributions to the conductivity spectra commonly overlap unlike the idealized schematics in Fig. 2.[13]

E. Extended Drude formalism and infrared response of a Fermi liquid

In a conducting system, physical processes responsible for renormalization of electronic lifetimes and effective masses also lead to deviations of the frequency-dependent conductivity from conventional Drude theory. These deviations can be captured through the extended Drude formalism (Götze and Wölfle, 1972; Allen and Mikkelsen, 1977):

$$4\pi\tilde{\sigma}(\omega, T) = \frac{i\omega_p^2}{\omega + M(\omega)} = \frac{\omega_p^2}{1/\tau(\omega) - i\omega[1 + \lambda(\omega)]}. \tag{15}$$

The complex memory function $M(\omega)$ has causal analytic properties and bears strong similarities with the electron self-energy for $\mathbf{k}$ points averaged over the Fermi surface. This analysis is particularly useful for the exploration of electron-boson coupling (see Sec. III.F) and of power-law behavior in quantum critical systems (see Sec. III.E). The subtle differences between $M(\omega)$ and the self-energy are discussed in a number of publications (Allen, 1971; Shulga *et al.*, 1991; Dolgov and Shulga, 1995).

In the absence of vertex corrections, the following approximate relation between $M(\omega)$ of an isotropic Fermi liquid and the single-particle self-energies was derived (Allen, 1971):

$$\frac{M(\omega)}{\omega} = \left\{\int \frac{f(\omega') - f(\omega' + \omega)}{\omega + \Sigma^*(\omega') - \Sigma(\omega' + \omega)} d\omega'\right\}^{-1} - 1, \tag{16}$$

where $\Sigma(\xi)$ is the self-energy of electrons with binding energy ξ, and $f(\xi)$ is the Fermi-Dirac distribution. The coupling of electrons to phonons or other bosonic fluctuations is described by the boson density of states multiplied with the square of the coupling constant, $\alpha^2F(\omega)$ for phonons, $I^2\chi(\omega)$ for spin fluctuations, and $\tilde{\Pi}(\omega)$ in general. The self-energy is within this approximation

$$\Sigma(\omega, T) = \int \tilde{\Pi}(\omega')K(\omega, \omega', T)d\omega', \tag{17}$$

where the kernel $K(\omega, \omega', T)$ is a material independent function given by the Fermi and Bose distributions (Allen, 1971). In this set of expressions a double integral relates $\tilde{\Pi}(\omega)$ to $M(\omega)$ and the optical conductivity, which is reduced to a single integral by the reasonably accurate Allen approximation (Allen, 1971; Shulga *et al.*, 1991)

[11] See, for exmple, Basov, Timusk *et al.* (1994), Basov, Liang *et al.* (1995), Liu *et al.* (1999), Dulić *et al.* (2001), Dordevic *et al.* (2002), Homes *et al.* (2004), and iron pnictides (Li, Hu *et al.*, 2008).

[12] See, for example, Abanov and Chubukov (2004), Toschi *et al.* (2005), Benfatto *et al.* (2006), Karakozov and Maksimov (2006), Marsiglio (2006), Norman *et al.* (2007), and Kuchinskii *et al.* (2008).

[13] Examples of extensive experimental literature on sum rule anomalies in correlated systems can be found in the following references: Basov *et al.* (1999), Katz *et al.* (2000a), Basov *et al.* (2001), Molegraaf *et al.* (2002), Kuzmenko *et al.* (2003), Boris *et al.* (2004), Homes, Dordevic *et al.* (2004), Santander-Syro *et al.* (2004), and LaForge *et al.* (2008, 2009).

$$1/\tau(\omega) = \frac{\pi}{\omega}\int_0^\infty \tilde{\Pi}(\omega')K'(\omega,\omega',T)d\omega', \tag{18}$$

where $K'(\omega, \omega', T)$ is a material independent kernel, different from $K(\omega, \omega', T)$. Marsiglio *et al.* (1998) derived, in the limit of weak coupling and zero temperature,

$$\frac{1}{2\pi}\frac{d^2}{d\omega^2}\frac{\omega}{\tau(\omega)} = \tilde{\Pi}(\omega), \tag{19}$$

which for the optical spectra of K_3C_{60} (Degiorgi, Nicol *et al.*, 1994) resulted in the qualitatively correct electron-phonon spectral function.

If the low-energy band structure can be approximated by a single effective band and the scattering γ is small, one may approximate the electron self-energy by a Fermi-liquid expansion $\Sigma = \Sigma(0) + (1 - 1/Z_F)\omega - i\gamma$, with $\gamma \ll T$. Here Z_F is the quasiparticle renormalization amplitude. The low-energy conductivity of such a Fermi liquid is given by

$$\tilde{\sigma}(\omega) = \frac{(\omega_p^0)^2/4\pi}{2\gamma - i(\omega/Z_F)} + \sigma_{\rm reg}(\omega), \tag{20}$$

where $(\omega_p^0)^2 = 4\pi e^2\sum_{\mathbf{k}}(v^{\mathbf{k}})^2\delta(\epsilon_{\mathbf{k}} - \mu_0)$ is the noninteracting plasma frequency, $\mu_0 = \mu - \Sigma(0)$ is the noninteracting chemical potential, and $\sigma_{\rm reg}$ is the regular part of the conductivity.

It is evident from Eq. (20) that the Drude weight is reduced by the quasiparticle renormalization amplitude Z_F, i.e., $\omega_p^2 = (\omega_p^0)^2 Z_F$. Within the band-structure method the Drude weight can be characterized by the effective density $n_{\rm eff}$ and the band mass m_b by $(\omega_p^0)^2 = n_{\rm eff}e^2/m_b$. The renormalized Drude weight, defined in Eq. (11), can be similarly expressed by $\omega_p^2 = n_{\rm eff}e^2/m^*$. Hence the renormalized quasiparticle mass is $m^* = m_b/Z_F$. As expected, the quasiparticle dispersion $\epsilon_{\mathbf{k}}Z_F$, measured by angle-resolved photoemission spectroscopy (ARPES), is also renormalized by the same amount.

The spectral form of the optical conductivity is usually more complicated than the Drude term alone and in addition contains both the incoherent spectral weight and many sidebands due to coupling to various excitations including magnetic and bosonic modes. These additional contributions are contained in $\sigma_{\rm reg}(\omega)$. The plasma frequency is hence modified due to renormalization of quasiparticles and the presence of other excitations by

$$\omega_p^2 = 8\int_0^\Lambda \sigma_1(\omega)d\omega = (\omega_p^0)^2 Z_F + 8w_{\rm reg}, \tag{21}$$

where $w_{\rm reg}$ is the integral of the regular part of σ_1 up to a cutoff Λ. The cutoff should exclude the interband transitions, but should be large enough to include the intraband transitions of some low-energy effective Hamiltonian. The total spectral weight ω_p^2, which is closely related to the kinetic energy of a corresponding low-energy Hamiltonian, defines the optical effective mass $m_{\rm opt}$ via $m_{\rm opt} = n_{\rm eff}e^2/\omega_p^2$, as shown in Fig. 2. Hence the optical mass renormalization over the band mass is $m_{\rm opt}/m_b = 1/[Z_F + 8w_{\rm reg}/(\omega_p^0)^2]$, which is smaller then the enhancement of the low-energy quasiparticle mass $m^*/m_b = 1/Z_F$, measured by ARPES. The optical mass enhancement is also shown in Fig. 2 as the high-energy limit of the effective mass $m^*(\omega)$. The low-energy quasiparticle effective mass is further enhanced by an amount $1 + 8w_{\rm reg}/(\omega_p^0)^2 Z_F$. This additional enhancement can be obtained using the extended Drude analysis. Comparing Eq. (15) with Eq. (20) in the zero-frequency limit, we see that $1 + \lambda(\omega = 0) = \omega_p^2/Z_F(\omega_p^0)^2 = 1 + 8w_{\rm reg}/(\omega_p^0)^2 Z_F$. Hence the quasiparticle effective mass is

$$m^*(\omega = 0) = m_{\rm opt}[1 + \lambda(\omega = 0)] = m_b/Z_F, \tag{22}$$

which is equal to the renormalization of the quasiparticle dispersion, as measured by ARPES. Hence the optical effective mass $m_{\rm opt}$ of a correlated metal can be obtained from optical conductivity data by comparing the total spectral weight below some cutoff Λ with the band-structure method. To obtain the quasiparticle effective mass m^*, one needs to further renormalize the mass by the factor $1 + \lambda$, which can be obtained by the extended Drude model analysis.

Finally, for a very anisotropic Fermi liquid with strong variation of quasiparticle weight $Z_F(\mathbf{q})$ across the Fermi surface, the formula for the effective mass needs to be corrected. As shown by Stanescu *et al.* (2008), the quasiparticle effective mass measured by optics is roughly proportional to $1/\langle Z_F(\mathbf{q})\rangle$, where $\langle\,\rangle$ stands for the average over the Fermi surface. The effective mass measured by other probes can be different. In particular, the Hall effect experiments measure the effective mass proportional to $\langle Z_F(\mathbf{q})\rangle/\langle Z_F^2(\mathbf{q})\rangle$, and quantum oscillation experiments measure the effective mass proportional to $\langle 1/Z_F(\mathbf{q})\rangle$ (Stanescu *et al.*, 2008).

F. Dynamical mean field theory

The theoretical modeling of correlated materials proved to be a difficult challenge for condensed matter theorists due to the absence of a small parameter for a perturbative treatment of correlations, such as the small ratio between the correlation energy and the kinetic energy, or a small electron radius r_s in the dense limit of the electron gas.

For realistic modeling of weakly correlated solids, the local density approximation (LDA) turns out to be remarkably successful in predicting the electronic band structure, as well as the optical constants. However, LDA cannot describe very narrow bands, found in many heavy-fermion materials, nor Hubbard bands. Not surprisingly, it fails to predict the insulating ground state in several Mott insulators and charge-transfer insulators. The combination of LDA with static Hubbard U correction, so-called LDA+U (Anisimov *et al.*, 1991), was able to predict the proper insulating ground state in numerous correlated insulators. Being a static approximation, LDA+U works well for many correlated insulators with long-range magnetic or orbital order. But the exaggerated tendency to spin and orbital order, the inability to describe the correlated metallic state, or capture the dynamic spectral-weight transfer in correlated metals hindered the applicability of the method. A perturbative band-structure method was developed over the course of several decades, named the *GW* method (Hedin, 1965), and it proved to be useful for moderately correlated materials. In particular, its quasiparticle self-consistent version (van Schilfgaarde *et al.*, 2006) successfully predicted band gaps of several semiconductors. However, its perturbative treatment of correlations does not

allow one to describe Mott insulators in a paramagnetic state, nor strongly correlated metals.

Theoretical tools were considerably advanced in the last two decades, mostly due to the development of the practical and powerful many-body method, DMFT (Georges *et al.*, 1996). This technique is based on the one-particle Green's function and is unique in its ability to treat quasiparticle excitations and atomiclike excitations on the same footing. The dynamic transfer of spectral weight between the two is the driving force for the metal insulator transition in Hubbard-like models as well as in transition-metal oxides.

Historically, it was not photoemission, but optical conductivity measurements, in combination with theory (Rozenberg *et al.*, 1995a), that first unraveled the process of the temperature-dependent spectral-weight transfer. In these early days it was difficult to probe bulk photoemission due to the issues with surface states that precluded the detection of the quasiparticle peak and its temperature dependence. On the other hand, the optical conductivity measurements on V_2O_3 (Rozenberg *et al.*, 1995a) unambiguously proved that a small decrease in temperature results in a redistribution of the optical spectral weight from high energy (of the order of a few electron volts) into the Drude peak and midinfrared peak. It was nearly a decade later before photoemission (Mo *et al.*, 2003) detected the subtle effects of the spectral-weight transfer between the quasiparticle peak and Hubbard band.

The accuracy of DMFT is based on the accuracy of the local approximation (Georges *et al.*, 1996) for the electron self-energy. It becomes exact in the limit of infinite lattice coordination (large dimension) and is very accurate in describing the properties of numerous three-dimensional materials (Kotliar *et al.*, 2006).

Just as the Weiss mean field theory (Weiss, 1907) for an Ising model reduces the lattice problem to a problem of a spin in an effective magnetic field, the DMFT approximation reduces the lattice problem to a problem of a single atom embedded in a self-consistent electronic medium. The medium is a reservoir of noninteracting electrons that can be emitted or absorbed by the atom. The local description of a correlated solid in terms of an atom embedded in a medium of noninteracting electrons corresponds to the celebrated Anderson impurity model, but now with an additional self-consistency condition on the impurity hybridization $\Delta(\omega)$ (Georges *et al.*, 1996). The central quantity of DMFT, the one-particle Green's function, is thus identified as an impurity Green's function of a self-consistent Anderson impurity problem. Diagrammatically, the DMFT approximation can be viewed as an approximation which sums up all local Feynman diagrams. Hence, the mapping to the Anderson impurity problem can be viewed as a trick to sum all local diagrams.

A second theoretical advance came when DMFT was combined with band-structure methods (Anisimov *et al.*, 1997), such as LDA, in an approximation dubbed LDA +DMFT (Kotliar *et al.*, 2006). This method does not require one to build the low-energy model to capture the essential degrees of freedom of a specific material, a step, which is often hard to achieve. In LDA+DMFT the extended sp and sometimes d orbitals are treated at the LDA level, while for the most correlated orbital, either f or d, one adds to the LDA Kohn-Sham potential all local Feynman diagrams, the diagrams which start at the specific atom and end at the same atom (Kotliar *et al.*, 2006).

The LDA+DMFT approach allows one to compute both the one-particle Green's function and the current vertex entering Eq. (6) for the optical response. These quantities are normally expressed in the Kohn-Sham basis in which the one-particle part of the Hamiltonian is diagonal. The DMFT one-particle Green's function $G^{ij}_{\mathbf{k}}$ (propagator in Fig. 6) in the Kohn-Sham (KS) basis is

$$G^{ij}_{\mathbf{k}} = \langle \psi_{\mathbf{k},i} | [(i\omega + \mu + \nabla^2 - V_{\mathrm{KS}})\delta(\mathbf{r} - \mathbf{r}') - \Sigma_\omega(\mathbf{r}, \mathbf{r}')]^{-1} | \psi_{\mathbf{k},j} \rangle, \tag{23}$$

where V_{KS} is the Kohn-Sham potential, and $\Sigma_\omega(\mathbf{r}, \mathbf{r}')$ is the DMFT self-energy. The procedure of embedding the DMFT impurity self-energy to the Kohn-Sham basis was extensively discussed by Haule *et al.* (2010). Finally, the two-particle vertex function $\Gamma(\mathbf{k}, \mathbf{q})$ (triangles in Fig. 6) can be computed from the fully irreducible two-particle vertex function $I(\mathbf{k}\mathbf{k}'; \mathbf{q})$ (squares in Fig. 6) through the Bethe-Salpeter equation shown in the second line of Fig. 6. Within the DMFT approximation, the two-particle irreducible vertex $I(\mathbf{k}\mathbf{k}'; \mathbf{q})$ is local, i.e., it does not depend on $\mathbf{k}$, $\mathbf{k}'$, or $\mathbf{q}$, and hence can be computed from the solution of the DMFT impurity problem (Georges *et al.*, 1996). It was first noticed by Khurana (1990) that the vertex corrections to the optical conductivity within the DMFT approximation vanish in the one-band Hubbard-like model. This is because the electron velocity $v_{\mathbf{k}}$ is an odd function of momentum $\mathbf{k}$, $I(\mathbf{k}, \mathbf{k}')$, and does not depend on $\mathbf{k}$ and $\mathbf{k}'$, and hence the vertex corrections to conductivity vanish. In general, for multiband situations encountered in LDA+DMFT, the vertex corrections do not necessarily vanish even though the two-particle irreducible vertex I is purely local in this approximation. This is because, in general, velocities are not odd functions of momentum, which is easy to verify in the strict atomic limit. Nevertheless, the vertex corrections are small in many materials because they vanish at low energy, where a single-band representation is possible, and are also likely subleading at intermediate and high energy, where the itinerant interband transitions dominate. To date, a careful study of the vertex correction effects within LDA+DMFT is lacking. In the context of the Hubbard model, Lin *et al.* (2009) demonstrated that vertex corrections substantially contribute to the optical conductivity at the scale of the Coulomb repulsion $\omega \sim U$, whereas negligible contributions were found to the Drude and the midinfrared peaks.

In the absence of vertex corrections, the optical constants [Eq. (4)] on the real axis take a simple form

$$\mathrm{Re}\{\sigma^{\mu\nu}(\omega)\} = \pi e^2 \sum_{\mathbf{k}} \int d\varepsilon \frac{f(\varepsilon - \omega) - f(\varepsilon)}{\omega} \times \mathrm{Tr}\{\rho_{\mathbf{k}}(\varepsilon) v^{\mathbf{k}\mu} \rho_{\mathbf{k}}(\varepsilon - \omega) v^{\mathbf{k}\nu}\}, \tag{24}$$

where $\rho_{\mathbf{k}}(\varepsilon) = (G^{\dagger}_{\mathbf{k}}(\varepsilon) - G_{\mathbf{k}}(\varepsilon))/(2\pi i)$ and the trace needs to be taken over all bands (Haule *et al.*, 2005). Equation (24) has been used in the majority of LDA+DMFT calculations.

III. EXCITATIONS AND COLLECTIVE EFFECTS

A. Free charge carriers

The electrical conduction of a material is governed by how freely charge carriers can move throughout it. In his seminal model, Drude (1900) considered the charge carriers to propagate independently. The span between two scattering events has an exponentially decaying probability characterized by the time τ and the mean free path ℓ. This scattering or relaxation time fully describes the dynamical response of the entire system to an external field, summarized in the complex frequency-dependent conductivity [Eq. (1)]. The Drude model does not take into account interactions with the underlying lattice, with electrons, or other quasiparticles. In his Fermi-liquid theory, Landau (1956) included electronic correlations, yielding an effective mass m^* and also an effective scattering time (Pines and Nozières, 1966).

In heavy-fermion materials the hybridization of nearly localized f-shell electrons with quasifree conduction electrons leads to an effective mass orders of magnitude larger than the bare electron mass (Fisk *et al.*, 1988; Grewe and Steglich, 1991). Accordingly, the spectral weight [proportional to n/m^* according to the sum rule Eq. (8)] and the scattering rate $1/\tau^* = (m/m^*)(1/\tau)$ are significantly reduced (C. Varma, 1985; C. M. Varma, 1985; Millis *et al.*, 1987; Millis and Lee, 1987). Hence, the charge carriers are extremely slow due to electron-electron interactions which shift the relaxation rate into the microwave regime. As shown in Fig. 7, Scheffler *et al.* (2005) probed the real and imaginary parts of the Drude response in UPd_2Al_3 and UNi_2Al_3 (Scheffler *et al.*, 2006, 2010) over 3 orders of magnitude in frequency and verified that the actual shape is perfectly described by Eq. (1), because impurity scattering still dominates over electron-electron scattering in spite of the strong renormalization.

More specific to the gigahertz range, Fermi-liquid theory predicts a renormalized frequency-dependent scattering rate (Abrikosov *et al.*, 1963; Pines and Nozières, 1966; Ashcroft and Mermin, 1976):

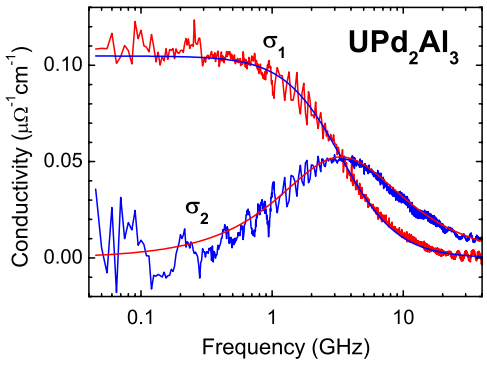

FIG. 7 (color online). Optical conductivity spectrum (real and imaginary parts) of UPd_2Al_3 at temperature $T = 2.75$ K. The fit by Eq. (1), with $\sigma_{dc} = 1.05 \times 10^5$ $(\Omega\,\mathrm{cm})^{-1}$ and $\tau = 4.8 \times 10^{-11}$ s, documents the excellent agreement of experimental data and the Drude prediction. The characteristic relaxation rate $1/(2\pi\tau)$ is marked by the decrease in σ_1 and the maximum in σ_2 around 3 GHz. From Scheffler *et al.*, 2005.

$$1/\tau^*(\omega, T) = A(k_B T)^2 + B(\hbar\omega)^2 \tag{25}$$

with the prefactors increasing as the square of the effective mass (Kadowaki and Woods, 1986), and A/B depending on the material properties (Rosch and Howell, 2005; Rosch, 2006). An experimental confirmation of Eq. (25) is still missing.

B. Charge transfer and excitons

Optical transparency of insulating compounds is a consequence of the energy gap in the spectrum for electron-hole pair excitations, which, if final-state interactions between the electron and the hole can be neglected, corresponds to the gap between the valence and the conduction band. Different physical origins of the gap are known, and the corresponding insulators can be classified accordingly. For this review we make a distinction between two main classes: (i) A gap caused by the periodic potential of the lattice. Standard semiconductors and insulating compounds fall in this class. (ii) A gap opened by on-site Coulomb repulsion (Hubbard U) on the transition-metal ion with an odd number of electrons per site. A further distinction in the latter group is made according to the value of U compared to the charge-transfer energy Δ needed for the excitation process $d^n \rightarrow d^{n+1}\underline{L}$, where $\underline{L}$ denotes a hole in the anion valence band (Zaanen *et al.*, 1985). When $U < \Delta$, processes of the type $d_i^n d_j^n \rightarrow d_i^{n+1} d_j^{n-1}$ are the dominant charge fluctuation corresponding to the optical gap at an energy U. On the other hand, when $U > \Delta$, $d^n \rightarrow d^{n+1}\underline{L}$ corresponds to the optical gap at energy Δ and fluctuations $d_i^n d_j^n \rightarrow d_i^{n+1} d_j^{n-1}$ at an energy U fall inside the interband transitions. The case $U < \Delta$ corresponds to the limit of a Mott-Hubbard insulator and is found on the left-hand side of the $3d$ series, i.e., vanadates and titanates, as well as organic compounds. The situation $U > \Delta$, indicated as "charge-transfer insulator" is common on the right-hand side of the $3d$ series; the cuprates and nickelates fall in this class. Coupling between different bands mixes the character of the bands on either side of the gap, which softens the transition from the Mott-Hubbard insulator to the charge-transfer insulator as a function of U/Δ. This is of particular relevance for substances with U and Δ of the same size, e.g., in Cr, Mn, and Fe oxides (Zaanen *et al.*, 1985; Imada *et al.*, 1998).

The Coulomb interaction can bind an electron and a hole to form an exciton, the energy of which is below the excitation threshold of unbound electron-hole pairs. This is illustrated by the example of cuprous oxide (Cu_2O). This material is important in the quest for Bose-Einstein condensation of excitons (Snoke *et al.*, 1990), a goal which until now has remained elusive (Denev and Snoke, 2002). Cu_2O is a conventional band insulator with a zone center gap of 2.17 eV. The valence and conduction bands have the same (positive) parity at the zone center, rendering direct transitions across the gap optically forbidden. The optical spectrum is therefore dominated by the $2p$, $3p$, $4p$, and $5p$ exciton lines situated 2 to 22 meV below the gap. The excitonic $1s$ ground state is split by the electron-hole exchange interaction into an optically forbidden singlet, and a triplet situated, respectively, 151 and 139 meV below the gap. The triplet corresponds to a

weakly dipole allowed transition at 2.034 eV, whereas the singlet (2.022 eV) can be optically detected in a finite magnetic field (Fishman *et al.*, 2009). Detection schemes employing terahertz radiation generated by $3p$-$2s$ transitions (Huber *et al.*, 2006) or terahertz absorption by $1s$-$2p$ excitations (Fishman *et al.*, 2006; Leinß *et al.*, 2008) of excitons created by laser excitation allow one to monitor the internal conversion of the excitons to the $1s$ ground state as a function of time.

In organic molecular crystals electron-hole pairs can be bound on a single molecule. Because of the larger band mass as compared to typical semiconductors, the exciton binding energy is relatively large: In a two-photon absorption experiment (Janner *et al.*, 1995) the ground-state exciton of C_{60} was observed at an energy 0.5 eV below the threshold of the electron-hole continuum at 2.3 eV.

When a gap is opened by the on-site Coulomb repulsion, a special situation arises due to the fact that the energy of a charge-neutral local configuration change can be smaller than the correlation gap. The result is again an excitonic bound state below the electron-hole continuum. For example, in the spin-Peierls system $CuGeO_3$, the upper Hubbard band is separated from the occupied oxygen $2p$ states by a 3 eV correlation gap. Bassi *et al.* (1996) observed a Cu d-d exciton at 1.75 eV (Fig. 8), far below the onset of the electron-hole continuum at 3 eV. This weak absorption is responsible for the transparent appearance of this compound. In the one-dimensional compound Sr_2CuO_3 (K. W. Kim *et al.*, 2008), sharp peaks observed at 10 K were attributed to weakly bound excitons. The $3d^8$ ground state in NiO is threefold degenerate, and the remaining 42 $3d^8$ states are spread over about 10 eV, grouped in 7 multiplets. About half of these are below the 4 eV correlation gap (Sawatzky and Allen, 1984). These excitons have been observed in optical absorption (Newman and Chrenko, 1959; Tsuboi and Kleemann, 1994). In $KCuF_3$ crystal field excitons were observed at 0.7, 1.05, 1.21, and 1.31 eV corresponding to a local d-d excitation from the $d_{x^2-y^2}$ ground state to d_z,d_{xy},d_{xz}, and d_{yz} excited states (Deisenhofer *et al.*, 2008).

For La_2CuO_4 the electron-hole threshold is at 1.9 eV; Ellis *et al.* (2008) observed a crystal field exciton at 1.8 eV, as well as a peak at 2.2 eV which they attribute to a quasibound electron-hole pair occupying neighboring copper and oxygen

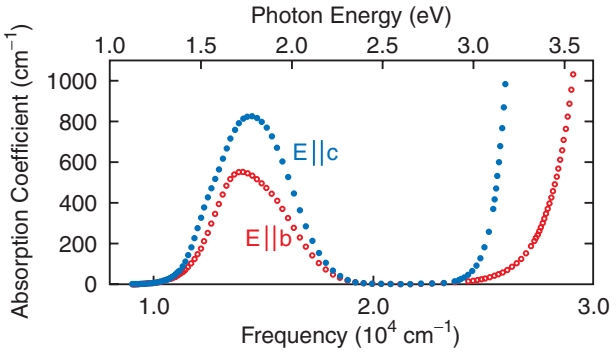

FIG. 8 (color online). Absorption spectrum of $CuGeO_3$ measured at 300 K for two different polarizations of the light. The band-gap energy is 3 eV. The peak at 1.75 eV is a phonon-assisted copper d-d exciton. From Bassi *et al.*, 1996.

atoms. $YTiO_3$ ($SmTiO_3$) has a 0.6 eV Mott-Hubbard gap; Gossling *et al.* (2008) reported excitons corresponding to processes of the type $d^1d^1 \rightarrow d^0d^2$ on two neighboring Y atoms, at 1.95 (1.8) eV, as well as other d^0d^2 configurations at higher energies, having strongly temperature-dependent spectral weight in the vicinity of the magnetic ordering transitions (Kovaleva *et al.*, 2007). Khaliullin *et al.* (2004) showed that, as a consequence of the temperature-dependent orbital correlations, both superexchange and kinetic energy have strong temperature and polarization dependences, leading to the observed temperature dependence of the spectral weight.

C. Polarons

Electron-phonon coupling quite generally renormalizes the mass, velocity, and scattering processes of an electron. The quasiparticles formed when phonons dress the bare electrons are referred to as polarons. However, different conditions in the solid require different theoretical approaches to the electron-phonon interaction. If the electron density is high, the Migdal approximation holds and standard Holstein-Migdal-Eliashberg theory is applied (Mahan, 2000). Historically, the concept of a polaron started from the opposite limit, i.e., a low density electron system interacting strongly with lattice vibrations. In this case the starting point is that of individual polarons, out of which a collective state of matter emerges when the density of polarons is increased. In many ways a polaron is different from an undressed electron. The polaron mass is higher and the Fermi velocity lower compared to those of the original electron, and a phonon-mediated polaron-polaron interaction arises in addition to the Coulomb interaction.

The original description by Landau and Pekar considered that an electron polarizes the surrounding lattice, which in turn leads to an attractive potential for the electron (Feynman, 1955; Mahan, 2000). The situation where the electron-phonon interaction is local is decribed by the Holstein model (Holstein, 1959a, 1959b). This potential is capable of trapping the electron, and a bound state is formed with binding energy E_p. In the literature a distinction is usually made between large and small polarons. Both in the Holstein and in the Fröhlich model the polaron diameter varies continuously from large to small as a function of the electron-phonon coupling parameter, but typically the Holstein (Fröhlich) model is used to describe small (large) polarons (Alexandrov and Mott, 1995). The Fröhlich model uses optical phonon parameters such as the longitudinal phonon frequency $\hbar\omega_{\mathrm{LO}}$, which can be measured spectroscopically (Calvani, 2001). In transition-metal oxides the dominant coupling is to an oxygen optical mode $\omega_{\mathrm{LO}} \sim 0.1$ eV. The binding energy and mass enhancement factor in the weak and strong coupling limits are summarized in Table I, where $\tilde{\varepsilon}_\infty^{-1} = \varepsilon_\infty^{-1} - \varepsilon(0)^{-1}$. In transition-metal oxides the band mass is typically $m_b \sim 2m_e$ and $\epsilon_\infty \sim 4$. The corresponding strong coupling values provide the upper limit for the binding energy ($E_p \sim 0.17$ eV) and the mass enhancement ($m^* \sim 5m_b$).

In general, if the electrons interact with a single Einstein mode, the spectrum consists of a zero-frequency mode and a

TABLE I. Expressions for the Fröhlich coupling constant α, polaron binding energy E_p, and mass enhancement m^*/m_b in the weak and strong coupling limits (Alexandrov and Kornilovitch, 1999).

	Weak coupling	Strong coupling
α^2	$(Ry/\tilde{\varepsilon}_\infty^2\hbar\omega_{\mathrm{LO}})m_b/m_e$	$(Ry/\tilde{\varepsilon}_\infty^2\hbar\omega_{\mathrm{LO}})m_b/m_e$
E_p	$\alpha\hbar\omega_{\mathrm{LO}}$	$0.1085\alpha^2\hbar\omega_{\mathrm{LO}}$
m^*/m_b	$1+(1/6)E_p/\hbar\omega_{\mathrm{LO}}$	$1.8(E_p/\hbar\omega_{\mathrm{LO}})^2$

series of sharp sidebands that describe the incoherent movement of a polaron assisted by $n=1,2,3,\ldots$ phonons (Devreese and Tempere, 1998). In real solids these sharp sidebands are smeared out due to the fact that phonons form bands, and usually only the envelope function is expected (Alexandrov and Bratkovsky, 1999). In a pump-probe experiment it is possible to move the electron suddenly away from the center of the surrounding lattice distortion. This sets up coherent lattice vibrations, which have recently been observed in GaAs using a midinfrared probe pulse (Gaal, 2007). Predictions of the energy of the midinfrared peak using the Fröhlich model are as high as $4.2E_p$ in the strong coupling limit (Myasnikova and Myasnikov, 2008), and $2E_p$ in the Holstein model (Fratini and Ciuchi, 2006). Consequently, in the case of transition-metal oxides, the Fröhlich coupling predicts a midinfrared peak at 0.7 eV at most.

If we now consider Table II, we observe that in most cases the peak maximum is below 0.75 eV. An exception is formed by the high-T_c superconductor $Ba_{1-x}K_xBiO_3$ where, in addition to a weaker peak between 0.33 and 0.45 eV, a strong peak has been observed at 1.2 eV. The latter peak was originally interpreted as a small-polaron midinfrared peak (Puchkov *et al.*, 1995) and more recently as a purely electronic transition (Ahmad and Uwe, 2005). The formalism has been extended to arbitrary density of Fröhlich polarons by Tempere and Devreese (2001). By fitting a moderate electron-phonon coupling ($m^*/m_b=1.3$), they obtained an excellent agreement with the optical data for $Nd_2CuO_{3.996}$ (Lupi *et al.*, 1999). In contrast, the one-polaron model does not capture the optical line shape near the maximum of these data, despite the very low doping level.

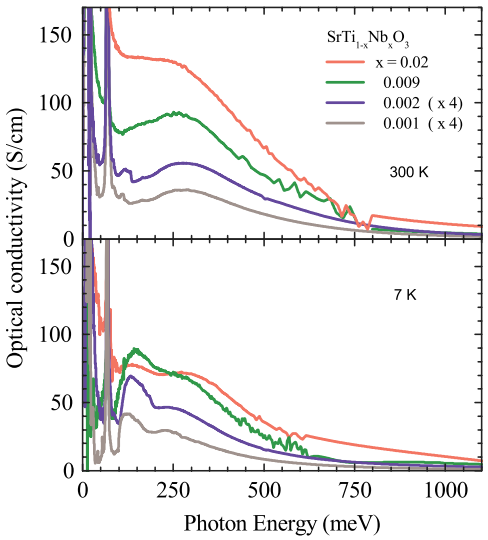

FIG. 9 (color online). Optical conductivity of $SrTi_{1-x}Nb_xO_3$ for $x=0.01$, 0.002, 0.009, and 0.02 at 300 K (top panel) and 7 K (bottom panel) (van Mechelen *et al.*, 2008). The broad, temperature-dependent, midinfrared band between 100 and 750 meV corresponds to (multi-)phonon sidebands of the Drude peak. The narrow Drude peak contains approximately the same amount of spectral weight as the sidebands, implying that $m^*/m_b\sim 2$.

Electrons doped into the unoccupied Ti $3d$ band of $SrTiO_3$ are believed to form polarons due to the Fröhlich-type electron-phonon coupling (Eagles *et al.*, 1995). Indeed, a midinfrared band characteristic of a polaron is observed at 0.25 eV (Calvani *et al.*, 1993; van Mechelen *et al.*, 2008), which redshifts and splits when the temperature decreases (see Fig. 9). The free-carrier mass derived from the Drude spectral weight is $m^*/m_b\approx 2$ implying moderate electron-phonon coupling and large Fröhlich polarons in this material.

A clear trend in Table II is the large values of E_p in transition-metal oxides containing Ni, Mn, or Fe, i.e.,

TABLE II. Midinfrared peak positions for various compounds.

Compound	E_{MIR}(eV)	Reference	T increase
$La_{1.5}Sr_{0.5}NiO_4$	0.75	Jung *et al.*, 2001	Weak redshift
Fe_3O_4	0.6	Park *et al.*, 1998	···
$La_{1-x}Sr_xNiO_4$	0.5	Bi *et al.*, 1993	···
$Pr_{1/2}Sr_{1/2}MnO_3$	0.5	J. H. Jung *et al.*, 2000	Blueshift
$Ba_{1-x}K_xBiO_3$	0.4 & 1.2	Ahmad and Uwe, 2005; Puchkov *et al.*, 1995	No shift
$La_{7/8}Sr_{1/8}MnO_3$	0.4	Jung *et al.*, 1999	Intensity loss
$\alpha'Na_{0.33}V_2O_5$	0.38	Presura *et al.*, 2003	No shift
$La_{1-y}Ca_yTiO_{3.4\pm\delta}$	0.31–0.38	Thirunavukkuarasu *et al.*, 2006	···
$LaTiO_{3.41}$	0.31	Kuntscher *et al.*, 2003	Blueshift
V_3O_5	0.38	Baldassarre *et al.*, 2007	Blueshift
$Bi_{1-x}Ca_xMnO_3$	0.25	Liu *et al.*, 1998	Intensity loss
$SrTiO_3$	0.25	van Mechelen *et al.*, 2008	Blueshift
$Eu_{1-x}Ca_xBa_2Cu_3O_6$	0.15	Mishchenko *et al.*, 2008	···
$Nd_2CuO_{4-\delta}$	0.1	Lupi *et al.*, 1999	···

materials where a transition metal has an open shell with more than one electron or hole. Recent LDA calculations of the electron-phonon coupling strength of $YBa_2Cu_3O_7$ (Heid *et al.*, 2009) gave $\lambda^{tr} = 0.26$, 0.27, and 0.23 along the *a*, *b*, and *c* axes, respectively. Addressing the problem of a single hole doped in the antiferromagnetic insulator, Cappelluti *et al.* (2007) and Mishchenko *et al.* (2008) argued that the electron-phonon and exchange coupling conspire to self-trap a polaron. Adopting $\lambda_{e\text{-ph}} = 0.39$ they predicted a double structure in the midinfrared similar to the experimental data, i.e., a phonon sideband at 0.1 eV and a sideband at 0.5 eV of mixed phonon-magnon character. In a similar way, the high energy of the midinfrared peak of the transition-metal oxides in the top of Table II may be a consequence of the combination of electron-phonon coupling and magnetic correlation.

D. Optical excitation of magnons

In correlated electron systems the spin degrees of freedom are revealed by the collective modes emanating from the interelectronic correlations. Depending on the state of matter, these modes can take the form of paramagnons for a regular metal (Monthoux *et al.*, 2007), spinons in the Luttinger liquid (Giamarchi, 2004a), triplons in spin dimers (Giamarchi *et al.*, 2008), triplet excitons in insulators (see Sec. III.B), or magnons in a ferromagnetic or antiferromagnetic state.

Ferromagnetic resonance (FMR) or antiferromagnetic resonance (AFMR) occurs by virtue of coupling of the electromagnetic field to zone-center magnons. If inversion symmetry is not broken, the only coupling to the electromagnetic field arises from the $\mathbf{B} \cdot \mathbf{S}$ term in Eq. (3). The selection rules are then those of a magnetic dipole transition. Hence the resonance features are present in the magnetic permeability $\mu(\omega)$, while being absent from the optical conductivity $\sigma(\omega)$. Asymmetry of the crystalline electric field upon the spins causes the AFMR frequency to be finite even at $k = 0$, the interaction occurring via the spin-orbit coupling. AFMR and FMR allow one to measure magnetocrystalline anisotropy and spin-wave damping in the hydrodynamic limit (Heinrich and Cochran, 1993). Langner *et al.* (2009) recently applied this technique to $SrRuO_3$ and demonstrated that the AFMR frequency and its damping coefficient are significantly larger than observed in transition-metal ferromagnets. Technological advances using synchrotron sources permit one to measure the absorption spectra as a function of magnetic field for $\omega > 4$ cm^{-1} and fields up to 14 T. The high sensitivity of this technique has led to the discovery of a novel, strongly field- and temperature-dependent mode in $LaMnO_3$ (Mihály *et al.*, 2004). Sensitive detection of FMR by the time-resolved magnetooptic Kerr effect measures the time evolution of the magnetization following an optical-pump pulse (Hiebert *et al.*, 1997).

Optical single-magnon excitations arise not exclusively from the $\mathbf{B} \cdot \mathbf{S}$ coupling: Spin-orbit interaction allows photons to couple to magnons through the $\mathbf{A} \cdot \mathbf{p}$ term of Eq. (3). Activation of this type of optical process requires the breaking of inversion symmetry, which is present in multiferroic materials due to their ferroelectric polarization (see Sec. V E). The optical excitation of a single magnon can be explained if the coupling to the electric field is an effective operator of Dzyaloshinski-Moriya symmetry (Cépas *et al.*, 2001). In the ordered spin state one of the two magnons in the Hamiltonian is replaced by the static modulation of spin density. In cases where magnons are electric dipole active, this has important consequences: Optical phonons and single-magnon waves of the same symmetry will mix. Moreover, two magnon and single magnons can be excited by the electric-field component of electromagnetic radiation (Katsura *et al.*, 2007).

An excitation at 44.5 cm^{-1} was observed by van Loosdrecht *et al.* (1996) in the infrared transmission spectrum of the spin-Peierls phase of $CuGeO_3$. The observed Zeeman splitting identified it as a magnetic excitation (Uhrig, 1997). However, the selection rules are those of an electric dipole (Damascelli, van der Marel *et al.*, 1997). Extensive magnetic field studies of the infrared spectra of $\alpha'NaV_2O_5$, $SrCu_2(BO_3)_2$, and $Sr_{14}Cu_{24}O_{41}$ indicated mixing of phonon and magnon excitations in these compounds (Rõõm *et al.*, 2004a, 2004b; Hüvonen *et al.*, 2007). For these examples a dynamical Dzyaloshinski-Moriya coupling has been proposed by Cépas and Ziman (2004).

The first optical spectra of double-magnon excitations were reported by Silvera and Halley (1966) in FeF_2 and interpreted by Tanabe *et al.* (1965) as the coupling of the electric-field vector to the effective transition dipole moment associated with a pair of magnons. The coupling is nonzero only in the absence of a center of symmetry between the two neighboring spins, as is indeed the case in FeF_2 rutile crystals. If the crystal lattice itself is centrosymmetric, electronic charge (dis)order can still provide the inversion symmetry breaking field: In the quarter-filled ladder compound $\alpha'NaV_2O_5$ the "charged" magnon effect (Popova *et al.*, 1997; Damascelli *et al.*, 1998) lent support to a symmetry breaking charge ordering transition at 34 K. Later investigations favored a zigzag type of charge order without the required inversion symmetry breaking. An alternative mechanism proposed by Mostovoy *et al.* (2002) requires a dynamically fluctuating symmetry breaking field rather than a static one. In this process the photon simultaneously excites one low-energy exciton and two spinons.

The inversion symmetry is not broken by pairs of Ni^{2+} ions in NiO. Yet, Newman and Chrenko (1959) reported a magnetic absorption at 0.24 eV. Mizuno and Koide (1964) attributed this to the simultaneous excitation of two magnons and an optical phonon, a process which is allowed by the electric dipole selection rules. Strong renewed interest in the magnetic fluctuations in transition-metal oxides was revived following the discovery of high-T_c superconductivity in cuprates. The observation of a peak at 0.4 eV in the antiferromagnetic Mott insulater La_2CuO_4 by Perkins *et al.* (1993)) was initially interpreted as an intra-atomic *d*-*d* exciton on the copper site. However, the lower bound of the *d*-*d* excitons was expected at about twice that energy based on microscopic calculations (Eskes *et al.*, 1990; McMahan *et al.*, 1990), as was confirmed by resononant inelastic x-ray scattering experiments (Kuiper *et al.*, 1998). Lorenzana and Sawatzky (1995a, 1995b) therefore postulated that the 0.4 eV peak is due to a phonon-assisted two-magnon process similar to NiO (Mizuno and Koide, 1964) and developed a theory for the optical conductivity spectra. This interpretation was confirmed by the excellent agreement between the

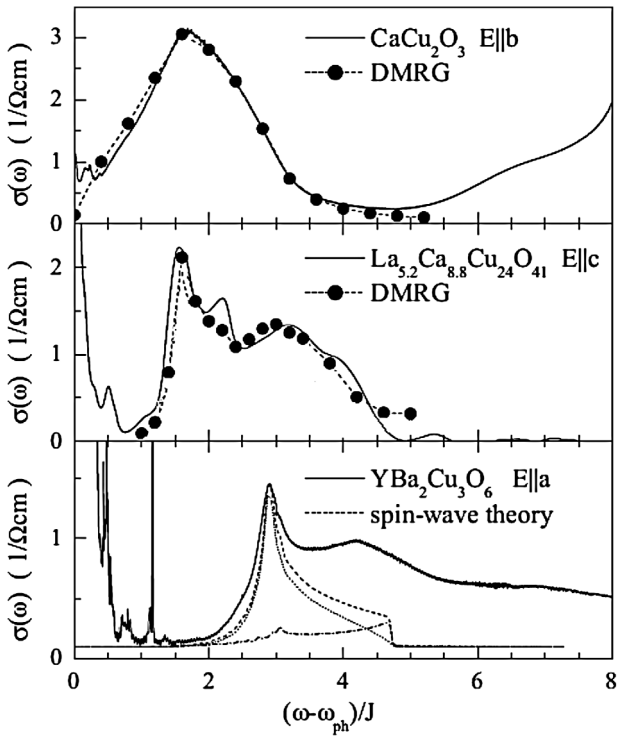

FIG. 10. Evolution of the optical conductivity from weakly coupled chains via two-leg ladders to 2D layers at $T = 4$ K. (Top panel) $\sigma_1(\omega)$ of $CaCu_2O_3$ for $E \parallel b$ (solid line), DMRG result (circles) for $J_\parallel/J_\perp = 5$ and $J_\perp = 1300$ cm^{-1}. (Middle panel) $\sigma(\omega)$ of $La_{5.2}Ca_{8.8}Cu_{24}O_{41}$ for $E \parallel c$ (solid line), DMRG calculation (closed symbols), for $J_\parallel/J_\perp = 1.3$, $J_{cyc}/J_\perp = 0.2$, and $J_\parallel = 1000$ cm^{-1} (Nunner *et al.*, 2002). (Bottom panel) $\sigma_1(\omega)$ of the 2D bilayer $YBa_2Cu_3O_6$ for $E \parallel a$ (solid line). In a bilayer, the two-magnon contribution from spin-wave theory (dashed line) contains an in-plane part (dotted line) and an interplane part (dash-dotted line). Here the in-plane exchange is $J = 780$ cm^{-1} and the interplane exchange amounts to $J_{12}/J = 0.1$ (Grüninger *et al.*, 2000). The two-magnon peak corresponds to $2.88J$ for $J_{12}/J = 0.1$, and to $2.73J$ for $J_{12} = 0$ (Grüninger *et al.*, 2003).

experimentally observed optical spectra and the two-magnon +phonon model for $S = 1/2$ moments in two dimensions (Grüninger *et al.*, 2000; Struzhkin *et al.*, 2000). The line shape of the phonon-assisted two-magnon optical absorption of the 1D spin chain $CaCu_2O_3$ (Suzuura *et al.*, 1996) is very well described by the two-spinon continuum (Lorenzana and Eder, 1997). In the ladder system $La_{5.2}Ca_{8.8}Cu_{24}O_{41}$ the spectrum of the on-rung triplet bound state was found in perfect agreement with the theory of two-triplon excitations, and it allowed the precise determination of the cyclic exchange constant (Windt *et al.*, 2001; Nunner *et al.*, 2002). The importance of quantum corrections to the linear spin-wave theory is shown by the comparison in Fig. 10 of the two-magnon plus phonon optical absorption spectra of chains, ladders, and 2D planes with dynamical mean field renormalization-group (DMRG) calculations and linear spin-wave theory (Grüninger *et al.*, 2003). The multimagnon excitations in the lower panel ($YBa_2Cu_3O_6$), having energies exceeding $5J$, are clearly not captured by linear spin-wave theory, an aspect which DMRG theory describes rather well as is demonstrated by the upper two panels.

E. Power-law behavior of optical constants and quantum criticality

In certain materials a quantum phase transition can occur at zero temperature (Sondhi *et al.*, 1997). A quantum critical state of matter has been anticipated in the proximity of these transitions (Sachdev, 1999; Varma *et al.*, 2002). This possibility has recently attracted much attention because the response of such a state of matter is expected to follow universal patterns defined by the quantum mechanical nature of the fluctuations (Belitz *et al.*, 2005). Candidates are, for example, found in heavy-fermion systems (Coleman and Schofield, 2005; v. Löhneysen *et al.*, 2007) and high-T_c superconductors (Varma *et al.*, 1989). Quantum fluctuations play a dominating role in one-dimensional systems causing *inter alia* the breakdown of the Fermi liquid into a Tomonaga-Luttinger (TL) liquid (Giamarchi, 2004a). Power-law behavior of the response functions is a natural consequence. Since $\ln(\sigma) = \ln(|\sigma|) + i \arctan(\sigma_2/\sigma_1)$, the phase $\arg(\sigma(\omega))$ and $\ln[|\sigma(\omega)|]$ are related by a Kramers-Kronig transformation. Because of the fact that $\int_0^\infty \sigma_1(\omega)d\omega$ is subject to the f-sum rule, we need $\alpha - 1 < 0$ for the integration to converge for $\omega \to 0$. Since in addition $\alpha - 1 \geq 0$ is needed to have a convergent result for $\omega \to \infty$, the integral diverges for any value of α. These divergencies can be avoided by limiting the power-law behavior to the range $\omega_L \ll \omega \ll \omega_H$ as in (van der Marel, 1999)

$$\tilde{\sigma}(\omega) = \frac{\omega_p^2}{4\pi} \frac{1}{(\omega_L - i\omega)^\alpha (\omega_H - i\omega)^{1-\alpha}}. \tag{26}$$

The optical conductivity follows the relation $\sigma_1(\omega) \propto \omega^{4n^2K_\rho - 5}$, where the TL parameter K_ρ characterizes the electron-electron interaction ($K_\rho > 1$ if the interaction is attractive), and n is the order of commensurability ($n = 1$ at half filling and $n = 2$ at quarter filling) (Giamarchi, 2008). This has been confirmed by experiments on the organic compound $(TMTSF)_2X$, where power-law behavior of the optical conductivity was observed with $K_\rho = 0.23$, indicating a repulsive electron-electron interaction (Schwartz *et al.*, 1998). Recent pressure-dependent studies of $(TMTSF)_2AsF_6$ indicate a pressure dependence where K_ρ increases from 0.13 (ambient pressure) to 0.19 (5 GPa), indicating a weakening of the electronic interaction (Pashkin *et al.*, 2006). A similar trend was reported by Lavagnini *et al.* (2009) for the charge-density-wave (CDW) system $LaTe_2$, where the exponent η in $\sigma_1(\omega) \propto \omega^{-\eta}$ evolves from 1.6 to 1.3 when the pressure increases from 0.7 to 6 GPa. Y.-S. Lee *et al.* (2005) measured the optical conductivity for the chain contribution in $YBa_2Cu_3O_y$ and observed a universal exponent $\eta = 1.6$ in the doping range $6.3 < y < 6.75$.

No exact solutions are known up to date for interacting particles in two or three dimensions. However, the preponderance of quantum fluctuations diminishes as the number of dimensions is increased, and consequently the breakdown of the Fermi liquid is not expected to be universal in dimensions higher than 1. An exception occurs when the system is tuned to a quantum phase transition. In this case a quantum critical state is approached and power-law behavior of the optical conductivity

$$\tilde{\sigma}(\omega) = C(1/\tau - i\omega)^{\alpha} \tag{27}$$

is a natural consequence for the response of charged bosons (Fisher *et al.*, 1990).[14] Whether for fermions similar behavior should be expected is a subject of intensive theoretical research (Cubrovic *et al.*, 2009). The limit of zero dissipation is described by $\alpha = -1$. Experimentally $\alpha = -0.4$ (Lee, Wu *et al.*, 2002; Kamal *et al.*, 2006) was observed for the paramagnetic metal (Cao *et al.*, 1997) $CaRuO_3$, while $\alpha = -0.5$ (Kostic *et al.*, 1998; Dodge *et al.*, 2000a) for the 3D ferromagnet $SrRuO_3$ with Curie temperature of 165 K having a large magnetization of $1.6\mu_B$/Ru (Randall and Ward, 1959; Callaghan *et al.*, 1966; Longo *et al.*, 1968) and the 3D helimagnetic metal MnSi (Mena *et al.*, 2003). Multiorbital correlations were shown to lead to an orbital non-FL metal with the observed frequency dependence (Laad *et al.*, 2008). At higher temperature, the power-law dependence of $SrRuO_3$ is cut off at a scale proportional to temperature, marked by dots in Fig. 11(a). In contrast, in $SrRuO_3$ the deviation from $\sigma \sim \omega^{-\alpha}$ occurs at $\omega\tau \gtrsim 1$ [see Eq. (27)]. At temperatures higher than 95 K, we found a deviation from Eq. (27) due to the appearance of a downturn at low frequency. This gapping [not shown in Fig. 11(b)] might be connected to the similar low-frequency downturn apparent also in $CaRuO_3$ [Fig. 11(a)], which Lee, Yu *et al.* (2002) interpreted as a generic feature of the paramagnetic state of ruthenates.

In cuprate high-T_c superconductors one obtains, near optimal doping, the coefficient $\alpha = -2/3$ (Schlesinger *et al.*, 1990; El Azrak *et al.*, 1994; van der Marel *et al.*, 2003; Hwang *et al.*, 2007). According to Eq. (27) the phase should be constant and equal to $-\pi\alpha/2$ (Baraduc *et al.*, 1996; Anderson, 1997). A crucial check therefore consists of a measurement of the phase angle of the optical conductivity $\arg\{\sigma(\omega)\}$. A constant phase angle of 60 degrees up to at least 5000 cm^{-1} is observed in optimally doped $Bi_2Sr_2CaCu_2O_8$ (van der Marel *et al.*, 2003; Hwang *et al.*, 2007), shown in Fig. 12.[15]

Sachdev (1999) showed that for $k_BT > \hbar\omega$ the system exhibits a classical relaxation dynamics. $\sigma_1(\omega, T)$ then becomes a universal function

$$\sigma_1(\omega, T) = T^{-\mu} g(\omega/T). \tag{28}$$

In the insulator-superconductor transition in two space dimensions, the optical conductivity is characterized by a single exponent $\mu = 0$ (Fisher *et al.*, 1990). Universal scaling was observed for $SrRuO_3$ with $\mu = 1/2$ and $g(\omega/T) = (\omega/T)^{1/2}\tanh(1.6\omega/T)$ (Lee, Yu *et al.*, 2002). This absence

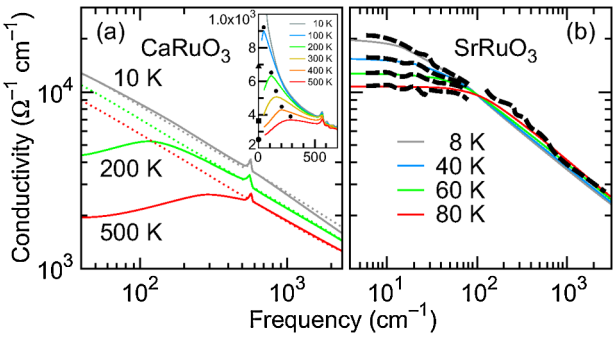

FIG. 11 (color online). (a) Temperature-dependent $\sigma_1(\omega)$ of $CaRuO_3$ shows the power-law scaling at three representative temperatures. The symbols in the inset mark the energy scale where power law $\omega_1^{-1/2}$ ceases to hold. From Y. S. Lee *et al.*, 2002. (b) Logarithmic plot of $\sigma_1(\omega)$ for $SrRuO_3$. The curves from the top correspond to temperatures $T = 8$ K, 40, 60, and 80 K, respectively. Dotted lines are fits to Eq. (27). From Dodge *et al.*, 2000b.

of any other characteristic scale but temperature is usually associated with quantum criticality. On the other hand, Kamal *et al.* (2006) argued that the ω/T scaling might be accidental in the temperature and frequency range measured, and might not be enough to prove the closeness of the quantum critical point. Another decade in the far infrared might be needed to fully establish the ω/T scaling. For the optimally doped

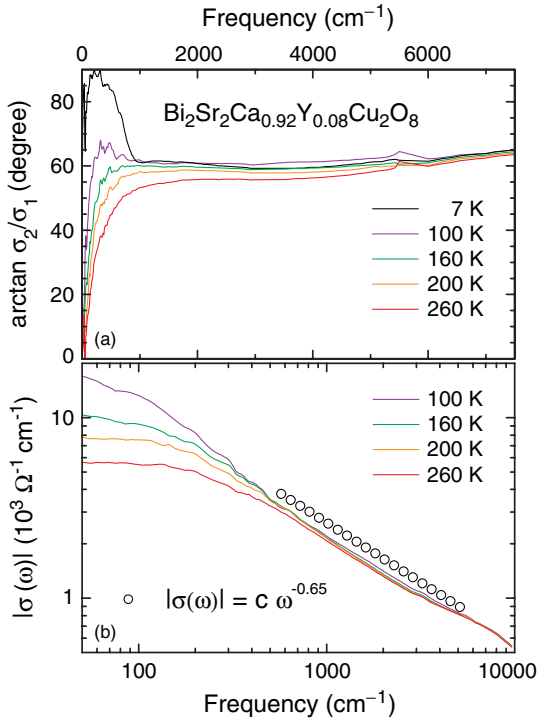

FIG. 12 (color online). Universal power law of the optical conductivity and the phase angle spectra of optimally doped $Bi_2Sr_2Ca_{0.92}Y_{0.08}Cu_2O_8$. (a) The phase function of the optical conductivity $\arg(\sigma(\omega))$. The error margins of $\epsilon_\infty = 4.5 \pm 0.5$ propagate to an uncertainty of $\pm 2°$ of the phase of $\sigma(\omega)$ for $\omega = 5000$ cm^{-1}. (b) The absolute value of the optical conductivity is plotted on a double logarithmic scale. The open symbols correspond to the power law $|\sigma(\omega)| = C\omega^{-0.65}$. From van der Marel *et al.*, 2003.

[14]When $\alpha > -1$ the spectral-weight integral $\int_0^\Omega \sigma_1(\omega)d\omega$ diverges for $\Omega \to \infty$. The power-law behavior is therefore necessarily limited to frequencies below some finite ultraviolet cutoff.

[15]The dielectric constant at finite frequencies is the superposition of the free-carrier contribution, $4\pi i\sigma(\omega)/\omega$, which is the focus of this discussion, and "bound charge" polarizability (see footnote 3 of Sec. II.A), the onset of which is above 1.5 eV for the cuprates (see Sec. III.B. Using ellipsometry between 0.8 and 4 eV, and reflectance data between 0.01 and 0.8 eV van der Marel *et al.* (2003) obtained $\epsilon_\infty = 4.5 \pm 0.5$ for optimally doped $Bi_2Sr_2Ca_{0.92}Y_{0.08}Cu_2O_8$. Using reflectance spectra in a broad frequency range Hwang *et al.* (2007) obtained ϵ_∞ between 4.3 and 5.6 for $Bi_2Sr_2CaCu_2O_8$ samples with different dopings.

cuprates scaling is found with $\mu = 1$ and $g(\omega/T) = C/(1 - iA\omega/T)$ (van der Marel *et al.*, 2006). Since $\mu = (2 - d)/z$, where d and z are dimension and critical exponent, respectively, a positive value for μ implies that z is negative, which is unusual if not impossible (Phillips and Chamon, 2005). Combining the two aspects of quantum critical behavior, the frequency power-law behavior [Eq. (27)] and ω/T scaling [Eq. (28)], required, in the case of the cuprates, the introduction of a nonuniversal energy (~ 50 meV) where the crossover takes place. This raises the question as to the role of such energy scale in a quantum critical scenario. It has been argued (Caprara *et al.*, 2007) that this nonuniversality occurs due to broken Galilean invariance under the influence of the crystal lattice, but that standard quantum criticality still provides the correct framework. Using the conventional framework of electron-boson coupling (see Sec. III.F), Norman and Chubukov (2006) related the power-law behavior of $\sigma(\omega)$ and the concave appearance of $1/\tau(\omega)$ to an electron-boson coupling function with an upper cutoff scale of the boson spectrum of about 300 meV, implying that spin fluctuations are involved in the electron-boson coupling function.

Power-law optical conductivity is not limited to sublinear behavior as in the materials discussed above. Superlinear behavior or ''universal dielectric response'' (Jonscher, 1977) associated with disorder has been observed in a large variety of materials (Dyre and Schrøder, 2000; Lunkenheimer and Loidl, 2003).

F. Electron-boson interaction

The theoretical approaches to the high-T_c pairing mechanism in the cuprates are divided into two main groups (Maier *et al.*, 2008) (see Sec. V.A.1): According to the first school electrons form pairs due to a retarded attractive interaction mediated by virtual bosonic excitations in the solid (Millis *et al.*, 1990). These bosons can be lattice vibrations (Shulga *et al.*, 1991), fluctuations of spin polarization (Scalapino *et al.*, 1986; Haslinger *et al.*, 2000), electric polarization, or charge density (Varma *et al.*, 1989). The second school concentrates on a pairing mechanism entirely due to the nonretarded Coulomb interaction (Phillips, 2006; Anderson, 2007). This section deals with the first group of ideas.

Munzar *et al.* (1999) obtained good agreement between experimental optical spectra for $YBa_2Cu_3O_{6.95}$ (Puchkov, Basov, and Timusk, 1996) and spectra calculated from a spin fluctuation model. Analysis of the optical conductivity of $YBa_2Cu_3O_{6.95}$ using Eq. (18) demonstrated a conspicuous peak in the coupling function at 60 meV (Carbotte *et al.*, 1999; Dordevic, Homes *et al.*, 2005). In addition, angle resolved photoemmision (Bogdanov *et al.*, 2000; Lanzara *et al.*, 2001; Meevasana *et al.*, 2006) and tunneling spectroscopy (Zasadzinski *et al.*, 2001; J. Lee *et al.*, 2006; Levy de Castro *et al.*, 2008) spectra show clear indications of a peak in the electron-boson coupling function at approximately the same energy. Hwang *et al.* (2004) observed a peak in $\mathrm{Re}\{M(\omega)\}$ [defined in Eq. (16)] of $Bi_2Sr_2CuO_6$, which makes its appearance at the superconducting T_c in overdoped copper oxides and slightly above T_c in the underdoped copper oxides. The question of whether the peak is due to a spin resonance, a phonon, or both is still open. Its intensity weakens with doping before disappearing completely at a critical doping level of 0.23 hole per copper atom where T_c is still 55 K. In addition, they found a broad background in $\mathrm{Re}\{M(\omega)\}$ at all doping levels and postulated that this provides a good candidate signature of the ''glue'' that binds the electrons (Hwang *et al.*, 2004).

Norman and Chubukov (2006) explained the spectral shape of $M(\omega)$ (see Sec. II.C) with a model of electrons coupled to a broad spectrum of spin fluctuations extending to about 300 meV, i.e., the scale of magnons in the insulating parent compounds (Hayden *et al.*, 1996). In the context of a discussion of the Hubbard model, it has been pointed out (Maier *et al.*, 2008) that the ''anomalous'' self-energy associated with the pairing has small but finite contributions extending to an energy as high as U, an aspect which is not captured by the approach of Eq. (16). Alternative approaches based on Eq. (16) assume that the bosonic spectral function is provided by (near quantum critical) orbital current fluctuations (Aji and Varma, 2007), or excitons (Little and Holcomb, 2004).

Extensive efforts have been made to infer $\tilde{\Pi}(\omega)$, introduced in Sec. II.E, from the experimental optical spectra. Usually, as the first step $1/\tau(\omega)$ is calculated from the original data. The most direct approach then uses Eq. (19) to calculate $\tilde{\Pi}(\omega)$ from $1/\tau(\omega)$. However, since this expression is only valid at zero temperature and for weak coupling, Dordevic, Homes *et al.* (2005) calculated $\tilde{\Pi}(\omega)$ from $1/\tau(\omega)$ from the inverse transformation of the integral equation (16) using the method of singular value decomposition. To fit the Allen approximation, Eq. (18), to the experimental $1/\tau(\omega)$ data Schachinger *et al.* (2006) implemented a maximum entropy method. Carbotte and Schachinger (2006) extended this analysis to the d-wave superconducting state at finite temperature by approximating the optical conductivity with a superposition of s-wave gaps. However, $1/\tau(\omega)$ is not a purely experimental quantity; to determine it a correction must be made for the interband transitions (see Sec. III.E) and a value of ω_p must be assumed. Therefore van Heumen, Kuzmenko, and van der Marel (2009) implemented a method which analyzes the original reflectance and ellipsometry spectra. A flexible parametrization of $\tilde{\Pi}(\omega)$ was used to calculate, using Eq. (16), respectively, $M(\omega)$, $\sigma(\omega)$, reflectance, and ellipsometry spectra. The parameters describing $\tilde{\Pi}(\omega)$, $\epsilon_b(\omega)$, and ω_p were varied using a numerical least-squares fitting routine with analytical derivatives, until convergence was reached to the experimental reflectance and ellipsometry data.

The universal description of optical and ARPES was demonstrated by extracting this way $\tilde{\Pi}(\omega)$ from optical and photoemission spectra of a series of $Bi_2Sr_2CuO_6$ crystals with different carrier concentrations (van Heumen, Meevasana *et al.*, 2009). Close to T_c the different methods give by and large the same $\tilde{\Pi}(\omega)$. However, for reasons which still need to be clarified, and as illustrated by the case of $HgBa_2CuO_4$, stronger temperature dependence of $\tilde{\Pi}(\omega)$ is obtained with the maximum entropy method (Yang, Hwang *et al.*, 2009) than with the least-squares fitting method (van Heumen, Muhlethaler *et al.*, 2009). Similar efforts were

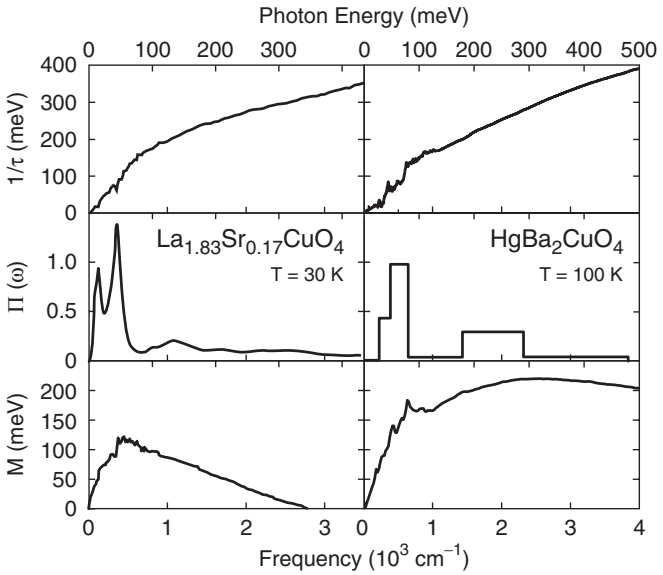

FIG. 13. Comparison at $T \approx T_c$ of the imaginary part $[1/\tau(\omega)]$ and the real part $[M(\omega)]$ of the optical self-energy, and the electron-boson coupling functions of $La_{1.83}Sr_{0.17}CuO_4$ ($T_c = 31$ K) (Hwang *et al.*, 2008) and $HgBa_2CuO_4$ ($T_c = 97$ K). From van Heumen, Muhlethaler *et al.*, 2009.

undertaken on the analysis of Raman spectra of cuprates (Devereaux and Hackl, 2007; Grilli *et al.*, 2009).

In Fig. 13, results are shown for two single-layer compounds, $La_{1.83}Sr_{0.17}CuO_4$ ($T_c = 31$ K) (Hwang *et al.*, 2008) and $HgBa_2CuO_4$ ($T_c = 97$ K) (van Heumen, Muhlethaler *et al.*, 2009). These spectra illustrate the main features of the bosonic spectrum observed in all cuprates, namely, a high-energy spectrum (extending to about 300 meV for the optimally and overdoped samples), and a peak between 50 and 70 meV in all cuprates. These aspects are also present in the spin fluctuation spectrum of Cásek *et al.* (2005) in their analysis of the optical spectra. For $La_{1.83}Sr_{0.17}CuO_4$, an additional peak was obtained at 18 meV, present only below 50 K (Hwang *et al.*, 2008). The intensity of the 50–70 meV peak decreases strongly as a function of doping, and on the overdoped side of the phase diagram only the high-energy part $\tilde{\Pi}(\omega)$ can account for the observed high T_c (van Heumen, Muhlethaler *et al.*, 2009). These observations support the idea that the pairing mechanism is, at least in part, of electronic nature, i.e., involves spin, charge, or orbital fluctuations.

G. Superconducting energy gap

Far-infrared spectroscopy has played an important role in the characterization of superconductors ever since the BCS phonon-mediated pairing mechanism was proposed and experimentally verified (Bardeen *et al.*, 1957). Mattis and Bardeen (1958) described the electrodynamics of superconductors and the opening of a spectroscopic gap $2\Delta_0$ for quasiparticle excitations. In weak-coupling BCS theory (Bardeen *et al.*, 1957), the gap value is given by $2\Delta_0 = 3.5k_BT_c$. The electrodynamics were experimentally measured by Glover and Tinkham (1957) using far-infrared techniques (Tinkham, 1996). Far-infrared spectroscopy continues to be

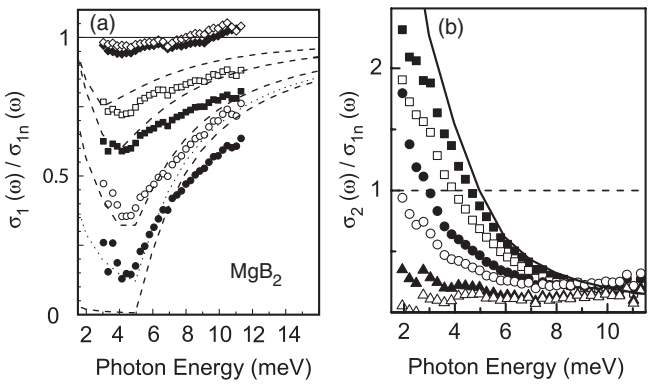

FIG. 14. Far-infrared conductivity of MgB_2. (a) σ_1/σ_n and (b) σ_2/σ_n as a function of frequency for various temperatures: 6 K (dots), 17.5 K (open circles), 24 K (solid squares), 27 K (open squares), 30 K (solid diamonds), and 50 K (open diamonds). The opening of a gap is clearly observed in (a), while (b) shows the characteristic $1/\omega$ inductive response of the condensate. From Kaindl *et al.*, 2001.

an important tool to investigate superconductors, especially considering recent discoveries of new superconducting compounds (Basov and Timusk, 2005).

MgB_2 provides one such example. Discovered in 2001, this material becomes superconducting below $T_c = 39$ K which was, at the time of discovery, an unexpected result for a simple intermetallic compound (Nagamatsu *et al.*, 2001). Shortly after its discovery, experiments using time-domain spectroscopy from 2 to 11 meV were performed on a 100-nm-thick MgB_2 film as shown in Fig. 14 (Kaindl *et al.*, 2001); complementary measurements in the frequency domain yield equivalent results (Pronin *et al.*, 2001; Pimenov *et al.*, 2002).

A useful way to analyze the electrodynamic properties of superconductors is to plot the ratio of the conductivity to its normal state value $\sigma_n(\omega)$. This is shown in Figs. 14(a) and 14(b) for the real and imaginary parts, respectively. A strong depletion in the real part $\sigma_1/\sigma_n(\omega)$ is evident in Fig. 14(a) as the temperature is decreased below T_c. This is the signature of the superconducting gap. The imaginary part $\sigma_2/\sigma_n(\omega)$ in Fig. 14(b) shows the buildup of a component in the superconducting state that strongly increases with decreasing frequency and the characteristic $1/\omega$ inductive condensate response. The lines in the figure are calculations using the Mattis-Bardeen theory for BCS superconductors with an isotropic *s*-wave gap (Mattis and Bardeen, 1958), valid in a "dirty limit," which occurs when the superconducting gap $2\Delta_0$ is much smaller than the normal state scattering time. The overall agreement is possible only when a gap value of $2\Delta_0 = 5$ meV is used in the calculations. This value is nearly a factor of 2 smaller than the ratio expected from the known T_c even in weak-coupling BCS theory, which predicts $2\Delta_0 = 3.5k_BT_c \approx 9$ meV. This small gap is a fundamental property of MgB_2 explained by the existence of two superconducting gaps, of which the smaller one dominates the optical conductivity.[16] First-principle band-structure calculations

[16]See, for example, Gorshunov *et al.* (2001), Kortus *et al.* (2001), Liu *et al.* (2001), Choi *et al.* (2002), Kuzmenko *et al.* (2002), and Pimenov *et al.* (2002).

confirm this novel physics and indicate that the dominant hole carriers in boron p orbitals are split into two distinct sets of bands with quasi-2D and -3D character. The coupling between these bands leads to a novel superconducting state with two gaps but a single T_c.

While far-infrared spectroscopy is clearly an important tool to investigate the electrodynamics of the condensate response of new superconductors (see, e.g., Sec. VI.E on the ferropnictides), there are also interesting studies on elemental superconductors in recent years. These experiments include detailed measurements of the microwave response of Al (Steinberg *et al.*, 2008) for comparison with BCS theory and probing the nonequilibrium condensate response of $DyBa_2Cu_3O_7$ (Feenstra *et al.*, 1997) and Pb (Carr *et al.*, 2000) using time-resolved far-infrared techniques.

As mentioned, far-infrared spectroscopy of the superconducting gap served as an important test of BCS in the early days. However, other predictions such as the coherence peak remained much more difficult to experimentally verify. In Pb and Nb the expected maximum in the temperature-dependent conductivity was not observed until the 1990s. The full frequency temperature and frequency dependence of the coherence peak was recently measured in Al ($T_c = 1.9$ K) using microwave spectroscopy from 45 MHz to 40 GHz (Steinberg *et al.*, 2008). The experiments were performed on a series of films with mean free paths ranging from 1.8 to 5.0 nm. The results are in agreement with the sum rule [Eq. (14)] and show a clear reduction in the coherence peak with increasing mean free path as the clean limit is approached.

Another area which has its roots in the 1960s efforts to experimentally verify the BCS response of conventional superconductors are nonequilibrium studies which originated in tunneling studies (Rothwarf and Cohen, 1963; Miller and Dayem, 1967). Early nonequilibrium studies of BCS superconductors showed that the time for quasiparticle recombination τ_R to Cooper pairs is sensitive to the magnitude of the superconducting gap (Kaplan *et al.*, 1976; Schuller and Gray, 1976; Gray, 1981). Quasiparticle recombination (i.e., the formation of a Cooper pair) is a fundamental process in a superconductor arising from the pairing of two quasiparticles which are thermally or otherwise excited out of the condensate. Thus, the goal of these initial experiments was to determine the bare quasiparticle recombination, where calculations taking into account the electron-phonon coupling suggest a time of ~100 ps in BCS superconductors.

Pair breaking by excess phonons, however, complicates matters as described by the phenomenological rate equations of Rothwarf and Taylor (1967). This model consists of two coupled rate equations describing the temporal evolution of the density of excess quasiparticles and phonons injected into a superconductor. The Rothwarf-Taylor equations are written as

$$\frac{dn}{dt} = \beta N - Rn^2 - 2Rnn_T, \tag{29a}$$

$$\frac{dN}{dt} = \frac{1}{2}[Rn^2 - \beta N] - \frac{N - N_0}{\tau_p}. \tag{29b}$$

Here n is the excess quasiparticle density, n_T is the thermal quasiparticle density, N is the excess density of phonons with energies greater than 2Δ, R is the bare quasiparticle recombination coefficient, β is the pair-breaking coefficient for ($>2\Delta$) phonons, and τ_p describes the relaxation time of the phonons either by anharmonic decay to phonons with energies $<2\Delta$ or through phonon escape from the sample (e.g., into the substrate). As Eqs. (29) reveal, in the limit of small n_T, the recombination of quasiparticles requires two quasiparticles to form one Cooper pair, hence the n^2 term. However, the direct determination of τ_R is difficult since it is masked by excess 2Δ phonons which break additional Cooper pairs (e.g., the βN term). Thus, in many measurements, it is actually the phonon decay τ_p that is measured. This has been termed the phonon bottleneck.[17]

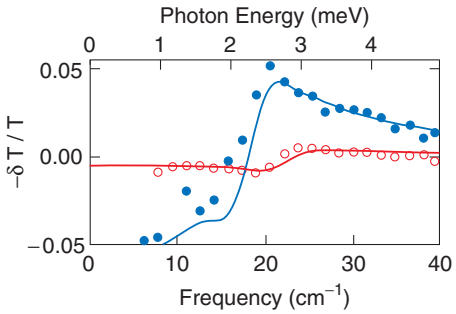

FIG. 15 (color online). Photoinduced change in the superconducting gap in Pb at $T = 3.7$ K. Photoexcitation reduces the condensate density which in turn leads to a decrease in the magnitude of the gap and a modified far-infrared transmission. The solid circles are data obtained following photoexcitation with 1.8 nJ pulses, while the open circles are for photoexcitation with 0.4 nJ pulses. The corresponding solid lines are fits to the change in transmission using BCS theory. From Carr *et al.*, 2000.

A recent example on Pb using femtosecond pump pulses synchronized to the far-infrared beam line at the National Synchrotron Light Source (NSLS) at Brookhaven producing pulses 300 ps in duration (Carr *et al.*, 2000). This permitted a direct probe of the recovery of the superconducting gap following photoexcitation with 800 nm pulses which reduce the condensate density by ~1% which is comparable to the excess thermal quasiparticle density. An exponential recovery of ~250 ps is related to the recombination of quasiparticles within the bottleneck regime. This assignment was verified through spectroscopic measurements of the induced change in the far-infrared transmission ($\delta T/T$) as shown in Fig. 15. The fits are using BCS theory with the spectral change related to the decrease in the gap due to the reduction in condensate density.

Similar experiments were performed on MgB_2 (Demsar *et al.*, 2003b). In these studies, the increased temporal resolution (~ 1 ps) afforded by electro-optic techniques enabled measurements of the quasiparticle recombination and the initial pair-breaking process. The pair-breaking process extended to 10 ps (~ 100 times the duration of the pair-breaking pulse) and is in contrast with Pb where the pair-breaking dynamics are complete in ~1 ps (Federici *et al.*,

[17]These phenomenological equations have been utilized to understand the dynamics of other gapped materials as described by Kabanov *et al.* (2005), Chia *et al.* (2006), Demsar, Thorsmolle *et al.* (2006), and Chia *et al.* (2007).

1992). Through analysis with Eqs. (29) this delay in the condensate reduction was attributed to a preferential phonon emission by the photoexcited quasiparticles which subsequently break additional Cooper pairs. It was also possible to extract β, R, and τ_p (Demsar *et al.*, 2003b).

These recent time-integrated and time-resolved experiments on BCS superconductors provide new insights into these materials and point the way toward experiments on more exotic superconductors such as the cuprates and pnictides (see Secs. V.A.1 and VI.E, respectively).

H. Pseudogap and density waves

The term ''pseudogap'' is heavily used in the physics of correlated electron materials in a variety of different contexts. Most generally, pseudogap describes a partial or incomplete gap in the density of states. Pseudogaps are common in doped Mott insulators in the vicinity of the insulator-to-metal transition (IMT) (see Sec. IV.A). The best studied class of materials displaying a pseudogap are cuprate superconductors, discussed in Sec. V.A.1. But cuprates are not the only class of materials which show a pseudogap in the charge response. In this regard, various one-dimensional analogs of cuprates have been recently synthesized. A prominent example is $Sr_{14-x}Ca_xCu_{24}O_{41}$.

This material has a layered structure and consists of two distinct one-dimensional objects: 1D two-leg ladders and 1D chains. The conductivity is primarily determined by the two-leg ladders (Osafune *et al.*, 1997). Namely, the holes on the chains are dimerized with periodicity $5c_{\text{chain}}$, as shown by neutron scattering experiments (Matsuda *et al.*, 1997). Hence the conductivity on the two-leg ladder subsystem is up to 1000 times larger than the conductivity along the chains.

The parent compound exhibits Mott-like insulating behavior, exhibiting spin and charge gaps. Because of chemical pressure the substitution of Sr^{2+} by isovalent Ca^{2+} introduces hole carriers, which form a CDW on the ladder subsystem [for a review, see Vuletić *et al.* (2006)]. At higher doping levels, the CDW is gradually suppressed and the CDW gap eventually vanishes at the critical doping. Vuletić *et al.* (2003) estimated the critical doping to be $x \approx 9$. For even larger doping $x \gtrsim 12$ under pressure, the system exhibits superconductivity with $T_c^{\max} \approx 12$ K (Uehara *et al.*, 1996).

Figure 16 shows the a-axis optical conductivity for two different hole doping levels $x = 8$ and 11 and few temperatures, measured by Osafune *et al.* (1999). Similar spectra for the same and lower hole dopings were obtained by Vuletić *et al.* (2003, 2005). Note, however, that the gap size at the same nominal doping is somewhat smaller in Vuletić *et al.* (2005) than measured by Osafune *et al.* (1999). The system develops a gap in the charge response at low temperatures. The low-frequency a-axis optical conductivity decreases with decreasing temperature, and the depressed spectral weight is transferred to much higher frequencies. The energy scale of this suppressed conductivity due to the CDW is very large and comparable to a pseudogap scale in cuprates. The optical conductivity in the c direction (not shown) also displays a gap (Vuletić *et al.*, 2005), although the gap size is somewhat smaller in the c direction compared to a, which is consistent

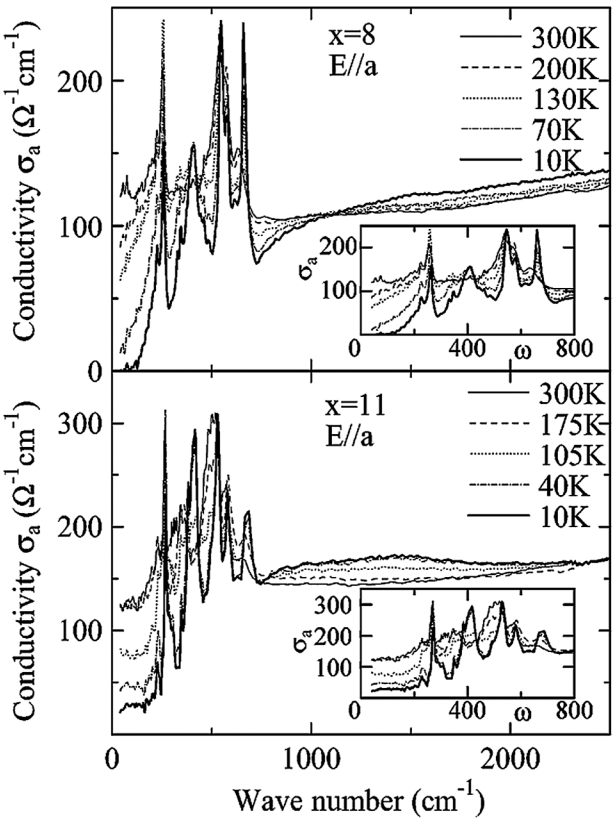

FIG. 16. The in-plane a-axis optical conductivity of the $Sr_{14-x}Ca_xCu_{24}O_{41}$ compound for doping $x = 8$ and 11. The insets show the enlargement of the low-frequency conductivity. From Osafune *et al.*, 1999.

with the conductivity being largest along the legs of the ladders.[18]

The existence of a CDW for $x = 0$ was well established from impedance measurements, a giant dielectric constant, and nonlinear current-voltage curve (Blumberg *et al.*, 2002; Gorshunov *et al.*, 2002). Direct detection of crystallization of holes with a periodicity of $5c_{\text{ladder}}$ was recently achieved by resonant x-ray scattering (Abbamonte *et al.*, 2004). Note that the material is intrinsically self-doped, and the $x = 0$ sample is already doped with holes at ~0.07 hole/Cu. The collective nature of the CDW is reflected in large effective masses of the CDW condensate. From c-axis conductivity, Osafune *et al.* (1999) estimated the effective mass to be of the order of $(100–200)m_e$. Vuletić *et al.* (2003) found a somewhat smaller but still large mass of the order of $(20–50)m_e$ from the CDW phason mode. The CDW develops in the a-c plane, while it does not develop true long-range order in the b direction. Hence no jump in temperature dependence of resistivity along the b direction was detected (Vuletić *et al.*, 2005).

While the electron-phonon interaction is crucial for development of CDWs, pure electron-electron interactions can drive the antiferromagnetic ordering of the conduction electrons, leading to a spin density wave (SDW). This was observed as a drop in the far-infrared reflectivity of Cr

[18]The optical conductivity in Fig. 16 resembles the c-axis conductivity of cuprates, first measured by Homes *et al.* (1993, 1995).

(Barker *et al.*, 1968), URu_2Si_2 (D. A. Bonn *et al.*, 1988), and $(TMTSF)_2PF_6$ (Degiorgi *et al.*, 1996) [see the inset of Fig. 48(c)]; and more recently in iron pnictides (Dong *et al.*, 2008; Hu *et al.*, 2008) [see Fig. 47(a)].

IV. OPTICAL PROBES OF INSULATOR-TO-METAL TRANSITIONS

A. Emergence of conducting state in correlated insulators

In Fig. 17 we display data revealing the evolution of the electromagnetic response across the IMT in four important examples of correlated electron systems. The top row presents results for V_2O_3 and $La_{2-x}Sr_xCuO_4$ which are two classes of Mott insulators. Transport and thermodynamics experiments revealed that V_2O_3 is driven toward the insulating state at $T < 150$ K by control of the electronic bandwidth W (McWhan *et al.*, 1971; Carter *et al.*, 1993) so that the strength of electronic correlations $\propto U/W$ is modified. In $La_{2-x}Sr_xCuO_4$ diavalent Sr substitutes trivalent La and the IMT is best understood in terms of band filling (Kumagai *et al.*, 1993). The electromagnetic response of bandwidth-controlled and filling-controlled Mott systems reveals a number of commonalities: (i) As expected, in the insulating state one finds evidence for the electronic gap where $\sigma_1(\omega) \to 0$ followed by a rapid increase of the conductivity. (ii) There is no obvious suppression of the gap in either bandwidth- or filling-controlled systems. Instead, the energy region below the gap is gradually "filled up" with states before any remanence of the gap disappears on the metallic side of the transition. (iii) A salient feature of both classes is that the redistribution of the electronic spectral weight involves a broad range of frequencies extending to several electron volts. In the case of V_2O_3 one therefore finds a large mismatch between the k_BT and $\hbar\omega$ scales near the IMT (Thomas *et al.*, 1994). (iv) The response on the metallic side of the transition is highly unconventional. The frequency-dependent conductivity is different from that of noninteracting systems. One commonly finds a Drude-like mode at far-IR frequencies attributable to mobile charges followed by a broad, incoherent part at higher energies. The oscillator strength of the Drude-like contribution to $\sigma_1(\omega)$ is significantly reduced compared to expectations of the band theories ignoring electronic correlations (Fig. 1). Cases (i)—(iv) can be regarded as universal attributes of the Mott transition obeyed both by oxides (Fig. 17) and also by organic compounds (Fig. 52). The evolution of optical constants upon variation of the U/W parameter has been monitored in $RTiO_3$ (R = La, Ce, Pr, Nd, Sm, Gd) systems (Crandles *et al.*, 1991; Katsufuji *et al.*, 1995; Okimoto *et al.*, 1995; Kobayashi *et al.*, 1998; Yang *et al.*, 2006). All of these systems reveal transfer of the electronic spectral weight to lower energies with increasing doping similar to cuprates and also consistent with the theoretical studies based on the Hubbard Hamiltonian (Dagotto, 1994). The rate of this spectral-weight transfer allows one to quantify the strength of electronic correlations U/W (Katsufuji *et al.*, 1995; Yang *et al.*, 2006).

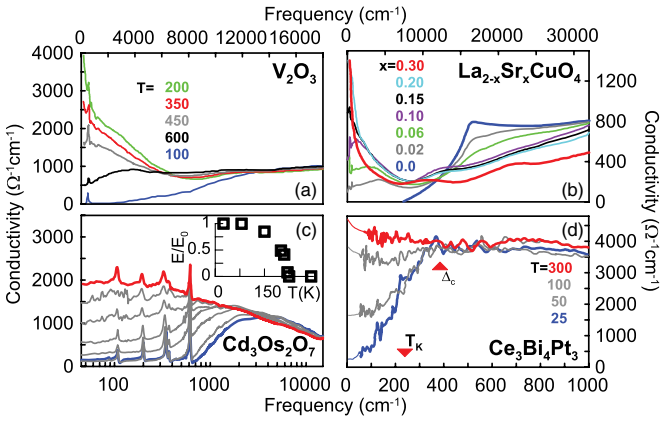

FIG. 17 (color online). Evolution of the optical conductivity across insulator-to-metal transitions. (a) Bandwidth controlled Mott transition in V_2O_3 (Baldassarre *et al.*, 2008). (b) Filling-controlled Mott transition in $La_{2-x}Sr_xCuO_4$ (Uchida *et al.*, 1991). (c) The Slater transition in $Cd_2Os_2O_7$ (Padilla *et al.*, 2002) [data plotted at the following temperatures (from top to bottom): 300, 250, 220, 210, 200, and 30 K; inset—the temperature dependence of the energy gap determined from the kink in $\sigma(\omega)$]. (d) Kondo system $Ce_3Bi_4Pt_3$ (Bucher *et al.*, 1994).

The energy gap in the optical data for Mott insulators is a direct consequence of the high energetic cost of double occupancy U. Doping of a Mott insulator partially releases the restriction for double occupancy and thus "unjams" the electronic conduction. Since doping typically impacts some but not all sites, doped Mott insulators are inherently inhomogeneous on the atomic scale. Their electromagnetic response combines features characteristics of an undoped insulator and a doped conductor. A partial electronic gap (or pseudogap) often persists in doped Mott insulators over an extended region of their phase diagram (Puchkov, Basov, and Timusk, 1996; Timusk and Statt, 1999; Y. S. Lee *et al.*, 2005) and in some cases has been linked to local inhomogeneities (Homes *et al.*, 2003). An extended Drude analysis commonly uncovers very strong dissipation on the metallic side of the transition (Orenstein *et al.*, 1990; Rotter *et al.*, 1991; El Azrak *et al.*, 1994; Basov *et al.*, 1996; Puchkov, Basov, and Timusk, 1996; Dodge *et al.*, 2000a; van der Marel *et al.*, 2003; Zaanen, 2004; Y. S. Lee *et al.*, 2005; Qazilbash *et al.*, 2006). Routinely, one finds that $1/\tau(\omega)$ exceeds the energy in the frequency region corresponding to the incoherent component. These results challenge the notion of well-defined quasiparticles.

A counterpart in dc transport is an exceptionally short electronic mean free path of the order of interatomic spacing commonly registered in doped Mott insulators (Emery and Kivelson, 1995a). An interdependence between the dc transport and incoherent (midinfrared) response has been analyzed within a framework based on the oscillator strength sum rule (Gunnarsson *et al.*, 2003; Qazilbash *et al.*, 2006). Currently, there is no consensus on a microscopic scenario for the midinfrared band.

The electronic spectral weight in filling-controlled systems proportional to n/m^* is vanishingly small on the insulating side of the transition and varies linearly with doping (Uchida *et al.*, 1991; van Heumen, Muhlethaler *et al.*, 2009). Both bandwidth- and filling-controlled classes of Mott systems

may reveal the divergence of the effective mass near the IMT. Thermodynamic measurements uncover mass enhancements in a bandwidth-controlled system: V_2O_3 (McWhan *et al.*, 1971; Carter *et al.*, 1993; Limelette *et al.*, 2003) but not in $La_{2-x}Sr_xCuO_4$ (Loram, 1989; Kumagai *et al.*, 1993). The behavior of the optical effective mass (see Sec. V.B.1) near the IMT boundary in V_2O_3 has not been investigated. A closely related VO_2 system (Qazilbash *et al.*, 2007) does reveal strong enhancement of m^* near the IMT boundary and so do organic materials with the bandwidth control of the transition (see Fig. 52) (Merino *et al.*, 2008; Dumm *et al.*, 2009). $Sr_{1-x}La_xTiO_3$ is an example of a filling-controlled system revealing nearly divergent behavior of m^* in proximity of the IMT (Fujishima *et al.*, 1992). On the contrary, the optical mass in high-T_c superconductors, which also belong to the filing-controlled class and include $La_{2-x}Sr_xCuO_4$ and $YBa_2Cu_3O_y$, shows no anomalies in proximity to the Mott phase (Padilla, Dumm *et al.*, 2005). This latter inference relies on the Hall data to discriminate between n and m^* contributions to infrared spectral weight and is therefore not unambiguous. Nevertheless, this finding is in accord with specific heat results (Kumagai *et al.*, 1993). Weak doping dependence of the optical mass in cuprates is in accord with DMFT analysis of the filling-controlled transition in these materials (see Sec. V.A.1).

Figure 17(d) shows the evolution of the electromagnetic response in a Kondo insulator $Ce_3Bi_4Pt_3$ (Bucher *et al.*, 1994). The gross features of this insulating state are best understood within the periodic Anderson model. This model predicts the formation of the energy gap in the vicinity of the Fermi energy as the result of hybridization between narrow d or f levels and conduction electrons (Hewson, 1993). Provided the Fermi energy falls inside the narrow hybridized band, the resultant behavior is metallic characterized by a large effective mass (see Sec. VI). However, if the Fermi energy is located within the hybridization gap, Kondo insulating behavior results. Quite remarkably, upon the transformation from the insulating to metallic state the conductivity spectra repeat universal characteristics of Mott insulators including gap filling, redistribution of the spectral weight across a broad energy range, and dominant incoherent contribution in the metallic state (see Sec. VI.B for a detailed discussion of the recent data).

In contrast, Slater insulators reveal much more conventional behavior across the IMT. The term refers to an insulating state produced by antiferromagnetic order alone due to a doubling of the magnetic unit cell (Slater, 1951). While there are numerous examples of Slater and SDW insulators in the realm of one-dimensional conductors (Degiorgi *et al.*, 1996; Vescoli *et al.*, 1999), very few three-dimensional systems fall under this classification. Elemental Cr is a poster child of a three-dimensional SDW system. Elemental Cr does reveal an optical gap below the Néel temperature but remains metallic (Fawcett, 1988), since only a portion of the Fermi surface is impacted by the gap. A rare example of a Slater insulator is $Cd_2Os_2O_7$ pyrochlore (Mandrus *et al.*, 2001; Padilla *et al.*, 2002). Unlike Mott and Kondo systems the insulating gap is reduced with the increase of temperature following the mean field behavior [see the inset of Fig. 17(c)]. The conductivity on the metallic side of the transition does not show a prominent incoherent component and is consistent with the Drude model. A redistribution of the electronic spectral weight primarily impacts the range of several energy gap values. Optical data for $Cd_2Os_2O_7$ along with the band-structure calculations (Singh *et al.*, 2002) yield $K_{\mathrm{exp}}/K_{\mathrm{band}} \simeq 1$ suggesting that correlations are mild in this compound. This latter result is in accord with the notion that proximity to antiferromagnetic order does not appreciably reduce the electronic kinetic energy of a conducting system (Qazilbash, Hamlin *et al.*, 2009).

B. Quasiparticles at the verge of localization

As mentioned in the Introduction, strong correlations arise due to the tendency of electrons to localize. While the hallmark of a metal is the decrease in conductivity with frequency, any sort of localization causes the overall conductivity $\sigma_1(\omega)$ to increase at low frequencies: $d\sigma_1/d\omega > 0$, because photon (or thermal) energy is required to overcome some barrier. This can be a geometrical localization in clusters or grains, Anderson localization in a disordered potential, confinement in a strong magnetic field (quantum Hall effect), or Mott localization by Coulomb repulsion.

In the two-dimensional electron gas of a Si inversion layer Anderson localization is observed as the electron density is lowered. At low temperatures Gold *et al.* (1982) measured a maximum in $\sigma_1(\omega)$ around 10–20 cm^{-1} as a precursor of the metal-insulator transition which is approached when the carrier concentration is reduced toward some critical value. In those strongly disordered systems transport can be largely understood without taking electronic correlations into account (Götze, 1978), although their fingerprints become observable at some point.[19]

The superconducting state of cuprates is known to be very sensitive to Zn impurities (Alloul *et al.*, 2009; and Logvenov *et al.*, 2009) and, further, the influence extends well into the normal state. Underdoped cuprates are, in particular, susceptible to localization since the Fermi energy is located slightly below the band edge. The optical spectra of Zn-doped $YBa_2Cu_4O_8$, for instance, are dominated by a peak around 120 cm^{-1}; hence Basov *et al.* (1998) concluded that the system tends to localize. The Drude peak present in the undoped compound $YBa_2(Cu_{1-y}Zn_y)_4O_8$ shifts to finite energies as y increases. Lupi *et al.* (2009) performed a similar far-infrared study on the MIT transitions in other hole-doped cuprates.

The optical conductivity of $La_{1.92}Sr_{0.08}CuO_4$ changes its behavior around $T^* \approx 250$ K, as shown in Fig. 18. This temperature evolution is not reflected in the dc resistivity

[19] Although most of the theoretical was done in the 1980s (Götze, 1978, 1979; Vollhardt and Wölfle, 1980a, 1980b; Belitz and Götze, 1981; Gold and Götze, 1981; Belitz and Kirkpatrick, 1994; Evers and Mirlin, 2008), experimental evidence was collected only recently. The frequency-dependent hopping conductivity changes its power law, for instance, when electron-electron interaction becomes relevant (Shklovskii and Efros, 1984), as nicely demonstrated in heavily doped silicon (Lee and Stutzmann, 2001; Helgren *et al.*, 2002, 2004; Hering *et al.*, 2007; Ritz and Dressel, 2008a, 2008b).

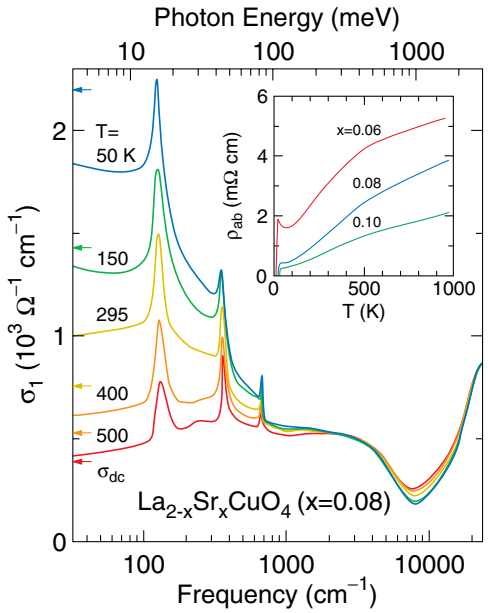

FIG. 18 (color online). In-plane optical conductivity of $La_{1.92}Sr_{0.08}CuO_4$ obtained from reflectivity measurements at different temperatures. The arrows on the left axis represent the dc conductivity. The inset shows the temperature dependence of the dc resistivity $\rho_{ab}(T)$ of $La_{2-x}Sr_xCuO_4$ for different doping levels. From Takenaka *et al.*, 2002.

(cf. the inset). At elevated temperatures, the far-infrared conductivity increases with frequency leading to a broad maximum that moves to lower energies as the temperature drops. The overall spectral weight shifts to lower energies, but only below T^* does a Drude-like peak develop that evidences coherent charge transport. At high temperatures the transport is incoherent (diffusive) with a finite-energy peak below 400 cm^{-1}. Takenaka *et al.* (2002) suggested this to be a consequence of a so-called dynamical localization. Also, in the extended Drude analysis, a clear distinction can be seen around T^* with a low-frequency divergence of $1/\tau(\omega)$ for $T > T^*$. As doping with Sr proceeds, the collective mode in the far infrared grows in intensity and the crossover temperature T^* increases. The intraband contribution becomes larger with x,; causing an overall enhancement of $\sigma_1(\omega)$ for $\omega < 5000$ cm^{-1}.

Phenomena very similar to the cuprates are observed in $SrRuO_3$ for which $\rho(T)$ increases linearly with T beyond the Ioffe-Regel limit without evidence of a crossover or saturation, suggesting bad metallic behavior (Emery and Kivelson, 1995a). The optical conductivity shows a $\sigma_1(\omega) \propto \omega^{-1/2}$ dependence (for a discussion of power laws, see Sec. III.E), yielding a linear increase in the scattering rate with frequency for low temperatures (Kostic *et al.*, 1998). At elevated temperatures the scattering rate of $SrRuO_3$ finally diverges for $\omega \to 0$ corresponding to the finite-energy peak (200 cm^{-1}) in the conductivity observed above ~150 K.

A violation of the so-called Mott or Ioffe-Regel condition means that $\rho(T)$ exceeds the upper limit fixed by the common understanding of a metal for which the mean free path ℓ should be larger than the atomic distance d (Ioffe and Regel, 1960; Mott, 1990). Numerous counterexamples, such as alkali-doped fullerenes A_3C_{60} (Gunnarsson and Han, 2000), weakly doped La_2CuO_4 (Calandra and Gunnarsson, 2002), or some organic conductors, for instance, θ-$(BEDT\text{-}TTF)_2I_3$ (Takenaka *et al.*, 2005; Gunnarsson and Vafayi, 2007), are discussed for different reasons. Gunnarsson *et al.* (2003) argued that in cuprates the resistivity saturates at some higher level due to a strong reduction of the kinetic energy caused by correlation effects, while for A_3C_{60} (and probably in a different way for the organics) coupling to phonons becomes important.

A general scenario can be sketched from the electrodynamics point of view: With increasing Coulomb repulsion the low-frequency conductivity drops before entering the insulating phase, leaving some maximum in $\sigma_1(\omega)$ at finite frequency (Mutou and Kontani, 2006). For two-dimensional conducting systems there is a strong redistribution of spectral weight as the Mott transition is approached with temperature (cf. Secs. IV.A and VII.C.1, for instance). Going from a half-filled to quarter-filled conduction band and further, the effect of intersite Coulomb repulsion V takes the leading role. Charge order develops in certain ways depending on the structural arrangement, the strength of on-site and intersite interaction compared to the bandwidth, but also on the electron-phonon interaction. Although an incomplete gap develops when the system approaches the metal-insulator transition, there always remains a Drude-like contribution to the optical conductivity as long as $V < V_c$ some critical value. In addition, a finite-energy peak is found in $\sigma_1(\omega)$ that is related to charge-order fluctuations which eventually may cause superconductivity (Merino and McKenzie, 2001). Recently collective excitations of the charge order have been observed which are linked to lattice vibrations. Prime examples are cuprates, doped manganites $R_{1-x}Ca_xMnO_3$ (R = Pr or Ca), or organic conductors of α-, β''-, and θ-$(BEDT\text{-}TTF)_2X$ type.[20]

C. Superconductor-insulator transition

Disorder has an influence on the superconducting state (Goldman and Markovic, 1998; Dubi *et al.*, 2007). While Anderson (1959) showed that weak disorder cannot destroy anisotropic s-wave superconductivity, the case is more complex for anisotropic systems; d- and p-wave superconductors are sensitive to disorder.[21] As far as two-dimensional systems

[20]For cuprates, see Tajima *et al.* (1999), and Dumm *et al.* (2002, 2003); for perovskite-type manganites, see Sec. V.C: Takenaka *et al.* (1999), Okimoto and Tokura (2000a), Takenaka *et al.* (2000), Kida and Tonouchi (2002), Nucara *et al.* (2008), Pignon *et al.* (2008), and Rusydi *et al.* (2008); for nickelates, see Lloyd-Hughes *et al.* (2008); organic materials are discussed in Sec. VII.C.2 and by Calandra *et al.* (2002), Dressel *et al.* (2003), Drichko, Dressel, Kuntscher *et al.* (2006), Merino *et al.* (2006), Dressel *et al.* (2010), and Drichko *et al.* (2010).

[21]Extensive investigations on high-T_c cuprates demonstrated that disorder causes localization in the quasi-two-dimensional transport of CuO_2 planes and acts as an efficient pair-breaking process; T_c is suppressed and the superconducting carrier density reduced (Basov, Puchkov *et al.*, 1994; Basov *et al.*, 1998; Tajima *et al.*, 1999; Dumm *et al.*, 2002).

are concerned, numerous experiments[22] have demonstrated a transition from a superconductor to an insulating state with increasing disorder or magnetic field. Strong disorder gives rise to spatial fluctuations of the local complex order parameter $\Psi(\mathbf{r}) = \Delta \exp\{i\phi\}$. Superconducting islands are surrounded by regions with relatively small Ψ and due only to tunneling of Cooper pairs between the islands are correlations sustained. With increasing B the superconducting islands lose their phase coherence, causing a magnetic-field-driven superconductor-insulator transition, although the amplitude of the order parameter vanishes only at higher fields. There seem to be links to superconducting phase fluctuations in underdoped cuprates and organic superconductors (Emery and Kivelson, 1995a; Corson *et al.*, 1999; Xu *et al.*, 2000; Spivak *et al.*, 2008; Müller and Shklovskii, 2009).

R. Crane *et al.* (2007), R. W. Crane *et al.* (2007) investigated superconducting InO_x films with $T_c = 2.28$ K (defined by a well-developed amplitude of the order parameter) and found that below the transition temperature the generalized superfluid stiffness acquires a distinct frequency dependence. Superconducting amplitude fluctuations cause a peak in the microwave dissipation [given by $\sigma_1(\omega, T)$] which shifts to higher temperatures and decreases in amplitude as ω increases from 9 to 106 GHz. The peak occurs when the time scale of the measurement probe matches the time scale of the superconducting fluctuations. The complex response measured for a finite magnetic field evidences that the superfluid stiffness is finite well into the insulating regime. From the frequency-dependent conductivity it can be inferred that short-range correlations exist at finite T, while long-range order does not. This insulating state with superconducting correlations is called a Bose insulator (Fisher *et al.*, 1989, 1990; Steiner *et al.*, 2008).

D. Conductivity scaling for metal-insulator transition

The superconductor-insulator transition is a prime example of a continuous quantum phase transition (Sondhi *et al.*, 1997; Sachdev, 1999) for which quantum fluctuations of diverging size and duration are important. There has been some work on the quantum critical behavior and on the conductivity scaling around metal-insulator transitions. Microwave and terahertz optical experiments on amorphous Nb_xSi alloys (Lee *et al.*, 1998), for instance, revealed a correspondence between the frequency- and temperature-dependent conductivity on both sides of the critical concentration x of the metal-insulator transition thus establishing a quantum critical nature of the transition. H.-L. Lee *et al.* (2000) determined a scaling function and critical exponents that shed light on the relationships between the temporal and spatial fluctuations; the location of the crossover and the dynamical exponent, however, lacks a theoretical explanation.

E. Photoinduced phase transitions

The emerging field of photoinduced phase transitions relies on optical techniques to initiate a cooperative response in a given material resulting in a new macroscopically ordered phase (Nasu, 2004; Kuwata-Gonokami and Koshihara, 2006; Yonemitsu and Nasu, 2008; Buron and Collet, 2005; Koshihara, 2009). The resultant change can be probed using x rays, dc transport, magnetic susceptibility, or a host of other electronic or structural probes. Optical spectroscopy is a powerful tool to monitor induced changes over a broad energy scale with temporal resolution from femtoseconds to days. Ultrafast optical spectroscopy is of particular interest as it provides the means to follow the dynamics of photoinduced phase transitions and, additionally, interrogate a metastable (though macroscopic) phase which may only exist for a few nanoseconds before thermal fluctuations drive the system back toward the true ground state.[23] Materials such as organics and transition-metal oxides with optically accessible on-site or intersite charge excitations (i.e., of a local nature) and competing degrees of freedom are ideal candidates in which to investigate photoinduced phase transitions.

Initial work on photoinduced phase transitions was on the reversible structural interconversion in polydiacetylenes highlighting a nonlinear excitation intensity dependence and the necessity of a photon energy ~0.5 eV above the exciton absorption peak (Koshihara, Tokura, Takeda *et al.*, 1990). Other influential experiments include the photoinduced phase transition on quasi-1D organic tetrathiafulvalene-p-chloranil (TTF-CA), where a photoinduced ionic to neutral transition was observed and has led to considerable theoretical effort (Koshihara, Tokura, Mitani *et al.*, 1990; Koshihara *et al.*, 1999). Figure 19 shows a simple picture capturing the essence of photoinduced phase transitions put forth by Nasu (2004) and Yonemitsu and Nasu (2008). The basic idea is that multistability can be investigated using photons to explore complex energy landscapes with correlated electron materials being of particular interest (Tokura, 2006). To date, the majority of experiments have focused on using pump photons $\gtrsim 1$ eV to "photodope" a material. This is depicted as the vertical arrow labeled (i) in Fig. 19. While numerous excitation pathways are possible, one of particular interest is photodoping holes into a Mott-Hubbard band. This can be accomplished by exciting electrons from the lower Hubbard band into a higher lying non-Hubbard band. At sufficient excitation intensity this could lead to a dynamic collapse of the Mott-Hubbard gap (Cavalleri *et al.*, 2005).

A recent example highlighting the power of ultrafast optical spectroscopy to monitor the evolution of a photoinduced phase transition are the experimental results of the photoinduced melting of the spin-Peierls phase in the organic charge-transfer compound K-tetracyanoquinodimethane (K-TCNQ) (Okamoto *et al.*, 2006). K-TCNQ is a

[22] Investigations have been performed on thin films of Nb_xSi alloys (Aubin *et al.*, 2006), amorphous InO_x (Sambandamurthy *et al.*, 2004, 2005; 2006), disordered TiN (Baturina, Mironov *et al.*, 2007; Baturina, Strunk *et al.*, 2007; Sacépé *et al.*, 2008; Vinokur *et al.*, 2008), or Ta (Qin *et al.*, 2006).

[23] In recent years ultrafast optical techniques have been extended to include time-resolved x-ray diffraction, electron diffraction, and photoemission, with interesting results obtained on various correlated electron materials (Cavalleri *et al.*, 2005; Perfetti *et al.*, 2006; Baum *et al.*, 2007; Gedik *et al.*, 2007).

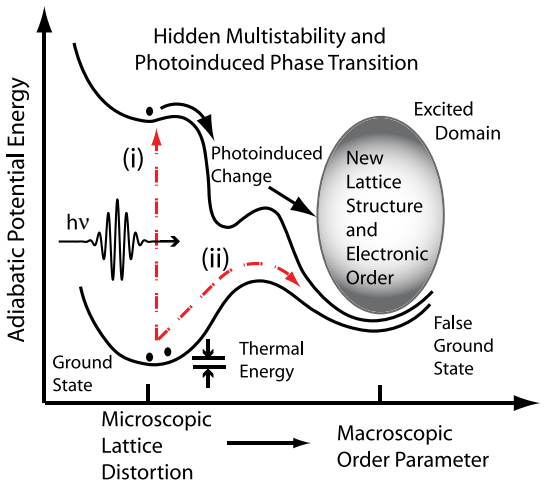

FIG. 19 (color online). Depiction of a photoinduced phase transition showing the potential energy as a function of a generalized structural coordinate. The basic idea is the so-called "domino effect": Photoexcitation initiates a structural change which, in turn, drives an electronic phase transition with an order parameter different from that in the ground state. The energy barrier to obtain the new long-range (though likely metastable) ordered phase is greater than k_bT. The dashed arrows labeled (i) and (ii) depict electronic and vibrational routes toward inducing a phase transition. From Nasu, 2004.

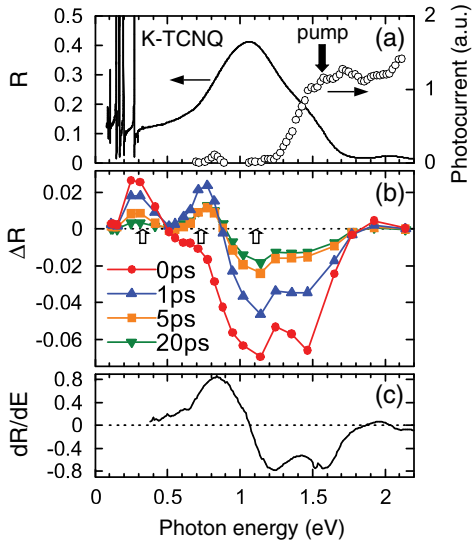

FIG. 20 (color online). (a) Reflectivity and photocurrent measured on K-TCNQ as a function of frequency taken at room temperature which is well below $T_{SP} = 395$ K. The peak at 1 eV corresponds to an excitonic charge-transfer excitation and the onset of a photocurrent response at ~0.5 eV above this is due to the excitation of unbound electron-hole pairs. (b) Spectral dependence of photoinduced absolute reflectivity change ΔR at various time delays following excitation. The lowest-energy peak arises from polaron formation while the change in the charge-transfer peak suggests "melting" of the spin-Peierls phase. (c) The derivative of reflectivity in (a) with respect to photon energy shows a similar spectral response to the time-resolved data which supports the interpretation of the dynamics. From Okamoto *et al.*, 2006.

one-dimensional organic with a half-filled π-electron band. Strong on-site Coulomb repulsion leads to a Mott-insulating state with a transition to a dimerized spin-Peierls (SP) state below $T_{SP} = 395$ K due to a strong spin-lattice interaction.

Photoexcitation creates localized carriers which destabilize the magnetic state resulting in melting of the spin-Peierls phase in <400 fs. Spectroscopic evidence for this is shown in Fig. 20. The peak at ~1 eV (solid line) in Fig. 20(a) is a charge-transfer transition, while the circles are photocurrent measurements of the onset of which is ~0.5 eV above the excitonic charge-transfer transition and corresponds to the creation of unbound electron-hole pairs. The photoinduced (150 fs, 1.55 eV pulses) absolute reflectivity change ΔR as a function of probe photon energy at various time delays is shown in Fig. 20(b). There are two features. A positive ΔR at lower energies is ascribed to small polarons. The ultrafast decrease of ΔR between 0.75 and 1.75 eV is spectrally similar to dR/dE [see Fig. 20(c)] determined using the static spectrum in Fig. 20(a). This differential response is associated with a decrease in dimerization based on analysis of the temperature-dependent redshift of the charge-transfer peak which follows the changes in the x-ray reflection intensity associated with dimerization. Thus, the picture that emerges is that photoexcitation leads to the formation of polarons which break spin-singlet dimers that, in turn, destabilize the spin-Peierls phase. Analysis of the oscillatory time-domain response of $\Delta R/R$ (not shown) indicates that this "melting" of the spin-Peierls phase initiates a coherent excitation of the 20 cm^{-1} mode corresponding to the lattice distortion associated with dimerization.

Further ultrafast studies using shorter pulses (sub-10 fs) comparing the response of the spin-Peierls compound K-TCNQ with a pure Mott analog (BEDT-TTF)(F_2TCNQ) [where BEDT-TTF or ET stands for bis-(ethylenedithio) tetrathiafulvalene] show remarkably different responses at early times (Okamoto *et al.*, 2007; Wall *et al.*, 2009; Uemura *et al.*, 2010), as shown in Fig. 21. These results

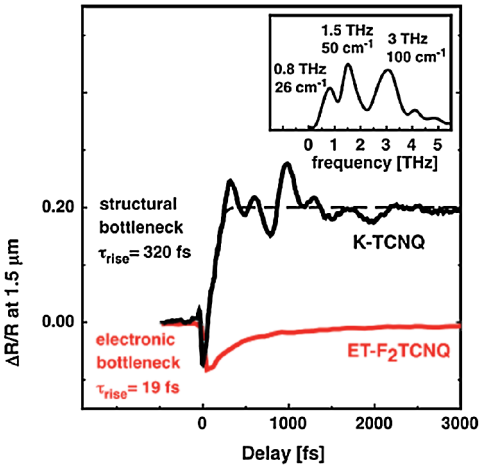

FIG. 21 (color online). Ultrafast dynamics measured on K-TCNQ and (BEDT-TTF)(F_2TCNQ). The spin-Pierels compound K-TCNQ (black line) shows a structural bottleneck in that the rise time is 320 fs while the Mott-Hubbard compound K-TCNQ (gray line), with a rise time of 19 fs, does not exhibit a structural bottleneck. In addition, the oscillations in the K-TCNQ data results from the coherent excitation of vibrational modes as shown in the inset. From Wall *et al.*, 2009.

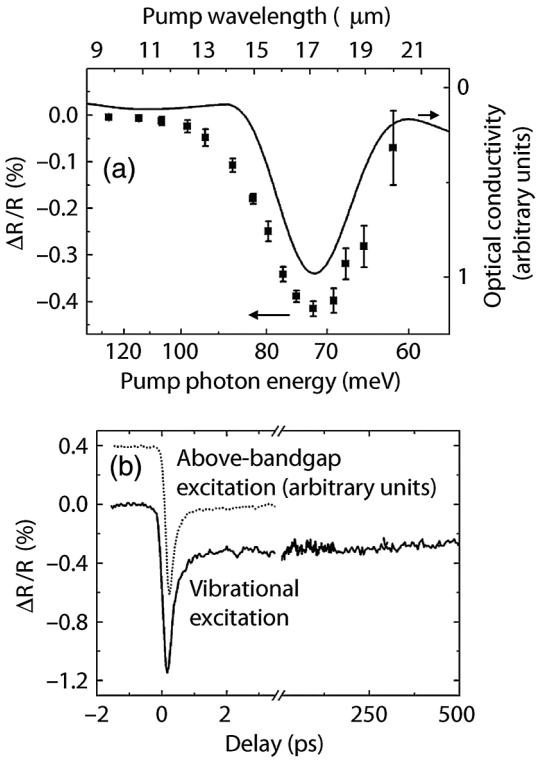

FIG. 22. (a) The induced change in the near-infrared (800 nm) reflectivity of $Pr_{0.7}Ca_{0.3}MnO_3$ as a function of pump photon energy at 30 K. The solid line is the time-integrated reflectivity of the 17 μm mode. The magnitude of the induced change at 800 nm tracks this mode. (b) Vibrational excitation at 17 μm initiates a dynamic response (solid black line) that is similar to electronic excitation (i.e., pumping directly at 800 nm), shown as a dotted line. From Rini *et al.*, 2007.

have been interpreted as a collapse of the Mott-insulating gap in (BEDT-TTF)(F_2TCNQ) occurring on a 20-fs time scale due to photodoping. This is in contrast to a 320-fs structural bottleneck in K-TCNQ corresponding to a quarter period coherent structural relaxation of the dimerization. This shows that ultrafast optical spectroscopy can track the initial steps of a photoinduced phase transition thereby providing a powerful discriminatory capability.

We mention a new area of research which has opened up with the recent demonstration of direct vibrational control over electronic phase transitions (Rini *et al.*, 2007). Referring to the simple schematic in Fig. 19, this would correspond to the arrow labeled (ii) where a phase transition is driven through vibrational excitation in the ground state. A plausible scenario in correlated electron materials is that of vibrationally driven bandwidth modulation. As described in the section on manganites (Sec. V.C), the narrow bandwidth manganite $Pr_{1-x}Ca_xMnO_3$ is insulating for all values of x. For intermediate values ($x \sim 0.3$ to 0.4) a "hidden" (i.e., thermally inaccessible) metallic phase is revealed upon application of a magnetic field (Tokura, 2000). Additionally, it has been shown that optical excitation drives $Pr_{1-x}Ca_xMnO_3$ to a metal-like state as observed in ultrafast reflectivity studies and the observation of stable paths for dc conduction between biased electrodes (Fiebig *et al.*, 1998, 2000). Recent experiments reveal that short pulse photoexcitation of the highest-frequency optical phonon (corresponding to a Mn-O stretching motion) at 17.5 μm leads to an ultrafast reflectivity change as occurs with optical excitation. This is shown in Fig. 22(b). Further, as shown in Fig. 22(a), the magnitude of $\Delta R/R$ follows the line shape of the optical phonon as the pump pulse is tuned across the resonance. In addition to the reflectivity changes in Fig. 22(a), photoexcitation of the phonons leads to an increase in the dc electrical conductivity increases by orders of magnitude (not shown). This demonstrates that vibrational excitation of an insulator-to-metal-like transition is viable. This motivates future efforts to explore vibrationally induced transitions in the electronic ground state of other correlated systems with the goal of clarifying the influence of specific modes and thermally inaccessible (i.e., coherent) structural distortions on the electronic state.

To conclude this section we mention the important topic of ultrafast demagnetization and magnetization control. In ferromagnetic metals, short pulse excitation initiates demagnetization on a sub-ps time scale (Beaurepaire *et al.*, 1996; Bigot *et al.*, 2009; G. P. Zhang *et al.*, 2009). Other experiments on antiferromagnetic orthoferrites and garnets have demonstrated optical control of the magnetization, where circularly polarized femtosecond pulses induce coherent magnon generation through the inverse Faraday effect (Kimel *et al.*, 2005, 2007). We mention these results since photoinduced phase transitions through optical manipulation of the magnetic degrees of freedom in strongly correlated electron materials are also of significant fundamental interest (Talbayev *et al.*, 2005).

F. Electronic phase separation

Electronic and magnetic phase separation is commonplace in correlated electron systems (Dagotto, 2005). It is believed to stem from the prominence of multiple simultaneously active and competing interactions of Coulomb, spin, orbital, and lattice origin. Optical studies of phase separated systems are complex. Under special circumstances, inhomogeneities may acquire a form of unidirectional elements extending over macroscopic dimensions (e.g., spin and charge stripes in high-T_c or organic superconductors). In this rather exceptional situation optical experiments performed on macroscopic specimens can be employed to probe the anisotropy associated with this order (Slater, 1951; Dumm *et al.*, 2003; Lee *et al.*, 2004; Drichko *et al.*, 2010). Provided the length scales associated with distinct electronic phases present in heterogeneous specimens are smaller than the wavelength of light one can introduce effective optical constants ϵ_{eff} for the material (Carr *et al.*, 1985).

Effective medium theories allowed one to evaluate the effective optical constants provided the dielectric functions and filling fractions of constituent phases are known (Bruggeman, 1935). Interpretation of these spectra has to be practiced with extreme caution since usual quantitative approaches suitable for homogeneous samples may easily produce erroneous answers.

Advances in IR and optical microscopy enabled imaging of phases separated in correlated systems (Okimoto *et al.*, 2004; Wu *et al.*, 2006; Nishi *et al.*, 2007; Qazilbash *et al.*, 2007; Qazilbash, Schafgans *et al.*, 2008; Frenzel *et al.*, 2009).

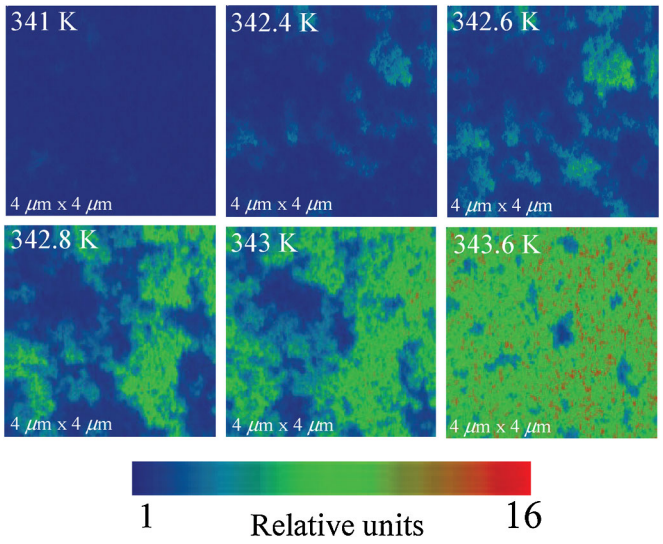

FIG. 23 (color online). Images of the near-field scattering amplitude over the same 4×4 μm^2 area at the infrared frequency $\omega = 930$ cm^{-1}. These images are displayed for representative temperatures in the insulator-to-metal transition regime of VO_2 to show percolation in progress. The metallic regions give higher scattering near-field amplitude compared with the insulating phase. Adapted from Qazilbash *et al.*, 2007.

Nanometer-scale inhomogeneities can be registered using a host of near-field techniques operational in different regions of the electromagnetic spectrum with the spatial resolution reaching 8–10 nm deep in the subdiffractional regime (H.-T. Chen *et al.*, 2004; Keilmann and Hillenbrand, 2004; Lai *et al.*, 2007; Huber *et al.*, 2008). Extended inhomogeneities occurring on the tens of microns length scale can be detected using conventional microscopy. This latter technique was employed to investigate the formation of stripes induced by the electrical current in prototypical organic Mott-Hubbard insulator (K-TCNQ) (Okimoto *et al.*, 2004). This material also exhibits the spin-Peierls-like structural transition associated with the dimerization of TCNQ molecules $T_c < 395$ K. Using a combination of IR and optical microscopies they have been able to register current-induced stripes with length scales over several microns. The striped contrast is produced by a different degree of dimerization.

Infrared microscopy has been applied to explore the metal-insulator transition in the correlated Mott system κ-$(BEDT\text{-}TTF)_2Cu[N(CN)_2]Br$ (Sasaki *et al.*, 2004; Nishi *et al.*, 2007). Microreflectance measurements in a magnetic field have identified coexisting metallic and insulating regions revealing markedly different behavior as a function of the applied field. Modest magnetic fields (5 T) enhanced the areal fraction of the phase attributable to the antiferromagnetic insulator. Further increase of the field up to 10 T has triggered the transition of the insulating antiferrromagnetic regions in the metallic state. In Mott systems, the magnetically induced metal-insulator transition is expected in the regime $U/W \simeq 1$ (Laloux *et al.*, 1994).

The highest spatial resolution of infrared experiments is achieved using near-field instruments based on atomic force microscopes coupled to IR lasers (Keilmann, 2004). This technique enables a contactless probe of local conductivity at the nanoscale (down to 8–10 nm). Near-field measurements uncovered the percolative nature of the IMT in VO_2 (Qazilbash *et al.*, 2007; Zhan *et al.*, 2007; Qazilbash, Schafgans *et al.*, 2008) (see Sec. V.B.1 for background and unresolved issues in this canonical correlated material). Representative scans in Fig. 23 show that the metallic regions nucleate, then grow with increasing temperature, and eventually interconnect. The observed phase separation results from an interplay of intrinsic physics such as the first-order nature of the transition in VO_2 and extrinsic effects including local strain, deviations from stoichiometry, and grain boundaries in these films. This interplay may result in enigmatic memory effects routinely observed in correlated oxides including VO_2 (Driscoll *et al.*, 2009).

G. Insights by numerical methods

Bandwidth controlled IMT phenomena at high temperatures and strong frustration are quite universal. The paramagnetic Mott-insulating phase competes with the correlated metallic phase of strongly renormalized quasiparticles. At a critical pressure and critical temperature, a first-order transition occurs and is accompanied by a hysteresis behavior. The critical exponents are of Ising type, as demonstrated in Cr-doped V_2O_3 (Limelette *et al.*, 2003). This universality enabled one to understand the Mott transition using a simple one-band Hubbard model studied in the limit of infinite dimension, or strong frustration. In this limit, DMFT is exact, and can be used to compute spectroscopic quantities as a function of temperature, pressure, and chemical doping.

The inset of Fig. 24(a) shows the evolution of the electronic states of the one-band Hubbard model within DMFT when the ratio of the Coulomb interaction U and the bandwidth W is varied. The main panel shows the corresponding optical conductivity. Within single-site DMFT, the Mott transition is achieved by a vanishing quasiparticle weight Z_F at critical interaction $U = U_{c2}$, and consequently the diverging effective band mass $m^*/m_b \propto 1/Z_F$. The interactions do not change the Fermi surface of a one-band model within DMFT. Shrinking of the quasiparticles leads to decreased Drude weight, being proportional to $D \propto Z_F \propto (U_{c2} - U)$ (Georges *et al.*, 1996). However, this metallic state is metastable at U_{c2}, and the first-order transition to the insulating state occurs in equilibrium before the U_{c2} point is reached. Thus, the effective mass does not truly diverge at finite temperatures, but it is strongly enhanced at the IMT. The optical conductivity in close proximity to the IMT has two additional peaks, one which is due to excitations from the Hubbard band into the quasiparticle peak [around $\omega \sim 0.25W$ for $U = 1.175W$ in Fig. 24(a)], and a second that is due to excitations from the lower to the upper Hubbard band (around $\omega \sim W \sim U$). Only the latter peak is present in the insulating state [$U/W = 1.2$ curve in Fig. 24(a)] where the quasiparticles cease to exist.

The qualitative features related to the IMT at finite temperature carry over to more general models having other integer orbital occupancies and band degeneracy, as well as including coupling to the lattice. To illustrate that, we show in Fig. 24(b) the realistic LDA+DMFT modeling of the IMT transition in V_2O_3, which was recently studied by Baldassarre

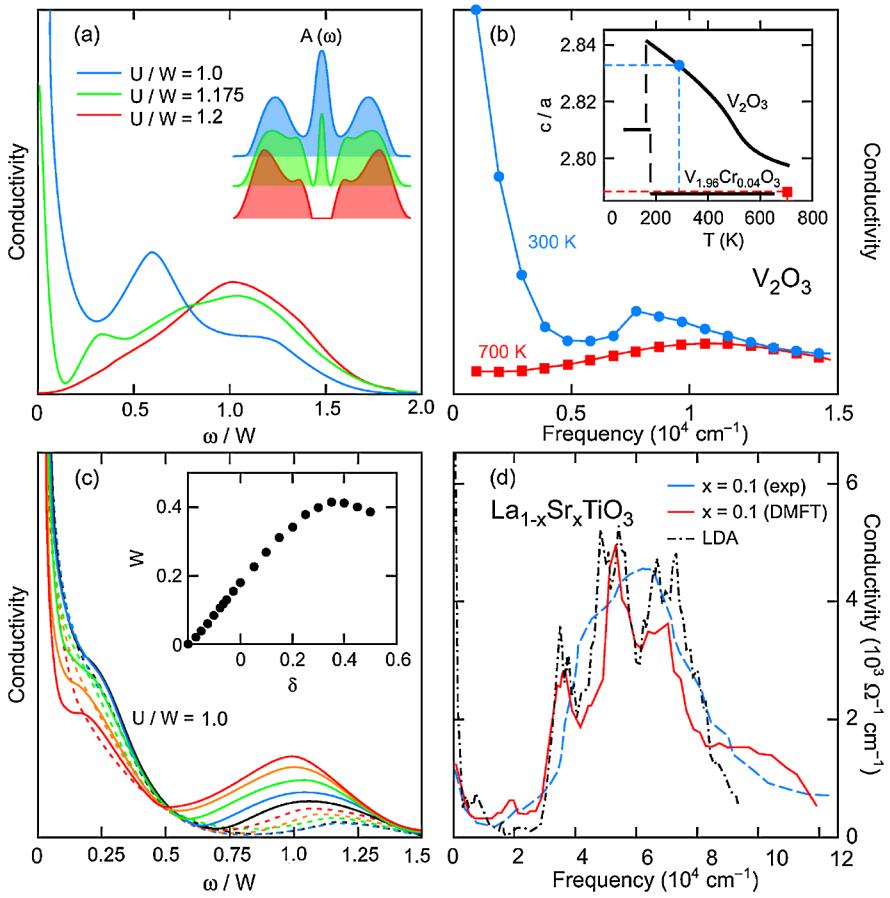

FIG. 24 (color online). (a) The optical conductivity of the bandwidth-controlled IMT of the one-band Hubbard model within DMFT approximation. The inset shows the electron spectral function for the same values of U/W. From Blümer, 2002. (b) The realistic calculation of the optical conductivity across the bandwidth-controlled IMT of V_2O_3. The inset shows the change of the lattice parameters with temperature, which was important to model the transition. From Baldassarre *et al.*, 2008. (c) The optical conductivity of the doping controlled IMT in the one-band Hubbard model within DMFT approximation. The inset shows the doping dependence of the Drude weight. From Jarrell *et al.*, 1995. (d) The realistic calculation of the optical conductivity in the material exhibiting the doping driven Mott transition. From Oudovenko *et al.*, 2004.

et al. (2008) and Rodolakis *et al.* (2010). Similar studies in the context of simplified models were previously carried out by Rozenberg *et al.* (1995a) and by Kajueter and Kotliar (1997). Baldassarre *et al.* (2008) emphasized that for the theory to quantitatively agree with experiment, it was important to include the variation of the lattice structure with temperature. The ratio c/a was taken from experiment (McWhan *et al.*, 1969) and is plotted in the inset of Fig. 24(b).

State-of-the-art calculations were recently carried out for VO_2 by Tomczak and Biermann (2008). The high-temperature rutile phase and the low-temperature monoclinic phase were modeled and favorable agreement with experiments was achieved. Since the low-temperature monoclinic phase shows simultaneous Mott and Peierls correlations, they had to go beyond single-site DMFT and include the tendency for dimerization by a cluster extension of DMFT Kotliar *et al.* (2001).

The optical conductivity in the vicinity of the filling-controlled IMT was first studied by DMFT by Jarrell *et al.* (1995). The results are reproduced in Fig. 24(c). The conductivity in the single-band Hubbard model shows the characteristic three peaks, Drude peak, midinfrared peak, and peak at U. With increasing doping, the midinfrared peak reduces in strength, while the Drude peak increases. The weight in the Drude peak is directly proportional to doping δ, as shown in the inset of Fig. 24(c).

A well-studied example of the 3D doping driven IMT is $La_{1-x}Sr_xTiO_{3+\delta/2}$ (Okimoto *et al.*, 1995). Its properties can be qualitatively explained by DMFT. The resistivity of the doped compound shows a T^2 Fermi-liquid behavior and the specific heat γ, which is proportional to the electron effective mass m^*, is enhanced significantly near the metal-insulator phase-transition boundary (Kumagai *et al.*, 1993). This large mass enhancement suggests a divergence of the effective electron mass due to the strong electronic correlation on approaching the metal-insulator transition.

A realistic LDA+DMFT calculation for $La_{1-x}Sr_xTiO_{3+\delta/2}$ was carried out by Oudovenko *et al.* (2004) with the results reproduced in Fig. 24(d). There are many contributions to the optical conductivity in this material. The Drude spectral weight is of the order of doping $\approx \delta$, just as in the model calculations. The onset of the Mott-Hubbard gap appears around 0.2 eV [see Okimoto *et al.* (1995)], and the peak around 0.5 eV is due to transitions between the two Hubbard bands. The rise in optical conductivity around 4 eV is the

charge-transfer gap between the O-2p filled state and the Ti-3d upper Hubbard band. The appearance of the p-d transitions at the higher energy than the excitations across the Mott-Hubbard gap in $LaTiO_3$ confirms that $LaTiO_3$ is a Mott-Hubbard insulator rather than a charge-transfer insulator in the scheme of Zaanen *et al.* (1985).

Owing to the success of the DMFT, we now have a firm understanding of the appearance of conducting states in very frustrated correlated material, or in systems with large lattice coordination, where DMFT predictions are accurate. The hallmark of the IMT transition in such systems is the vanishing of the quasiparticle weight and consequently a diverging effective mass.

Inclusion of short-range nonlocal correlations, when these are weakly frustrated, considerably modifies the IMT in the small doping regime. The most prominent example is the appearance of pseudogap in the cuprates. In recent years, cluster extensions of the DMFT were developed (Maier *et al.*, 2005; Kotliar *et al.*, 2006), which treat short-range correlations exactly, while long-range correlations are treated on the mean field level. The inclusion of commensurate short-range spin fluctuations does not change the order of the bandwidth-controlled IMT (Park *et al.*, 2008), which remains first order. However, the quasiparticle residue Z_F no longer diverges at the transition. Finite Z_F at the IMT might wrongly suggest nonvanishing Drude weight at the transition. However, short-range spin fluctuations also strongly modify the Fermi surface in the vicinity of the IMT (Civelli *et al.*, 2005), such that the plasma frequency vanishes at the IMT. This is because the active part of the Fermi surface shrinks, while Z_F remains finite on this active part of the Fermi surface. In Fig. 25(a) we show that ω_p^2, within cluster DMFT, is an approximately linear function of doping, just as in single-site DMFT. However, the effective mass $1+\lambda$ is not diverging at the doping controlled transition, in accord with experimental data by Padilla, Lee *et al.* (2005) on the cuprates. The increase in the effective mass from the overdoped to the underdoped regime is of the order of 2, in agreement with measurements by van Heumen, Muhlethaler *et al.* (2009).

In Fig. 25(b) we reproduce optical conductivity for the t-J model computed by cluster DMFT on the plaquette (Haule and Kotliar, 2007). Compared to single-site DMFT, the mid-infrared peak is now at much lower frequency and scales as

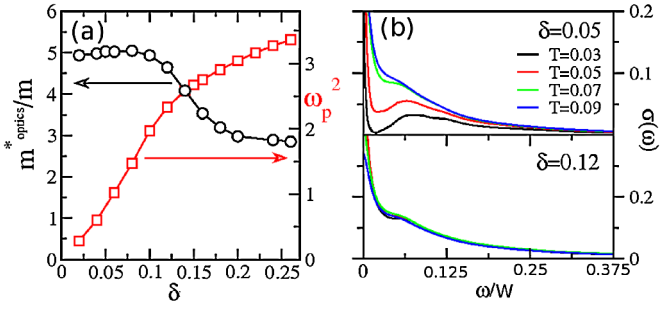

FIG. 25 (color online). (a) The optical mass $1+\lambda = m^*/m_{\rm opt}$ and the plasma frequency as a function of doping for the t-J model within the cluster DMFT approach for a 2D unfrustrated square lattice. (b) The optical conductivity of the same model at two selected doping levels and few temperatures. From Haule and Kotliar, 2007.

$2J$. Hence, it comes from spin fluctuations. This peak is quickly suppressed by doping and is barely visible at $\delta = 0.12$.

From the theoretical perspective, the Mott transition can thus lead to a diverging effective mass at the transition or not, depending on the degree of frustration of the system. In the absence of long-range magnetic order, and in the limit of strong frustration (or large lattice connectivity) the Mott transition does involve divergence of the effective mass. In this limit, the single-site dynamical mean field theory describes the Mott transition correctly, and the quasiparticle renormalization amplitude Z_F is only weakly momentum dependent, and the effective mass is inversely proportional to Z_F.

Note, however, that the transition is first order at finite temperatures; hence, the truly diverging effective mass occurs only if one follows the metastable metallic state to the point where it ceases to exist.

In the opposite limit of very weak frustration, such as in the Hubbard model in two dimensions, the Mott transition is accompanied by a strong differentiation in momentum space and strong momentum dependence of the quasiparticle renormalization amplitude (Parcollet *et al.*, 2004; Civelli *et al.*, 2005). In this limit, the effective mass at the Mott transition remains finite (Park *et al.*, 2008), and only a part of the Fermi surface becomes metallic at IMT (Werner *et al.*, 2009). Moreover, the Fermi surface appears gradually with increasing doping or increasing the bandwidth.

Studies of correlated electron models, such as the Hubbard and the t-J model, have a long history. The most successful method among the numerical methods for computing optical response was exact diagonalization of small clusters using the Lanczos algorithm [for a review, see Dagotto (1994)]. A series of these numerical studies[24] established the fact that the Hubbard model has a charge gap in the Mott state. The Drude weight in the doping controlled IMT increases continuously with doping (Dagotto *et al.*, 1992), roughly linearly with the doping level (Tohyama, 2006). These studies also showed that, for small doping, a large part of the optical spectral weight is incoherent and is located inside the original charge gap.[25] The midinfrared peak appears around $2J$ (Moreo and Dagotto, 1990; Sega and Prelovšek, 1990; Stephan and Horsch, 1990; Chen and Schüttler, 1991), which is ascribed to a propagating hole dressed by spin excitations. Upon increasing doping, the Drude-like part of the spectra grows, and the weight is progressively transferred from the higher-energy region above the charge gap of the insulator to the region inside the gap. The low-frequency optical spectral weight and its doping dependence was studied by a variety of other methods, including the variational quantum

[24]See, for example, Maldague (1977), Loh and Campbell (1988), Inoue and Maekawa (1990), Moreo and Dagotto (1990), Sega and Prelovšek (1990), Stephan and Horsch (1990), Chen and Schüttler (1991), Dagotto *et al.* (1992), Tohyama *et al.* (1999), Zemljic and Prelovšek (2005), and Tohyama (2006).

[25]See, for example, Inoue and Maekawa (1990), Moreo and Dagotto (1990), Sega and Prelovšek (1990), Stephan and Horsch (1990), Chen and Schüttler (1991), and Zemljic and Prelovšek (2005).

Monte Carlo method (Millis and Coppersmith, 1990), slave boson mean field methods (Grilli *et al.*, 1990), and memory function approach (Jackeli and Plakida, 1999).

These numerical methods proved to be useful in unraveling the IMT in a simple one-band model, such as the Hubbard and the *t-J* model. Their generalization to realistic materials, however, is prohibitively expensive. On the other hand, density functional theory (DFT) methods were developed, and it was empirically established that the DFT band structure of simple metals is very close to the experimentally established excitation spectrum. It was also realized that the high-energy excitation spectrum (Jones and Gunnarsson, 1989; Pickett, 1989) as well as the Fermi surface (Andersen *et al.*, 1994; Schabel *et al.*, 1998) of many correlated materials is well described by DFT. This was not expected since DFT is a ground-state theory. Because of this unexpected success, the optical conductivity of the DFT free carriers turned out to be surprisingly similar to optical spectra of simple metals and even transition metals (Maksimov *et al.*, 1988, 1989), owing to careful implementation of velocity matrix elements (Uspenski *et al.*, 1983; Maksimov *et al.*, 1988; Ambrosch-Draxl and Sofob, 2006). Although the Mott-insulating state cannot be described by DFT, nor the anomalous metallic state in the vicinity of the IMT, high-energy interband transitions are usually satisfactorily given by this method (Maksimov *et al.*, 1989; Kircher *et al.*, 1993). The itinerant metallic state away from the IMT in transition-metal compounds is routinely found to be well described by DFT (Maksimov *et al.*, 1989), with the exception of the reduction of the Drude weight. Given the simplicity and speed of DFT methods, as well as their *ab initio* standing, they are invaluable tools for understanding and predicting material properties. Their combination with the perturbative *GW* method (Onida *et al.*, 2002) and dynamical mean field theory (Kotliar *et al.*, 2006) makes them even more attractive for the description of correlated materials.

V. TRANSITION-METAL OXIDES

A. Cuprates

1. Steady-state spectroscopy

The key unresolved issue in the physics of the high-T_c cuprates is the mechanism of superconductivity. Despite an unprecedented research effort it remains unclear if superconducting pairing is mediated by strong coupling to bosonic modes in a fashion not dissimilar to the BCS theory or whether a totally new mechanism is operational in this class of materials (Bonn, 2006). Arguably, the most significant departure from the BCS scheme in high-T_c cuprate superconductors is revealed by optical studies (Basov *et al.*, 1999; Leggett, 2006), which indicate that electronic processes occurring on the energy scale $(10^2–10^3)k_BT_c$ are often involved in the formation of the superconducting condensate.[26] These high-frequency optical effects have been observed in the response of the CuO_2 planes: the key building block of all cuprates as well as in the response along the less conducting interplane direction. An appealing interpretation of these effects is in terms of electronic kinetic energy savings at $T < T_c$ (Hirsch, 1992; Chakravarty *et al.*, 1999) and is at odds with predictions of BCS theory. The low-energy spectral weight is not conserved in the normal state either as discussed in Sec. II.D, where we also analyze some of the caveats of possible interpretations.

The cuprates offer the best studied example of the filling-controlled Mott transition. Superconductivity in this class of materials occurs as undoped antiferromagnetic insulators are being transferred into a fairly conventional Fermi liquid on the overdoped side. Much of the currently accepted phenomenology of high-T_c phases has been established with a strong involvement of optical techniques (Basov and Timusk, 2005). This includes strong dissipation and unconventional power-law behavior of the scattering rate in the normal state, the formation of a partial electronic gap or pseudogap, and strong anisotropy of both normal state and superconducting properties.

In particular, pseudogap state physics has captured unparalleled attention. The pseudogap state is realized in the moderately doped materials with a T_c lower than the maximum T_c for a given series. Transport and spectroscopic probes reveal a pseudogap in the normal state that resembles the superconducting gap in magnitude and symmetry leading to the common view that the origin of the pseudogap may be intimately related to superconducting pairing at $T > T_c$ (Puchkov, Basov, and Timusk, 1996; Timusk and Statt, 1999; P. A. Lee *et al.*, 2006). The pseudogap is not unexpected by continuity with fully gapped insulating counterparts but is in conflict with Landau Fermi-liquid theory. However, studies focusing on strongly underdoped samples uncovered different doping trends between the superconducting gap and the pseudogap (Y. S. Lee *et al.*, 2005; Le Tacon *et al.*, 2006; Tanaka *et al.*, 2006; Hüfner *et al.*, 2008). These latter experiments point to the different microscopic origins of superconductivity and the pseudogap. Yet another alternate point of view asserts that the pseudogap represents a state that competes with superconductivity (P. A. Lee *et al.*, 2006; Kondo *et al.*, 2009). Infrared signatures of the pseudogap include a suppression of the scattering rate at $\omega < 500$ cm^{-1} in the conductivity probed along CuO_2 planes (Orenstein *et al.*, 1990; Rotter *et al.*, 1991; Basov *et al.*, 1996; Puchkov, Basov, and Timusk, 1996; Puchkov *et al.*, 1996) with the simultaneous development of a gaplike structure in the interplane *c*-axis conductivity (Basov, Mook *et al.*, 1995; Tajima *et al.*, 1997; Bernhard *et al.*, 1999; Homes *et al.*, 2003). These trends are common between several different families of hole-doped cuprates. In electron-doped materials a gaplike structure can be identified directly in the conductivity spectra (Onose *et al.*, 2001; Millis *et al.*, 2005; Zimmers *et al.*, 2005; Homes, Lobo *et al.*, 2006). The electronic kinetic energy is most strongly suppressed compared to the K_{band} value in underdoped materials characterized by the pseudogap (see Fig. 1).

Electrodynamics of the superconducting condensate has been explored at zero and finite magnetic fields. Microwave

[26] See, for example, Katz *et al.* (2000), Basov *et al.* (2001), Rübhausen *et al.* (2001), Molegraaf *et al.* (2002), Norman and Pépin (2002), Kuzmenko *et al.* (2003), Boris *et al.* (2004), Homes, Dordevic *et al.* (2004), Santander-Syro *et al.* (2004), and LaForge *et al.* (2008).

studies of the temperature dependence of the superfluid density within the CuO_2 planes have first hinted to the unconventional *d*-wave nature of the order parameter (Hardy *et al.*, 1993) later confirmed through direct phase sensitive measurements (Van Harlingen, 1995). The layered nature of the cuprates implies strong anisotropy of the superfluid density ρ_s. The properties of the interlayer components of ρ_s can be understood in terms of Josephson coupling of the CuO_2 planes (Basov, Timusk *et al.*, 1994; Shibauchi *et al.*, 1994; Dordevic *et al.*, 2002). The formation of the (stripe-like) magnetic order within the CuO_2 frustrates the Josephson coupling leading to two-dimensional superconductivity within the CuO_2 layers in several families of cuprates (Homes, Dordevic *et al.*, 2006; Berg *et al.*, 2007; LaForge *et al.*, 2010; Schafgans *et al.*, 2010; Tranquada *et al.*, 2010), in particular, La_2CuO_4. The in-plane superfluid density reveals universal scaling with T_c: $\rho_{CuO_2} \propto T_c$ (Uemura *et al.*, 1991; Uemura, 2003). This effect is regarded as one of the most evident manifestations of phase fluctuations in a doped Mott insulator (Emery and Kivelson, 1995b). Deviations from the Uemura plot primarily in the overdoped crystals are captured with $\rho_{CuO_2} \propto \sigma_{DC} T_c$ (Homes, Dordevic *et al.*, 2004; Homes, Dordevic, Bonn *et al.*, 2005; Homes, Dordevic, Valla, and Strongin *et al.*, 2005). Physics underlying this latter universal behavior seen in many classes of exotic superconductors (see Fig. 26) may involve strong dissipation in the normal state characteristic of conducting correlated electron systems (Zaanen, 2004). Systematic studies of ρ_s in weakly doped ultrathin films indicate that the disappearance of superconductivity at low dopings may be due to quantum fluctuations near a two-dimensional quantum critical point (Hetel *et al.*, 2007). On the contrary, the behavior of the in-plane superfluid density in weakly doped $YBa_2Cu_3O_{6+y}$ single crystals of high purity is consistent with the notion of a quantum phase transition in the $(3 + 1)$-dimensional *XY* universality class (Broun *et al.*, 2007).

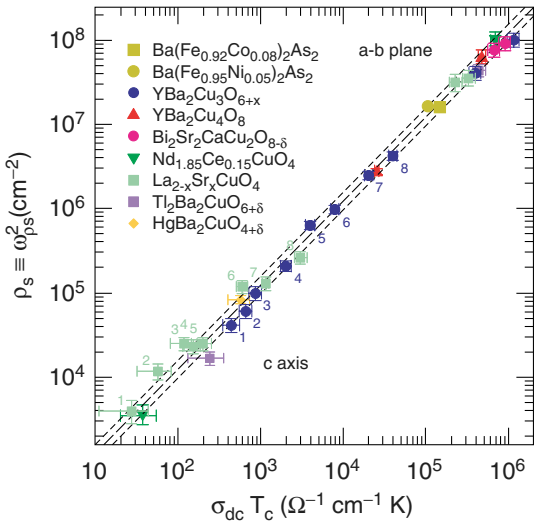

FIG. 26 (color online). The log-log plot of the spectral weight of the superfluid density $\rho_{s,0}$ for a variety of superconductors probed along both the conducting *a*-*b*-plane direction and the interplane *c*-axis direction. From Homes *et al.*, 2004 supplemented by iron-pnictide data from Wu *et al.*, 2010a.

Low values of the superfluid density in underdoped phases in combination with the short coherence length all realized in the environment of the copper-oxygen plane give rise to prominent fluctuations effects both below and above T_c (Kamal *et al.*, 1994; Corson *et al.*, 1999). One remarkable observation pertains to the survival of superconducting fluctuations at temperature above T_c by 10–30 K (Corson *et al.*, 1999) later confirmed through systematic studies of the Nernst effect (Wang *et al.*, 2006). These findings indicate that the energy scale associated with the fluctuation regime is much smaller than the pseudogap scale implying that the two phenomena may be of different origin. Anomalies of the in-plane superfluid density in weakly doped cuprates have been interpreted by Homes (2009) in terms of Josephson phases: a regime of isolated superconducting regions experiencing Josephson coupling.

The electromagnetic response in the presence of the magnetic field is dominated by the dynamics of both pancake and Josephson vortices (Matsuda *et al.*, 1995; Kojima *et al.*, 2002; Dordevic, Komiya *et al.*, 2005; LaForge *et al.*, 2007). Terahertz spectroscopy of the nondiagonal components of the conductivity tensor in the magnetic field (often referred to as Hall angle experiments) (Parks *et al.*, 1997; Grayson *et al.*, 2002; Rigal *et al.*, 2004) concur that the charge dynamics near optimal doping is fairly conventional and governed by a single relaxation rate (contrary to earlier theoretical proposals). Magneto-optics data for moderately underdoped samples of the $YBa_2Cu_3O_7$ (YBCO) family are indicative of density-wave-like reconstruction of the Fermi surface (Rigal *et al.*, 2004). This latter result is of interest in the context of quantum oscillations observed in high purity underdoped samples of YBCO (Doiron-Leyraud *et al.*, 2007; Jaudet *et al.*, 2008; Sebastian *et al.*, 2008; Yelland *et al.*, 2008). Quantum oscillations signal the presence of coherent quasiparticles. Virtually all attempts to explain the oscillating phenomena invoke Fermi surface reconstruction due to some type of density-wave order (Harrison *et al.*, 2007; Millis and Norman, 2007; Chakravarty, 2008). An alternative proposal (LaForge *et al.*, 2010; Tranquada *et al.*, 2010) is aimed at reconciling quantum oscillations data with transport, and infrared and photoemission experiments highlight the role of stripes.

2. Pump-probe spectroscopy

Given the ability to directly measure electron-phonon coupling in metals and the work on nonequilibrium dynamics in BCS superconductors, it is natural that time-resolved spectroscopy would be utilized to investigate quasiparticle recombination in the cuprates with a view toward obtaining insights into the pairing mechanism. Initial studies using all-optical pump-probe spectroscopy on $YBa_2Cu_3O_{7-\delta}$ thin films revealed a response that changed dramatically at T_c showing, for example, a slow (bolometric) induced increase in $\Delta R/R$ above T_c crossing over to a fast induced decrease in $\Delta R/R$ below T_c (Han *et al.*, 1990; Chekalin *et al.*, 1991; Stevens *et al.*, 1997). Below T_c, these data were interpreted in terms of a fast (i.e., 300 fs) avalanche process followed by quasiparticle recombination to Cooper pairs on a picosecond time scale limited by the 2Δ phonon relaxation time similar to BCS superconductors. Importantly, the time scales in the

cuprates are much faster than in BCS superconductors given the larger gap (Kabanov *et al.*, 1999; Carbotte and Schachinger, 2004).

The initial studies on cuprates have been extended since 1999 to include more detailed investigations of the nonequilibrium dynamics using all-optical pump-probe spectroscopy and, additionally, low-energy probes in the mid and far infrared.[27] These results reveal a marked sensitivity to the onset and subsequent evolution of the superconducting state with decreasing temperature. Photoinduced changes at 1.5 eV were performed on $Y_{1-x}Ca_xBa_2Cu_3O_{7-\delta}$ single crystals for $x = 0$ ($T_c = 93$ K) and $x = 0.132$ ($T_c = 75$ K). A two exponent relaxation was observed. The slow component (3 ps) was interpreted (Demsar *et al.*, 1999) as the recombination time where $\tau_{\rm exp} \sim 1/\Delta$ with pair breaking due to phonons with energies greater than 2Δ limiting the recovery time. The fast component (0.5 ps) was associated with a temperature-independent gap (i.e., the pseudogap). These results show that the recovery dynamics of $\Delta R/R$ at probe frequencies well above the gap energy are strongly sensitive to the superconducting gap and to the pseudogap and that the reformation time of the condensate is rapid.

Ultrafast measurements of $YBa_2Cu_3O_{7-\delta}$ thin films in the mid-IR (60–200 meV) which probe in the vicinity of the superconducting gap also revealed (i) a picosecond recovery of the superconducting condensate, (ii) a subpicosecond response related pseudogap correlations, and (iii) a temperature dependence of the amplitude that follows the antiferromagnetic 41 meV peak observed in neutron scattering (Kaindl *et al.*, 2000). These dynamics are similar to the 1.5 eV measurements except for a difference in the temperature dependence of the amplitudes that remains unexplained.

Optical-pump terahertz-probe studies of $YBa_2Cu_3O_{7-\delta}$ revealed that it is possible to simultaneously monitor the dynamics of excess quasiparticles and the condensate recovery which manifests as a strong $1/\omega$ component in the imaginary conductivity. The first far-infrared optical-pump terahertz-probe experiments were performed on near-optimally doped and underdoped samples of $YBa_2Cu_3O_{7-\delta}$ (Averitt, Rodriguez *et al.*, 2001; Averitt *et al.*, 2002). The measurements were made on epitaxial thin films including $YBa_2Cu_3O_{7-\delta}$ with $T_c = 89$ K. Figure 27 shows $\sigma_2(\omega)$ as a function of frequency at various delays following photoexcitation. There is a rapid decrease in the condensate fraction followed by a fast, picosecond recovery. The condensate recovery is nearly complete by 10 ps, in dramatic contrast to conventional superconductors. In the optimally doped films the condensate recovery is ~1.7 ps (in comparison to >100 ps in conventional superconductors) and increases near T_c, consistent with a decrease in the superconducting gap. Above T_c at 95 K, the lifetime has decreased to 2 ps and is likely a measure of electron-phonon equilibration in the normal state. Furthermore, the lifetime is independent of fluence indicative of the absence of bimolecular kinetics. In contrast, for underdoped films ($YBa_2Cu_3O_{6.5}$, $T_c = 50$ K) the lifetime was constant at 3 ps even above T_c, suggestive of a pseudogap.

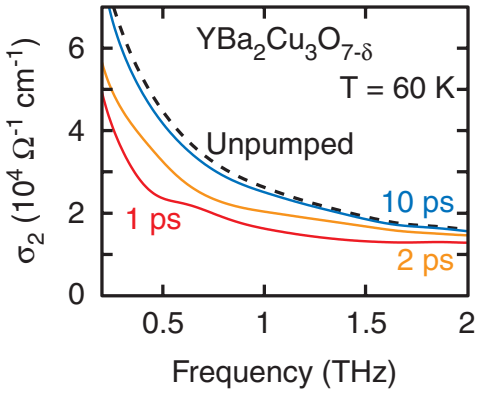

FIG. 27 (color online). Imaginary part of the far-infrared conductivity in a $YBa_2Cu_3O_{7-\delta}$ film as a function of frequency for various times following photoexcitation. An initial reduction in the condensate density yields a reduction in the $1/\omega$ response which recovers in ~2 ps. From Averitt, Rodriguez *et al.*, 2001.

All-optical pump-probe experiments have been performed on high quality YBCO ortho II single crystals, an underdoped cuprate superconductor with a T_c of 60 K (Segre *et al.*, 2002; Gedik *et al.*, 2004). The goal was to determine whether quasiparticle relaxation is described by one- or two-particle kinetics. In one-particle (unimolecular) kinetics, the excitation created by the pump has an intrinsic lifetime and the decay is expected to be exponential. In two-particle (bimolecular) kinetics the photon creates a pair of excitations, for example, an electron and a hole, that inelastically scatter off each other in order to recombine. In this case the decay rate is expected to follow a power law in time and to become faster as the initial excitation density increases. Direct evidence for the importance of bimolecular kinetics in cuprates superconductors was reported by Segre *et al.* (2002) and Gedik *et al.* (2004). Bimolecular recombination was observed, indicative of the recombination of a pair of opposite spin quasiparticles.

Recently, detailed optical-pump terahertz-probe experiments were performed on $Bi_2Sr_2CaCu_2O_{8+\delta}$ (Kaindl *et al.*, 2005) The pump-induced change $\Delta\sigma(\omega)$ of the in-plane terahertz conductivity was measured in 62 nm thick optimally doped $Bi_2Sr_2CaCu_2O_{8+\delta}$ films. As in $YBa_2Cu_3O_{7-\delta}$, the superconducting state exhibits a $1/\omega$ component in the imaginary part of conductivity $\sigma_2(\omega)$. This response, as is well known (see Sec. III.G), provides a direct measure of the condensate density and, therefore, its temporal evolution is a direct measure of the condensate recovery dynamics. In these studies, bimolecular recombination (i.e., a two-particle process) was also observed consistent with the pairwise interaction of quasiparticles as they recombine into Cooper pairs.

There have also been careful all-optical pump-probe studies on $Bi_2Sr_2Ca_{1-y}Dy_yCu_2O_{8+\delta}$ as a function of doping. While an optical-pump terahertz probe has the advantage of directly probing the low-energy dynamics, all-optical pump-probe spectroscopy has advantages in the sensitivity and that small single crystals can be measured with comparable ease. Figure 28 summarizes time-resolved measurements of the

[27]See, for example, Demsar *et al.* (1999), Gay *et al.* (1999), Kaindl *et al.* (2000), Averitt, Rodriguez *et al.* (2001), Demsar *et al.* (2001), Schneider *et al.* (2002), Segre *et al.* (2002), Gedik *et al.* (2003), Gedik *et al.* (2004), Gedik *et al.* (2005), Kaindl *et al.* (2005), Chia *et al.* (2007), and Kaindl and Averitt (2007).

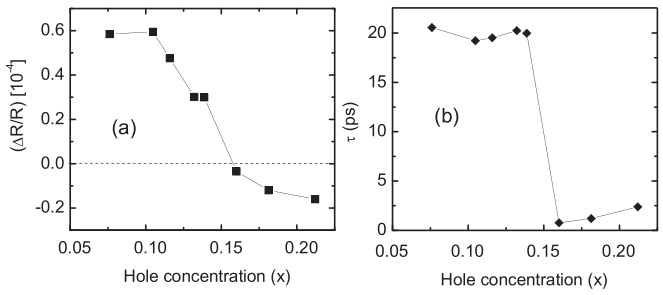

FIG. 28. (a) Peak induced change in $\Delta R/R$ at 1.55 eV and (b) recovery lifetime as a function of hole concentration in $Bi_2Sr_2Ca_{1-y}Dy_yCu_2O_{8+\delta}$ at $T = 5$ K. An abrupt change in the dynamics occurs at optimal doping ($x \sim 0.15$). Note that the values of hole doping x are obtained through a variation of Dy and the oxygen stoichiometry. From Gedik *et al.*, 2005.

photoinduced change in reflectivity $\Delta R/R$ at 1.5 eV in $Bi_2Sr_2Ca_{1-y}Dy_yCu_2O_{8+\delta}$ as a function of hole concentration (Gedik *et al.*, 2005). The quasiparticle decay and the sign of $\Delta R/R$ change abruptly at the maximum of the superconducting transition temperature with respect to doping. This reveals that a sharp transition in the quasiparticle dynamics takes place precisely at optimal doping in $Bi_2Sr_2Ca_{1-y}Dy_yCu_2O_{8+\delta}$. The sign change was interpreted in terms of the change in the real part of the dielectric function arising from spectral-weight transfer from the condensate. This is consistent with time-integrated optical conductivity measurement experiments directly measuring the spectral-weight transfer due to thermal depletion of the condensate as a function of doping (Basov *et al.*, 1999; Molegraaf *et al.*, 2002).

The change in the dynamics indicates different quasiparticle relaxation dynamics for overdoping and underdoping [see Fig. 28(b)]. In the underdoped side, the recombination rate depends linearly on the density, consistent with pairwise bimolecular kinetics. In contrast, for the overdoped side the decay is fast and independent of excitation density. The fact that the amplitude of ΔR depends linearly on excitation density suggests that the photoinduced quasiparticles are antinodal, as the spectral-weight transfer due to nodal quasiparticles would lead to $\Delta R \propto n^{0.33}$ (Carbotte and Schachinger, 2004). Thus, the intensity-dependent dynamics might indicate that the antinodal quasiparticles are metastable on the underdoped side of the phase diagram while readily decaying into other excitations for overdoping. We mention that time-integrated experiments of the interplane response measure the antinodal conductivity (Basov *et al.*, 1999). Thus, time-resolved studies of the c-axis optical conductivity might provide additional insight into the dynamics of antinodal quasiparticles.

From the optical-pump terahertz-probe experiments described above the decrease in superfluid density demonstrates that Cooper pairs are broken following photoexcitation. Nonetheless, it is not known whether the resulting quasiparticle population is nodal, antinodal, or both. A step toward this identification was the direct observation of the diffusion coefficient of the photoinduced quasiparticles in YBCO ortho II (Gedik *et al.*, 2003). The diffusion coefficient at low temperature was determined to be 24 cm^2/s, which is ~200 times less than would be expected from nodal quasiparticle transport measurements on the same crystals. This indicates that antinodal quasiparticles are present in the photoexcited state, possibly together with nodal quasiparticles.

B. Vanadium oxides

1. Steady-state spectroscopy

Vanadium oxides are canonical examples of transition-metal oxides with correlated electrons. Vanadium dioxide shows a transition from the insulating phase to metallic phase as T rises across $T_{IMT} = 340$ K accompanied by a structural phase transition (Morin, 1959; Goodenough, 1971). Vanadium sesquioxide (V_2O_3) undergoes a first-order insulator-metal transition at $T_{IMT} = 150$ K from a low-temperature AF insulating phase to a high-temperature paramagnetic metallic phase. The crystal structure deforms from monoclinic in the insulating phase to rhombohedral symmetry in the metallic phase. Transport and thermodynamic measurements present solid evidence for a bandwidth controlled form of the Mott transition in V_2O_3 (McWhan *et al.*, 1971; Carter *et al.*, 1993). The low-T insulating phase of VO_2 shows no AF ordering but does reveal charge ordering of vanadium pairs along the c axis. The presence of such vanadium chains imparts a quasi-one-dimensional character to what is essentially a three-dimensional system and prompted an interpretation of the IMT in terms of the Peierls physics.

There has been considerable controversy over the relative importance of the Peierls scenario and electronic correlations representing Mott physics.[28] A number of experimental studies indicates that the electronic IMT transition in VO_2 precedes the structural phase transition (Kim *et al.*, 2006; Arcangeletti *et al.*, 2007; B.-J. Kim *et al.*, 2007). These results motivated time-resolved optical and structural studies discussed in Sec. V.B.2. Ternary and quarternary vanadium oxide reveal a number of fascinating phenomena including heavy-fermion behavior in LiV_2O_4 (Kondo *et al.*, 1997), optical anisotropy induced by orbital effects in pseudocubic $La_{1-x}Sr_xVO_3$ (Fujioka *et al.*, 2006), 1D magnetic chains in α'-NaV_2O_5 (Damascelli *et al.*, 2000), and many others.

Early experiments first uncovered dramatic modification of optical properties of both VO_2 and V_2O_3 across the IMT (Barker *et al.*, 1966; Barker and Remeika, 1970). Thomas *et al.* (1994), and Rozenberg *et al.* (1995b, 1996) discovered a redistribution of the electronic spectral weight in V_2O_3 associated with the IMT. As pointed out in Sec. IV.A such a nonlocal redistribution of spectral weight involving the conductivity range extending up to several electron volts is now generally regarded as a salient feature of a correlated electron state. Experiments for thin film samples reaffirm these earlier findings (Choi *et al.*, 1996; Okazaki *et al.*, 2006; Baldassarre *et al.*, 2007; Qazilbash *et al.*, 2007; Perucchi *et al.*, 2009). Ellipsometric data for $\sigma_1(\omega)$ of VO_2 displayed in Fig. 29 visualize the issue of the spectral-weight transfer with utmost

[28]See, for example, Zylbersztejn and Mott (1975), Rice *et al.* (1994), Wentzcovitch *et al.* (1994), H. Kim *et al.* (2004), Biermann *et al.* (2005), Haverkort *et al.* (2005), Kim, *et al.* (2006), Hilton *et al.* (2007), Qazilbash *et al.* (2007), Donev *et al.* (2009), and Perucchi *et al.* (2009).

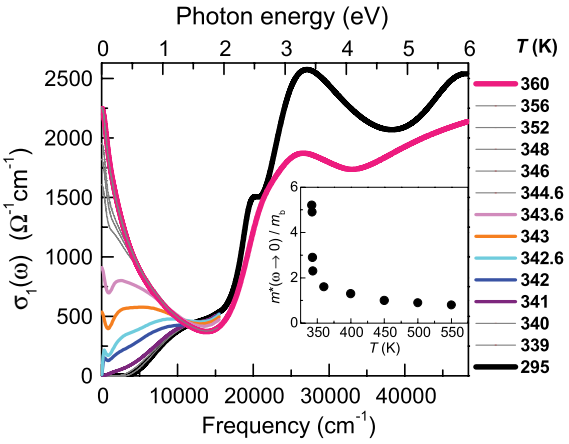

FIG. 29 (color online). The real part of the optical conductivity of VO_2 film extracted from ellipsometric measurements in mid-IR–UV in combination with reflectance in far-IR. The transformation of these spectra across the IMT reveal spectral-weight transfer over the energy scale beyond 6 eV common to other correlated electron systems. Spectra in the transition region (339–352 K) are representative of electronic phase separation of VO_2 in metallic and insulating regions. Applying the effective medium theory to the analysis of these data one can extract the electromagnetic response of metallic puddles. This response is characterized by nearly divergent behavior of the effective mass (inset). From Qazilbash *et al.*, 2007.

clarity. Spectra taken in the transition region reveal the ''filling'' of a 0.6 eV gap with states.

One obstacle toward quantitative analysis of these latter spectra is phase separation (see Fig. 23). The effective medium analysis of a combination of near-field and broadband ellipsometric data (Qazilbash *et al.*, 2009a) revealed strong enhancement of the quasiparticle effective mass in newborn metallic nanoclusters. This result supports the notion of the dominant role of electron-electron interaction (Brinkman and Rice, 1970) in the IMT physics of VO_2 similarly to its V_2O_3 counterpart (Baldassarre *et al.*, 2007). The electronic kinetic energy of the metallic phases is reduced compared to band-structure results in both VO_2 and V_2O_3 attesting to correlated character of the metallic regime (see Fig. 1).

Optical studies of yet another vanadium oxide V_3O_5 (Baldassarre *et al.*, 2007) are in stark contrast with the observations for both VO_2 and V_2O_3 (Perucchi *et al.*, 2009). Specifically, the spectral-weight redistribution in V_3O_5 across $T_{IMT} = 420$ K is confined the region within 1 eV. The forms of the optical spectra and their evolution with temperature and pressure are indicative of prominent polaronic effects. Thus, data for V_3O_5 show that lattice effects and structural phase transitions can lead only to a fairly conventional picture of electrodynamics across the insulator-to-metal transition. This may imply that the role of lattice effects in other vanadium oxides is also fairly mundane, whereas exotic effects of metallic transport of VO_2 and V_2O_3 likely originate from the proximity to Mott insulating state.

The insulator-to-metal transition in both VO_2 and V_2O_3 can be tuned not only by temperature but also by doping, the electric field (Qazilbash, Li *et al.*, 2008), pressure (Marezio *et al.*, 1972; Carter *et al.*, 1993), and photoexcitation (see Sec. V.B.2). While all these stimuli promote metallicity, it is not evident that either the nature of the transition or the end metal phase are identical in all these cases. At least in V_2O_3 x-ray absorption data revealed that the metallic phase reached under pressure is different from the one obtained by changing doping or temperature (Rodolakis *et al.*, 2010). Since electronic phase separation is clearly playing a prominent role in the insulator-transition physics (see Fig. 23), more detailed insights can be expected from the exploration of transport, spectroscopic, and structural aspects of the transition using experimental probes with adequate spatial resolution at the nanoscale.

2. Pump-probe spectroscopy

The insulator-to-metal transition in VO_2 has been extensively investigated using ultrafast optical spectroscopy with experiments spanning from the far infrared through the visible including, in addition, time-resolved x-ray and electron diffraction studies.[29] For VO_2, a primary motivation of these photoinduced phase-transition experiments (see Sec. IV.E) is to determine the relative influence upon the IMT transition of structural distortions (associated with the vanadium dimerization) and correlation effects using the temporal discrimination ultrafast optical spectroscopy provides. The existing body of work reveals a prompt nonthermal photoinduced transition which occurs on a subpicosecond time scale and a slower thermally induced phase transition which is sensitive to a softening of the insulating phase. A fluence threshold to drive the phase transition is observed and is a well-known feature of photoinduced phase transitions (Koshihara, *et al.*, 1999; Nasu, 2004), where the cooperative nature of the dynamics results in a nonlinear conversion efficiency as a function of the number of absorbed photons.

The approach of these experiments is that, starting from the insulating phase, excitation with the above band-gap photons leads to a reduction from half filling in the lower Hubbard band (photodoping) which initiates a collapse of the Hubbard gap on a subpicosecond time scale. For example, an all-optical pump-probe study of the dynamics revealed that for pulses shorter than 70 fs the transition time is constant (Cavalleri *et al.*, 2004). This indicates a structural bottleneck in obtaining the metallic phase in contrast to what would be expected for a purely electronic phase transition, suggesting that lattice effects must be considered in any complete scenario of the photoinduced IMT transition in VO_2 and other systems. This is consistent with time-resolved x-ray diffraction experiments, where the photoinduced change in diffraction of the rutile phase shows an initial subpicosecond increase and a longer ~15 ps increase related to the nucleation and growth of the metallic phase (Cavalleri *et al.*, 2001). This is also consistent with the discussion at the end of Sec. V.B.1 discussing multiple pathways in driving a IMT (Rodolakis *et al.*, 2010). Along these lines, the physics of a photoinduced IMT may be considerably different than IMTs

[29]See, for example, Cavalleri *et al.* (2001), Cavalleri *et al.* (2004), Cavalleri *et al.* (2005), Baum *et al.* (2007), Hilton *et al.* (2007), Kübler *et al.* (2007), Nakajima *et al.* (2008), and Rini *et al.* (2008).

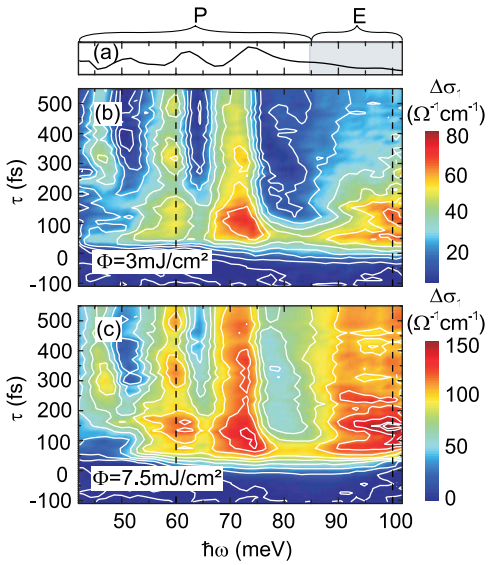

FIG. 30 (color online). Optical-pump terahertz probe on VO_2 at $T = 250$ K. (a) In the 40–85 meV range, the temporal evolution of the optical phonons probes the lattice degree of freedom, while changes above 85 meV are representative of the electronic response. (b), (c) Two-dimensional evolution of the optical conductivity as a function of time and frequency. In (b) the excitation fluence is below the threshold to drive the transition while (c) shows the above threshold dynamics which reveal a prompt increase in the conductivity above 85 meV. From Kübler *et al.*, 2007.

driven by temperature, electric or magnetic fields, or applied currents and is a topic of considerable interest.

Figure 30 shows results using electric-field resolved mid-IR spectroscopy which have been used to probe the nonthermal photoinduced phase transition (Kübler *et al.*, 2007). The two-dimensional scans highlight the power of this technique showing the temporal evolution of the optical conductivity. Figure 30(b) is the response at 3 mJ/cm^2 which (at 300 K) is below the fluence threshold to drive VO_2 to the metallic state, while Fig. 30(c) reveals the response at an excitation fluence of 7.5 mJ/cm^2. There is a clear increase in conductivity above 85 meV that is established within 100 fs. A simple model was proposed whereby photoexcitation from bonding to antibonding orbitals initiates coherent wave packet motion that, above threshold, overcomes correlations which stabilize the insulating state. This is similar to the case of K-TCNQ discussed in Sec. IV.E.[30]

Finally, we mention investigations of the photoinduced metal-insulator transition using far-infrared pulses (Hilton *et al.*, 2007). In these experiments, a threshold fluence was also observed with additional evidence of a softening of the photoinduced transition with increasing temperature in the insulating state. Interestingly, even at the highest excitation fluence, the evolution toward metallicity required tens of picoseconds. This is in contrast with other studies and also in contrast with ultrafast electron-phonon thermalization which typically occurs on a picosecond time scale. To interpret these results, a model was developed based on Bruggeman's effective medium theory, where photoexcitation rapidly drives the temperature above T_c followed by dynamic growth and percolation of metallic domains. An important aspect to consider in photoinduced phase transitions is that photodoping and thermal effects must be considered simultaneously. For VO_2, there are interesting aspects which require further effort such as the potential role of midgap states on the dynamics and the exact nature of the prompt metallic state. For example, is it truly indicative of the metallic phase in thermal equilibrium or is it more closely related to the enhanced effective-mass state observed in mid-IR microscopy experiments (Qazilbash *et al.*, 2007)?

C. Manganites

A strong resurgence in manganite research occurred upon the observation of negative magnetoresistance in lanthanum-based manganite thin films. This "colossal" negative magnetoresistance (CMR) was observed near the Curie temperature T_C coinciding with the transition from paramagnetic semiconductor to ferromagnetic metal (Jin *et al.*, 1994).[31] Recently, work has emphasized the diversity of phenomena in the manganites including charge and orbital ordering, electronic phase separation and quenched disorder, and investigations of other families of manganites and related materials. This includes the two-dimensional Ruddlesden-Poper phases and, to a lesser extent, pyrochlores such as $Tl_2Mn_2O_7$ which also exhibit CMR (Shimakawa *et al.*, 1996; Ramirez, 1997). Numerous reviews are available describing the properties and physics of manganites (Ramirez, 1997; Tokura, 2000; Salamon and Jaime, 2001; Dagotto, 2003).

The parent compounds of manganites (as with the cuprates) are antiferromagnetic Mott insulators. The canonical example is $LaMnO_3$ with octahedrally coordinated Mn^{3+} and a coherent Jahn-Teller effect (i.e., orbital ordering) due to the occupation of a single electron in the doubly degenerate e_g^1 level. There is also a lower lying t_{2g}^3 level to which the e_g levels are slaved to through on-site ferromagnetic exchange coupling. Divalent substitution leads to hole doping in the e_g derived band with transport described by double exchange between adjacent Mn ions hybridized with O_{2p} orbitals strongly influenced by Jahn-Teller distortions (Millis *et al.*, 1995, 1996). In addition, the bandwidth of manganites can be sensitively controlled. The Mn-O-Mn bond angle depends on the ionic sizes of the rare earth and the dopants. As a function of decreasing ion radius the Mn-O-Mn bond angle decreases with a gradual structural change from cubic to rhomboheral to, eventually, orthorhombic.

The observed properties of manganites show a strong correlation to this bond angle (Hwang *et al.*, 1995). For example, $La_{0.7}Sr_{0.3}MnO_3$ is classified as an intermediate bandwidth material exhibiting a transition ($T_c \approx 260$ K) from ferromagnetic metal to paramagnetic semiconductor.

[30]In this experiment on VO_2, the full conductivity of the metallic state is not obtained and the role of intragap dynamics cannot be strictly ruled out.

[31]It was during the 1950s that mixed valence manganites ($Re_{1-x}D_xMnO_3$, where Re is a rare-earth such as La or Nd and D is a divalent alkali such as Sr or Ca) were first synthesized and extensively studied (Jonker and van Santen, 1950).

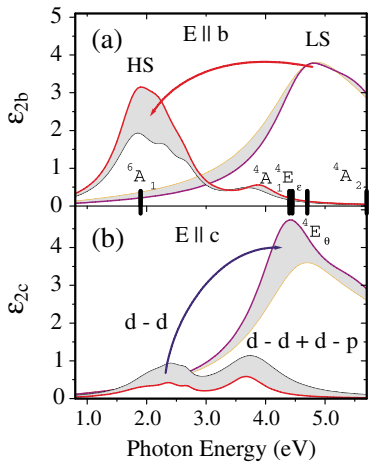

FIG. 31 (color online). Summary of the optical response of $LaMnO_3$ upon crossing from the orbitally ordered state to the antiferromagnetic state. (a) The imaginary part of the dielectric function ϵ_{2b} along the b axis. As the temperature decreases below T_N, there is a transfer of spectral weight from the low-spin (LS) to high-spin (HS) configuration which is consistent with what is expected for d-d intersite transition. (b) The imaginary part of the dielectric function ϵ_{2c} along the c axis. From Kovaleva *et al.*, 2004.

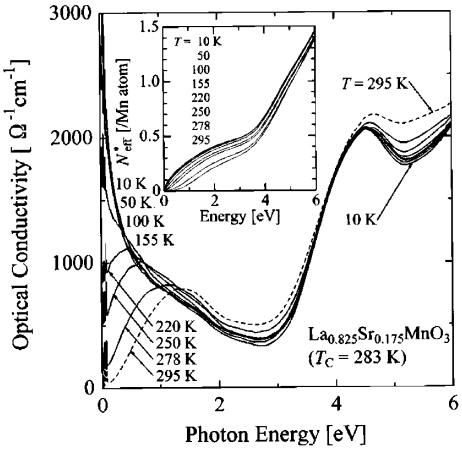

FIG. 32. σ_1 as a function of photon energy for various temperatures measured on a cleaved single crystal of $La_{0.825}Sr_{0.175}MnO_3$. The polaron peak at ~1 eV gradually redshifts with decreasing temperature to a Drude peak. The inset shows the integrated spectral weight as a function of energy for various temperatures. From Takenaka *et al.*, 1999.

In contrast, the narrow bandwidth manganite $Pr_{0.6}Ca_{0.4}MnO_3$ does not exhibit metallic behavior instead entering a charge-ordered phase with decreasing temperature though, as described below, it is very sensitive to external perturbations. These properties manifest in dramatic fashion in optical spectroscopy with significant redistribution of spectral weight from the far infrared through the visible. Considerable insight into the electronic properties of manganites has been obtained from optical conductivity measurements.[32]

For example, $LaMnO_3$ is orbitally ordered below 780 K with an onset of antiferromagnetic ordering at $T_N = 140$ K, where spins ferromagnetically align in the a-b plane with antiferromagnetic ordering along the c axis. Optical conductivity measurements to elucidate the character of the lowest lying transition (~ 2 eV) in $LaMnO_3$ must distinguish between on-site d-d transitions [allowed through hybridization with O($2p$) orbitals], charge transfer [O($2p$)-Mn($3d$)], or $d_i \rightarrow d_j$ intersite transitions. Early studies on detwinned single crystals revealed a strong anisotropy in the optical conductivity arising from orbital ordering (Tobe *et al.*, 2001). A lack of spectral-weight transfer in the vicinity of T_N was taken as an indication of the charge-transfer character of the transition as this would be insensitive to spin ordering.

A recent experiment, however, exhibited dramatic spectral-weight transfer upon antiferromagnetic ordering (Kovaleva *et al.*, 2004). The results are summarized in Fig. 31 which plots the imaginary part of the dielectric response as a function of energy above and below T_N. Figure 31(a) is presented with the electric field polarized along the b axis ($E \parallel b$), while Fig. 31(b) is for the electric field parallel to c ($E \parallel c$). The strong anisotropy arises from orbital ordering, as mentioned. For $E \parallel b$ spectral weight shifts from higher energies to lower energies with decreasing temperature while the converse is true for $E \parallel c$. Focusing on Fig. 31(a), the spectral-weight transfer is from a low-spin (LS) state to a high-spin (HS) state. The HS state should, in fact, be favored in comparison to the LS state because of ferromagnetic spin alignment in the a-b plane below T_N.[33] That is, the increase in spectral weight at 2.0 eV is consistent with an intersite transition from a singly occupied e_g orbital to an unoccupied e_g orbital on an adjacent site. The peak at 3.8 eV is assigned to a $t_{2g} - e_g$ high-spin transition while the 4.7 eV peak is likely a charge-transfer transition. These results are consistent with $LaMnO_3$ as a Mott-Hubbard insulator and are a representative example of how optical spectroscopy can discern the character of multiorbital transitions as influenced by spin correlations.

Hole doping of $LaMnO_3$ creates mobile carriers which (for appropriate doping in intermediate bandwidth manganites) leads to incoherent hopping of Jahn-Teller polarons in the paramagnetic phase crossing over to coherent transport in the low-temperature ferromagnetic metallic state. This manifests in the optical conductivity as shown in Fig. 32 for $La_{0.825}Sr_{0.175}MnO_3$ ($T_c = 283$ K). The optical conductivity shows a redshift of an incoherent peak at ~1 eV at 293 K to lower energies with the clear onset of a Drude response below 155 K (Takenaka *et al.*, 1999). These data were obtained from reflection measurements on a cleaved single crystal yielding a considerably larger Drude spectral weight extending to higher energies than previously obtained on polished samples (Okimoto and Tokura, 2000b). Figure 32 shows that even on a pristine cleaved crystal the incoherent response persists well into the ferromagnetic phase suggestive of

[32]See, for example, Okimoto *et al.* (1997), Kim *et al.* (1998), Quijada *et al.* (1998), Simpson *et al.* (1999), J. Jung *et al.* (2000), Okimoto and Tokura (2000b), Cooper (2001), H. Lee *et al.* (2002), M. Kim *et al.* (2007), and Rusydi *et al.* (2008).

[33]See Kovaleva *et al.* (2004), and references therein, and also M. W. Kim *et al.* (2004) for a similar analysis.

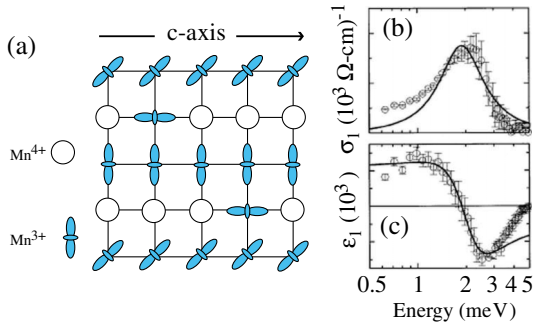

FIG. 33 (color online). (a) Depiction of charge and orbitally ordered state. (b) $\sigma_1(\omega)$ and (c) $\epsilon_1(\omega)$ measured on $Pr_{0.7}C_{0.3}MnO_3$ thin film at 4 K. From Kida and Tonouchi, 2002.

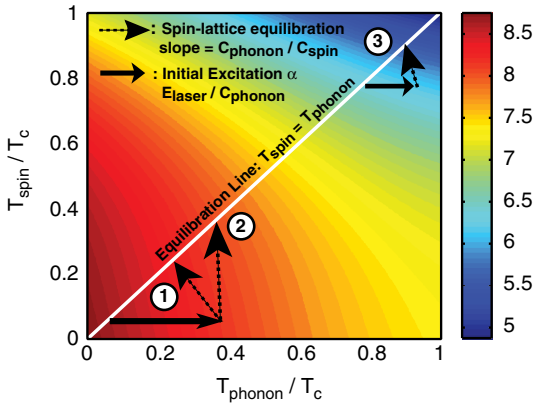

FIG. 34 (color online). Plot of the natural logarithm of the conductivity in the phonon-spin temperature plane [the color bar denotes the magnitude of $\ln(\sigma)$]. The white diagonal line denotes the equilibrium line ($T_{\text{spin}} = T_{\text{phonon}}$) of conventional time-integrated measurements. Photoexcitation provides access to the lower half of the plane. The dynamics can be dominated by changes in the phonon temperature as is the case for arrow 1 or dominated by changes in the spin temperature as indicated by arrow 3. From Averitt, Lobad *et al.*, 2001.

residual polaronic effects which may be strongly influenced by the orbital degrees of freedom.

Contrasting with this are narrower bandwidth manganites that are not metallic at any temperature. For example, with decreasing temperature, $Pr_{0.6}Ca_{0.4}MnO_3$ transitions from a paramagnetic semiconductor to a charge-ordered insulator ($T_{co} = 235$ K). However, an applied magnetic field "melts" the charge order with a Drude-like peak emerging in $\sigma_1(\omega)$ between 6 and 7 T (Okimoto and Tokura, 2000b). This highlights the sensitivity of the optical and electronic properties of manganites resulting from nearly degenerate ground states with differing order parameters.

In the charge-ordered manganites a subgap collective mode excitation of the charge-density condensate has been reported by Kida and Tonouchi (2002). Specifically, a pinned phason mode occurs at terahertz frequencies. Figure 33 shows the first observation of a collective mode of the charge-ordered state measured on epitaxial $Pr_{0.7}Ca_{0.3}MnO_3$ thin films. The observed response persisted above the charge ordering temperature which could arise from mixed phase behavior, though other effects could not be ruled out. Recently, optical conductivity measurements on commensurate charge-ordered manganites including single crystal $Nd_{0.5}Ca_{0.5}MnO_3$ and polycrystalline pellets of $La_{1-n/8}Sr_{n/8}MnO_3$ ($n = 5, 6, 7$) have also shown a pinned phason response that, however, did not persist above the charge ordering transition (Nucara *et al.*, 2008). An alternative explanation assigns the mode to former acoustic phonons folded back optically activated due to charge ordering (Zhang *et al.*, 2010; Zhukova *et al.*, 2010). Future studies of collective mode excitations in the manganites as a function of applied magnetic field or in the vicinity of a phase transition could provide further insights into the nature of charge localization and fluctuations as has been the case for two-dimensional metal organics (see Sec. VII.C).

Ishikawa *et al.* (2000) performed optical conductivity measurements on the layered manganites $La_{2-2x}Sr_{1+2x}Mn_2O_7$. Similar to the cuprates, the charge transport is highly anisotropic with metallic conductivity in plane and activated conduction along the c axis. The results of optical conductivity measurements coupled with ARPES and scanning tunneling microscopy suggest a picture of a metal with a highly anisotropic band structure and very strong electron-phonon coupling (Mannella *et al.*, 2005; Ronnow *et al.*, 2006; Sun *et al.*, 2006, 2007).

There have also been interesting time-resolved studies on the manganites and related materials with a focus on probing the quasiparticle dynamics within a given phase.[34] Photoexcitation with a probe pulse results in a dynamic redistribution of spectral weight whose subsequent temporal evolution is monitored with a probe pulse. The time scales over which this occurs provide information about which degrees of freedom are involved in the dynamic spectral-weight transfer (Lobad *et al.*, 2000, 2001). In the perovskite manganites, optical-pump terahertz-probe measurements in the ferromagnetic metallic phase revealed a two-exponential decrease in the optical conductivity (Averitt, Lobad *et al.*, 2001). A short ~1 ps response is associated with electron-phonon equilibration, while the longer (> 10 ps) relaxation is due to spin-lattice thermalization.

It is possible to use time-resolved data to extrapolate the conductivity in the T_S-T_L plane where T_S and T_L are the spin and lattice temperatures, respectively. Results are shown in Fig. 34 as contours of constant $\ln(\sigma_1)$ in the T_S-T_L plane (Averitt, Lobad *et al.*, 2001). Conventional measurement techniques do not deviate from equilibrium as indicated by the white diagonal line. However, optical-pump terahertz-probe experiments, while starting from a point on the equilibrium line, allow for access to the portion of the T_S-T_L plane below the diagonal equilibrium line since the excited electrons couple preferentially to the phonons during the initial 2 ps. Depending on the initial temperature the observed conductivity decrease can depend predominantly on T_L and/or T_S. The ultrafast conductivity dynamics in

[34]See, for example, Lobad *et al.* (2000), Kise *et al.* (2000), Averitt, Lobad *et al.* (2001), Lobad *et al.* (2001), Ogasawara *et al.* (2001), Ogasawara *et al.* (2003), Tomimoto *et al.* (2003), McGill *et al.* (2004), Prasankumar *et al.* (2005), Talbayev *et al.* (2005), Matsubara *et al.* (2007), Polli *et al.* (2007), Prasankumar *et al.* (2007), Y. H. Ren *et al.* (2008), and Mazurenko *et al.* (2008).

$La_{2/3}Ca_{1/3}MnO_3$ (LCMO) and $La_{2/3}Sr_{1/3}MnO_3$ thin films show that $\partial\sigma/\partial T$ is determined primarily by phonons at low temperatures and by spin fluctuations at higher temperatures. Other manganites including charge-order materials have been investigated using similar techniques. These studies are distinct from those described in Sec. IV.E on photo-induced phase transitions in that the goal is to probe the quasiparticles within a given phase as opposed to dynamically initiating a phase change with photoexcitation.

D. Ruthenates

Although Sr_2RuO_4 (a member of the Ruddlesden-Popper series) possesses a crystal structure very similar to cuprates, the electronic properties are distinctively different (Lichtenberg, 2002; Mackenzie and Maeno, 2003). The resistivity is strongly anisotropic by about 3 orders of magnitude, but both in-plane ρ_{ab} and out-of-plane ρ_c exhibit a T^2 dependence at low temperatures consistent with the Fermi-liquid theory of metals (Hussey *et al.*, 1998). This implies coherent conduction in all three directions with an anisotropic effective mass, found in various low-dimensional compounds (Dordevic, Basov, Dynes, and Bucher, 2001; Ruzicka *et al.*, 2001; Dordevic *et al.*, 2002), similar to the example of $(TMTSF)_2PF_6$ discussed in Sec. VII.A. This behavior is opposite to that of the cuprates where Fermi-liquid-like in-plane properties are accompanied with incoherent c-axis transport.

Optical investigations by Katsufuji *et al.* (1996) support this idea: As shown in Fig. 35, for the in-plane polarization there is a sharp increase in reflectivity below 15 000 cm^{-1} and it increases even more for low temperatures owing to a strong Drude contribution. In the perpendicular direction ($E \parallel c$), $\sigma_1(\omega)$ remains basically constant below 4000 cm^{-1}, except for some phonons. A closer inspection of the low-frequencies properties shown in Fig. 36, however, reveals that a narrow Drude-like contribution develops below 130 K (Katsufuji *et al.*, 1996; Hildebrand *et al.*, 2001; Pucher *et al.*, 2003). The c-axis spectral weight and charge carrier density responsible for the coherent transport are only weakly temperature dependent, much lower than expected from band-structure calculations (Singh, 1995). Slight doping by Ti destroys the coherent transport (Minakata and Maeno, 2001; Pucher *et al.*, 2003).

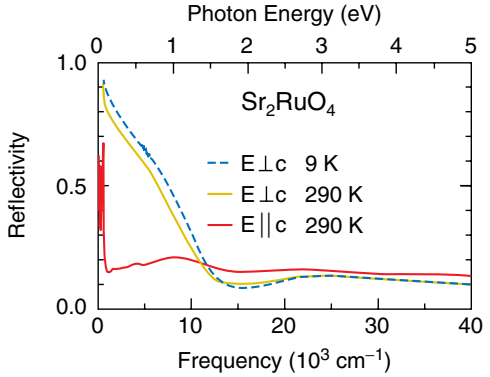

FIG. 35 (color online). Reflectivity of Sr_2RuO_4 for $E \parallel c$ and $E \perp c$ at different temperatures as indicated. From Katsufuji *et al.*, 1996.

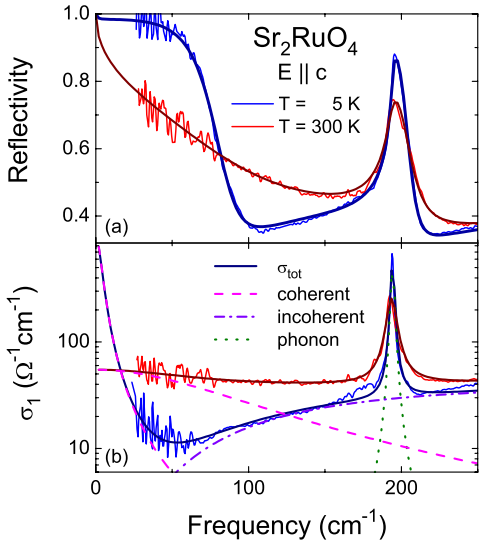

FIG. 36 (color online). The far-infrared properties of Sr_2RuO_4 show the development of a plasma edge around 70 cm^{-1} for $E \parallel c$ related to a Drude contribution of the low-temperature conductivity (Pucher *et al.*, 2003). The total conductivity $\sigma_{tot}(\omega)$ can be separated into a coherent (dashed line) and incoherent (dash-dotted line) contribution.

From the extended Drude analysis a large mass enhancement of $m^*/m_c \approx 30$ is found below 200 cm^{-1} leading to $m_c/m_{ab} \approx 100$. The scattering rate $1/\tau_c(\omega)$ exhibits a maximum around 100 cm^{-1} and is strongly suppressed below (Katsufuji *et al.*, 1996; Hildebrand *et al.*, 2001).

The low transition temperature of up to 1.4 K makes the superconducting state difficult to explore by optical experiments, even when the gap is considerably larger than expected from mean field theory (Rao *et al.*, 2006). Microwave experiments find a drop in surface resistance and a small peak in the ac conductivity right below T_c (Gough *et al.*, 2004; Thoms, 2004; Ormeno *et al.*, 2006); a finite quasiparticle fraction is inferred with a temperature-independent relaxation rate. Because of its spin-triplet superconducting state with a $d = \Delta_0\hat{z}(k_x \pm ik_y)$ symmetry, order-parameter collective modes were predicted in Sr_2RuO_4 similar to the clapping mode in the A phase of superfluid ^{3}He (Higashitani and Nagai, 2000; Kee *et al.*, 2000). They should show up in the acoustic properties as well as in the electromagnetic absorption at $\hbar\omega = \sqrt{2}\Delta$, i.e., in the GHz range, but have so far defied experimental verification.

E. Multiferroics

Because of their fundamentally different behavior with respect to time and space reversal, no linear coupling can exist between static polarization and magnetization. On the other hand, space and time dependent polarization and magnetization do couple provided that certain special conditions are met. Multiferroics, such as $TbMnO_3$, $Ni_3V_2O_8$, $MnWO_4$, and CuO, are materials where these special conditions are present, thus offering the prospect of controlling charges by applied magnetic fields and spins by applied voltages (Cheong and Mostovoy, 2007). A crucial role in the phenomenological description of magnetoelectric coupling is

played by the symmetry of the crystal lattice, the symmetry of the unit cell, and of the magnetic order (Kenzelmann *et al.*, 2005). For example, a spiral spin state (Sushkov *et al.*, 2008) induces, through the Dzyaloshinski-Moriya exchange (Dzyaloshinski, 1958; Moriya, 1960), a polar lattice distortion and accordingly a static electric polarization. In the ordered spin state, one of the two magnons in the Hamiltonian is replaced by the static modulation of spin density. Together, the symmetry breaking caused by the static electric polarization and the spin-orbit interaction render magnons electric dipole active (see Sec. III.D). Consequently, optical phonons and single-magnon waves of the same representation will mix. Also, two-magnon and single magnons can be excited by the electric-field component of electromagnetic radiation (Katsura *et al.*, 2007). This is at the heart of the phenomenon of electromagnons, and it offers interesting perspectives for the coupling of electric and magnetic polarization in multiferroic materials (Cheong and Mostovoy, 2007).

Indeed strong ''electromagnon'' modes are observed in the infrared transmission spectra of $GdMnO_3$, $TbMnO_3$ (see Fig. 37), $Gd_{0.7}Tb_{0.3}MnO_3$, and $Eu_{0.75}Y_{0.25}MnO_3$ at ~20 and 60 cm^{-1} (Pimenov, Mukhin *et al.*, 2006; Pimenov, Rudolf *et al.*, 2006; Sushkov *et al.*, 2007; Aguilar *et al.*, 2007; Kida *et al.*, 2008; Sushkov *et al.*, 2008; Aguilar *et al.*, 2009; Pimenov *et al.*, 2009). Recent observation of the coincidence of two AFMR modes with electromagnons at 18 and 26 cm^{-1} illustrates the close relationship of electromagnons to AFMR (Pimenov *et al.*, 2009). Whereas a single zone-boundary magnon seems the most plausible interpretation of the 60 cm^{-1} peak (Aguilar *et al.*, 2009), the interpretation of the 25 cm^{-1} peak as either a rotation mode of the spiral spin plane (Katsura *et al.*, 2007) or a two-magnon process (Kida *et al.*, 2008) is still the subject of discussion. Talbayev, LaForge *et al.* (2008) observed AFMR at 43 cm^{-1} in multiferroic hexagonal $HoMnO_3$ and demonstrated the ferromagnetic nature of the rare-earth and Mn exchange. The magnetoelectric response in a multiferroic material enables monitoring the oscillation of coherent magnons in the time domain following femtosecond excitation: The magnetic precession modulates the material's dielectric tensor, and this is seen as a modulation of the intensity of a light beam reflected at the surface of the sample (Talbayev, Trugman *et al.*, 2008).

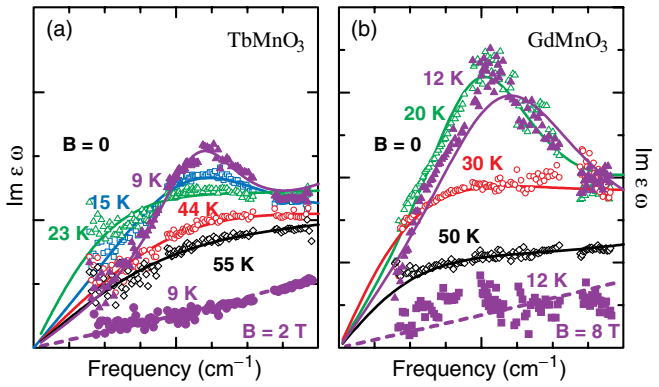

FIG. 37 (color online). Frequency dependence of the imaginary parts of the terahertz-dielectric function in (a) $TbMnO_3$ and (b) $GdMnO_3$ with $e \parallel a$ and $b \parallel c$. Open symbols represent experimental data in zero external magnetic field and in the IC-AFMR phase. Solid lines represent model calculations adding an overdamped Lorentzian (dashed lines) to the residual high-frequency contribution. Filled spheres represent the data in the CA-AFMR state obtained by applying $B = 2$ T ($GdMnO_3$) and $B = 8$ T ($TbMnO_3$) along the c axis. The corresponding zero-field data are shown by filled triangles. From Pimenov, Mukhin *et al.*, 2006.

F. Iridates

Moon *et al.* (2008) studied a Ruddlesden-Popper series of Ir oxides with chemical formula $Sr_{n+1}Ir_nO_{3n+1}$, where $n = 1$, 2, and ∞. The optical conductivity of Sr_2IrO_4 and $Sr_3Ir_2O_7$ single crystals, as well as epitaxially thin films of $SrIrO_3$ grown on cubic MgO substrate, is reproduced in Fig. 38. The role of the substrate was to ensure the perovskite phase of $SrIrO_3$, which is otherwise stable only at higher pressure and temperature (Longo *et al.*, 1971). To measure the $SrIrO_3$ optical response, far-infrared ellipsometry was combined with transmittance and reflectance measurements to obtain accurate results over an extended energy range.

Figure 38(a) shows that Sr_2IrO_4 ($n = 1$) has an optical gap of ~0.1 eV, $Sr_3Ir_2O_7$ ($n = 2$) has a much smaller gap, and $SrIrO_3$ ($n = \infty$) is a metal. Hence there is a metal-insulator transition in the Ruddlesden-Popper series for n in the range $2 < n < \infty$.

The optical conductivity in Figs. 38(a) and 38(b) displays a pronounced two peak structure in both insulators, with peaks α and β, which slightly decrease with n. In the metal, only the higher-energy peak β is identified. Moon *et al.* (2008)

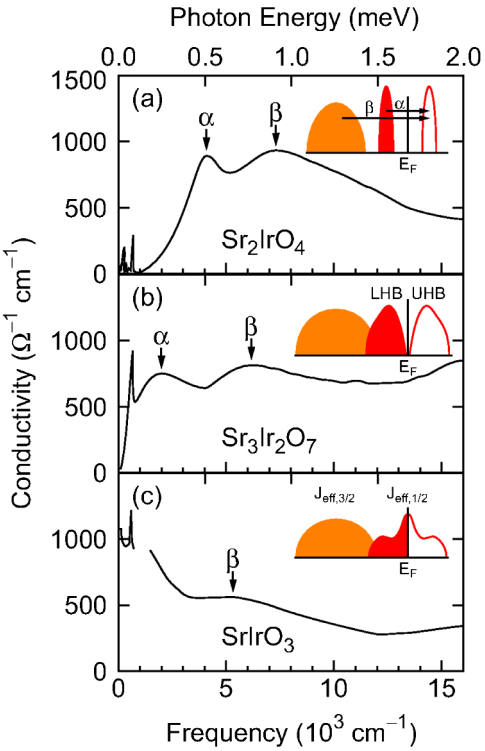

FIG. 38 (color online). Optical conductivity of the Ruddlesden-Popper series $Sr_{n+1}Ir_nO_{3n+1}$, where $n = 1$, 2, and ∞. The insets sketch the $t2g$ density of states in the three materials. From Moon *et al.*, 2008.

interpreted these peaks as excitations across the Hubbard bands, shown in Fig. 38(b).

The band-structure LDA+U calculations for ferromagnetic Sr_2IrO_4 (B. J. Kim *et al.*, 2008) suggested that the t_{2g} bands split due to large spin-orbit coupling ($\xi \approx 0.4$ eV) into two sets of states, a set of bands with an effective angular momentum $J_{\text{eff}} = 3/2$, and a band with an effective $J_{\text{eff}} = 1/2$. The former states are lower in energy and thus completely filled, while the $J_{\text{eff}} = 1/2$ band is half filled [see Fig. 38(b)]. Although the Hubbard U in the LDA+U calculation was only $U = 2$ eV, it opened the gap in the half-filled $J_{\text{eff}} = 1/2$ band, and split the Hubbard bands of $J_{\text{eff}} = 1/2$ for roughly 0.5 eV. B. J. Kim *et al.* (2008) suggested that the excitations across these $J_{\text{eff}} = 1/2$ bands give rise to the peak α in optical conductivity, while the excitations from $J_{\text{eff}} = 3/2$ into the unoccupied $J_{\text{eff}} = 1/2$ give rise to the peak marked β in Fig. 38(a).

Moon *et al.* (2008) suggested that the bandwidth W of the Ruddlesden-Popper series increases with n. They argued that this is a natural consequence of the connectivity z of the Ir atom. The connectivity is only $z = 4$ in Sr_2IrO_4, but becomes $z = 5$ and 6 in $Sr_3Ir_2O_7$ and $SrIrO_3$, respectively. Hence, using the same small $U \sim 2$ eV within LDA+U, Moon *et al.* (2008) showed that the gap in Sr_2IrO_4 is indeed very small and that it disappears in $SrIrO_3$, in qualitative agreement with experiment. Moreover, the optical conductivity data of Moon *et al.* (2008) suggest that the metallic state of $SrIrO_3$ is very correlated with heavy effective mass of the order of $m^*/m_b \sim 7$. This enhancement of the mass cannot be captured by the LDA+U method, but it is expected for a correlated metal.

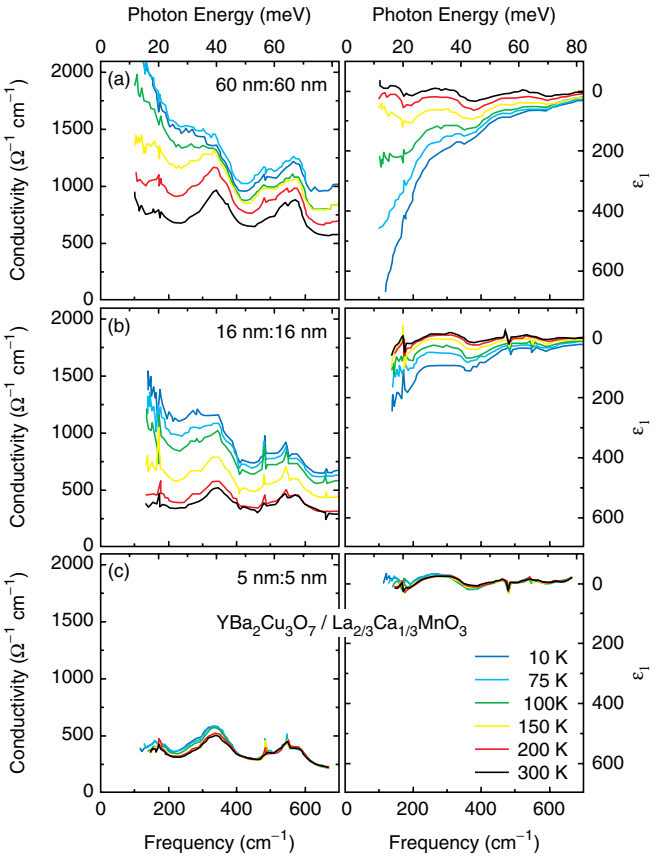

FIG. 39 (color online). Optical conductivity and dielectric constant of superlattices consisting of equal thickness of YBCO and LCMO layer. The thickness of each layer in (a), (b), and (c) is 60, 16, and 5 nm, respectively. From Holden *et al.*, 2004.

G. Oxide heterostructures

Artificial multilayers of complex transition-metal oxides attract much attention as possible building blocks of novel and useful functional materials. In particular, heterostructures of superconducting YBCO and ferromagnetic LCMO offer a unique opportunity to study the interplay between two antagonistic orders, ferromagnetism and high-temperature superconductivity.

The similar lattice constants of perovskite materials YBCO and LCMO allow one to grow high quality superlattices of any layer thickness and with perfect atomically sharp interface. The pure cuprate high-T_c YBCO is superconducting below $T_c = 90$ K and is metallic above T_c. Bulk LCMO exhibits colossal magnetoresistance and is a ferromagnetic metal below $T_{\text{Curie}} = 245$ K and a paramagnetic insulator above T_{Curie}.

Using spectral ellipsometry, Holden *et al.* (2004) measured the effective dielectric function ϵ_1 and effective optical conductivity σ_1 of superlattices, which are equal to the volume average of the superlattice components (Aspnes, 1982). Figure 39 shows σ_1 and ϵ_1 for several YBCO/LCMO superlattices with thickness ratio d_{YBCO}: d_{LCMO} of 60:60, 16:16, and 5:5 nm. Given the metallic properties of the pure YBCO and LCMO in the extended range of temperatures, one would expect that the superlattice also should exhibit a strong metallic response. Instead Figs. 39(a)–39(c) highlight the fact that the YBCO/LCMO superlattice exhibits a drastic decrease of carrier concentration and their mobility. For the fairly thick superlattice of 60:60 nm the decrease of metallicity is not yet very pronounced, and one can even observe signatures of superconducting gapping in 10 K data of Fig. 39(a).

The metallic response is strongly suppressed in other superlattices with thinner layers. The absolute value of σ_1 and ϵ_1 is drastically reduced in 5:5 nm superlattice at all temperatures [see Fig. 39(c)]. The Curie temperature and superconducting temperature of this superlattice are ~120 and 60 K, respectively. Hence insulatinglike behavior below 120 K is completely unexpected and surprising.

To shed some light on the origin of such strong suppression of the free-carrier response, the optical conductivity was calculated for a model of a superlattice consisting of 16 nm of LCMO and 16 nm of a material with a small Drude-like response with $\omega_p^2 = 2 \times 10^6$ cm^{-2}. The idea for such a "fit layer" comes from the results on 5:5 nm superlattice, which gives roughly the Drude weight of comparable magnitude $\omega_p^2 = 2 \times 10^6$ cm^{-2}. Agreement between the measurements and such a model calculation was found to be very good (Holden *et al.*, 2004), which might suggest that the LCMO response does not change much with the layer thickness, while superconducting YBCO becomes almost insulating in thin layers. Note that the superconducting T_c remains relatively high around 60 K. A model for a superlattice with 16 nm of YBCO and 16 nm of a Drude-like layer with

arbitrary ω_p does not give satisfactory agreement with measurements.

Holden *et al.* (2004) also measured the conductivity of superlattices consisting of YBCO and material X, where X was insulating $PrBa_2Cu_3O_7$, paramagnetic metal $LaNiO_3$, and ferromagnetic metal $SrRuO_3$. Ferromagnetic $SrRuO_3$ shows a similar suppression of charge carriers as LCMO, while this effect is absent for paramagnetic metal $LaNiO_3$ or insulator $PrBa_2Cu_3O_7$. Hence the competition of ferromagnetism and superconductivity is likely responsible for the measured suppression of the conductivity. It should be noted that superlattices of YBCO/LCMO with the YBCO layer much thicker than LCMO, such as 60:15, 30:15, and 8:3 nm, do not show a strong suppression of conductivity; hence only comparable thickness of the two layers gives the intriguing effect of suppressed conductivity (Holden *et al.*, 2004). Similar suppression of the superconducting condensate density in the superlattices of comparable thickness was observed in terahertz measurements by F. Chen *et al.* (2004).

Understanding of the electronic states at the interface between a high-T_c material and a ferromagnet is far from complete; hence the origin of the conductivity suppression is at present unknown. However, there are various proposals for the origin of these phenomena. In the most straightforward interpretation, there is a massive transfer of holes from YBCO to LCMO, such that YBCO becomes underdoped and LCMO is driven into a charge-ordered state, similar to the one observed for Ca content of $x > 0.45$ (Holden *et al.*, 2004; Yunoki *et al.*, 2007). However, metallic $LaNiO_3$ does not give rise to this effect, while ferromagnetic $SrRuO_3$ does. Thus, the magnetic proximity effect might play a major role in affecting the YBCO superconductor (Buzdin, 2005).

Indeed there are some indications of interesting interfacial phenomena in YBCO/LCMO superlattices. X-ray spectroscopy and neutron measurements by Chakhalian *et al.* (2006) showed that Cu atoms in the first Cu-O layer of YBCO acquire a ferromagnetic polarization, likely due to canting of Cu magnetic moments. This is due to coupling between the Cu-O layer and Mn-O layer at the interface. The LCMO ferromagnetic layer at the interface has a somewhat suppressed ferromagnetic moment and is coupled antiferromagnetically to the net Cu-polarized moment (Stahn *et al.*, 2005). Resonant x-ray spectroscopy by Chakhalian *et al.* (2007) furthermore suggested a major change in orbital occupation of the electronic states on the Cu atom at the interface. The $3d_{3z^2-r^2}$ Cu orbital is almost fully occupied and inactive in bulk YBCO, but becomes partially occupied at the interface.

There are indications of a strong modification of the ferromagnetic LCMO layers, obtained by neutron spectroscopy experiments (Hoppler *et al.*, 2009). It was suggested that every second LCMO layer might lose as much as 90% of the magnetic moment, while the remaining half of the LCMO layers might have strongly enhanced magnetic moments, such that the average magnetization remains unchanged. While these unusual interfacial effects do not directly explain the origin of the strong suppression of the conductivity, they show that the interface physics and proximity effects might be far more complicated than previously thought and might be relevant for correct interpretation of the measured conductivity suppression.

Numerous other oxide heterostructures were synthesized recently, such as $LaTiO_3/SrTiO_3$ (Ohtomo *et al.*, 2002), $CaRuO_3/CaMnO_3$ (Takahashi *et al.*, 2001), and $La_2CuO_4/La_{1.55}Sr_{0.45}CuO_4$ (Gozar *et al.*, 2008). For a recent review, see Ahn *et al.* (2006). More recently, far-infrared spectral ellipsometry was applied to superlattice of correlated paramagnetic metal $CaRuO_3$ and the antiferromagnetic insulator $CaMnO_3$ (Freeland *et al.*, 2010). It was found that the ferromagnetic polarization is due to canted Mn spins in $CaMnO_3$ penetrated unexpectedly deep into the $CaMnO_3$ layer (3–4 unit cells).

VI. INTERMETALLIC COMPOUNDS AND MAGNETIC SEMICONDUCTORS

The properties of intermetallic compounds containing elements with f electrons (such as U, Ce, or Yb) are governed by the competition between Kondo and Ruderman-Kittel-Kasuya-Yosida (RKKY) interactions (Doniach, 1977; Hewson, 1993; Fulde *et al.*, 2006). While magnetic ground states occur when RKKY ordering dominates, Kondo interaction links localized f electrons and conduction electrons. Their hybridization severely influences the density of states. The Anderson model contains the essential physics of d and f states in heavy fermions, but is also crucial for the understanding of magnetic impurities in simpler systems such as (Ga,Mn)As. After early reviews by Millis (1992) and Wachter (1994), the electrodynamic properties have been extensively discussed by Degiorgi (1999); thus we confine ourselves to some recent developments.

A. Heavy-fermion metals

The heavy-fermion phenomenon exists in a number of lanthanide and actinide compounds[35] and manifests in the apparent existence of quasiparticles with large effective mass m^* below some characteristic temperature T^*. These materials have partially filled f orbitals, which hybridize with lighter and more spatially extended s, p, and d orbitals. At low temperature, the electrons can form a *heavy* Fermi-liquid state, a composite of f-electron spins, and conduction-electron charges. Alternatively, the f electrons can magnetically order, or the heavy quasiparticles can superconduct [for reviews, see Stewart (2001, 2006)].

In a simple picture these correlations reduce the scattering rate $1/\tau$ and spectral weight (Varma, 1985a, 1985b; Coleman, 1987; Millis *et al.*, 1987; Millis and Lee, 1987). In other words, the Drude response becomes extremely narrow. As pointed out by Scheffler *et al.* (2005, 2006, 2009, 2010), the Fermi velocity v_F is small (cf. Sec. III.A and Fig. 7).

In addition to the narrow Drude-like response, a midinfrared absorption peak around ω_{mir} is commonly observed

[35]Kondo *et al.* (1997) also discovered heavy-fermion characteristics in the d-electron system LiV_2O_4. Optical experiments reveal that it behaves more like a "bad metal" close to a correlation-driven insulating state and that the spectral weight is transferred over an extremely wide energy range (Jönsson *et al.*, 2007). Hydrostatic pressure suppresses the Drude response and a charge-order insulator develops (Irizawa *et al.*, 2009).

that scales as $\omega_{\mathrm{mir}} \propto \sqrt{T^*}$ (Garner *et al.*, 2000; Degiorgi *et al.*, 2001; Hancock *et al.*, 2004; Hancock *et al.*, 2006; Okamura *et al.*, 2007). From optical and magneto-optical experiments on numerous nonmagnetic systems, Dordevic, Basov, Dilley *et al.* (2001), Dordevic *et al.* (2006) confirmed the scaling relation $m^*/m_b = (\Delta/k_B T^*)^2$ between the magnitude of m^* and the hybridization gap Δ.

Extending previous experiments (Bonn, Klassen *et al.*, 1988; Bommeli *et al.*, 1997) to lower frequencies and temperatures, Holden *et al.* (2003) observed coherent transport in UBe_{13} with an abrupt decrease in scattering rate and a strong increase of the effective mass. The strongest enhancement of the effective mass is observed in heavy-fermion systems with a magnetically ordered ground state. UPd_2Al_3 is a prime example for which Dressel *et al.* (2000), Dressel, Kasper, Petukhov, Gorshunov *et al.*, 2002, and Dressel, Kasper, Petukhov, Peligrad *et al.*, 2002) measured the low-temperature optical properties in a wide frequency range. As shown in Fig. 40, below $T^* \approx 50$ K, the hybridization gap opens around 10 meV. As the temperature decreases

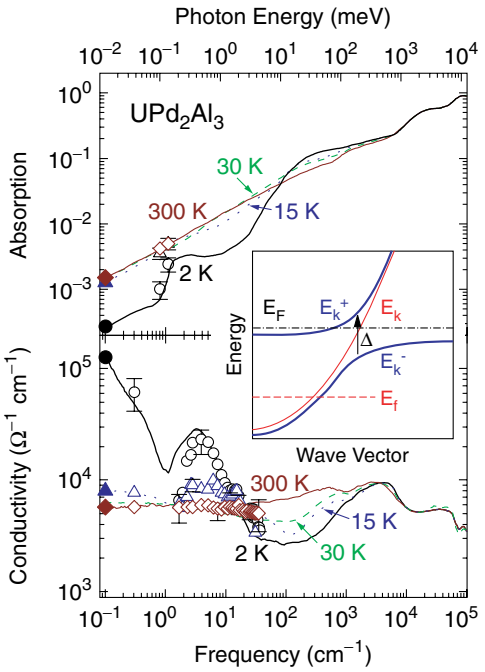

FIG. 40 (color online). Frequency-dependent absorptivity $A(\omega) = 1 - R(\omega)$ and optical conductivity of UPd_2Al_3 at different temperatures shown over a wide frequency range. The solid symbols on the left axis are from dc measurements; the open symbols in the microwave range are obtained by cavity perturbation technique. In the terahertz range the optical conductivity is determined directly using the transmission and the phase shift measured by the Mach-Zehnder interferometer. The lines are from various optical investigations [transmission through films and reflection of bulk samples (Degiorgi, Dressel *et al.*, 1994)] and simultaneously match the directly measured conductivity and dielectric constant (Dressel, Kasper, Petukhov, Gorshunov *et al.*, 2002, Dressel, Kasper, Petukhov, Peligrad *et al.*, 2002). Inset: Renormalized band structure calculated from the Anderson lattice Hamiltonian. E_k and E_f denote bands of free carriers and localized f electrons. At low temperatures, a direct gap Δ opens. The Fermi level E_F is near the bottom of the upper band E_k^+, resulting in enhanced effective mass of the quasiparticles.

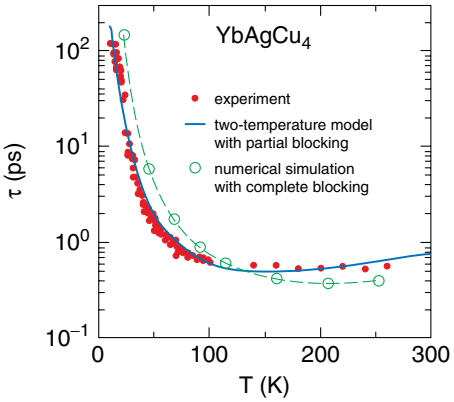

FIG. 41 (color online). Temperature dependence of the relaxation time on YbAgCu4. Numerical simulations have been performed assuming suppressed scattering of heavy electrons by phonons; the solid line corresponds to simulations by a two-temperature model with a partial reduction of the scattering. An equally good description is obtained by coupled Boltzmann equations when the electron-phonon coupling is suppressed for electronic states within the Abrikosov-Suhl peak in the density of states (Demsar, Averitt *et al.*, 2003; Ahn *et al.*, 2004).

further ($T \leq 20$ K), a well-pronounced pseudogap of ~0.2 meV develops in the optical response that may be related to the antiferromagnetic ordering, $T_N \approx 14$ K. Similar observations are reported for UPt_3 (Donovan *et al.*, 1997; Tran *et al.*, 2002), UNi_2Al_3 (Scheffler *et al.*, 2010), and URu_2Si_2 (Morales and Escudero, 2009).

The heavy-fermion compound $CeCoIn_5$ with the highest superconducting transition, $T_c = 2.3$ K, is subject to intense optical investigations (Singley, Basov *et al.*, 2002; Mena *et al.*, 2005; Burch *et al.*, 2007; Sudhakar Rao *et al.*, 2009) without giving insight into the superconducting state yet.

Time-resolved optical investigations on $YbAgCu_4$ reveal that the electron-phonon thermalization increases below T^* by more than 2 orders of magnitude (see Fig. 41), because heavy quasiparticles acquire a large specific heat and their scattering on phonons is suppressed (Demsar, Averitt *et al.*, 2003). In conventional metals (Groeneveld *et al.*, 1995; Hase *et al.*, 2005a, 2005b) the relaxation time can be well described by coupling the electrons to the lattice bath (two-temperature model), but it fails at low temperatures when electron-electron thermalization becomes the limiting factor. In the case of heavy fermions, the latter process is much faster; however, the scattering of the heavy electrons on phonons is suppressed due to the extremely slow Fermi velocity v_F compared to the sound velocity. An alternative scenario is based on the bottleneck idea of Rothwarf and Taylor (1967) (cf. Sec. III.G): the recombination of a photoexcited quasiparticle across the hybridization gap is the limiting factor in heavy-fermion metals as well as in Kondo insulators or spin-density-wave systems (Chia *et al.*, 2006; Demsar, lle *et al.*, 2006; Demsar, Sarrao, and Taylor *et al.*, 2006).

B. Kondo insulators

In a few cases the hybridization of conduction electrons and f electrons leads to semiconducting characteristics with a

small energy gap (of the order of 10 meV) and a van Vleck–like susceptibility at low temperatures (Aeppli and Fisk, 1992; Wachter, 1994; Degiorgi, 1999; Riseborough, 2000). A canonical example of a Kondo insulator is $Ce_3Bi_4Pt_4$, for which the gap opening below 100 K is shown in Fig. 17(d). The depleted spectral weight grows linearly with temperature and is displaced to energies much larger than the gap.

Numerous efforts have been undertaken to elucidate the nature of the gap and possible states inside (Riseborough, 2003). Experiments by Okamura *et al.* (1998), 2000, 2004, 2005 shed light on the optical properties of the ytterbium compounds. The infrared conductivity of YbB_{12} and $YbAl_3$ is governed by a broad peak centered at 2000 cm^{-1} related to direct transitions between the Yb $4f$-derived narrow band and the broad conduction band. The behavior can be reproduced by calculations based on the electronic band structure (Antonov *et al.*, 2002a, 2002b; Saso, 2004). As shown in Fig. 42(a) for the case of YbB_{12}, below $T = 80$ K an energy gap opens around 320 cm^{-1}. In $YbAl_3$ a similar behavior is found at 500 cm^{-1}, although the compound remains metallic. It is argued that these excitations are indirect transitions within the hybridization state. The correlated nature of the low-temperature state is reflected in the mass enhancement $m^*/m_b \approx 12$ and $1/\tau \propto \omega^2$ dependence of YbB_{12} obtained from a generalized Drude analysis (Gorshunov, Haas *et al.*, 2006; Gorshunov, Prokhorov *et al.*, 2006). For $T \leq 10$ K the conductivity onset is 15 meV, which agrees with the renormalized band model (Hewson, 1993). Resistivity, Hall effect, photoemission, and specific heat measurements yield comparable values of the gap (Iga *et al.*, 1999; Takeda *et al.*, 2004). Substituting Yb^{3+} by nonmagnetic Lu^{3+} lowers the electronic correlations: similar to the temperature increase, the gap gradually fills in [Fig. 42(b)] without shifting the shoulder at 300 cm^{-1}. The midinfrared peak, however, moves to lower energies in $Yb_{1-x}Lu_xB_{12}$ with x increasing until it is lost for $x \geq 0.75$ because the coherence among the Kondo singlets vanishes (Okamura *et al.*, 2000); the same effect is reached by rising temperature.

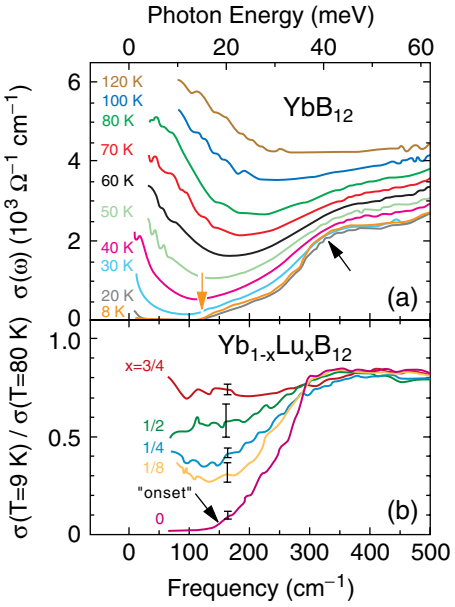

FIG. 42 (color online). (a) Optical conductivity of YbB_{12} at different temperatures. The arrows indicate the shoulder and the conduction onset. (b) Substitution of Yb by Lu decreases correlations; the corresponding energy gap does not shift but disappears (Okamura *et al.*, 2000, 2005).

Dressel *et al.* (1999) and Gorshunov *et al.* (1999) extended previous optical experiments on the intermediate-valence compound SmB_6 by Travaglini and Wachter (1984) and Nanba *et al.* (1993) to extremely low frequencies ($\nu > 1$ cm^{-1}). Within the 19 meV energy gap in the density of states they found an additional narrow donor-type band only 3 meV below the bottom of the upper conduction band, seen as an absorption peak at 24 cm^{-1}. At $T < 5$ K, only the charge carriers within the narrow band contribute to the ac conductivity. Correlation effects cause a sizable effective-mass enhancement $m^* \approx 30m_b$ which is discussed in the frame of a specific exciton-polaron formation at low temperatures when moving carriers get self-trapped (Kikoin and Mishchenko, 1990; Curnoe and Kikoin, 2000; Sluchanko *et al.*, 2000). However, field- and pressure-dependent NMR and transport experiments (Caldwell *et al.*, 2007; Derr *et al.*, 2008) evidence the intrinsic nature and magnetic origin of the in-gap states. The observations are explained by antiferromagnetic correlations based on a localized Kondo model (Kasuya, 1996; Riseborough, 2000, 2003).

Matsunami *et al.* (2009) succeeded in tuning the Kondo insulator to a heavy-fermion metal by applying high pressure. In the well-studied insulator (Degiorgi *et al.*, 2001; Dordevic, Basov, Dilley *et al.*, 2001) the gap between the f band and conduction electrons closes above 8 GPa and metallic behavior with heavy carriers is observed.

While Yb_4As_3, TmSe, or FeSi are often subsumed under Kondo insulators, the viewpoint has shifted in recent years. Fulde *et al.* (1995) pointed out that the unusual properties of Yb_4As_3 can be explained by charge ordering of the Yb ions which at low temperatures are self-doped leading to strong electronic correlations of the $4f$ holes in charge-ordered Yb chains. In accord with broadband reflection measurements by Kimura *et al.* (1996, 1997, and 2002), magneto-optical investigations on Sb-substituted crystals yield an energy difference of 0.42 eV between the occupied and empty $4f^{14}$ state (Pittini *et al.*, 1998). In TmSe, $\sigma(\omega)$ reveals a gaplike feature below 100 cm^{-1} for $5 < T < 50$ K, which is accounted for as a mobility gap due to localization of d electrons on local Kondo singlets rather than a hybridization gap in the density of states (Dumm *et al.*, 2005; Gorshunov *et al.*, 2005). As discussed in Sec. VI.D.3, extensive investigations of the narrow-gap semiconductor FeSi and related compounds, such as $Fe_{1-x}Co_xSi$, MnSi, and FeGe, consider FeSi as an itinerant semiconductor whose properties can be explained without a local Kondo-like interaction.[36]

[36]Previous investigations (Schlesinger *et al.*, 1993; Degiorgi, Hunt *et al.*, 1994; Paschen *et al.*, 1997) were hampered by sample quality, but also the point of view has changed over the years (Damascelli *et al.*, 1997; van der Marel *et al.*, 1998; Mena *et al.*, 2003, 2006; Guritanu *et al.*, 2007; Zur *et al.*, 2007; Klein *et al.*, 2008).

C. Beyond the Anderson model

The Anderson lattice model adequately describes the gross features of the heavy electron physics (see Sec. VI) and Kondo insulating behavior (see Sec. VI.B). Specifically, the model accounts for the fingerprints of electrodynamics of a heavy-fermion metal including massive quasiparticles, the hybridization gap (Degiorgi, 1999), as well as the scaling of these observables with the coherence temperature T^*. DMFT results (Grenzebach *et al.*, 2006) reproduce all qualitative features of the complex conductivity characteristic to a typical heavy-fermion system. Nevertheless, optical data for a class of Ce-based heavy fermions with chemical formula $CeXIn_5$ (X = Co, Rh, Ir) (Singley, Basov *et al.*, 2002; Mena *et al.*, 2005; Burch *et al.*, 2007) reveal significant departures from these established trends. Spectra shown in Fig. 43(b) do not reveal a clear hybridization gap. Instead a continuum of states extends down to lowest energies; this later behavior is most clearly seen in data by Singley, Basov *et al.* (2002). Burch *et al.* (2007) interpreted this unusual response in terms of the distribution of the energy gaps and conjectured that the strength of the hybridization may be momentum dependent.

Microscopically, a momentum dependence in the hybridization is hardly surprising given the fact that the local-moment orbitals are of f type and may hybridize with several conduction-electron orbitals. Weber and Vojta (2008) considered heavy-fermion metals with hybridization nodes and concluded that the low-temperature specific heat of these type of systems is dominated by heavy quasiparticles, whereas the electrical conductivity at intermediate temperatures is carried by unhybridized light electrons. Calculations of the optical conductivity carried out by Weber and Vojta (2008) confirm smearing of the hybridization gap feature. The LDA+DMFT calculations by Shim *et al.* (2007), reproduced in Fig. 43(a), revealed that the "in-gap" states are related to excitations across a second hybridization gap. Namely, at low temperature, the Ce local moment is strongly coupled to electrons on neighboring In atoms. The coupling is strong with the out-of-plane In, and weaker with the in-plane In, which results in variation of the hybridization gap in momentum space [see Fig. 43(c)]. The larger (smaller) hybridization gap gives rise to a peak at higher (lower) frequency of ~0.075 eV (~ 0.03 eV). At higher temperature, the electronic states which are strongly coupled to Ce moments (and result in a large hybridization gap at low temperature) become highly scattered and acquire large broadening of the bands [see Fig. 43(d)], a signature of the local-moment regime.

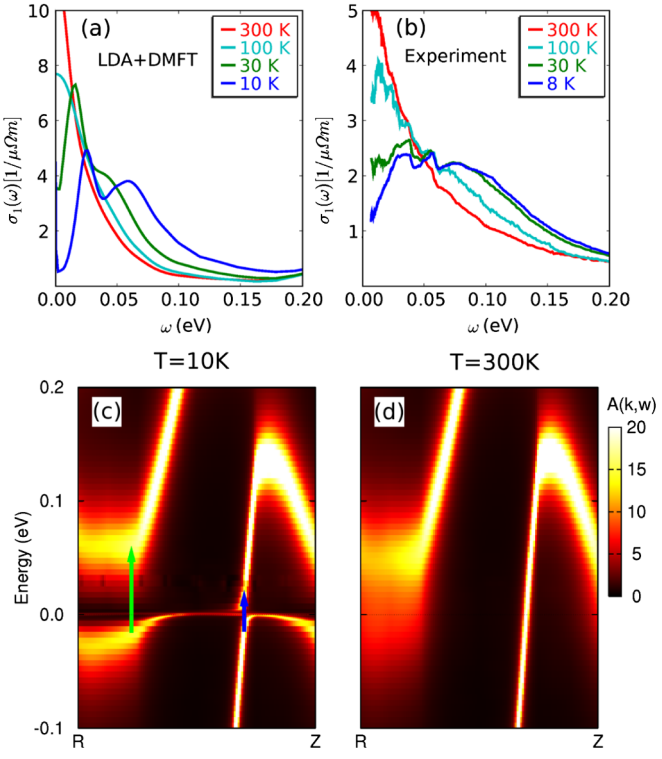

FIG. 43 (color online). The development of the hybridization gap in the heavy-fermion compound $CeIrIn_5$. (a) The optical conductivity calculated by LDA+DMFT method. From Shim *et al.*, 2007. (b) Experimental optical conductivity for the same compound measured by Mena *et al.* (2005). (c) Theoretical momentum-resolved non-f spectral function at low temperature. The two types of hybridization gaps are marked by arrows in (c). (d) Same as (c) but for higher temperature.

D. Magnetic semiconductors

In this section we provide an overview of the optical properties of several different classes of ferromagnetic semiconductors including III-Mn-As, EuB_6, and transition-metal silicides. A common denominator between these systems is low carrier density n and plasma frequency ω_p. Furthermore, in all of these systems the formation of magnetic order is associated with significant changes of the plasma frequency and low-energy conductivity. In both borides and III-Mn-As the plasma frequency increases below the Curie temperature T_{Curie} revealing scaling with the magnetization. In silicides the dominant contribution to the transformation of optical properties below T_{Curie} is due to magnetic disorder leading to suppressed metalicity in the ferromagnetic state.

1. III-Mn-As

The discovery of ferromagnetism in III-V hosts heavily doped with Mn has propelled research in this class of materials (Ohno *et al.*, 1996). From the applications point of view, FM semiconductors are appealing because magnetic, electronic, and optical effects in these systems are intimately entangled. These properties, combined with Curie temperatures as high as $T_{\mathrm{Curie}} = 170$ K, may enable new device functionalities (Žutić *et al.*, 2004; Awschalom, 2007). The fundamental physics of FM semiconductors is equally exciting. The detailed understanding of complex behavior of III-Mn-V ferromagnetic semiconductors relies on resolving the roles played by electron-electron interactions and disorder in the previously unexplored regime of exceptionally high concentration of magnetic dopants. Magnetic impurities radically modify the IMT in this class of materials (Jungwirth *et al.*, 2006; Burch *et al.*, 2008). The most studied system, $Ga_{1-x}Mn_xAs$, undergoes the IMT in the impurity band that survives well on the metallic side of the transition (Burch *et al.*, 2008). On general grounds, one expects strong

electronic correlations to be an essential element of physics of a system where transport phenomena are dominated by states in the impurity band (Jungwirth *et al.*, 2006).

$Ga_{1-x}Mn_xAs$ is commonly referred to as a "prototypical" ferromagnetic semiconductor. An Mn ion in a GaAs host has a half-filled d shell and acts as a $S = 5/2$ local moment. The spin degeneracy of a Mn_{Ga} acceptor is lifted due to the large on-site Coulomb repulsion $U = 3.5$ eV. Itinerant carriers produced by Mn substituting Ga are locally magnetically coupled to the Mn spins via an exchange coupling. The exchange between the Mn local moments and the carriers they produce plays a key role in the physics of III-Mn-V diluted magnetic semiconductors and is responsible for mediating ferromagnetism. Another important aspect of the exchange coupling is its tendency to localize the holes around the Mn. The effect of disorder tends to be stronger in magnetic semiconductors compared to nonmagnetic counterparts (Timm, 2003; Ohno and Dietl, 2008). Mn doping introduces the insulator-to-metal transition near $x = 1$–2%. The IMT concentration depends on the presence of compensating donors (As antisites and interstitially doped Mn) and disorder.

Infrared and optical properties of $Ga_{1-x}Mn_xAs$ were a subject of detailed experimental (Nagai *et al.*, 2001; Singley, Kawakami *et al.*, 2002; Seo *et al.*, 2003; Singley *et al.*, 2003; Burch *et al.*, 2004, 2005, 2006) and theoretical (Sinova *et al.*, 2002; Moca *et al.*, 2009) investigations. Figure 44 shows the evolution of the electromagnetic response of $Ga_{1-x}Mn_xAs$ in the process of doping. A brief inspection of these data shows a dramatic change of the optical conductivity upon doping in the frequency range within the band gap of the GaAs host. Ferromagnetic films of $Ga_{1-x}Mn_xAs$ reveal two new features in the intragap conductivity. The first is a broad resonance initially centered at ~ 2000 cm^{-1}, whose center energy redshifts with doping (see inset of Fig. 44). The second key feature is the presence of finite conductivity in the limit of $\omega \to 0$: a signature of metallic behavior. The oscillator strength of both features increases with additional Mn doping. The redshift of the midinfrared resonance (Burch *et al.*, 2006) and further theoretical analysis of this behavior (Moca *et al.*, 2009) established that the formation of the metallic state occurs within the impurity band most likely overlapping the valence band of the GaAs host. This viewpoint on the electronic structure of ferromagnetic $Ga_{1-x}Mn_xAs$ ($x < 7\%$) is supported by magneto-optics measurements, time-resolved optical techniques, and also photoemission studies (Burch *et al.*, 2008). One can anticipate that with increasing doping concentration the Fermi energy will eventually move into the valence band (Jungwirth *et al.*, 2006).[37]

Analysis of the optical effective masses associated with the free-carrier absorption is indicative of correlation effects in $Ga_{1-x}Mn_xAs$. IR measurements reveal optical masses of the order $10m_e$ (Singley *et al.*, 2003; Burch *et al.*, 2006), a result recently confirmed by studies of the mobility and IMT in

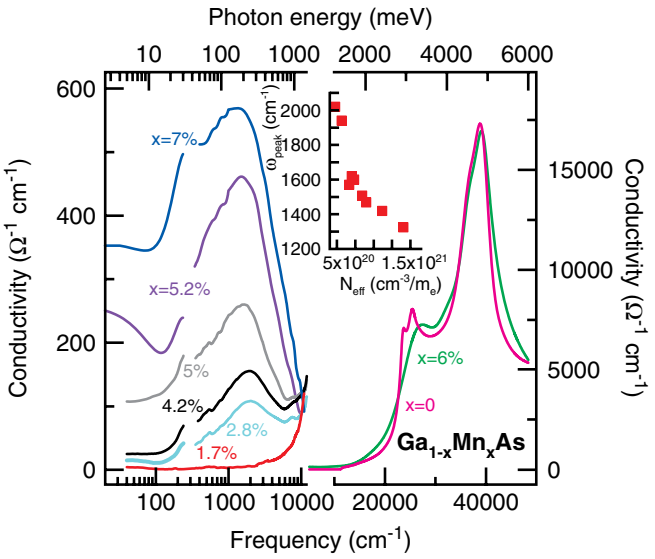

FIG. 44 (color online). The optical conductivity of $Ga_{1-x}Mn_xAs$ in the energy region below the band gap of the GaAs host (left panel) and above the gap (right panel). Data reveal systematic enhancement of the intragap conductivity with Mn doping and only weak modification of the van Hove singularities due to interband transitions. Data from Singley, Kawakami *et al.* (2002) and Burch *et al.* (2006). Inset: The peak position of the mid-IR resonance vs the spectral weight below 6450 cm^{-1}, which is proportional to the number of holes added through the doping process as described in detail by Burch *et al.* (2006). A prominent redshift of the resonance is apparent. All infrared data (left panel and the inset) at $T = 8$ K. Ellipsometry data in the right panel are at room temperature.

$Ga_{1-x-y}Mn_xAsBe_y$ and $Ga_{1-x}Mn_xAs_{1-y}P_y$ (Alberi *et al.*, 2008). It is yet to be determined if these heavy masses originate solely from impurity band physics or if many-body effects play a role in mass enhancement as well. Furthermore, in the ferromagnetic state the optical mass is reduced and scales with the magnetization (Singley *et al.*, 2003). This latter finding is in accord with the results reported for colossal magnetoresistance manganites: another class of correlated carrier mediated ferromagnets (see Sec. V.C).

2. EuB_6

Magnetic semiconductors have attracted interest not only for their potential use in spintronics, but also because of the fundamental question of how a magnetic metal can be derived from a paramagnetic insulator. The most common method, as described, involves insertion of transition-metal atoms into common semiconductors such as GaAs. Another important magnetic semiconductor is EuB_6 and its alloys. The Eu^{2+} ions have $S = 7/2$ magnetic moments. The material is a ferromagnetic semimetal at low temperature containing 10^{-2} carrier per formula unit. The transition to the paramagnetic state takes place in two steps, at $T_{Curie} = 12.5$ K and $T_M = 15.3$ K. If no magnetic field is applied, the unscreened plasma frequency shrinks spectacularly from 5200 cm^{-1} at low temperature to 2200 cm^{-1} at T_{Curie}, where it stabilizes (Degiorgi *et al.*, 1997). At all temperatures an externally applied magnetic field of a few Tesla increases the plasma

[37]In nonmagnetic semiconductors (Si:P, for example) the latter effect occurs at carrier densities exceeding the critical IMT concentration by the factor of 8–10 (Alexander and Holcomb, 1968). Then similar "valence band transition" in $Ga_{1-x}Mn_xAs$ can be anticipated at Mn concentrations near 20%.

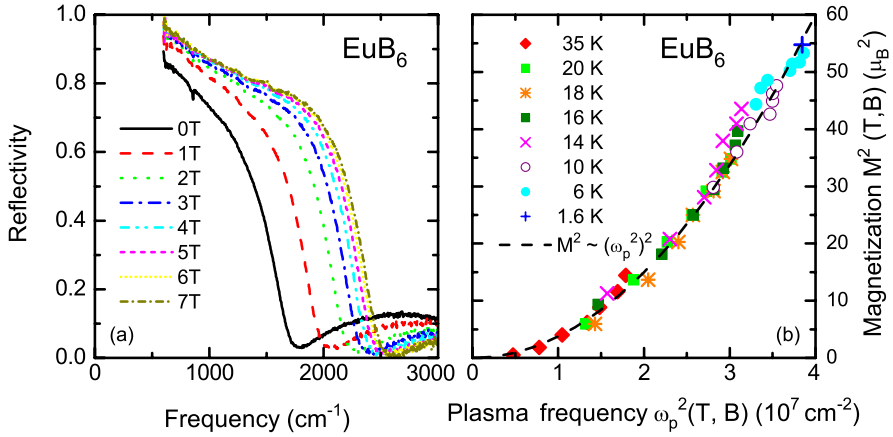

FIG. 45 (color online). (a) Magneto-optical reflectivity of EuB_6 at 16 K; (b) scaling of magnetization and plasma frequency. From Broderick *et al.*, 2002.

frequency. Moreover, ω_p and the magnetization M satisfy the simple scaling relation (Broderick *et al.*, 2002) $\omega_p^2 = cM$, as illustrated in Fig. 45, an effect which Pereira *et al.* (2004) explained using a double exchange model: The itinerant carriers move in a spin-background potential which is disordered by thermal fluctuations. The disorder is suppressed when the temperature is lowered and/or and the magnetic field is increased, and localized charge carriers are released into itinerant states. Consequently, the Drude weight grows upon magnetizing the system. Upon substituting Ca on the Eu site the plasma frequency of $Eu_{1-x}Ca_xB_6$ decreases to a small value at $x_c = 0.35$, and a finite free-carrier density remains for $x > x_c$ (Kim *et al.*, 2005). The scattering rate decreases strongly as a function of magnetization (Perucchi *et al.*, 2004; Caimi *et al.*, 2006), and the spectral weight (described by the parameter ω_p^2) follows the exponential relation $\omega_p^2(M) = \omega_{p0}^2 e^{cM}$. This behavior was ascribed to the inhibiting effect on the charge transport of magnetic domain walls and as such represents a spin-filter effect. The preponderance of the domain walls decreases when M increases, so that the scattering diminishes as is observed experimentally.

3. Transition-metal silicides

Other routes to create magnetic semiconductors are based on tuning the free charge carrier density of stoichiometric semiconducting compounds of transition metals or rare-earth ions and other elements such as Si or boron. The itinerant ferromagnets FeGe and MnSi belong to the same class of transition-metal silicides and germanates. Substituting Ge on the Si site of FeSi results in the metal-insulator transition at the composition $FeSi_{0.75}Ge_{0.25}$. It has been predicted (Anisimov *et al.*, 2002) that application of a high magnetic field to the semiconductor induces a highly spin-polarized ferromagnetic state. Pure FeGe is a good metal, which undergoes a transition to a helimagnetic ordered state when cooled below at $T_{\text{Curie}} = 280$ K. The stoichimetric ferromagnets MnSi ($T_{\text{Curie}} = 29.5$ K) (Mena *et al.*, 2003) and FeGe present an evolution of the scattering rate, which resembles more that of EuB_6 than that of the disordered ferromagnets $Fe_{1-x}Co_xSi$: At the temperature where magnetic order occurs, a distinct and narrow free-carrier response develops, with a strong decrease of the frequency-dependent scattering rate in the zero-frequency limit. $m^*(\omega, T)$ for $\omega \to 0$ is enhanced at low temperatures and falls gradually as a function of increasing frequency. Similar trends of $m^*(\omega, T)$ and $1/\tau(\omega, T)$ have been observed in the heavy-fermion uniaxial ferromagnet UGe_2 ($T_{\text{Curie}} = 53$ K) (Guritanu *et al.*, 2008), the nearly ferromagnetic metal $SrFe_4Sb_{12}$ ($T_{\text{Curie}} = 53$ K) (Kimura, *et al.*, 2006), and the itinerant ferromagnet $ZrZn_2$ ($T_{\text{Curie}} = 28$ K) (Kimura *et al.*, 2007).

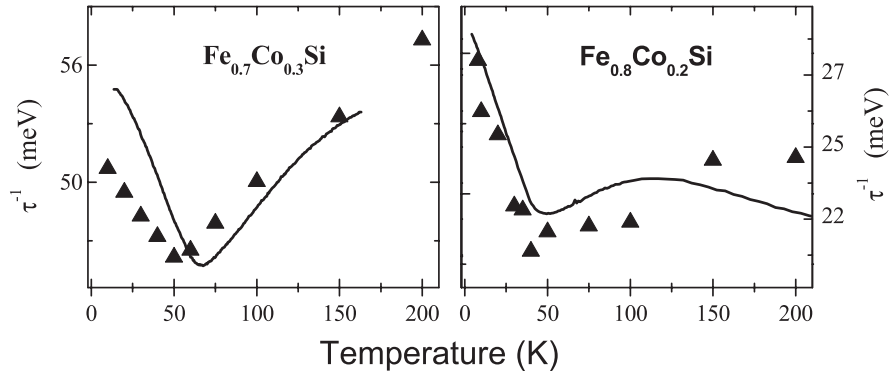

FIG. 46. Temperature dependence of the optical scattering rates $\hbar/\tau$ (triangles) of $Fe_{1-x}Co_xSi$ for two different doping concentrations, and dc resistivities scaled as to overlay the scattering rates (solid curves). From Mena *et al.*, 2006.

The far-infrared reflectivity of Co-doped FeSi samples is suppressed and the scattering increases when magnetic order sets in (Mena *et al.*, 2006) (see Fig. 46). The physics differs in an essential way from that of Ca-doped EuB_6 because FeSi is characterized by a small gap in the density of states and a *nonmagnetic* ground state. It has a large 300 K response to magnetic fields that vanishes as T approaches zero, due to the opening of a correlation gap at low temperature (Schlesinger *et al.*, 1993). The substitution of Co on the Fe site dopes one hole per Co atom, and, contrary to Ca-doped EuB_6, where the pristine material is already ferromagnetic, here the spin-polarized state is created by Co doping (Manyala *et al.*, 2008). Through the exchange interaction the spin polarization deepens the potential wells presented by the randomly distributed Co atoms to the majority spin carriers (Mena *et al.*, 2006). Consequently, the scattering increases (Fig. 46), causing the gradual suppression of the metallic conductivity.

E. Iron pnictides

The iron-based superconductor $LaFeAsO_{1-x}F_x$ discovered by Kamihara *et al.* (2008) opened the way to a new class of materials with interesting magnetic and superconducting properties. The common building block of iron pnictides are layers of edge-shared tetrahedra, where the central Fe atoms are surrounded by four As, P, or Se atoms. Four major groups can be distinguished: (i) 1111 materials with chemical formula *Re*FeAsO (with *Re* = La, Ce, Nd, Pr, or Sm) under electron doping; (ii) 122 materials with chemical formula AFe_2As_2 (with A = Ca, Sr, Ba, or Eu) under hole doping, or, substitution of Fe by Co or Ni (electron doping); (iii) 11 materials of type $FeSe_{1-x}$ and $Fe(Se_{1-x}Te_x)_{0.82}$; and (iv) 111 material LiFeAs. Many other chemically similar compounds with lower superconducting transition temperature were synthesized, including nickelates and phosphorus-based Fe-oxypnictide LaFePO (Ishida *et al.*, 2009).

The parent compounds of the 1111 and 122 iron pnictides are semimetals with an antiferromagnetic transition in the temperature range between 130 and 200 K that is accompanied by a structural transition. Substitutional doping (but also pressure) gradually suppresses the magnetic order and finally the materials become superconducting with T_c's up to 56 K (Z.-A. Ren *et al.*, 2008; H. Chen *et al.*, 2009; Chu *et al.*, 2009; Rotter *et al.*, 2009). Optical experiments by Dong *et al.* (2008) first showed the development of a spin-density wave. However, the nesting affects only part of the Fermi surface, and the systems remain metallic. In the parent compounds, below T_{SDW}, the SDW gap opens around 1000 cm^{-1} with the spectral weight piling up right above; Fig. 47(a) shows the example of $BaFe_2As_2$ (Hu *et al.*, 2008, 2009). A prominent in-plane infrared-active phonon mode, likely connected with orbital ordering, was also observed in a parent compound at 253 cm^{-1} (Akrap *et al.*, 2009; Wu *et al.*, 2009). Besides a large background, a sizable Drude contribution is present at all temperatures and narrows upon cooling. This general feature was confirmed by measurements on $SrFe_2As_2$, $EuFe_2As_2$, and $BaNi_2As_2$ (Z. G. Chen *et al.*, 2009; Hu *et al.*, 2009; Wu *et al.*, 2009; Chen *et al.*, 2010; Wu *et al.*, 2010b). The extended Drude analysis yields a linear behavior of the frequency-dependent scattering rate below

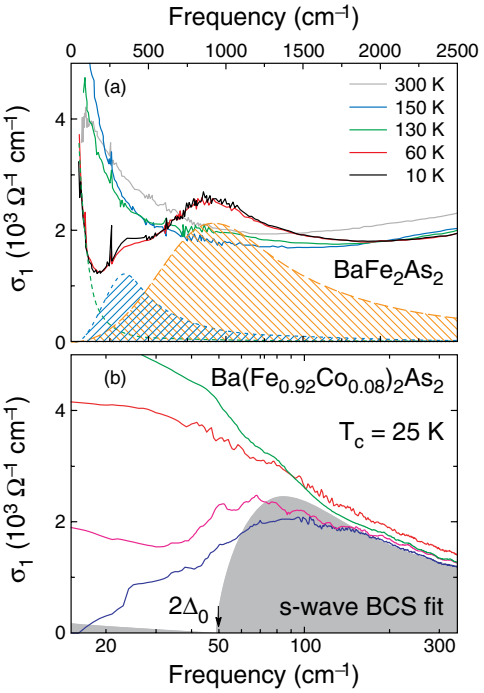

FIG. 47 (color online). (a) Optical conductivity of $BaFe_2As_2$ from room temperature, and across the antiferromagnetic transition around 140 K, down to 10 K. The partial gap due to SDW is clearly visible. Hu *et al.* (2008, 2009) associated the two peaks depicted with the excitations across the SDW gap. (b) Low-frequency conductivity of $Ba(Fe_{0.92}Co_{0.08})_2As_2$ above and below the superconducting transition T_c = 25 K. The curve given by the shaded area is calculated using the theory of Mattis and Bardeen (1958) for the lowest temperature with a gap of $2\Delta_0^{(1)} = 50$ cm^{-1}. From Wu *et al.*, 2010b.

T_{SDW}, indicating an interaction between the charge carriers and spin fluctuations in the spin-density-wave state (Wu *et al.*, 2009; Yang, Hüvonen *et al.*, 2009). For the superconducting compounds, such as $Ba(Fe_{1-x}M_x)_2As_2$, its resistivity follows a T^2 behavior, implying that superconductivity develops out of a Fermi liquid. Optical studies of both LaFePO and $BaFe_2As_2$ (Fig. 1) reveal suppression of the electronic kinetic energy comparable to that of other strongly correlated superconductors including high-T_c cuprates (Qazilbash, Hamlin *et al.*, 2009; Chen *et al.*, 2010), emphasizing the importance of correlation effects in iron pnictides (Haule *et al.*, 2008; Si, 2009).

In accord with theory, most experimental methods evidence a fully gapped superconductor with no nodes of the order parameter. Its symmetry might be a $s_{\pm}$ wave, i.e., reverses sign for electron and hole pockets of the Fermi surface. Reflection experiments (G. Li *et al.*, 2008; Hu *et al.*, 2009; Wu *et al.*, 2010b) and transmission through films (Gorshunov *et al.*, 2010) yield a reduction of the optical conductivity for $T < T_c$. In accordance with ARPES measurements (Evtushinsky *et al.*, 2009) two gaps—different in energy by a factor of 2—in certain parts of the Fermi surface evolve simultaneously below T_c. In Fig. 47(b) the optical conductivity of $Ba(Fe_{0.98}Co_{0.08})_2As_2$ is plotted for various temperatures. It can be sufficiently well described by the BCS theory (shaded area). The missing spectral weight extends up

to $6\Delta \approx 150\ \mathrm{cm}^{-1}$ and according to the Ferrell-Glover-Tinkham sum rule [Eq. (14)], it corresponds to a superconducting density in accord (Wu *et al.*, 2010a) with Homes's scaling plotted in Fig. 26.

VII. ORGANIC AND MOLECULAR CONDUCTORS

Organic ligands are utilized to arrange metal ions in chains similar to $K_2Pt(CN)_4Br_{0.3} \cdot 3H_2O$ (KCP), the canonical example of a one-dimensional metal (Keller, 1975; Schuster, 1975; Kagoshima *et al.*, 1988). In organic solids extended molecules with delocalized π electrons form stacks or layers with orbital overlap in certain directions causing a large anisotropy of the electronic properties (Farge, 1994; Ishiguro *et al.*, 1998; Schwoerer and Wolf, 2007). They serve as model systems for investigating the physics in reduced dimension (Dressel, 2003, 2007; Toyota *et al.*, 2007; Lebed, 2008).

The discovery of the first organic metal TTF-TNCQ in the early 1970s kicked off a broad endeavor to understand the one-dimensional metallic properties as well as the charge-density-wave ground state below 54 K. Optical experiments by Tanner *et al.* (1974, 1976, 1981), and others (Eldridge and Bates, 1983; Eldridge, 1985; Gorshunov *et al.*, 1986; Basista *et al.*, 1990) turned out to be challenging and even today no agreement has been reached about collective modes below $100\ \mathrm{cm}^{-1}$.[38]

A. One-dimensional molecular crystals

In the Bechgaard salts $(TMTSF)_2X$ coherent electronic transport develops along the stacks of tetramethyl-tetraselena-fulvalene molecules; the conduction band is split due to dimerization, yielding a half-filled system. The interaction between the stacks can be varied when selenium is replaced by sulfur or anions X of different size are selected. In the extremely one-dimensional case of $(TMTTF)_2AsF_6$, for instance, Coulomb repulsion drives the system Mott insulating. With increasing interchain coupling, a deconfinement transition occurs to a Luttinger liquid and two-dimensional metal (Biermann *et al.*, 2001; Giamarchi, 2004a, 2004b; Vescoli *et al.*, 1998); it corresponds to a horizontal movement in the phase diagram shown in the inset of Fig. 48(b). Application of pressure is a way to continuously tune the interaction between chains (Pashkin *et al.*, 2006, 2010). Eventually at $p = 12$ kbar $(TMTSF)_2PF_6$ becomes superconducting around $T_c = 1$ K.

The quasi-one-dimensional metal $(TMTSF)_2PF_6$ exhibits a large anisotropy in the plasma frequency of a factor of 10 (see Fig. 48). As first shown by Jacobsen, Mortensen *et al.* (1981), Jacobsen *et al.* (1983), with decreasing temperature the system becomes metallic even in the b direction [development of a plasma edge in Figs. 48(b) and 48(c) compared to Fig. 48(a)], indicating a crossover from a one- to a two-dimensional metal (vertical movement in the phase diagram). At high frequencies ($\hbar\omega > t_\perp$, the transfer integral perpendicular to the chains), the low-temperature optical conductivity follows a power law $\sigma_1(\omega) \propto \omega^{-1.3}$ (Schwartz *et al.*,

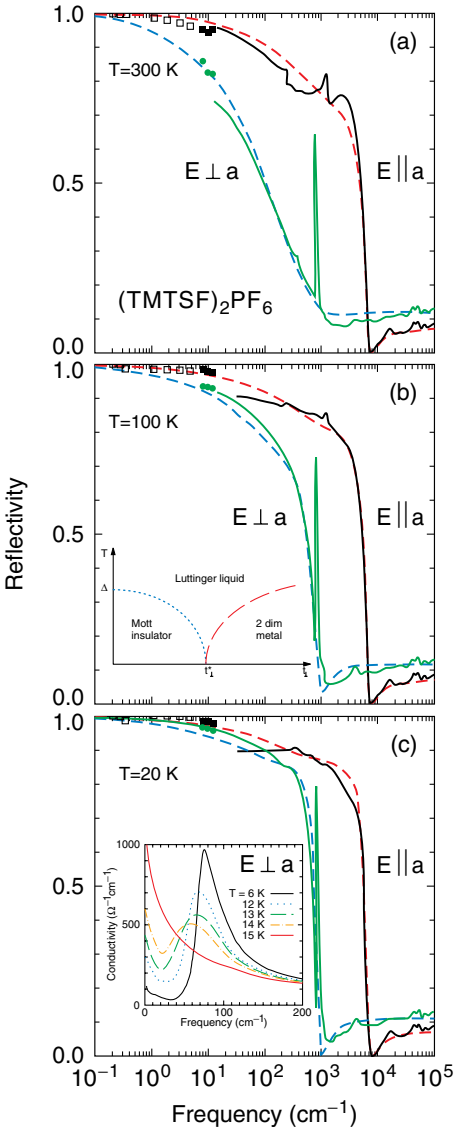

FIG. 48 (color online). (a) Reflectivity spectra of $(TMTSF)_2PF_6$ measured at different temperatures along the stacking axis a and perpendicular to it. The filled symbols are obtained by a coherent source terahertz spectrometer, the open symbols are calculated from microwave experiments (Donovan *et al.*, 1994; Dressel *et al.*, 1996). The dashed lines represent a Drude fit. The inset of (b) shows the schematic phase diagram of the deconfinement transition for a system of weakly coupled conducting chains as suggested by Biermann *et al.* (2001) and Giamarchi (2004b). The transition from a Mott insulator to a two- or three-dimensional metallic state occurs at $T = 0$ when $t_\perp$ reaches a critical value $t_\perp^*$. At high enough temperature, the increase in $t_\perp$ leads to a transition from a Mott-insulating to a one-dimensional Luttinger liquid and further to a dimensional crossover into a metallic state. The development of the SDW gap at 70 cm^{-1} is seen from the low-temperature conductivity $E \perp a$ plotted in the inset of (c). From Degiorgi *et al.*, 1996.

[38]The electrodynamic properties of conducting polymers also continue to attract attention concerning coherent transport (Kohlman *et al.*, 1995; Romijn *et al.*, 2003), CDW instabilities (K. Lee *et al.*, 2000), and solitons and polarons (Kaiser, 2001; Tanner *et al.*, 2004). We skip these topics as well as fullerenes and carbon nanotubes (Wu *et al.*, 2004; Kamaras *et al.*, 2006, 2008), and limit ourselves to the discussion of graphene in Sec. VII.D.

1998) in agreement with transport measurements (Moser *et al.*, 1998; Dressel *et al.*, 2005) and with calculations based on an interacting Luttinger liquid (Giamarchi, 1991, 1997).[39]

At $T_{SDW} = 12$ K $(TMTSF)_2PF_6$ enters a SDW state with a sharp increase in resistivity due to the opening of an energy gap over the entire Fermi surface (Jacobsen, Mortensen *et al.*, 1981; Dressel *et al.*, 2005).[40] Degiorgi *et al.* (1996) discovered a single-particle gap around $2\Delta = 70$ cm^{-1} in the optical properties (Henderson *et al.*, 1999; Vescoli *et al.*, 1999) as shown in the inset of Fig. 48(c). In addition collective excitations of the SDW are observed along the nesting vector leading to a pinned mode resonance in the microwave range (Donovan *et al.*, 1994; Petukhov and Dressel, 2005). It does not make up for the spectral weight lost upon entering the insulating state at T_{SDW}.

B. *MX* chains

Halogene-bridged metal complexes forming -*M*-*X*-*M*-*X*- linear chains constitute one-dimensional Peierls-Hubbard systems, where the electron-phonon interaction, the electron transfer, and the on-site and intersite Coulomb repulsion energies compete and cooperate with one another. In $[Ni(chxn)_2Br]Br_2$ (chxn = cylohexanediamine), for instance, four nitrogen atoms of two ligand units coordinating a Ni ion [cf. Fig. 49(a)] produce such a strong ligand field that the Ni^{3+} ion is in a low-spin state with an unpaired electron in the d_{z^2} orbital. The strong on-site Coulomb repulsion among the Ni 3*d* electrons causes a Mott-Hubbard gap (~ 5 eV) with the occupied Br 4*p* band located inside. Thus the lowest-energy electronic excitation goes from the Br 4*p* band to the Ni 3*d* upper Hubbard band indicated by the sharp absorption band around 1.3 eV as shown by Takaishi and Yamishita (2008). For *M* = Pd and Pt the ionic radius is larger and thus the electron-electron interaction is weak compared to the electron-lattice interaction. The bridging halogen ions are distorted from midpoint between the neighboring two metal ions, giving rise to the CDW states or $M^{II}M^{IV}$ mixed-valence states (-M^{II}-$XM^{IV}X$-M^{II}-). Accordingly, the half-filled metallic bands split by a finite Peierls gap into the occupied valence bands and the unoccupied conduction bands. The compounds exhibit unique optical and dynamical properties, such as dichroic and intense intervalence charge-transfer bands (Tanaka *et al.*, 1984), resonance Raman spectra (Clark, 1983, 1990), luminescences with large Stokes shift (Tanino and Kobayashi, 1983), and midgap absorptions attributable to the solitons and polarons (Okamoto *et al.*, 1992; Okamoto and Yamashita, 1998).

1. Mott insulators

Iwano *et al.* (2002) explained the small Raman Stokes shift observed in the nickel-chain compound by a suppression

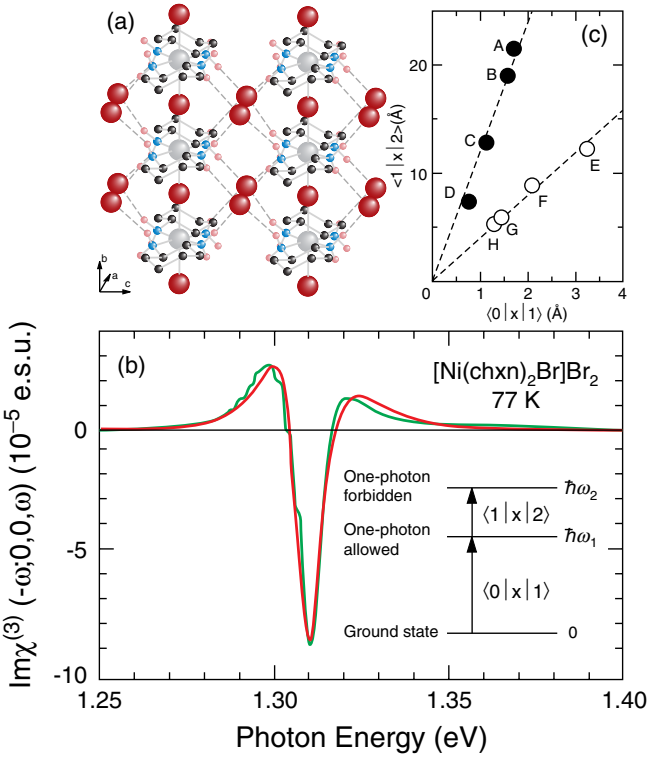

FIG. 49 (color online). (a) Arrangement of the Ni and Br ions along chains in $[Ni(chxn)_2Br]Br_2$ leads to an overlap of the Ni $3d_{x^2}$ and Br $4p_z$ orbitals. From Takaishi and Yamishita, 2008. (b) $\mathrm{Im}\chi^{(3)}(-\omega;0,0,\omega)$ spectra of $[Ni(chxn)_2Br]Br_2$ at $T = 77$ K. The lines are the experimental and calculated results. The energy levels are sketched in the lower panel. (c) Relation between the transition dipole moments of $\langle 0|x|1\rangle$ and $\langle 1|x|2\rangle$ for one-dimensional Mott insulators [solid circles: A, $[Ni(chxn)_2Br]Br_2$; B, $[Ni(chxn)_2Cl]Cl_2$; C, $[Ni(chxn)_2Cl](NO_3)_2$; D, Sr_2CuO_3) compared to other one-dimensional materials]; [empty circles: E, $[Pt(en)_2][Pt(en)_2I_2](ClO_4)_4$; F, $[Pt(en)_2][Pt(en)_2Br_2](ClO_4)_4$; G, $[Pt(en)_2][Pt(en)_2Cl_2](ClO_4)_4$; H, polydihexylsilane (PDHS)]. From Kishida *et al.*, 2000.

of the electron-lattice interaction, in agreement with dynamical density-matrix renormalization-group calculations incorporating lattice fluctuations (Iwano, 2006). The dominance of strong electronic correlations enhances the nonlinear optical properties, including the third-order susceptibility $\chi^{(3)}$ (Kishida *et al.*, 2000; Ono *et al.*, 2004) shown in Fig. 49(b). The main reasons are the small energy splitting of about 10 meV between the two excited states ω_1 and ω_2 and the large transition dipole moments $\langle 0|x|1\rangle$ and $\langle 1|x|2\rangle$ between the ground state $|0\rangle$, the one-photon allowed state $|1\rangle$, and the one-photon forbidden state $|2\rangle$; here $\langle 1|x|2\rangle$ describes the spatial extension of the electron-hole wave function in the excited state, as shown in Fig. 49(c). Thus one-dimensional Mott insulators have a larger potential for nonlinear optical devices than one-dimensional band insulators, such as silicon polymers and Peierls insulators of π-conjugated polymers (Takaishi and Yamishita, 2008).

When $[Ni(chxn)_2Br]Br_2$ is irradiated by light, electrons are excited, leading to an enhancement of the Drude-like low-energy component in the optical conductivity

[39]It is interesting to note that in one-dimensional Cu-O chains of $YBa_2Cu_3O_{7-\delta}$ a similar power law was observed (Lee *et al.*, 2004; Y.-S. Lee *et al.*, 2005). See also Sec. III.E.

[40]Similar investigations have been performed on various sister compounds $(TMTSF)_2X$ (Jacobsen *et al.*, 1983; Ng *et al.*, 1984, 1985; Eldridge and Bates, 1986; Kornelsen *et al.*, 1987).

immediately after photoirradiation as demonstrated by Iwai *et al.* (2003) and shown in Fig. 50. This suggests a Mott transition by photodoping with an ultrashort lifetime $t_d =$ 0.5 ps of the metallic state. For very low excitation density x_{ph} of about 10^{-3} photon per Ni site a midgap absorption is observed around 0.4–0.5 eV. Following the analysis of chemical-doped Mott insulators, the effective number of carriers $N_{eff}(\omega)$ is obtained by integrating the optical conductivity to the measurement frequency ω. This yields the total spectral-weight transfer from the charge-transfer band to the innergap region and indicates that the photoinduced midgap absorption is due solely to electron-type charge carriers since the hole-type carriers are localized by electron-lattice interaction. Interestingly, the palladium-chain compounds remain insulating with a finite optical gap even after photoexcitation (Yonemitsu and Nasu, 2008).

Theoretical studies using one- and two-band extended Peierls-Hubbard models deal with ground state, excitation spectrum, and the nonlinear optical properties of MX chains (Gammel *et al.*, 1992; Weber-Milbrodt *et al.*, 1992; Saxena *et al.*, 1997). Other platium-halide ladder compounds are treated by a multiband extended Peierls-Hubbard Hamiltonian to reproduce the optical spectra (Yamamoto and Ohara, 2007).

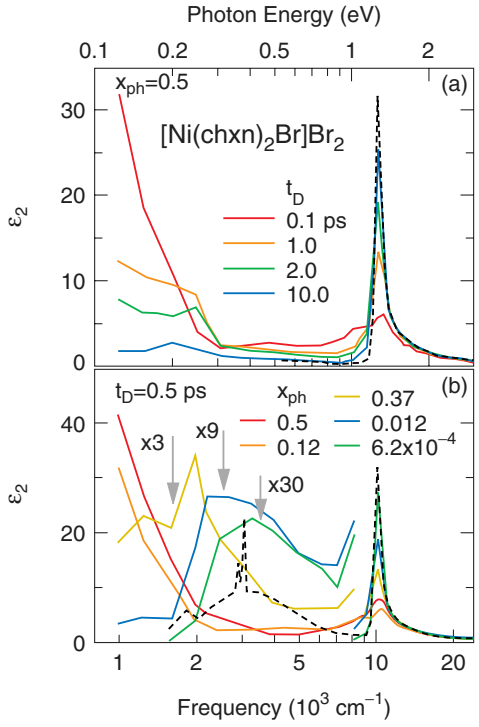

FIG. 50 (color online). Room-temperature spectra of the imaginary part of the dielectric constant ϵ_2 of $[Ni(chxn)_2Br]Br_2$. (a) Data are taken prior to the photoexcitation (dashed line) and at delay times t_d after the photoexcitation (solid lines) with an excitation density x_{ph} is 0.5 photon per Ni site. The polarization of the pump and probe is parallel to the chain axis. (b) Dependence of $\epsilon_2(\omega)$ on the excitation density as indicated ($t_d = 01$ ps). The dotted line shows the spectrum before the photoexcitation obtained by direct measurements of the polarized absorption. From Iwai *et al.*, 2003.

2. Peierls systems

$[Pt(en)_2][Pt(en)_2Br_2] \cdot (PF_6)_4$ (en = ethylene-diamine) shows both the periodic charge disproportionation (mixed valence, commensurate CDW) and the periodic bond-length distortion (Peierls distortion) as shown in Fig. 51(a). Femtosecond impulsive excitation causes a coherent oscillation at the ground-state vibrational frequency of 180 cm^{-1} [known from Raman experiments (Love *et al.*, 1993)] and its harmonics. In addition, a self-trapped excition state is observed at 110 cm^{-1} (Dexheimer *et al.*, 2000a, 2000b). The phase of this rapidly damped component shifts systematically with detection wavelength changing by ~180° between 830 and 940 nm. Using even shorter pulses (5 fs) transmission measurements reveal low-frequency modes around 60–70 cm^{-1} assigned to asymmetric vibrational modes of the self-trapped excition state (Araoka *et al.*, 2007). Similar findings have been made by time-resolved reflectivity (Sugita *et al.*, 2001) and luminescence spectroscopy (Tomimoto *et al.*, 2002) on various PtX chains with $X =$ Cl, Br, or I with an decrease in lifetime from 30 to 0.65 ps.

Recent investigations by ultrafast laser pulses could establish low-dimensional organic compounds as model

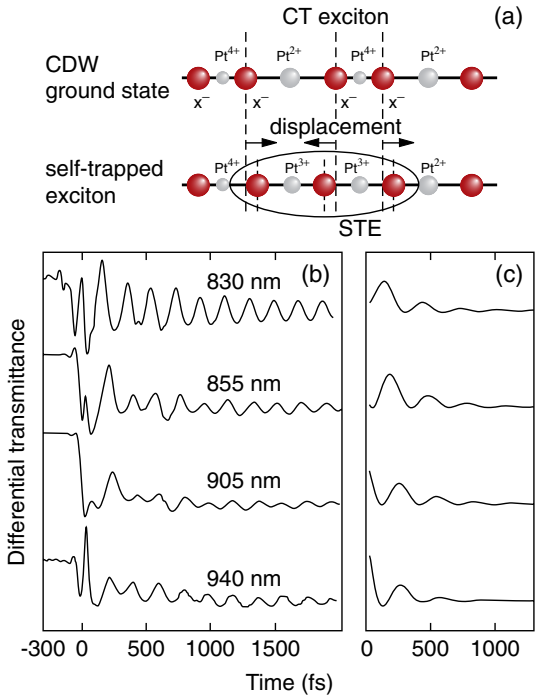

FIG. 51 (color online). (a) Schematic of the linear chain in a halogen bridged Pt complex. In the ground state a charge density is commensurately modulated; a self-trapped exciton is formed in the excited state (Suemoto and Tomimoto, 2002). (b) Time-resolved differential transmittance of $[Pt(en)_2][Pt(en)_2Br_2] \cdot (PF_6)_4$ following excitation of the intervalence charge-transfer band with 35 fs pulses centered at 800 nm. Measurements were taken at a series of detection wavelengths selected from a broadband femtosecond continuum. (c) The sum of the low-frequency component and the zero-frequency component extracted by linear prediction and singular value decomposition, showing the excited state contributions to the response and the systematic phase shift of the wave packet oscillation with detection wavelength. From Dexheimer *et al.*, 2000b.

compounds for photoinduced phase transitions, as discussed in Sec. IV.E.

C. Two-dimensional molecular crystals

Among the layered organic crystals, bis-(ethylenedithio) tetrathiafulvalene (BEDT-TTF) molecules are of paramount interest due to their versatility of forming (super-)conducting salts with different anions in a large variety of patterns (Mori, 1998, 1999; Mori *et al.*, 1999; Mori, 2000). The fine-tuning of molecular interactions provides the possibility to study bandwidth controlled Mott transitions, the interplay of charge order and superconductivity, etc. (Dressel and Drichko, 2004).[41]

1. Mott insulator versus Fermi liquid

The κ-phase BEDT-TTF compounds, for instance, form an anisotropic triangular lattice; the upper band is half filled leading to a Mott transition when U/W exceeds some critical value. The antiferromagnetic insulating ground state is next to superconductivity with the maximum T_c of 14 K which triggered numerous theoretical studies (Powell and McKenzie, 2005; Watanabe *et al.*, 2006; Powell and McKenzie, 2007; Clay *et al.*, 2008; Mazumdar and Clay, 2008; Peters and Pruschke, 2009). The optical spectra are dominated by a strong charge-transfer band in the midinfrared and electron-molecular vibrational (emv) coupled modes (Eldridge *et al.*, 1991; Kornelsen *et al.*, 1991b, 1992). These excitations can be separated from contributions of the itinerant electrons (Faltermeier *et al.*, 2007; Dressel *et al.*, 2009) giving insight into the dynamics of charge carriers at the verge of localization. Replacing Cl by Br in the anion layer of κ-(BEDT-TTF)$_2$Cu[N(CN)$_2$]Br$_x$Cl$_{1-x}$ serves as chemical pressure that increases the bandwidth. As shown in Fig. 52(a), spectral weight is redistributed from high to low frequencies as the Mott transition is approached at $x \approx 0.7$; a similar shift is caused by temperature. The effective mass of the quasiparticles also increases considerably; at low frequencies the scattering rate follows a $1/\tau(\omega) \propto \omega^2$ behavior (Dumm *et al.*, 2009) in accordance with the quadratic temperature dependence of the resistivity (Dressel *et al.*, 1997; Yasin, 2008).

A dynamical mean field theory treatment of the relevant Hubbard model gives a good quantitative description of the experimental data as shown in Fig. 52. The calculations are performed on a frustrated square lattice at half filling taking the nearest-neighbor hopping amplitudes to be $t_2 = -0.03$ eV and $t_1 = 0.8t_2$ (as known from band-structure calculations) that leads to a noninteracting bandwidth of $W \approx 0.3$ eV, comparable to values from density functional theory calculations (Merino and McKenzie, 2000; Merino *et al.*, 2008; Dumm *et al.*, 2009).

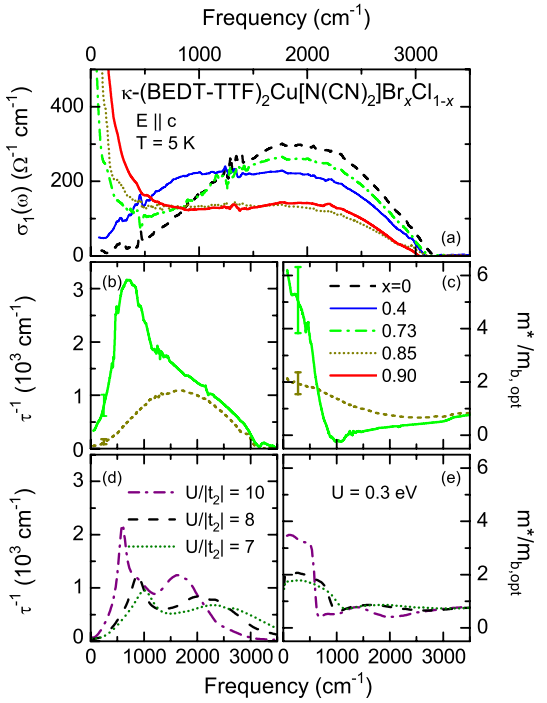

FIG. 52 (color online). (a) Low-temperature optical conductivity of κ-(BEDT-TTF)$_2$Cu[N(CN)$_2$]Br$_x$Cl$_{1-x}$ for different Br content x, which serves as chemical pressure and decreases the effective Coulomb interaction U/W. The contributions from intradimer transitions and vibrational modes are subtracted; the $\sigma_1(\omega)$ spectra plotted here represent the correlated charge carriers. (b), (c) The frequency dependence of the scattering rate and effective mass extracted from an extended Drude model analysis of the conductivity (a). (d), (e) The corresponding results of DMFT calculations plotted for different U/W and $T = 50$ K. Clearly as the Mott-insulating phase is approached, the effective mass and the scattering rate increase significantly. From Merino *et al.*, 2008; Dumm *et al.*, 2009.

Sasaki *et al.* (2007, 2008) suggested that the Mott insulator κ-(BEDT $-$ TTF)$_2$Cu[N(CN)$_2$]Cl can be effectively doped by charge carriers when irradiated by x rays. Considerable spectral weight is transferred from the midinfrared region to low frequencies as the Mott gap collapses with increasing irradiation time as shown in Fig. 53. Nevertheless, no Drude-like peak is present even after 590 h at a dose of 0.5 MGy/h, suggesting that the crystals transform to a weakly disordered metal.

2. Charge order and superconductivity

In the A_2B stoichiometry the conduction band is quarter filled when the BEDT-TTF molecules are not arranged in dimers. Because of strong intersite Coulomb repulsion V, the materials are subject to an electronically driven charge order (Calandra *et al.*, 2002; Seo *et al.*, 2004, 2006), which (besides NMR and x-ray scattering) can be seen from the splitting of the charge-sensitive intramolecular BEDT-TTF vibrations. Raman and infrared investigations can quantitatively estimate the charge disproportionation and yield information on the charge-order pattern (Yamamoto *et al.*, 2002; Wojciechowski *et al.*, 2003; Musfeldt *et al.*, 2005; Drichko *et al.*, 2009).

[41]The search for indications of a superconducting gap in the optical properties (Kornelsen *et al.*, 1991a; Ugawa and Tanner, 2000) led to success only recently (Drichko *et al.*, 2002, 2010). There is some debate on whether the organic superconductor follows the universal scaling presented in Fig. 26 (Pratt and Blundell, 2005).

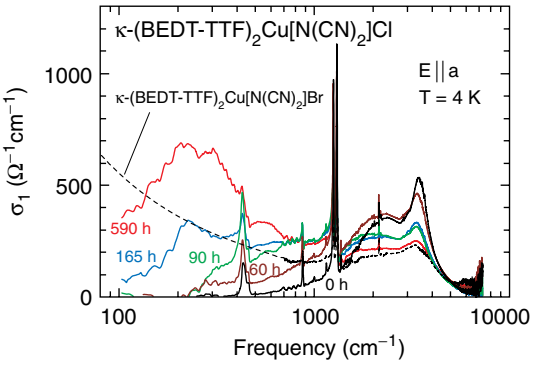

FIG. 53 (color online). Low-temperature optical conductivity of κ-(BEDT-TTF)$_2$Cu[N(CN)$_2$]Cl before and after x-ray irradiation. The dashed curve represents $\sigma_1(\omega)$ of the nonirradiated κ-(BEDT-TTF)$_2$Cu[N(CN)$_2$]Br. From Sasaki *et al.*, 2008.

Mori, Tanaka, and Mori (1998), Mori, Tanaka, Mori, and Kobayashi (1998), and Mori *et al.* (1995) introduced the θ-(BEDT-TTF)$_2MM'$(SCN)$_4$ family for which by variation of the metal ions M and M' the transfer integrals t_1 and t_2 can be chosen in such a way that horizontal and vertical charge-order patterns form [cf. Fig. 54(a)]. While θ-(BEDT-TTF)$_2$CsZn(SCN)$_4$ remains metallic down to 20 K, the Drude contribution to the optical response of θ-(BEDT-TTF)$_2$RbCo(SCN)$_4$ vanishes upon passing through the charge-order transition at 190 K, and the spectrum becomes semiconductorlike, as shown in Fig. 54 (Tajima

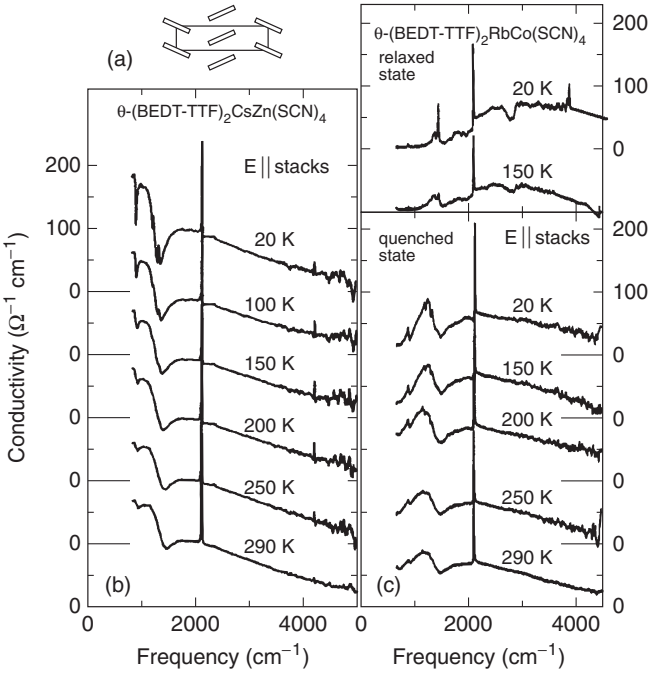

FIG. 54. (a) The structural arrangement of the θ phase reveals two stacks of BEDT-TTF molecules in a herringbone fashion. Optical conductivity of (b) θ-(BEDT-TTF)$_2$CsZn(SCN)$_4$ and (c) θ-(BEDT-TTF)$_2$RbCo(SCN)$_4$ measured along the stacks (c axis) for different temperatures. The charge-ordered state in the latter is only reached when slowly cooled (0.1 K/min), for rapid cooling (1 K/min) the crystal remains metallic (Tajima *et al.*, 2000). The curves for different temperatures are displaced.

et al., 2000); similar results are obtained for θ-(BEDT-TTF)$_2$RbZn(SCN)$_4$.

Within the two-dimensional conducting layer, the organic BEDT-TTF molecules are arranged in stacks which are more or less coupled; hence the charge disproportionation in the stacks can form certain patterns of stripes. The actual arrangement of horizontal, vertical, or diagonal stripes very much depends upon the interplay of the different interactions. A detailed understanding needs to go beyond a pure electronic model because coupling of the charge order to the underlying lattice has to be taken into account (Tanaka and Yonemitsu, 2007, 2008; Miyashita and Yonemitsu, 2008; Tanaka and Yonemitsu, 2009). These effects are weak in the α compounds where the molecular rearrangement is small compared with those in the θ phase. Their photoinduced dynamics studied by femtosecond reflection spectroscopy (Tajima *et al.*, 2005; Iwai *et al.*, 2007, 2008) are qualitatively different: θ-(BEDT-TTF)$_2$RbZn(SCN)$_4$ exhibits local melting of the charge order and ultrafast recovery, while α-α-(BEDT-TTF)$_2$I$_3$ exhibits critical slowing down.

Comprehensive optical studies on metallic compounds in the vicinity of the charge-ordered phase (by varying V/W) reveal the development of a pseudogap, charge-order fluctuations, and collective charge-order excitations which are coupled to lattice vibrations (Dressel *et al.*, 2003, 2004; Drichko, Dressel, Kuntscher *et al.*, 2006, Drichko, Dressel, Merino *et al.*, 2006, Drichko *et al.*, 2010). Evidence has accumulated that charge-order fluctuations induce superconductivity in these organic charge-ordered systems similar to $Na_{0.35}CoO_2 \cdot 1.3H_2O$ (Merino and McKenzie, 2001; Greco *et al.*, 2005; Watanabe and Ogata, 2005, 2006). Changing the band filling beyond one-quarter results in a strong increase in the spectral weight of the Drude term (Drichko *et al.*, 2005, 2007).

D. Graphene

Apart from organic conductors reviewed in Secs. VII.A–VII.C, hallmarks of electronic correlations are found in a variety of carbon-based systems. Examples include Luttinger liquid behavior of carbon nanotubes (Bockrath *et al.*, 1999) and polymers (Yuen *et al.*, 2009) as well as a Mott-Hubbard state in A_4C_{60} (A = Na, K, Rb, or Cs) (Knupfer and Fink, 1997). Graphene—a one-atom-thick sheet of carbon—is emerging as an extremely interesting electronic system to investigate the role of correlations and many-body physics in optical and transport properties (Peres *et al.*, 2006; Neto *et al.*, 2009). The "relativistic" nature of the quasiparticles in graphene, albeit with a speed of propagation 300 times smaller than the speed of light, is expected to give rise to unusual spectroscopic, transport, and thermodynamic properties that are at odds with the standard Fermi-liquid theory of metals (González *et al.*, 1999; Polini *et al.*, 2007; Sarma *et al.*, 2007).

Electronic phenomena in single-layered and multilayered graphene can be readily altered by applied voltage. Importantly, the interaction of electrons and holes with each other and with the honeycomb lattice also can be controlled by the gate voltage (Goerbig *et al.*, 2007; Neto and Guinea, 2007; Yan *et al.*, 2007; Kuzmenko, Benfatto *et al.*, 2009).

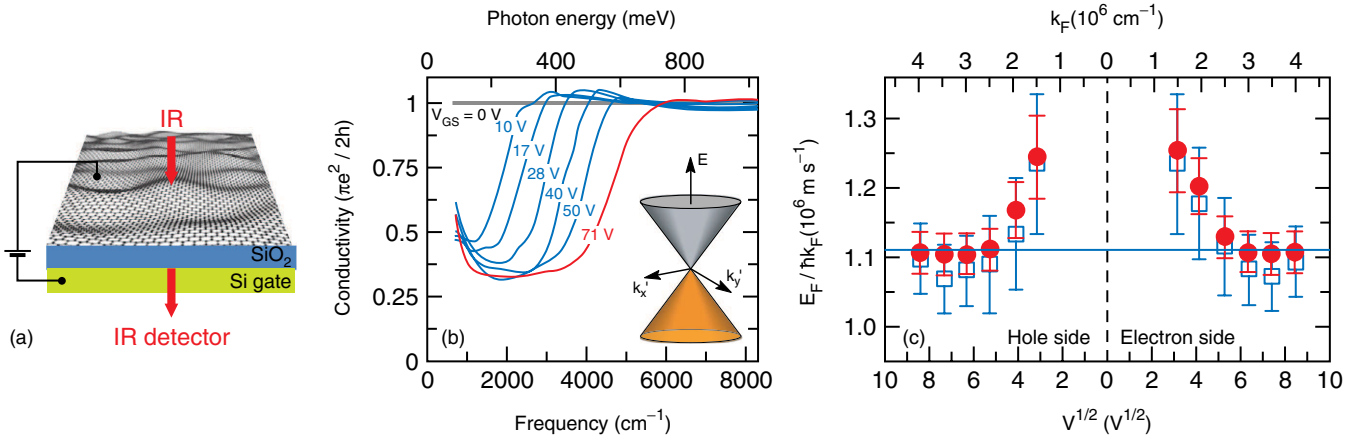

FIG. 55 (color online). (a) Schematic of graphene-based gated structure. (b) The optical conductivity of graphene extracted from $R(\omega)$ and $T(\omega)$ synchrotron-based microscopy for various gate voltages. The threshold feature is due to interband transitions at $2E_F$ shown schematically in the inset. (c) Magnitude of v_F extracted from the conductivity data in (b). An enhancement of v_F at small biases is indicative of many-body effects in graphene as discussed in the text. From Z. Q. Li *et al.*, 2008.

Interactions among "massless" Dirac quasiparticles in graphene are of fundamental interest and are also of relevance for the understanding of superconductivity with relatively high transition temperature in various other forms of carbon including nanotubes, doped C_{60} crystals, doped diamond, as well as graphite intercalation compounds. Spectroscopic investigations of graphene physics, to a large extent, rely on measurements of gated structures. Infrared experiments of the gated structures are relatively scarce in view of the technical complexity of monitoring subtle changes of properties in ultrathin accumulation and depletion layers. Following the pioneering work for Si MOSFETs (metal–oxide–semiconductor field-effect transistor) (Tsui, 1978), infrared studies of gated devices were extended to field effect transistors with active elements made of polymers (Brown *et al.*, 2001; Li *et al.*, 2006), molecular crystals (Fischer *et al.*, 2006; Li *et al.*, 2007), oxides (J. Kim *et al.*, 2008; Qazilbash, Li *et al.*, 2008), and most recently graphene.

In charge-neutral monolayer graphene the Fermi energy is located exactly between the two linearly dispersing cones characteristic of Dirac quasiparticles. This dispersion leads to the frequency-independent conductivity leveling at the universal value (Ando *et al.*, 2002; Gusynin and Sharapov, 2006; Peres *et al.*, 2006; Kuzmenko *et al.*, 2008; Mak *et al.*, 2008; Nair *et al.*, 2008; Li *et al.*, 2009). Infrared data taken under applied gate voltage V_g revealed significant modification of optical properties consistent with the expectations based on the electronic structure (Wang *et al.*, 2008; Li *et al.*, 2009). The dominant feature of the conductivity data (see Fig. 55) is a formation of a threshold feature in $\sigma_1(\omega, V_g)$ that systematically hardens with the increase of V_g. This form of the conductivity is consistent with the notion of Pauli blocking: Direct interband transitions between the bottom and top cones are prohibited by momentum conservation for $\hbar\omega < 2E_F$.

The spectral weight lost from the region below $2E_F$ is transferred to the Drude conductivity due to mobile Dirac quasiparticles in partially filled bands. The Pauli blocking in graphene is not complete and substantial absorption can be recognized in the data down to the lowest frequencies. At least in part the residual response can be attributed to impurities and interaction with phonons (Stauber *et al.*, 2008). A different proposal accounts for Pauli-prohibited absorption within the marginal Fermi-liquid theory of Dirac quasiparticles (Grushin *et al.*, 2009) originally proposed to explain anomalous scattering processes in high-T_c superconductors. Residual absorption observed in single-layer graphene is also found in bilayer graphene samples (Zhang *et al.*, 2008; Kuzmenko, van Heumen *et al.*, 2009; Li *et al.*, 2009). A new property of the latter systems is a gate-induced energy gap between the valence and conduction bands revealed by recent experiments (Kuzmenko, Crassee *et al.*, 2009; Mak *et al.*, 2009; Y. Zhang *et al.*, 2009).

The evolution of the $2E_F$ feature with V_g allows one to probe the Fermi velocity of Dirac quasiparticles. Experiments are in accord with nearly linear variation of $2E_F(V_g)$ implied by the linear dispersion with $v_F \simeq (1.12\text{–}1.2) \times 10^6$ ms^{-1}. However, at small biases one witnesses a systematic enhancement of v_F. Thus, in graphene, Coulomb interaction favors electron and hole delocalization offering an intriguing counterexample to properties of most other systems discussed in this review, where strong interactions typically impede electronic transport. The Fermi velocity in graphene can be independently obtained from infrared studies of cyclotron resonance (Deacon *et al.*, 2007; Jiang *et al.*, 2007; Henriksen *et al.*, 2008). These latter experiments carried out for both single-layer and bilayer graphene yield v_F which is enhanced by 20%–30% compared to that of the bulk graphite.

The renormalization of v_F is interesting in the context of electronic correlations in graphene since it can be attributed to Coulomb interaction of Dirac quasiparticles (González *et al.*, 1999). A salient feature of magneto-optics data for both single-layer and bilayer graphene is the violation to the Kohn theorem (Kohn, 1961). The theorem predicts only a negligible role of the electron-electron interaction in the properties of conventional 2D electron gas with quadratic dispersion but appears to be violated for the linearly dispersing Dirac quasiparticles. The theoretical analysis of cyclotron resonance absorption of graphene supports the notion of strong electron-electron interaction (Iyengar *et al.*, 2007; Bychkov and Martinez, 2008).

Several reported studies of both zero-field and high magnetic-field response of epitaxial graphene (Sadowski *et al.*, 2006; Dawlaty *et al.*, 2008; Plochocka *et al.*, 2008; Choi *et al.*, 2009). One potential problem with the quantitative interpretation of these latter data is that epitaxial graphene obtained through high-temperature thermal decomposition of SiC substrates is not continuous and in addition reveals substantial variation of thickness along wafers.

VIII. OUTLOOK

The hypothesis of Mott and Peierls (1937) on the paramount role of the Coulomb interaction in insulating behavior of NiO and other unconventional insulators has proven to be accurate. Arguably, Mott-Hubbard insulators present the best understood example of a strongly correlated system. Optical experiments have made preeminent contributions toward establishing an experimental picture of these materials through direct measurements of the energy gap and detailed studies of the spectral weight redistribution with doping (see Sec. IV.A). An in-depth understanding of the parent insulating systems is a precondition for the description of some of the most enigmatic effects in *doped* Mott insulators including unconventional superconductivity and ferromagnetism accompanied with colossal magnetoresistance. A similar level of understanding is yet to be achieved for conducting-doped Mott insulators.

The term optical as applied in this review to the electrodynamic response of complex correlated materials should be understood colloquially since investigations of the frequency-dependent response readily extend from microwaves through terahertz and IR to UV. Largely due to technical innovations in the 1990s and 2000s, femtosecond studies of correlated matter have now become commonplace. The parameter space of optical investigations of correlated materials often limited to temperature during the not so distance past is now beginning to include high pressure, static and pulsed magnetic fields, and nanoscale spatial resolution. The breadth of applicability of ''optical methods'' to investigate correlations is further highlighted by important insights rapidly obtained for newly discovered materials such as graphene and iron pnictides.

Several highlights are as follows:

(1) The formation of a conducting state in a correlated insulator is associated with the development of low-energy spectral weight at the expense of suppression of excitations in the charge-transfer and/or U region. Optical tools enable a comprehensive inquiry into this behavior revealing common physics between oxide and organic Mott systems.

(2) Sum rule analysis of the optical conductivity provides a potent experimental method to classify complex materials based on the strength of their correlations (Fig. 1). The development of low-energy spectral weight with doping that can be determined with the help of sum rules yields a reliable estimate of W/U for a correlated material (see Secs. V and VII.C).

(3) The analysis of optical constants offers detailed information on renormalization of effective masses and Fermi velocities for electrons or holes in a correlated host. The energy dependence of these renormalized quantities is most valuable for uncovering the fundamental interactions ultimately responsible for renormalizations in oxides, heavy-fermion, and organic systems.

(4) Several classes of doped correlated materials become superconducting. Infrared optics allows one to measure both the energy gap and the superfluid density tensor. Relatively small values of the superfluid density are believed to be an essential aspect of superconductivity of synthetic conductors also pointing to the prominence of phase fluctuations in these systems. Advances in the experimental precision and reproducibility of optical spectroscopy have made it possible to routinely obtain detailed spectra of the glue to which the electrons near the Fermi energy are coupled (see Sec. III.F). Correlations between the glue spectra and T_c are being established.

(5) Optical methods have shown that the gross features of both Kondo insulating and heavy-fermion behavior are understood with the Anderson lattice model. New measurements extending data to the very far-IR and microwave regions uncovered systematic deviations from this model, some of which are captured by DMFT analysis (see Sec. VI).

(6) Pump-probe spectroscopy of correlated electron materials has made considerable headway during the past decade. This has primarily been through the judicious application of femtosecond studies to all of the material classes discussed in this review coupled with developments in generating short pulses through the far to midinfrared portions of the spectrum. Initial experiments suggest that the sensitivity of correlated materials to external perturbations makes them promising candidates to investigate the physics of photo-induced phase transitions (see Sec. IV.E).

(7) Frequency-domain spectroscopy rests upon a well-developed theoretical foundation (see Sec. II.C) with DMFT emerging as a powerful tool to calculate the optical response of correlated electron materials. The qualitative agreement of the main experimental spectral features with DMFT calculations for Hubbard-like and Kondo-like systems is an important step forward (see Fig. 5). Of perhaps even greater importance is its combination with (*ab initio*) structure, such as LDA calculations and the potential for quantitative material-specific predictions with the first encouraging successes V_2O_3 [see Fig. 24(b)] and $CeIrIn_5$ (see Fig. 44).

One challenge for future work, of course, is to advance our basic understanding of the role of correlations with the longer term view toward developing, in conjunction with theory, predictive capabilities of the electronic properties of specific materials. As the understanding of correlated electron materials advances hand in hand with the ability to synthesize new materials with specific properties, it will be crucial to investigate possible technological applications. The sensitivity of numerous correlated electron materials to external

perturbations would seem to be of some promise for applications ranging from novel switches to chemical sensors. Recent examples in this direction include oxide heterostructures (see Fig. 39) and graphene (see Fig. 55). Time-integrated and time-resolved optical spectroscopy will undoubtedly play an important role toward investigating potential applications as has been the case in characterizing semiconductor heterostructures and devices.

Apart from predictive capabilities it is imperative to develop ways to tune and control properties of correlated materials. Again, oxide heterostructures offer some interesting approaches. A 2D electron gas at interfaces can have high mobility and can be gated. Recent advances enable local control of this 2D gas using scanning probes techniques to write real-space structures. Memory effects are equally appealing for applications and control. For example, it has only recently been demonstrated that ferromagnetics can be demagnetized on a subpicosecond time scale using femtosceond pulses (Beaurepaire *et al.*, 1996; Kimel *et al.*, 2005; Koopmans *et al.*, 2005; Bigot *et al.*, 2009; G. P. Zhang *et al.*, 2009). The ramification of such a possibility is under active investigation and includes the possibility of ultrafast memory storage. It can be envisioned that, in a similar vein, interesting possibilities exist in correlated materials including multiferroics and organics.

There are nascent experimental techniques that build on the intellectual and technological developments associated with ''conventional'' optical spectroscopy that are of considerable promise for future studies of electronic correlations. For example, as discussed in Sec. V.F, electronic phase separation and intrinsic (or extrinsic) inhomogeneities are of considerable importance. Spatially resolved optical probes provide an exciting approach in the study of electronic phase separation complementing well-developed techniques such as scanning-probe tunneling spectroscopy. In the future, it will be important to broaden the spectral range over which such studies can be carried out and also to extend nanoscopy to cryogenic temperatures.

To date, the majority of time-resolved optical experiments have been limited to pumping in the 1.5–3.0 eV range, leading to a cascade of scattering processes as highly energetic quasiparticles relax to low-energy states which can (though not always) result in a fairly indirect and uncontrolled way to perturb a material. However, the development of intense pulses at lower photon energies (mid-IR to terahertz pulses) will help to alleviate this issue. For example, interesting experiments on semiconductors have probed the nonequilibrium physics of polarons and, in the future, resonant excitation of superconductors with intense terahertz pulses at the gap energy will likely provide new insights into their nonequilibrium properties. Further, as discussed in Sec. IV.E on photoinduced phase transitions, high intensity coupled with spectral agility provides the ability to pump phonon modes with a view toward vibrational excitation and control of the electronic properties of complex materials. These pump-probe studies may also provide means to manipulate components of the pairing glue in novel superconductors. There is also a need to increase the sensitivity of time-resolved experiments as this directly translates to the ability to photexcite at lower fluences. This is important in the investigation of materials with low transition temperatures and in delicately probing the dynamics within a given phase of particular material. We also stress that the theoretical underpinnings of time-domain spectroscopy of correlated electron materials is far less developed and, while presenting a considerable challenge, offers numerous opportunities. This includes, as examples, basic questions ranging from the information content of time-resolved spectroscopy in comparison to steady-state spectroscopy to the physics of photodoping-induced phase transitions.

Increased spatial and temporal resolution of optical probes enables experiments away from steady-state and homogeneous samples. These previously unattainable regimes may require a revision of basic ideas behind an optical probe of phenomena introduced within a conventional description of electrons in the momentum space. Progress with the studies of inhomogeneous systems critically relies on advances enabling one to deal with the spatial variation of properties literally at the nanoscale. Ultrashort pulses of extreme intensity changes our common understanding of electronic excitations in the frequency domain. For optics this means to reconsider many fundamental issues, including but not limited to locality, equilibrium, linearity, and Kramers-Kronig consistency.

ACKNOWLEDGMENTS

Over the past years we had the privilege of working with a large number of collaborators, postdocs, and students and their contributions strongly influenced many parts of this review. We had many valuable discussions with colleagues on different occasions and we want to thank all of them. D. B. received support from the Alexander von Humboldt Foundation during his stay in Stuttgart. We also want to acknowledge support from the National Science Foundation (NSF), the Department of Energy (DOE), the Airforce Office of Scientific Research (AFOSR), the Office of Naval Research (ONR), the Electronics and Telecommunications Research Institute (ETRI), the Deutsche Forschungsgemeinschaft (DFG), the Swiss National Science Foundation, and the National Center of Competence in Research (MaNEP).

REFERENCES

Abanov, A., and A. V. Chubukov, 2004, Phys. Rev. B **70**, 100504.

Abbamonte, P., G. Blumberg, A. Rusydi, A. Gozar, P. Evans, T. Siegrist, L. Venema, H. Eisaki, E. Isaacs, and G. Sawatzky, 2004, Nature (London) **431**, 1078.

Abrikosov, A. A., L. P. Gor'kov, and I. Y. Dsyaloshinskii, 1963, *Methods of Quantum Field Theory in Statistical Physics* (Prentice-Hall, Englewood).

Aeppli, G., and Z. Fisk, 1992, Comments Condens. Matter Phys. **16**, 155.

Agranovich, V., 2009, *Excitations in Organic Solids* (Oxford University Press, Oxford).

Agranovich, V. M., and V. L. Ginzburg, 1984, *Crystal Optics with Spatial Dispersion and the Theory of Excitons* (Springer-Verlag, Berlin), 2nd ed.

Aguilar, R. V., M. Mostovoy, A. B. Sushkov, C. L. Zhang, Y. J. Choi, S.-W. Cheong, and H. D. Drew, 2009, Phys. Rev. Lett. **102**, 047203.

Aguilar, R. V., A. B. Sushkov, C. L. Zhang, Y. J. Choi, S.-W. Cheong, and H. D. Drew, 2007, Phys. Rev. B **76**, 060404.

Ahmad, J., and H. Uwe, 2005, Phys. Rev. B **72**, 125103.

Ahn, C. H., *et al.*, 2006, Rev. Mod. Phys. **78**, 1185.

Ahn, K. H., M. J. Graf, S. A. Trugman, J. Demsar, R. D. Averitt, J. L. Sarrao, and A. J. Taylor, 2004, Phys. Rev. B **69**, 045114.

Aji, V., and C. Varma, 2007, Phys. Rev. Lett. **99**, 067003.

Akrap, A., J. J. Tu, L. J. Li, G. H. Cao, Z. A. Xu, and C. C. Homes, 2009, Phys. Rev. B **80**, 180502.

Alberi, K., K. M. Yu, P. R. Stone, O. D. Dubon, W. Walukiewicz, T. Wojtowicz, X. Liu, and J. K. Furdyna, 2008, Phys. Rev. B **78**, 075201.

Alexander, M. N., and D. F. Holcomb, 1968, Rev. Mod. Phys. **40**, 815.

Alexandrov, A. S., and A. M. Bratkovsky, 1999, Phys. Rev. B **60**, 6215.

Alexandrov, A. S., and P. E. Kornilovitch, 1999, Phys. Rev. Lett. **82**, 807.

Alexandrov, A. S., and N. F. Mott, 1995, *Polarons and Bipolarons* (World Scientific, Singapore).

Allen, J. W., and J. C. Mikkelsen, 1977, Phys. Rev. B **15**, 2952.

Allen, P. B., 1971, Phys. Rev. B **3**, 305.

Allen, P. B., 1987, Phys. Rev. Lett. **59**, 1460.

Alloul, H., J. Bobroff, M. Gabay, and P. J. Hirschfeld, 2009, Rev. Mod. Phys. **81**, 45.

Ambrosch-Draxl, C., and J. O. Sofob, 2006, Comput. Phys. Commun. **175**, 1.

Andersen, O. K., O. Jepsen, A. I. Liechtenstein, and I. I. Mazin, 1994, Phys. Rev. B **49**, 4145.

Anderson, P. W., 1959, J. Phys. Chem. Solids **11**, 26.

Anderson, P. W., 1997, Phys. Rev. B **55**, 11785.

Anderson, P. W., 2007, Science **316**, 1705.

Ando, T., Y. Zheng, and H. Suzuura, 2002, J. Phys. Soc. Jpn. **71**, 1318.

Anisimov, V., A. Poteryaev, M. Korotin, A. Anokhin, and G. Kotliar, 1997, J. Phys. Condens. Matter **9**, 7359.

Anisimov, V. I., R. Hlubina, M. A. Korotin, V. V. Mazurenko, T. M. Rice, A. O. Shorikov, and M. Sigrist, 2002, Phys. Rev. Lett. **89**, 257203.

Anisimov, V. I., J. Zaanen, and O. K. Andersen, 1991, Phys. Rev. B **44**, 943.

Antonov, V. N., B. N. Harmon, and A. N. Yaresko, 2002a, Phys. Rev. B **66**, 165208.

Antonov, V. N., B. N. Harmon, and A. N. Yaresko, 2002b, Phys. Rev. B **66**, 165209.

Araoka, F., A. Ozawa, D. Kawakami, S. Takaishi, M. Yamashita, and T. Kobayashi, 2007, Phys. Rev. B **75**, 224304.

Arcangeletti, E., L. Baldassarre, D. D. Castro, S. Lupi, L. Malavasi, C. Marini, A. Perucchi, and P. Postorino, 2007, Phys. Rev. Lett. **98**, 196406.

Ashcroft, N. W., and N. D. Mermin, 1976, *Solid State Physics* (Saunders College Publishing, Fort Worth).

Aspnes, D. E., 1982, Am. J. Phys. **50**, 704.

Aubin, H., C. A. Marrache-Kikuchi, A. Pourret, K. Behnia, L. Bergé, L. Dumoulin, and J. Lesueur, 2006, Phys. Rev. B **73**, 094521.

Averitt, R. D., A. I. Lobad, C. Kwon, S. A. Trugman, V. K. Thorsmolle, and A. J. Taylor, 2001, Phys. Rev. Lett. **87**, 017401.

Averitt, R. D., G. Rodriguez, A. I. Lobad, J. L. W. Siders, S. A. Trugman, and A. J. Taylor, 2001, Phys. Rev. B **63**, 140502.

Averitt, R. D., and A. J. Taylor, 2002, J. Phys. Condens. Matter **14**, R1357.

Averitt, R. D., V. K. Thorsmolle, Q. X. Jia, S. A. Trugman, and A. J. Taylor, 2002, Physica (Amsterdam) **312B–313B**, 86.

Awschalom, D. D., and M. E. Flatté , 2007, Nature Phys. **3**, 153.

Axt, V., and T. Kuhn, 2004, Rep. Prog. Phys. **67**, 433.

Baeriswyl, D., J. Carmelo, and A. Luther, 1986, Phys. Rev. B **33**, 7247.

Baeriswyl, D., C. Gros, and T. M. Rice, 1987, Phys. Rev. B **35**, 8391.

Baldassarre, L., A. Perucchi, E. Arcangeletti, D. Nicoletti, D. D. Castro, P. Postorino, V. A. Sidorov, and S. Lupi, 2007, Phys. Rev. B **75**, 245108.

Baldassarre, L., *et al.*, 2008, Phys. Rev. B **77**, 113107.

Baraduc, C., A. El Azrak, and N. Bontemps, 1996, J. Supercond. **9**, 3.

Bardeen, J., L. N. Cooper, and J. R. Schrieffer, 1957, Phys. Rev. **108**, 1175.

Barker, A. S., B. I. Halperin, and T. M. Rice, 1968, Phys. Rev. Lett. **20**, 384.

Barker, A. S., and J. P. Remeika, 1970, Solid State Commun. **8**, 1521.

Barker, A. S., H. W. Verleur, and H. J. Guggenheim, 1966, Phys. Rev. Lett. **17**, 1286.

Basista, H., D. A. Bonn, T. Timusk, J. Voit, D. Jérome, and K. Bechgaard, 1990, Phys. Rev. B **42**, 4088.

Basov, D. N., B. Dabrowski, and T. Timusk, 1998, Phys. Rev. Lett. **81**, 2132.

Basov, D. N., C. C. Homes, E. J. Singley, M. Strongin, T. Timusk, G. Blumberg, and D. van der Marel, 2001, Phys. Rev. B **63**, 134514.

Basov, D. N., R. Liang, D. A. Bonn, W. N. Hardy, B. Dabrowski, M. Quijada, D. B. Tanner, J. P. Rice, D. M. Ginsberg, and T. Timusk, 1995, Phys. Rev. Lett. **74**, 598.

Basov, D. N., R. Liang, B. Dabrowski, D. A. Bonn, W. N. Hardy, and T. Timusk, 1996, Phys. Rev. Lett. **77**, 4090.

Basov, D. N., H. A. Mook, B. Dabrowski, and T. Timusk, 1995, Phys. Rev. B **52**, R13141.

Basov, D. N., A. V. Puchkov, R. A. Hughes, T. Strach, J. Preston, T. Timusk, D. A. Bonn, R. Liang, and W. N. Hardy, 1994, Phys. Rev. B **49**, 12165.

Basov, D. N., E. J. Singley, and S. V. Dordevic, 2002, Phys. Rev. B **65**, 054516.

Basov, D. N., and T. Timusk, 2005, Rev. Mod. Phys. **77**, 721.

Basov, D. N., T. Timusk, B. Dabrowski, and J. D. Jorgensen, 1994, Phys. Rev. B **50**, 3511.

Basov, D. N., S. I. Woods, A. S. Katz, E. J. Singley, R. C. Dynes, M. Xu, D. G. Hinks, C. C. Homes, and M. Strongin, 1999, Science **283**, 49.

Bassi, M., P. Camagni, R. Rolli, G. Samoggia, F. Parmigiani, G. Dhalenne, and A. Revcolevschi, 1996, Phys. Rev. B **54**, R11030.

Baturina, T. I., A. Y. Mironov, V. M. Vinokur, M. R. Baklanov, and C. Strunk, 2007, Phys. Rev. Lett. **99**, 257003.

Baturina, T. I., C. Strunk, M. R. Baklanov, and A. Satta, 2007, Phys. Rev. Lett. **98**, 127003.

Baum, P., D.-S. Yang, and A. H. Zewail, 2007, Science **318**, 788.

Beaurepaire, E., J. Merle, A. Daunois, and J. Bigot, 1996, Phys. Rev. Lett. **76**, 4250.

Belitz, D., and W. Götze, 1981, Philos. Mag. B **43**, 517.

Belitz, D., and T. R. Kirkpatrick, 1994, Rev. Mod. Phys. **66**, 261.

Belitz, D., T. R. Kirkpatrick, and T. Vojta, 2005, Rev. Mod. Phys. **77**, 579.

Benfatto, L., J. P. Carbotte, and F. Marsiglio, 2006, Phys. Rev. B **74**, 155115.

Benfatto, L., and S. G. Sharapov, 2006, Low Temp. Phys. **32**, 533.

Benfatto, L., S. G. Sharapov, N. Andrenacci, and H. Beck, 2005, Phys. Rev. B **71**, 104511.

Berg, E., E. Fradkin, E.-A. Kim, S. A. Kivelson, V. Oganesyan, J. M. Tranquada, and S. C. Zhang, 2007, Phys. Rev. Lett. **99**, 127003.
Bernhard, C., D. Munzar, A. Wittlin, W. König, A. Golnik, C. T. Lin, M. Kläser, T. Wolf, G. Müller-Vogt, and M. Cardona, 1999, Phys. Rev. B **59**, R6631.
Bethe, H., 1928, Ann. Phys. (Leipzig) **392**, 55.
Bi, X.-X., P. C. Eklund, and J. M. Honig, 1993, Phys. Rev. B **48**, 3470.
Biermann, S., A. Georges, A. Lichtenstein, and T. Giamarchi, 2001, Phys. Rev. Lett. **87**, 276405.
Biermann, S., A. Poteryaev, A. I. Lichtenstein, and A. Georges, 2005, Phys. Rev. Lett. **94**, 026404.
Bigot, J.-Y., M. Vomir, and E. Beaurepaire, 2009, Nature Phys. **5**, 515.
Bloch, F., 1929, Z. Phys. **57**, 545.
Blumberg, G., P. Littlewood, A. Gozar, B. Dennis, N. Motoyama, H. Eisaki, and S. Uchida, 2002, Science **297**, 584.
Blümer, N., 2002, Ph.D. thesis (Universität Augsburg).
Bockrath, M., D. Cobden, J. Lu, A. Rinzler, R. Smalley, T. Balents, and P. McEuen, 1999, Nature (London) **397**, 598.
Bogdanov, P. V., *et al.*, 2000, Phys. Rev. Lett. **85**, 2581.
Bommeli, F., L. Degiorgi, P. Wachter, F. B. Anders, and A. V. Mitin, 1997, Phys. Rev. B **56**, R10001.
Bonn, D., R. Klassen, J. Garrett, T. Timusk, J. Smith, and Z. Fisk, 1988, Physica (Amsterdam) **153C–155C**, 453.
Bonn, D. A., 2006, Nature Phys. **2**, 159.
Bonn, D. A., J. D. Garrett, and T. Timusk, 1988, Phys. Rev. Lett. **61**, 1305.
Boris, A., N. Kovaleva, O. Dolgov, T. Holden, C. Lin, B. Keimer, and C. Bernhard, 2004, Science **304**, 708.
Brinkman, W. F., and T. M. Rice, 1970, Phys. Rev. B **2**, 4302.
Broderick, S., B. Ruzicka, L. Degiorgi, H. R. Ott, J. L. Sarrao, and Z. Fisk, 2002, Phys. Rev. B **65**, 121102.
Broun, D. M., W. A. Huttema, P. J. Turner, S. Özcan, B. Morgan, R. Liang, W. N. Hardy, and D. A. Bonn, 2007, Phys. Rev. Lett. **99**, 237003.
Brown, P. J., H. Sirringhaus, M. Harrison, M. Shkunov, and R. H. Friend, 2001, Phys. Rev. B **63**, 125204.
Bruggeman, D. A. G., 1935, Ann. Phys. (Leipzig) **416**, 636.
Bucher, B., Z. Schlesinger, P. C. Canfield, and Z. Fisk, 1994, Phys. Rev. Lett. **72**, 522.
Burch, K. S., D. D. Awschalom, and D. N. Basov, 2008, J. Magn. Magn. Mater. **320**, 3207.
Burch, K. S., S. V. Dordevic, F. P. Mena, A. B. Kuzmenko, D. van der Marel, J. L. Sarrao, J. R. Jeffries, E. D. Bauer, M. B. Maple, and D. N. Basov, 2007, Phys. Rev. B **75**, 054523.
Burch, K. S., D. B. Shrekenhamer, E. J. Singley, J. Stephens, B. L. Sheu, R. K. Kawakami, P. Schiffer, N. Samarth, D. D. Awschalom, and D. N. Basov, 2006, Phys. Rev. Lett. **97**, 087208.
Burch, K. S., E. J. Singley, J. Stephens, R. K. Kawakami, D. D. Awschalom, and D. N. Basov, 2005, Phys. Rev. B **71**, 125340.
Burch, K. S., J. Stephens, R. K. Kawakami, D. D. Awschalom, and D. N. Basov, 2004, Phys. Rev. B **70**, 205208.
Buron, M., and E. Collet, 2005, J. Phys. Conf. Ser. **21**.
Buzdin, A. I., 2005, Rev. Mod. Phys. **77**, 935.
Bychkov, Y. A., and G. Martinez, 2008, Phys. Rev. B **77**, 125417.
Caimi, G., A. Perucchi, L. Degiorgi, H. R. Ott, V. M. Pereira, A. H. C. Neto, A. D. Bianchi, and Z. Fisk, 2006, Phys. Rev. Lett. **96**, 016403.
Calandra, M., and O. Gunnarsson, 2003, Europhys. Lett. **61**, 88.
Calandra, M., J. Merino, and R. McKenzie, 2002, Phys. Rev. B **66**, 195102.
Caldwell, T., A. P. Reyes, W. G. Moulton, P. L. Kuhns, M. J. Hoch, P. Schlottmann, and Z. Fisk, 2007, Phys. Rev. B **75**, 075106.
Callaghan, A., C. W. Moeller, and R. Ward, 1966, Inorg. Chem. **5**, 1572.
Calvani, P., 2001, Riv. Nuovo Cimento Soc. Ital. Fis. **24**, 1.
Calvani, P., M. Capizzi, F. Donato, S. Lupi, P. Maselli, and D. Peschiaroli, 1993, Phys. Rev. B **47**, 8917.
Cao, G., S. McCall, M. Shepard, J. E. Crow, and R. P. Guertin, 1997, Phys. Rev. B **56**, 321.
Cappelluti, E., S. Ciuchi, and S. Fratini, 2007, Phys. Rev. B **76**, 125111.
Caprara, S., M. Grilli, C. D. Castro, and T. Enss, 2007, Phys. Rev. B **75**, 140505.
Carbotte, J., and E. Schachinger, 2004, Phys. Rev. B **70**, 014517.
Carbotte, J., and E. Schachinger, 2006, Ann. Phys. (N.Y.) **15**, 585.
Carbotte, J. P., 1990, Rev. Mod. Phys. **62**, 1027.
Carbotte, J. P., E. Schachinger, and D. N. Basov, 1999, Nature (London) **401**, 354.
Cardona, M., 1969, *Modulation Spectroscopy* (Academic Press, Berlin).
Carr, G. L., R. Lobo, J. LaVeigne, D. H. Reitze, and D. B. Tanner, 2000, Phys. Rev. Lett. **85**, 3001.
Carr, G. L., S. Perkowitz, and D. B. Tanner, 1985, *Far Infrared Properties of Inhomogeneous Materials*, edited by K. J. Button, Infrared and Millimeter Waves Vol 13 (Academic Press, Orlando), pp. 171–263.
Carter, S. A., T. F. Rosenbaum, P. Metcalf, J. M. Honig, and J. Spalek, 1993, Phys. Rev. B **48**, 16 841.
Cásek, P., C. Bernhard, J. Humlíek, and D. Munzar, 2005, Phys. Rev. B **72**, 134526.
Cavalleri, A., T. Dekorsy, H. Chong, J. Kieffer, and R. Schoenlein, 2004, Phys. Rev. B **70**, 161102.
Cavalleri, A., M. Rini, H. H. W. Chong, S. Fourmaux, T. E. Glover, P. A. Heimann, J. C. Keiffer, and R. W. Schoenlein, 2005, Phys. Rev. Lett. **95**, 067405.
Cavalleri, A., C. Toth, C. W. Siders, J. A. Squier, F. Raksi, P. Forget, and J. C. Keiffer, 2001, Phys. Rev. Lett. **87**, 237401.
Cépas, O., K. Kakurai, L. P. Regnault, T. Ziman, J. P. Boucher, N. Aso, M. Nishi, H. Kageyama, and Y. Ueda, 2001, Phys. Rev. Lett. **87**, 167205.
Cépas, O., and T. Ziman, 2004, Phys. Rev. B **70**, 024404.
Chakhalian, J., *et al.*, 2006, Nature Phys. **2**, 244.
Chakhalian, J., J. W. Freeland, H.-U. Habermeier, G. Cristiani, G. Khaliullin, M. van Veenendaal, and B. Keimer, 2007, Science **318**, 1114.
Chakravarty, S., 2008, Science **319**, 735.
Chakravarty, S., H.-Y. Kee, and E. Abrahams, 1999, Phys. Rev. Lett. **82**, 2366.
Chekalin, S., V. Farztdinov, V. Golovlyov, V. Letokhov, Y. Lozovik, Y. Matveets, and A. Stepanov, 1991, Phys. Rev. Lett. **67**, 3860.
Chemla, D., and J. Shah, 2001, Nature (London) **411**, 549.
Chen, C.-X., and H.-B. Schüttler, 1991, Phys. Rev. B **43**, 3771.
Chen, F., B. Gorshunov, G. Cristiani, H. Habermeier, and M. Dressel, 2004, Solid State Commun. **131**, 295.
Chen, H., *et al.*, 2009, Europhys. Lett. **85**, 17 006.
Chen, H.-T., S. Kraatz, G. C. Cho, and R. Kersting, 2004, Phys. Rev. Lett. **93**, 267401.
Chen, Z. G., G. Xu, W. Z. Hu, X. D. Zhang, P. Zheng, G. F. Chen, J. L. Luo, Z. Fang, and N. L. Wang, 2009, Phys. Rev. B **80**, 094506.
Chen, Z. G., R. H. Yuan, T. Dong, and N. L. Wang, 2010, Phys. Rev. B **81**, 100502(R).
Cheong, S.-W., and M. Mostovoy, 2007, Nature Mater. **6**, 13.
Chia, E., J.-X. Zhu, D. Talbayev, R. D. Averitt, A. J. Taylor, K.-H. Oh, I.-S. Jo, and S.-I. Lee, 2007, Phys. Rev. Lett. **99**, 147008.

Chia, E. E. M., J.-X. Zhu, H. J. Lee, N. O. Morena, E. D. Bauer, T. Durakiewicz, R. D. Averitt, J. L. Sarrao, and A. J. Taylor, 2006, Phys. Rev. B **74**, 140409.
Choi, H., F. Borondics, D. A. Siegel, S. Y. Zhou, M. C. Martin, A. Lanzara, and R. A. Kaindl, 2009, Appl. Phys. Lett. **94**, 172102.
Choi, H. J., D. Roundy, H. Sun, M. L. Cohen, and S. G. Louie, 2002, Nature (London) **418**, 758.
Choi, H. S., J. S. Ahn, J. H. Jung, T. W. Noh, and D. H. Kim, 1996, Phys. Rev. B **54**, 4621.
Chu, J.-H., J. G. Analytis, C. Kucharczyk, and I. R. Fisher, 2009, Phys. Rev. B **79**, 014506.
Civelli, M., M. Capone, S. S. Kancharla, O. Parcollet, and G. Kotliar, 2005, Phys. Rev. Lett. **95**, 106402.
Clark, R. J. H., 1983, Adv. Infrared Raman Spectrosc. **11**, 95.
Clark, R. J. H., 1990, Chem. Soc. Rev. **19**, 107.
Clay, R. T., H. Li, and S. Mazumdar, 2008, Phys. Rev. Lett. **101**, 166403.
Cohen-Tannoudji, C., 2004, *Atoms in Electromagnetic Fields*, World Scientific Series on Atomic, Molecular and Optical Physics Vol. 3 (World Scientific, Singapore), 2nd ed.
Coleman, P., 1987, Phys. Rev. Lett. **59**, 1026.
Coleman, P., and A. J. Schofield, 2005, Nature (London) **433**, 28.
Cooper, S. L., 2001, Structure and Bonding (Berlin) **98**, 161.
Corson, J., R. Mallozzi, J. Orenstein, and J. N. Eckstein, 1999, Nature (London) **398**, 221.
Crandles, D. A., T. Timusk, and J. E. Greedan, 1991, Phys. Rev. B **44**, 13 250.
Crane, R., N. P. Armitage, A. Johansson, G. Sambandamurthy, D. Shahar, and G. Grüner, 2007, Phys. Rev. B **75**, 184530.
Crane, R. W., N. P. Armitage, A. Johansson, G. Sambandamurthy, D. Shahar, and G. Grüner, 2007, Phys. Rev. B **75**, 094506.
Cubrovic, M., J. Zaanen, and K. Schalm, 2009, Science **325**, 439.
Curnoe, S., and K. A. Kikoin, 2000, Phys. Rev. B **61**, 15 714.
Dagotto, E., 1994, Rev. Mod. Phys. **66**, 763.
Dagotto, E., 2003, *Nanoscale Phase Separation and Colossal Magnetoresistance* (Springer-Verlag, Berlin).
Dagotto, E., 2005, Science **309**, 257.
Dagotto, E., A. Moreo, F. Ortolani, J. Riera, and D. J. Scalapino, 1992, Phys. Rev. B **45**, 10 107.
Damascelli, A., Z. Hussain, and Z.-X. Shen, 2003, Rev. Mod. Phys. **75**, 473.
Damascelli, A., C. Presura, D. van der Marel, J. Jegoudez, and A. Revcolevschi, 2000, Phys. Rev. B **61**, 2535.
Damascelli, A., K. Schulte, D. van der Marel, and A. A. Menovsky, 1997, Phys. Rev. B **55**, R4863.
Damascelli, A., D. van der Marel, M. Grüninger, C. Presura, T. T. M. Palstra, J. Jegoudez, and A. Revcolevschi, 1998, Phys. Rev. Lett. **81**, 918.
Damascelli, A., D. van der Marel, F. Parmigiani, G. Dhalenne, and A. Revcolevschi, 1997, Phys. Rev. B **56**, R11373.
Dawlaty, J. M., S. Shivaraman, J. Strait, P. George, M. Chandrashekhar, F. Rana, M. G. Spencer, D. Veksler, and Y. Chen, 2008, Appl. Phys. Lett. **93**, 131905.
Deacon, R. S., K.-C. Chuang, R. J. Nicholas, K. S. Novoselov, and A. K. Geim, 2007, Phys. Rev. B **76**, 081406.
Degiorgi, L., 1999, Rev. Mod. Phys. **71**, 687.
Degiorgi, L., F. Anders, and G. Grüner, 2001, Eur. Phys. J. B **19**, 167.
Degiorgi, L., M. Dressel, G. Grüner, P. Wachter, N. Sato, and T. Komatsubara, 1994, Europhys. Lett. **25**, 311.
Degiorgi, L., M. Dressel, A. Schwartz, B. Alavi, and G. Grüner, 1996, Phys. Rev. Lett. **76**, 3838.
Degiorgi, L., E. Felder, H. R. Ott, J. L. Sarrao, and Z. Fisk, 1997, Phys. Rev. Lett. **79**, 5134.
Degiorgi, L., M. B. Hunt, H. R. Ott, M. Dressel, B. J. Feenstra, G. Grüner, Z. Fisk, and P. Canfield, 1994, Europhys. Lett. **28**, 341.
Degiorgi, L., E. J. Nicol, O. Klein, G. Grüner, P. Wachter, S.-M. Huang, J. Wiley, and R. B. Kaner, 1994, Phys. Rev. B **49**, 7012.
Deisenhofer, J., I. Leonov, M. V. Eremin, C. Kant, P. Ghigna, F. Mayr, V. V. Iglamov, V. I. Anisimov, and D. van der Marel, 2008, Phys. Rev. Lett. **101**, 157406.
Dekorsy, T., H. Auer, H. J. Bakker, H. G. Roskos, and H. Kurz, 1996, Phys. Rev. B **53**, 4005.
Demsar, J., R. D. Averitt, K. H. Ahn, M. J. Graf, S. A. Trugman, V. V. Kabanov, J. L. Sarrao, and A. J. Taylor, 2003a, Phys. Rev. Lett. **91**, 027401.
Demsar, J., R. Hudej, J. Karpinski, V. Kabanov, and D. Mihailovic, 2001, Phys. Rev. B **63**, 054519.
Demsar, J., V. K. T. lle, J. L. Sarrao, and A. J. Taylor, 2006, Phys. Rev. Lett. **96**, 037401.
Demsar, J., B. Podobnik, V. V. Kabanov, T. Wolf, and D. Mihailovic, 1999, Phys. Rev. Lett. **82**, 4918.
Demsar, J., J. L. Sarrao, and A. J. Taylor, 2006, J. Phys. Condens. Matter **18**, R281.
Demsar, J., V. Thorsmolle, J. Sarrao, and A. Taylor, 2006, Phys. Rev. Lett. **96**, 037401.
Demsar, J., *et al.*, 2003b, Phys. Rev. Lett. **91**, 267002.
Denev, S., and D. W. Snoke, 2002, Phys. Rev. B **65**, 085211.
Derr, J., G. Knebel, D. Braithwaite, B. Salce, J. Flouquet, K. Flachbart, S. Gabáni, and N. Shitsevalova, 2008, Phys. Rev. B **77**, 193107.
Devereaux, T. P., and R. Hackl, 2007, Rev. Mod. Phys. **79**, 175.
Devreese, J., and J. Tempere, 1998, Solid State Commun. **106**, 309.
Devreese, J. T., L. F. Lemmens, and J. Van Royen, 1977, Phys. Rev. B **15**, 1212.
Dexheimer, S. L., A. D. Van Pelt, J. A. Brozik, and B. I. Swanson, 2000a, J. Phys. Chem. A **104**, 4308.
Dexheimer, S. L., A. D. Van Pelt, J. A. Brozik, and B. I. Swanson, 2000b, Phys. Rev. Lett. **84**, 4425.
Dodge, J. S., C. P. Weber, J. Corson, J. Orenstein, Z. Schlesinger, J. W. Reiner, and M. R. Beasley, 2000a, Phys. Rev. Lett. **85**, 4932.
Dodge, J. S., C. P. Weber, J. Corson, J. Orenstein, Z. Schlesinger, J. W. Reiner, and M. R. Beasley, 2000b, Phys. Rev. Lett. **85**, 4932.
Doiron-Leyraud, N., C. Proust, D. LeBoeuf, J. Levallois, J.-B. Bonnemaison, R. Liang, D. A. Bonn, W. N. Hardy, and L. Taillefer, 2007, Nature (London) **447**, 565.
Dolgov, O., and S. Shulga, 1995, J. Supercond. **8**, 611.
Donev, E. U., R. Lopez, L. C. Feldman, and R. F. Haglund, Jr., 2009, Nano Lett. **9**, 702.
Dong, J., *et al.*, 2008, Europhys. Lett. **83**, 27 006.
Doniach, S., 1977, Physica (Amsterdam) **91B**, 231.
Donovan, S., Y. Kim, L. Degiorgi, M. Dressel, G. Grüner, and W. Wonneberger, 1994, Phys. Rev. B **49**, 3363.
Donovan, S., A. Schwartz, and G. Grüner, 1997, Phys. Rev. Lett. **79**, 1401.
Dordevic, S. V., D. N. Basov, N. R. Dilley, E. D. Bauer, and M. B. Maple, 2001, Phys. Rev. Lett. **86**, 684.
Dordevic, S. V., D. N. Basov, R. C. Dynes, and E. Bucher, 2001, Phys. Rev. B **64**, 161103.
Dordevic, S. V., K. S. D. Beach, N. Takeda, Y. J. Wang, M. B. Maple, and D. N. Basov, 2006, Phys. Rev. Lett. **96**, 017403.
Dordevic, S. V., C. C. Homes, J. J. Tu, T. Valla, M. Strongin, P. D. Johnson, G. D. Gu, and D. N. Basov, 2005, Phys. Rev. B **71**, 104529.
Dordevic, S. V., S. Komiya, Y. Ando, Y. J. Wang, and D. N. Basov, 2005, Phys. Rev. B **71**, 054503.

Dordevic, S. V., E. J. Singley, D. N. Basov, S. Komiya, Y. Ando, E. Bucher, C. C. Homes, and M. Strongin, 2002, Phys. Rev. B **65**, 134511.
Dressel, M., 2003, Naturwissenschaften **90**, 337.
Dressel, M., 2007, Naturwissenschaften **94**, 527.
Dressel, M., and N. Drichko, 2004, Chem. Rev. **104**, 5689.
Dressel, M., N. Drichko, and S. Kaiser, 2010, Physica (Amsterdam) **470C**, S589.
Dressel, M., N. Drichko, J. Schlueter, O. Bogdanova, E. Zhilyaeva, R. Lyubovskaya, A. Greco, and J. Merino, 2004, J. Phys. IV France **114**, 183.
Dressel, M., N. Drichko, J. Schlueter, and J. Merino, 2003, Phys. Rev. Lett. **90**, 167002.
Dressel, M., D. Faltermeier, M. Dumm, N. Drichko, B. Petrov, V. Semkin, R. Vlasova, C. Meźière, and P. Batail, 2009, Physica (Amsterdam) **404B**, 541.
Dressel, M., B. Gorshunov, N. Kasper, B. Nebendahl, M. Huth, and H. Adrian, 2000, J. Phys. Condens. Matter **12**, L633.
Dressel, M., B. Gorshunov, N. Sluchanko, A. Volkov, W. Henderson, B. Alavi, G. Grüner, G. Knebel, A. Loidl, and S. Kunii, 1999, Phys. Status Solidi B **215**, 161.
Dressel, M., and G. Grüner, 2002, *Electrodynamics of Solids: Optical Properties of Electrons in Matter* (Cambridge University Press, Cambridge, UK).
Dressel, M., G. Grüner, J. E. Eldridge, and J. M. Williams, 1997, Synth. Met. **85**, 1503.
Dressel, M., N. Kasper, K. Petukhov, B. Gorshunov, G. Grüner, M. Huth, and H. Adrian, 2002, Phys. Rev. Lett. **88**, 186404.
Dressel, M., N. Kasper, K. Petukhov, D. N. Peligrad, B. Gorshunov, M. Jourdan, M. Huth, and H. Adrian, 2002, Phys. Rev. B **66**, 035110.
Dressel, M., K. Petukhov, B. Salameh, P. Zornoza, and T. Giamarchi, 2005, Phys. Rev. B **71**, 075104.
Dressel, M., and M. Scheffler, 2006, Ann. Phys. (Leipzig) **15**, 535.
Dressel, M., A. Schwartz, G. Grüner, and L. Degiorgi, 1996, Phys. Rev. Lett. **77**, 398.
Drichko, N., M. Dressel, C. Kuntscher, A. Pashkin, A. Greco, J. Merino, and J. Schlueter, 2006, Phys. Rev. B **74**, 235121.
Drichko, N., M. Dressel, J. Merino, A. Greco, and J. Schlueter, 2006, J. Low Temp. Phys. **142**, 345.
Drichko, N., M. Dumm, D. Faltermeier, M. Dressel, J. Merino, and A. Greco, 2007, Physica (Amsterdam) **460C–462C**, 125.
Drichko, N., P. Haas, B. Gorshunov, D. Schweitzer, and M. Dressel, 2002, Europhys. Lett. **59**, 774.
Drichko, N., S. Kaiser, A. Greco, J. A. Schlueter, G. L. Gard, and M. Dressel, 2010 (unpublished).
Drichko, N., S. Kaiser, Y. Sun, C. Clauss, M. Dressel, H. Mori, J. Schlueter, E. Zhyliaeva, S. Torunova, and R. Lyubovskaya, 2009, Physica (Amsterdam) **404B**, 490.
Drichko, N., K. Peukhov, M. Dressel, O. Bogdanova, E. Zhilyaeva, R. Lyubovskaya, A. Greco, and J. Merino, 2005, Phys. Rev. B **72**, 024524.
Driscoll, T., H. T. Kim, B. G. Chae, B. J. Kim, Y.-W. Lee, N. M. Jokerst, S. Palit, D. Smith, M. Di Ventra, and D. N. Basov, 2009, Science **325**, 1518.
Drude, P., 1900, Phys. Z. **1**, 161.
Dubi, Y., Y. Meir, and Y. Avishai, 2007, Nature (London) **449**, 876.
Dulić, D., *et al.*, 2001, Phys. Rev. Lett. **86**, 4144.
Dumm, M., D. N. Basov, S. Komiya, Y. Abe, and Y. Ando, 2002, Phys. Rev. Lett. **88**, 147003.
Dumm, M., D. Faltermeier, N. Drichko, M. Dressel, C. Meźière, and P. Batail, 2009, Phys. Rev. B **79**, 195106.
Dumm, M., B. P. Gorshunov, M. Dressel, and T. Matsuma, 2005, Europhys. Lett. **72**, 103.
Dumm, M., S. Komiya, Y. Ando, and D. N. Basov, 2003, Phys. Rev. Lett. **91**, 077004.
Dyre, J. C., and T. B. Schrøder, 2000, Rev. Mod. Phys. **72**, 873.
Dzyaloshinski, I., 1958, J. Phys. Chem. Solids **4**, 241.
Eagles, D., R. Lobo, and F. Gervais, 1995, Phys. Rev. B **52**, 6440.
Eckstein, M., and K. Kollar, 2008, Phys. Rev. B **78**, 205119.
El Azrak, A., R. Nahoum, N. Bontemps, M. Guilloux-Viry, C. Thivet, A. Perrin, S. Labdi, Z. Z. Li, and H. Raffy, 1994, Phys. Rev. B **49**, 9846.
Eldridge, J. E., 1985, Phys. Rev. B **31**, 5465.
Eldridge, J. E., and F. E. Bates, 1983, Phys. Rev. B **28**, 6972.
Eldridge, J. E., and G. S. Bates, 1986, Phys. Rev. B **34**, 6992.
Eldridge, J. E., K. Kornelsen, H. H. Wang, J. M. Williams, A. V. D. Crouch, and D. M. Watkins, 1991, Solid State Commun. **79**, 583.
Ellis, D. S., J. P. Hill, S. Wakimoto, R. J. Birgeneau, D. Casa, T. Gog, and Y.-J. Kim, 2008, Phys. Rev. B **77**, 060501.
Emery, V. J., and S. A. Kivelson, 1995a, Phys. Rev. Lett. **74**, 3253.
Emery, V. J., and S. A. Kivelson, 1995b, Nature (London) **374**, 434.
Eskes, H., L. H. Tjeng, and G. A. Sawatzky, 1990, Phys. Rev. B **41**, 288.
Evers, F., and A. D. Mirlin, 2008, Rev. Mod. Phys. **80**, 1355.
Evtushinsky, D. V., *et al.*, 2009, Phys. Rev. B **79**, 054517.
Faltermeier, D., J. Barz, M. Dumm, M. Dressel, N. Drichko, B. Petrov, V. Semkin, R. Vlasova, C. Meźière, and P. Batail, 2007, Phys. Rev. B **76**, 165113.
Fann, W. S., R. Storz, H. W. K. Tom, and J. Bokor, 1992, Phys. Rev. Lett. **68**, 2834.
Farge, J.-P., 1994, Ed., *Organic Conductors: Fundamentals and Applications* (Dekker, New York).
Farnworth, B., and T. Timusk, 1974, Phys. Rev. B **10**, 2799.
Fawcett, E., 1988, Rev. Mod. Phys. **60**, 209.
Federici, J. F., B. I. Greene, P. N. Saeta, D. R. Dykaar, F. Sharifi, and R. C. Dynes, 1992, Phys. Rev. B **46**, 11 153.
Feenstra, B., J. Schutzmann, D. van der Marel, R. Pinaya, and M. Decroux, 1997, Phys. Rev. Lett. **79**, 4890.
Feynman, R., 1955, Phys. Rev. **97**, 660.
Fiebig, M., K. Miyano, Y. Tomioka, and Y. Tokura, 1998, Science **280**, 1925.
Fiebig, M., K. Miyano, Y. Tomioka, and Y. Tokura, 2000, Appl. Phys. B **71**, 211.
Fischer, M., M. Dressel, B. Gompf, A. K. Tripathi, and J. Pflaum, 2006, Appl. Phys. Lett. **89**, 182103.
Fisher, M. P. A., G. Grinstein, and S. M. Girvin, 1990, Phys. Rev. Lett. **64**, 587.
Fisher, M. P. A., P. B. Weichman, G. Grinstein, and D. S. Fisher, 1989, Phys. Rev. B **40**, 546.
Fishman, D., C. Faugeras, M. Potemski, A. Revcolevschi, and P. H. M. van Loosdrecht, 2009, Phys. Rev. B **80**, 045208.
Fishman, D. A., A. Revcolevschi, and P. H. M. van Loosdrecht, 2006, Phys. Status Solidi C **3**, 2469.
Fisk, Z., D. Hess, C. Pethick, D. Pines, J. Smith, J. Thompson, and J. Willis, 1988, Science **239**, 33.
Fratini, S., and S. Ciuchi, 2006, Phys. Rev. B **74**, 075101.
Freeland, J. W., J. Chakhalian, A. V. Boris, J. M. Tonnerre, J. J. Kavich, P. Yordanov, S. Grenier, P. Popovich, H. N. Lee, and B. Keimer, 2010, Phys. Rev. B **81**, 094414.
Frenzel, A., M. M. Qazilbash, M. Brehm, B.-G. Chae, B.-J. Kim, H.-T. Kim, A. V. Balatsky, F. Keilmann, and D. N. Basov, 2009, Phys. Rev. B **80**, 115115.
Fujioka, J., S. Miyasaka, and Y. Tokura, 2006, Phys. Rev. Lett. **97**, 196401.
Fujishima, Y., Y. Tokura, T. Arima, and S. Uchida, 1992, Phys. Rev. B **46**, 11 167.

Fulde, P., B. Schmidt, and P. Thalmeier, 1995, Europhys. Lett. **31**, 323.
Fulde, P., P. Thalmeier, and G. Zwicknagl, 2006, in *Strongly Correlated Electrons*, edited by H. Ehrenreich and F. Spaepen, Solid State Physics: Advances in Research and Applications Vol. 60 (Academic Press, San Diego), pp. 1–180.
Gaal, P., W. Kuehn, K. Reimann, M. Woerner, T. Elsaesser, and R. Hey, 2007, Nature (London) **450**, 1210.
Gammel, J. T., A. Saxena, I. Batisti, A. R. Bishop, and S. R. Phillpot, 1992, Phys. Rev. B **45**, 6408.
Garner, S. R., J. N. Hancock, Y. W. Rodriguez, Z. Schlesinger, B. Bucher, Z. Fisk, and J. L. Sarrao, 2000, Phys. Rev. B **62**, R4778.
Gay, P., D. Smith, C. Stevens, C. Chen, G. Yang, S. Abell, D. Wang, J. Wang, Z. Ren, and J. Ryan, 1999, J. Low Temp. Phys. **117**, 1025.
Gedik, N., P. Blake, R. C. Spitzer, J. Orenstein, R. Liang, D. A. Bonn, and W. N. Hardy, 2004, Phys. Rev. B **70**, 014504.
Gedik, N., D.-S. Yang, G. Logvenov, I. Bozovic, and A. H. Zewail, 2007, Science **316**, 425.
Gedik, N., M. Langer, J. Orenstein, S. Ono, Y. Abe, and Y. Ando, 2005, Phys. Rev. Lett. **95**, 117005.
Gedik, N., J. Orenstein, R. X. Liang, D. A. Bonn, and W. N. Hardy, 2003, Science **300**, 1410.
Georges, A., G. Kotliar, W. Krauth, and M. Rozenberg, 1996, Rev. Mod. Phys. **68**, 13.
Giamarchi, T., 1991, Phys. Rev. B **44**, 2905.
Giamarchi, T., 1997, Physica (Amsterdam) **230B–232B**, 975.
Giamarchi, T., 2004a, *Quantum Physics in One Dimension* (Oxford University Press, Oxford).
Giamarchi, T., 2004b, Chem. Rev. **104**, 5037.
Giamarchi, T., 2008, in *The Physics of Organic Superconductors and Conductors*, edited by A. Lebed (Springer-Verlag, Berlin/Heidelberg), pp. 719–743.
Giamarchi, T., C. Ruegg, and O. Tchernyshyov, 2008, Nature Phys. **4**, 198.
Glover, R. E., and M. Tinkham, 1957, Phys. Rev. **108**, 243.
Goerbig, M. O., J.-N. Fuchs, K. Kechedzhi, and V. I. Fal'ko, 2007, Phys. Rev. Lett. **99**, 087402.
Gold, A., S. J. Allen, B. A. Wilson, and D. C. Tsui, 1982, Phys. Rev. B **25**, 3519.
Gold, A., and W. Götze, 1981, J. Phys. C **14**, 4049.
Goldman, A. M., and N. Markovic, 1998, Phys. Today **51**, 39.
González, J., F. Guinea, and M. A. H. Vozmediano, 1999, Phys. Rev. B **59**, R2474.
Goodenough, J. B., 1971, J. Solid State Chem. **3**, 490.
Gorshunov, B., P. Haas, T. Rõõm, M. Dressel, T. Vuletić, B. Korin-Hamzić, S. Tomić, J. Akimitsu, and T. Nagata, 2002, Phys. Rev. B **66**, 060508.
Gorshunov, B., P. Haas, O. Ushakov, M. Dressel, and F. Iga, 2006, Phys. Rev. B **73**, 045207.
Gorshunov, B., C. A. Kuntscher, P. Haas, M. Dressel, P. F. Mena, A. B. Kuzmenko, D. van der Marel, T. Muranaka, and J. Akimitsu, 2001, Eur. Phys. J. B **21**, 159.
Gorshunov, B., A. S. Prokhorov, I. E. Spektor, A. A. Volkov, M. Dressel, M. Dumm, and T. Matsumura, 2005, Zh. Eksp. Teor. Fiz. **128**, 1047 [JETP **101**, 913 (2005)].
Gorshunov, B., A. S. Prokhorov, I. E. Spektor, A. A. Volkov, M. Dressel, and F. Iga, 2006, Zh. Eksp. Teor. Fiz. **130**, 1039 [JETP **103**, 897 (2006)].
Gorshunov, B., N. Sluchanko, A. Volkov, M. Dressel, G. Knebel, A. Loidl, and S. Kunii, 1999, Phys. Rev. B **59**, 1808.
Gorshunov, B., D. Wu, A. A. Voronkov, P. Kallina, K. Ida, S. Haindl, F. Kurth, L. Schultz, B. Holzapfel, and M. Dressel, 2010, Phys. Rev. B **81**, 060509(R).
Gorshunov, B. P., G. V. Kozlov, A. A. Volkov, V. Železný, J. Petzelt, and C. S. Jacobsen, 1986, Solid State Commun. **60**, 681.
Gossling, A., R. Schmitz, H. Roth, M. W. Haverkort, T. Lorenz, J. A. Mydosh, E. Muller-Hartmann, and M. Gruninger, 2008, Phys. Rev. B **78**, 075122.
Götze, W., 1978, Solid State Commun. **27**, 1393.
Götze, W., 1979, J. Phys. C **12**, 1279.
Götze, W., and P. Wölfle, 1972, Phys. Rev. B **6**, 1226.
Gough, C. E., R. J. Ormeno, M. A. Hein, A. Sibley, J. J. Wingfield, J. Powell, A. Porch, G. Yang, Y. Maeno, and Z. Q. Mao, 2001, J. Supercond. **14**, 73.
Gozar, A., G. Logvenov, L. Fitting Kourkoutis, A. T. Bollinger, L. A. Giannuzzi, D. A. Muller, and B. I., 2008, Nature (London) **455**, 782.
Gray, K. E., 1981, *Nonequilibrium Superconductivity, Phonons, and Kaptiza Boundaries* (Plenum, New York).
Grayson, M., L. B. Rigal, D. C. Schmadel, H. D. Drew, and P.-J. Kung, 2002, Phys. Rev. Lett. **89**, 037003.
Greco, A., J. Merino, A. Foussats, and R. H. McKenzie, 2005, Phys. Rev. B **71**, 144502.
Grenzebach, C., F. B. Anders, G. Czycholl, and T. Pruschke, 2006, Phys. Rev. B **74**, 195119.
Grewe, N., and F. Steglich, 1991, in *Heavy Fermions*, edited by K. A. Gschneidner Jr., and L. Eyring, Handbook on the Physics and Chemistry of Rare Earths Vol. 14 (Elsevier, Amsterdam), p. 343.
Grilli, M., S. Caprara, C. D. Castro, T. Enss, R. Hackl, B. Muschler, and W. Prestel, 2009, Physica (Amsterdam) **404B**, 3070.
Grilli, M., B. G. Kotliar, and A. J. Millis, 1990, Phys. Rev. B **42**, 329.
Groeneveld, R. H. M., R. Sprik, and A. Lagendijk, 1995, Phys. Rev. B **51**, 11433.
Grüninger, M., D. van der Marel, A. Damascelli, A. Erb, T. Nunner, and T. Kopp, 2000, Phys. Rev. B **62**, 12 422.
Grüninger, M., M. Windt, E. Benckiser, T. S. Nunner, K. P. Schmidt, G. S. Uhrig, and T. Kopp, 2003, Adv. Solid State Phys. **43**, 95.
Grushin, A. G., B. Valenzuela, and M. A. H. Vozmediano, 2009, Phys. Rev. B **80**, 155417.
Gunnarsson, O., M. Calandra, and J. E. Han, 2003, Rev. Mod. Phys. **75**, 1085.
Gunnarsson, O., and J. E. Han, 2000, Nature (London) **405**, 1027.
Gunnarsson, O., and K. Vafayi, 2007, Phys. Rev. Lett. **98**, 219802.
Guritanu, V., N. P. Armitage, R. Tediosi, S. S. Saxena, A. Huxley, and D. van der Marel, 2008, Phys. Rev. B **78**, 172406.
Guritanu, V., D. van der Marel, J. Teyssier, T. Jarlborg, H. Wilhelm, M. Schmidt, and F. Steglich, 2007, Phys. Rev. B **75**, 155114.
Gusynin, V. P., and S. G. Sharapov, 2006, Phys. Rev. B **73**, 245411.
Han, S. G., Z. V. Vardeny, K. S. Wong, O. G. Symko, and G. Koren, 1990, Phys. Rev. Lett. **65**, 2708.
Hancock, J. N., T. McKnew, Z. Schlesinger, J. L. Sarrao, and Z. Fisk, 2004, Phys. Rev. Lett. **92**, 186405.
Hancock, J. N., T. McKnew, Z. Schlesinger, J. L. Sarrao, and Z. Fisk, 2006, Phys. Rev. B **73**, 125119.
Hardy, W. N., D. A. Bonn, D. C. Morgan, R. Liang, and K. Zhang, 1993, Phys. Rev. Lett. **70**, 3999.
Harrison, N., R. D. McDonald, and J. Singleton, 2007, Phys. Rev. Lett. **99**, 206406.
Hase, M., K. Ishioka, J. Demsar, K. Ushida, and M. Kitajima, 2005a, Phys. Rev. B **72**, 189902.
Hase, M., K. Ishioka, J. Demsar, K. Ushida, and M. Kitajima, 2005b, Phys. Rev. B **71**, 184301.
Haslinger, R., A. V. Chubukov, and A. Abanov, 2000, Phys. Rev. B **63**, 020503.
Haule, K., and G. Kotliar, 2007, Phys. Rev. B **76**, 104509.

Haule, K., V. Oudovenko, S. Y. Savrasov, and G. Kotliar, 2005, Phys. Rev. Lett. **94**, 036401.
Haule, K., J. H. Shim, and G. Kotliar, 2008, Phys. Rev. Lett. **100**, 226402.
Haule, K., C.-H. Yee, and K. Kim, 2010, Phys. Rev. B **81**, 195107.
Haverkort, M. W., *et al.*, 2005, Phys. Rev. Lett. **95**, 196404.
Hayden, S. M., G. Aeppli, H. A. Mook, T. G. Perring, T. E. Mason, W. Cheong, and Z. Fisk, 1996, Phys. Rev. Lett. **76**, 1344.
Hedin, L., 1965, Phys. Rev. **139**, A796.
Heid, R., R. Zeyher, D. Manske, and K.-P. Bohnen, 2009, Phys. Rev. B **80**, 024507.
Heinrich, B., and J. F. Cochran, 1993, Adv. Phys. **42**, 523.
Helgren, E., N. P. Armitage, and G. Grüner, 2002, Phys. Rev. Lett. **89**, 246601.
Helgren, E., N. P. Armitage, and G. Grüner, 2004, Phys. Rev. B **69**, 014201.
Henderson, W., V. Vescoli, P. Tran, L. Degiorgi, and G. Grüner, 1999, Eur. Phys. J. B **11**, 365.
Henriksen, E. A., Z. Jiang, L.-C. Tung, M. E. Schwartz, M. Takita, Y.-J. Wang, P. Kim, and H. L. Stormer, 2008, Phys. Rev. Lett. **100**, 087403.
Hering, M., M. Scheffler, M. Dressel, and H. v. Löhneysen, 2007, Phys. Rev. B **75**, 205203.
Hetel, I., T. R. Lemberger, and M. Randeria, 2007, Nature Phys. **3**, 700.
Hewson, A. C., 1993, *The Kondo Problem in Heavy Fermions* (Cambridge University Press, Cambridge, UK).
Hiebert, W. K., A. Stankiewicz, and M. R. Freeman, 1997, Phys. Rev. Lett. **79**, 1134.
Higashitani, S., and K. Nagai, 2000, Phys. Rev. B **62**, 3042.
Hildebrand, M. G., M. Reedyk, T. Katsufuji, and Y. Tokura, 2001, Phys. Rev. Lett. **87**, 227002.
Hilton, D., R. P. Prasankumar, S. Fourmaux, A. Cavalleri, D. Brassard, M. A. El Khakani, J. C. Keiffer, A. J. Taylor, and R. D. Averitt, 2007, Phys. Rev. Lett. **99**, 226401.
Hilton, D. J., R. P. Prasankumar, S. A. Trugman, A. J. Taylor, and R. D. Averitt, 2006, J. Phys. Soc. Jpn. **75**, 011006.
Hirsch, J. E., 1992, Physica (Amsterdam) **199C**, 305.
Holden, A. A. B., G. M. Wardlaw, M. Reedyk, and J. L. Smith, 2003, Phys. Rev. Lett. **91**, 136401.
Holden, T., *et al.*, 2004, Phys. Rev. B **69**, 064505.
Holstein, T., 1959a, Ann. Phys. (N.Y.) **8**, 325.
Holstein, T., 1959b, Ann. Phys. (N.Y.) **8**, 343.
Homes, C. C., 2009, Phys. Rev. B **80**, 180509.
Homes, C. C., S. V. Dordevic, D. A. Bonn, R. Liang, and W. N. Hardy, 2004, Phys. Rev. B **69**, 024514.
Homes, C. C., S. V. Dordevic, D. A. Bonn, R. Liang, W. N. Hardy, and T. Timusk, 2005, Phys. Rev. B **71**, 184515.
Homes, C. C., S. V. Dordevic, G. D. Gu, Q. Li, T. Valla, and J. M. Tranquada, 2006, Phys. Rev. Lett. **96**, 257002.
Homes, C. C., S. V. Dordevic, T. Valla, and M. Strongin, 2005, Phys. Rev. B **72**, 134517.
Homes, C. C., R. P. S. M. Lobo, P. Fournier, A. Zimmers, and R. L. Greene, 2006, Phys. Rev. B **74**, 214515.
Homes, C. C., T. Timusk, R. Liang, D. A. Bonn, and W. N. Hardy, 1993, Phys. Rev. Lett. **71**, 1645.
Homes, C. C., T. Timusk, R. Liang, D. A. Bonn, and W. N. Hardy, 1995, Physica (Amsterdam) **254C**, 265; **432C**, 316(E) (2005).
Homes, C. C., J. M. Tranquada, Q. Li, A. R. Moodenbaugh, and D. J. Buttrey, 2003, Phys. Rev. B **67**, 184516.
Homes, C. C., *et al.*, 2004, Nature (London) **430**, 539.
Hoppler, J., *et al.*, 2009, Nature Mater. **8**, 315.
Howell, P. C., A. Rosch, and P. J. Hirschfeld, 2004, Phys. Rev. Lett. **92**, 037003.
Hu, W., Q. Zhang, and N. Wang, 2009, Physica (Amsterdam) **469C**, 545.
Hu, W. Z., J. Dong, G. Li, Z. Li, P. Zheng, G. F. Chen, J. L. Luo, and N. L. Wang, 2008, Phys. Rev. Lett. **101**, 257005.
Huber, A. J., F. Keilmann, J. Wittborn, J. Aizpurua, and R. Hillenbrand, 2008, Nano Lett. **8**, 3766.
Huber, R., B. A. Schmid, Y. R. Shen, D. S. Chemla, and R. A. Kaindl, 2006, Phys. Rev. Lett. **96**, 017402.
Huber, R., F. Tauser, A. Brodschelm, M. Bichler, G. Abstreiter, and A. Leitenstorfer, 2001, Nature (London) **414**, 286.
Hüfner, S., M. A. Hossain, A. Damascelli, and G. A. Sawatzky, 2008, Rep. Prog. Phys. **71**, 062501.
Hussey, N. E., A. P. Mackenzie, J. R. Cooper, Y. Maeno, S. Nishizaki, and T. Fujita, 1998, Phys. Rev. B **57**, 5505.
Hüvonen, D., U. Nagel, T. Rõõm, P. Haas, M. Dressel, J. Hwang, T. Timusk, Y. J. Wang, and J. Akimitsu, 2007, Phys. Rev. B **76**, 134418.
Hwang, H. Y., S.-W. Cheong, P. G. Radaelli, M. Marezio, and B. Batlogg, 1995, Phys. Rev. Lett. **75**, 914.
Hwang, J., E. Schachinger, J. P. Carbotte, F. Gao, D. B. Tanner, and T. Timusk, 2008, Phys. Rev. Lett. **100**, 137005.
Hwang, J., T. Timusk, and G. D. Gu, 2004, Nature (London) **427**, 714.
Hwang, J., T. Timusk, and G. D. Gu, 2007, J. Phys. Condens. Matter **19**, 125208.
Iga, F., S. Hiura, J. Klijn, N. Shimizu, T. Takabatake, M. Ito, Y. Matsumoto, F. Masaki, T. Suzuki, and T. Fujita, 1999, Physica (Amsterdam) **259B–261B**, 312.
Imada, M., A. Fujimori, and Y. Tokura, 1998, Rev. Mod. Phys. **70**, 1039.
Inoue, J.-I., and S. Maekawa, 1990, J. Phys. Soc. Jpn. **59**, 2110.
Ioffe, A. F., and A. R. Regel, 1960, Prog. Semicond. **4**, 237.
Irizawa, A., K. Shimai, K. Sato, K. Iizuka, M. Nishiyama, T. Nanba, S. Niitaka, and H. Takagi, 2009, J. Phys. Conf. Ser. **150**, 042070.
Ishida, K., Y. Nakai, and H. Hosono, 2009, J. Phys. Soc. Jpn. **78**, 062001.
Ishiguro, T., K. Yamaji, and G. Saito, 1998, in *Organic Superconductors*, Springer Series in Solid State Sciences Vol. 88 (Springer-Verlag, Berlin), 2nd ed.
Ishikawa, T., K. Tobe, T. Kimura, T. Katsufuji, and Y. Tokura, 2000, Phys. Rev. B **62**, 12 354.
Iwai, S., M. Ono, A. Maeda, H. Matsuzaki, H. Kishida, H. Okamoto, and Y. Tokura, 2003, Phys. Rev. Lett. **91**, 057401.
Iwai, S., K. Yamamoto, F. Hiramatsu, H. Nakaya, Y. Kawakami, and K. Yakushi, 2008, Phys. Rev. B **77**, 125131.
Iwai, S., K. Yamamoto, A. Kashiwazaki, F. Hiramatsu, H. Nakaya, Y. Kawakami, K. Yakushi, H. Okamoto, H. Mori, and Y. Nishio, 2007, Phys. Rev. Lett. **98**, 097402.
Iwano, K., 2006, Phys. Rev. B **74**, 125104.
Iwano, K., M. Ono, and H. Okamoto, 2002, Phys. Rev. B **66**, 235103.
Iyengar, A., J. Wang, H. A. Fertig, and L. Brey, 2007, Phys. Rev. B **75**, 125430.
Jackeli, G., and N. M. Plakida, 1999, Phys. Rev. B **60**, 5266.
Jacobsen, C. S., K. Mortensen, M. Weger, and K. Bechgaard, 1981, Solid State Commun. **38**, 423.
Jacobsen, C. S., D. B. Tanner, and K. Bechgaard, 1981, Phys. Rev. Lett. **46**, 1142.
Jacobsen, C. S., D. B. Tanner, and K. Bechgaard, 1983, Phys. Rev. B **28**, 7019.
Janner, A.-M., R. Eder, B. Koopmans, H. T. Jonkman, and G. A. Sawatzky, 1995, Phys. Rev. B **52**, 17158.
Jarrell, M., J. K. Freericks, and T. Pruschke, 1995, Phys. Rev. B **51**, 11704.

Jaudet, C., *et al.*, 2008, Phys. Rev. Lett. **100**, 187005.
Jiang, Z., E. A. Henriksen, L. C. Tung, Y.-J. Wang, M. E. Schwartz, M. Y. Han, P. Kim, and H. L. Stormer, 2007, Phys. Rev. Lett. **98**, 197403.
Jin, S., T. H. Tiefel, M. McCormack, R. A. Fastnacht, R. Ramesh, and L. H. Chen, 1994, Science **264**, 413.
Jones, R. O., and O. Gunnarsson, 1989, Rev. Mod. Phys. **61**, 689.
Jonker, G. H., and J. H. van Santen, 1950, Physica (Amsterdam) **16**, 337.
Jonscher, A. K., 1977, Nature (London) **267**, 673.
Jönsson, P. E., K. Takenaka, S. Niitaka, T. Sasagawa, S. Sugai, and H. Takagi, 2007, Phys. Rev. Lett. **99**, 167402.
Jung, J., H. Lee, T. Noh, E. Choi, Y. Moritomo, Y. Wang, and X. Wei, 2000, Phys. Rev. B **62**, 481.
Jung, J. H., D.-W. Kim, T. W. Noh, H. C. Kim, H.-C. Ri, S. J. Levett, M. R. Lees, D. M. Paul, and G. Balakrishnan, 2001, Phys. Rev. B **64**, 165106.
Jung, J. H., K. H. Kim, H. J. Lee, J. S. Ahn, N. J. Hur, T. W. Noh, M. S. Kim, and J.-G. Park, 1999, Phys. Rev. B **59**, 3793.
Jung, J. H., H. J. Lee, J. Yu, T. W. Noh, E. J. Choi, and Y. Moritomo, 2000, Phys. Rev. B **61**, 14 656.
Jungwirth, T., J. Sinova, J. Mašek, J. Kučera, and A. H. MacDonald, 2006, Rev. Mod. Phys. **78**, 809.
Kabanov, V., J. Demsar, and D. Mihailovic, 2005, Phys. Rev. Lett. **95**, 147002.
Kabanov, V., J. Demsar, B. Podobnik, and D. Mihailovic, 1999, Phys. Rev. B **59**, 1497.
Kadowaki, K., and S. Woods, 1986, Solid State Commun. **58**, 507.
Kagoshima, S., H. Nagasawa, and T. Sambongi, 1988, *One-Dimensional Conductors*, Springer Series in Solid-State Sciences Vol. 72 (Springer-Verlag, Berlin).
Kaindl, R., M. Woerner, T. Elsaesser, D. Smith, J. Ryan, G. Farnan, M. McCurry, and D. Walmsley, 2000, Science **287**, 470.
Kaindl, R. A., and R. D. Averitt, 2007, in *Time-Resolved THz Studies of Carrier Dynamics in Semiconductors, Superconductors, and Strongly Correlated Electron Materials*, edited by S. Dexheimer (CRC Press, Boca Raton), pp. 119–170.
Kaindl, R. A., M. A. Carnahan, D. S. Chemla, S. Oh, and J. N. Eckstein, 2005, Phys. Rev. B **72**, 060510(R).
Kaindl, R. A., M. A. Carnahan, J. Orenstein, D. S. Chemla, H. M. Christen, H. Y. Zhai, M. Paranthaman, and D. H. Lowndes, 2001, Phys. Rev. Lett. **88**, 027003.
Kaiser, A., 2001, Rep. Prog. Phys. **64**, 1.
Kajueter, H., and G. Kotliar, 1997, Int. J. Mod. Phys. B **11**, 729.
Kamal, S., D. A. Bonn, N. Goldenfeld, P. J. Hirschfeld, R. Liang, and W. N. Hardy, 1994, Phys. Rev. Lett. **73**, 1845.
Kamal, S., D. M. Kim, C. B. Eom, and J. S. Dodge, 2006, Phys. Rev. B **74**, 165115.
Kamaras, K., A. Pekker, M. Bruckner, F. Borondics, A. G. Rinzler, D. B. Tanner, M. E. Itkis, R. C. Haddon, Y. Tan, and D. E. Resasco, 2008, Phys. Status Solidi B **245**, 2229.
Kamaras, K., A. G. Rinzler, D. B. Tanner, and D. A. Walters, 2006, Phys. Status Solidi B **243**, 3126.
Kamihara, Y., T. Watanabe, M. Hirano, and H. Hosono, 2008, J. Am. Chem. Soc. **130**, 3296.
Kaplan, S. B., C. C. Chi, D. N. Langenberg, J. J. Chang, S. Jafarey, and D. J. Scalapino, 1976, Phys. Rev. B **14**, 4854.
Karakozov, A., and E. Maksimov, 2006, Solid State Commun. **139**, 80.
Kasuya, T., 1996, J. Phys. Soc. Jpn. **65**, 2548.
Katsufuji, T., M. Kasai, and Y. Tokura, 1996, Phys. Rev. Lett. **76**, 126.
Katsufuji, T., Y. Okimoto, and Y. Tokura, 1995, Phys. Rev. Lett. **75**, 3497.
Katsura, H., A. V. Balatsky, and N. Nagaosa, 2007, Phys. Rev. Lett. **98**, 027203.
Katz, A. S., S. I. Woods, E. J. Singley, T. W. Li, M. Xu, D. G. Hinks, R. C. Dynes, and D. N. Basov, 2000, Phys. Rev. B **61**, 5930.
Kee, H.-Y., Y. B. Kim, and K. Maki, 2000, Phys. Rev. B **62**, 5877.
Keilmann, F., 2004, J. Electron Microsc. **53**, 187.
Keilmann, F., and R. Hillenbrand, 2004, Phil. Trans. R. Soc. A **362**, 787.
Keller, H., 1975, Ed., *Low Dimensional Cooperative Phenomena*, NATO Advanced Study Institutes Series B Vol. 7 (Plenum Press, New York).
Kenzelmann, M., A. Harris, S. Jonas, C. Broholm, J. Schefer, S. Kim, C. Zhang, S. Cheong, O. Vajk, and J. Lynn, 2005, Phys. Rev. Lett. **95**, 087206.
Khaliullin, G., P. Horsch, and A. M. Oleś, 2004, Phys. Rev. B **70**, 195103.
Khurana, A., 1990, Phys. Rev. Lett. **64**, 1990.
Kida, N., and M. Tonouchi, 2002, Phys. Rev. B **66**, 024401.
Kida, N., Y. Yamasaki, R. Shimano, T.-h. Arima, and Y. Tokura, 2008, J. Phys. Soc. Jpn. **77**, 123704.
Kikoin, K. A., and A. S. Mishchenko, 1990, J. Phys. Condens. Matter **2**, 6491.
Kim, B. J., *et al.*, 2008, Phys. Rev. Lett. **101**, 076402.
Kim, B.-J., Y. W. Lee, B.-G. Chae, S. J. Yun, S.-Y. Oh, H.-T. Kim, and Y.-S. Lim, 2007, Appl. Phys. Lett. **90**, 023515.
Kim, H., B. Chae, D. Youn, S. Maeng, G. Kim, K. Kang, and Y. Lim, 2004, New J. Phys. **6**, 52.
Kim, H.-T., Y. W. Lee, B.-J. Kim, B.-G. Chae, S. J. Yun, K.-Y. Kang, K.-J. Han, K.-J. Yee, and Y.-S. Lim, 2006, Phys. Rev. Lett. **97**, 266401.
Kim, J., S. Jung, E. J. Choi, K. Kim, K. Lee, and S. Im, 2008, Appl. Phys. Lett. **93**, 241902.
Kim, J.-H., Y. Lee, C. C. Homes, J.-S. Rhyee, B. K. Cho, S.-J. Oh, and E. J. Choi, 2005, Phys. Rev. B **71**, 075105.
Kim, K., J. Jung, and T. Noh, 1998, Phys. Rev. Lett. **81**, 1517.
Kim, K. W., G. D. Gu, C. C. Homes, and T. W. Noh, 2008, Phys. Rev. Lett. **101**, 177404.
Kim, M., H. J. Lee, B. J. Yang, K. H. Kim, Y. Moritomo, J. Yu, and T. W. Noh, 2007, Phys. Rev. Lett. **98**, 187201.
Kim, M. W., P. Murugavel, S. Parashar, J. S. Lee, and T. W. Noh, 2004, New J. Phys. **6**, 156.
Kimel, A., A. Kirilyuk, F. Hansteen, R. Pisarev, and T. Rasing, 2007, J. Phys. Condens. Matter **19**, 043201.
Kimel, A., A. Kirilyuk, P. Usachev, R. Pisarev, A. Balbashov, and T. Rasing, 2005, Nature (London) **435**, 655.
Kimura, S., M. Ikezawa, A. Ochiai, and T. Suzuki, 1996, J. Phys. Soc. Jpn. **65**, 3591.
Kimura, S., N. Kimura, and H. Aoki, 2007, J. Phys. Soc. Jpn. **76**, 084710.
Kimura, S., A. Ochiai, H. Iwata, T. Nishi, H. Aoki, and A. Ochiai, 2002, Physica (Amsterdam) **312B–313B**, 356.
Kimura, S., A. Ochiai, and T. Suzuki, 1997, Physica (Amsterdam) **230B–232B**, 705.
Kimura, S.-I., T. Mizuno, H. Im, K. Hayashi, E. Matsuoka, and T. Takabatake, 2006, Phys. Rev. B **73**, 214416.
Kircher, J., M. Cardona, A. Zibold, H.-P. Geserich, E. Kaldis, J. Karpinski, and S. Rusiecki, 1993, Phys. Rev. B **48**, 3993.
Kise, T., T. Ogasawara, M. Ashida, Y. Tomioka, Y. Tokura, and M. Kuwata-Gonokami, 2000, Phys. Rev. Lett. **85**, 1986.
Kishida, H., H. Matsuzaki, H. Okamoto, T. Manabe, M. Yamashita, Y. Taguchi, and Y. Tokura, 2000, Nature (London) **405**, 929.
Klein, M., D. Zur, D. Menzel, J. Schoenes, K. Doll, J. Röder, and F. Reinert, 2008, Phys. Rev. Lett. **101**, 046406.

Klingshirn, C., 1995, *Semiconductor Optics* (Springer-Verlag, Berlin).
Knupfer, M., and J. Fink, 1997, Phys. Rev. Lett. **79**, 2714.
Kobayashi, T., T. Okada, T. Kobayashi, K. A. Nelson, and S. De Silvestri, 2005, in *Ultrafast Phenomena XIV—Proceedings of the 14th International Conference*, Springer Series in Chemical Physics Vol. 79 (Springer, Berlin).
Kobayashi, Y., C. L. Wang, K. Hirata, W. Zheng, and C. Zhang, 1998, Phys. Rev. B **58**, 5384.
Kohlman, R. S., J. Joo, Y. Z. Wang, J. P. Pouget, H. Kaneko, T. Ishiguro, and A. J. Epstein, 1995, Phys. Rev. Lett. **74**, 773.
Kohn, W., 1961, Phys. Rev. **123**, 1242.
Kojima, K. M., S. Uchida, Y. Fudamoto, and S. Tajima, 2002, Phys. Rev. Lett. **89**, 247001.
Kondo, S., *et al.*, 1997, Phys. Rev. Lett. **78**, 3729.
Kondo, T., R. Khasanov, T. Takeuchi, J. Schmalian, and A. Kaminski, 2009, Nature (London) **457**, 296.
Koopmans, B., J. J. M. Ruigrok, F. Dalla Logna, and W. J. M. de Jonge, 2005, Phys. Rev. Lett. **95**, 267207.
Kornelsen, K., J. E. Eldridge, and G. S. Bates, 1987, Phys. Rev. B **35**, 9162.
Kornelsen, K., J. E. Eldridge, H. H. Wang, H. A. Charlier, and J. M. Williams, 1992, Solid State Commun. **81**, 343.
Kornelsen, K. E., J. E. Eldridge, H. H. Wang, and J. M. Williams, 1991a, Solid State Commun. **76**, 1009.
Kornelsen, K., J. E. Eldridge, H. H. Wang, and J. M. Williams, 1991b, Phys. Rev. B **44**, 5235.
Kortus, J., I. I. Mazin, K. D. Belashchenko, V. P. Antropov, and L. Boyer, 2001, Phys. Rev. Lett. **86**, 4656.
Koshihara, S.-Y., 2009, J. Phys. Conf. Ser. **148**, 011001.
Koshihara, S.-Y., Y. Tokura, T. Mitani, G. Saito, and T. Koda, 1990, Phys. Rev. B **42**, 6853.
Koshihara, S., Y. Takahashi, H. Sakai, Y. Tokura, and T. Luty, 1999, J. Phys. Chem. B **103**, 2592.
Koshihara, S.-Y., Y. Tokura, K. Takeda, T. Koda, and A. Kobayashi, 1990, J. Chem. Phys. **92**, 7581.
Kostic, P., Y. Okada, N. C. Collins, Z. Schlesinger, J. W. Reiner, L. Klein, A. Kapitulnik, T. H. Geballe, and M. R. Beasley, 1998, Phys. Rev. Lett. **81**, 2498.
Kotliar, G., S. Y. Savrasov, K. Haule, V. S. Oudovenko, O. Parcollet, and C. A. Marianetti, 2006, Rev. Mod. Phys. **78**, 865.
Kotliar, G., S. Y. Savrasov, G. Pálsson, and G. Biroli, 2001, Phys. Rev. Lett. **87**, 186401.
Kovaleva, N., A. V. Boris, C. Bernhard, A. Kulakov, A. Pimenov, A. M. Balbashov, G. Khaliullin, and B. Keimer, 2004, Phys. Rev. Lett. **93**, 147204.
Kovaleva, N. N., *et al.*, 2007, Phys. Rev. B **76**, 155125.
Kübler, K., H. Ehrka, R. Huber, R. Lopez, A. Halabica, R. Haglund, Jr., and A. Leitenstorfer, 2007, Phys. Rev. Lett. **99**, 116401.
Kubo, R., 1957, J. Phys. Soc. Jpn. **12**, 570.
Kuchinskii, E. Z., N. A. Kuleeva, I. A. Nekrasov, and M. V. Sadovskii, 2008, J. Exp. Theor. Phys. **107**, 281.
Kuiper, P., J.-H. Guo, C. Såthe, L.-C. Duda, J. Nordgren, J. J. M. Pothuizen, F. M. F. de Groot, and G. A. Sawatzky, 1998, Phys. Rev. Lett. **80**, 5204.
Kumagai, K., T. Suzuki, Y. Taguchi, Y. Okada, Y. Fujishima, and Y. Tokura, 1993, Phys. Rev. B **48**, 7636.
Kuntscher, C. A., D. van der Marel, M. Dressel, F. Lichtenberg, and J. Mannhart, 2003, Phys. Rev. B **67**, 035105.
Kuwata-Gonokami, M., and S.-y. Koshihara, 2006, J. Phys. Soc. Jpn. **75**, 011001.
Kuzmenko, A., *et al.*, 2002, Solid State Commun. **121**, 479.
Kuzmenko, A. B., L. Benfatto, E. Cappelluti, I. Crassee, D. van der Marel, P. Blake, K. S. Novoselov, and A. K. Geim, 2009, Preprint.
Kuzmenko, A. B., I. Crassee, D. van der Marel, P. Blake, and K. S. Novoselov, 2009, Preprint.
Kuzmenko, A. B., N. Tombros, H. J. A. Molegraaf, M. Grüninger, D. van der Marel, and S. Uchida, 2003, Phys. Rev. Lett. **91**, 037004.
Kuzmenko, A. B., E. van Heumen, F. Carbone, and D. van der Marel, 2008, Phys. Rev. Lett. **100**, 117401.
Kuzmenko, A. B., E. van Heumen, D. van der Marel, P. Lerch, P. Blake, K. S. Novoselov, and A. K. Geim, 2009, Phys. Rev. B **79**, 115441.
Laad, M., I. Bradarić, and F. Kusmartsev, 2008, Phys. Rev. Lett. **100**, 096402.
LaForge, A. D., W. J. Padilla, K. S. Burch, Z. Q. Li, S. V. Dordevic, K. Segawa, Y. Ando, and D. N. Basov, 2007, Phys. Rev. B **76**, 054524.
LaForge, A. D., W. J. Padilla, K. S. Burch, Z. Q. Li, A. A. Schafgans, K. Segawa, Y. Ando, and D. N. Basov, 2008, Phys. Rev. Lett. **101**, 097008.
LaForge, A. D., W. J. Padilla, K. S. Burch, Z. Q. Li, A. A. Schafgans, K. Segawa, Y. Ando, and D. N. Basov, 2009, Phys. Rev. B **79**, 104516.
LaForge, A. D., *et al.*, 2010, Phys. Rev. B **81**, 064510.
Lai, K., M. B. Ji, N. Leindecker, M. A. Kelly, and Z. X. Shen, 2007, Rev. Sci. Instrum. **78**, 063702.
Laloux, L., A. Georges, and W. Krauth, 1994, Phys. Rev. B **50**, 3092.
Landau, L. D., 1956, Zh. Eksp. Teor. Fiz. **30**, 1058 [Sov. Phys. JETP **3**, 920 (1957)].
Langner, M. C., C. L. S. Kantner, Y. H. Chu, L. M. Martin, P. Yu, J. Seidel, R. Ramesh, and J. Orenstein, 2009, Phys. Rev. Lett. **102**, 177601.
Lanzara, A., *et al.*, 2001, Nature (London) **412**, 510.
Lavagnini, M., *et al.*, 2009, Phys. Rev. B **79**, 075117.
Lebed, A. G., 2008, Ed., *The Physics of Organic Superconductors and Conductors*, Springer Series in Materials Science Vol. 110 (Springer-Verlag, Berlin).
Lee, H., K. Kim, M. Kim, T. Noh, B. Kim, T. Koo, S. Cheong, Y. Wang, and X. Wei, 2002, Phys. Rev. B **65**, 115118.
Lee, H.-L., J. P. Carini, D. V. Baxter, and G. Grüner, 1998, Phys. Rev. Lett. **80**, 4261.
Lee, H.-L., J. P. Carini, D. V. Bexter, W. Henderson, and G. Grüner, 2000, Science **287**, 633.
Lee, J., *et al.*, 2006, Nature (London) **442**, 546.
Lee, K., R. Menon, A. J. Heeger, K. H. Kim, Y. H. Kim, A. Schwartz, M. Dressel, and G. Grüner, 2000, Phys. Rev. B **61**, 1635.
Lee, M., and M. L. Stutzmann, 2001, Phys. Rev. Lett. **87**, 056402.
Lee, P. A., N. Nagaosa, and X.-G. Wen, 2006, Rev. Mod. Phys. **78**, 17.
Lee, Y. S., K. Segawa, Z. Q. Li, W. J. Padilla, M. Dumm, S. V. Dordevic, C. C. Homes, Y. Ando, and D. N. Basov, 2005, Phys. Rev. B **72**, 054529.
Lee, Y. S., J. Yu, J. S. Lee, T. W. Noh, T.-H. Gimm, H.-Y. Choi, and C. B. Eom, 2002, Phys. Rev. B **66**, 041104(R).
Lee, Y.-S., K. Segawa, Y. Ando, and D. N. Basov, 2004, Phys. Rev. B **70**, 014518.
Lee, Y.-S., K. Segawa, Y. Ando, and D. N. Basov, 2005, Phys. Rev. Lett. **94**, 137004.
Leggett, A., 2006, Nature Phys. **2**, 134.
Leinß, S., T. Kampfrath, K. v. Volkmann, M. Wolf, J. T. Steiner, M. Kira, S. W. Koch, A. Leitenstorfer, and R. Huber, 2008, Phys. Rev. Lett. **101**, 246401.
Le Tacon, M., A. Sacuto, A. Georges, G. Kotliar, Y. Gallais, D. Colson, and A. Forget, 2006, Nature Phys. **2**, 537.

Levy de Castro, G., C. Berthod, A. Piriou, E. Giannini, and O. Fischer, 2008, Phys. Rev. Lett. **101**, 267004.
Li, G., W. Z. Hu, J. Dong, Z. Li, P. Zheng, G. F. Chen, J. L. Luo, and N. L. Wang, 2008, Phys. Rev. Lett. **101**, 107004.
Li, Z., G. Wang, N. Sai, D. Moses, M. Martin, M. Di Ventra, A. Heeger, and D. Basov, 2006, Nano Lett. **6**, 224.
Li, Z. Q., E. A. Henriksen, Z. Jiang, Z. Hao, M. C. Martin, P. Kim, H. L. Stormer, and D. N. Basov, 2008, Nature Phys. **4**, 532.
Li, Z. Q., E. A. Henriksen, Z. Jiang, Z. Hao, M. C. Martin, P. Kim, H. L. Stormer, and D. N. Basov, 2009, Phys. Rev. Lett. **102**, 037403.
Li, Z. Q., V. Podzorov, N. Sai, M. C. Martin, M. E. Gershenson, M. D. Ventra, and D. N. Basov, 2007, Phys. Rev. Lett. **99**, 016403.
Lichtenberg, F., 2002, Prog. Solid State Chem. **30**, 103.
Limelette, P., A. Georges, D. Jerome, P. Wzietek, P. Metcalf, and J. Honig, 2003, Science **302**, 89.
Lin, N., E. Gull, and A. J. Millis, 2009, Phys. Rev. B **80**, 161105.
Little, W., and M. Holcomb, 2004, J. Supercond. **17**, 551.
Liu, A. Y., I. I. Mazin, and J. Kortus, 2001, Phys. Rev. Lett. **87**, 087005.
Liu, H. L., S. L. Cooper, and S.-W. Cheong, 1998, Phys. Rev. Lett. **81**, 4684.
Liu, H. L., *et al.*, 1999, J. Phys. Condens. Matter **11**, 239.
Lloyd-Hughes, J., D. Prabhakaran, A. T. Boothroyd, and M. B. Johnston, 2008, Phys. Rev. B **77**, 195114.
Lobad, A. I., R. D. Averitt, and A. J. Taylor, 2000, Appl. Phys. Lett. **77**, 4025.
Lobad, A. I., R. D. Averitt, and A. J. Taylor, 2001, Phys. Rev. B **63**, 060410(R).
Logvenov, G., A. Gozar, and I. Bozovic, 2009, Science **326**, 699.
Loh, E., and D. Campbell, 1988, Synth. Met. **27**, A499.
Longo, J. M., J. A. Kafalas, and R. J. Arnott, 1971, J. Solid State Chem. **3**, 174.
Longo, J. M., P. M. Raccah, and J. B. Goodenough, 1968, J. Appl. Phys. **39**, 1327.
Loram, 1989, Physica (Amsterdam) **162C–164C**, 498.
Lorenzana, J., and R. Eder, 1997, Phys. Rev. B **55**, R3358.
Lorenzana, J., and G. A. Sawatzky, 1995a, Phys. Rev. Lett. **74**, 1867.
Lorenzana, J., and G. A. Sawatzky, 1995b, Phys. Rev. B **52**, 9576.
Love, S. P., S. C. Huckett, L. A. Worl, T. M. Frankcom, S. A. Ekberg, and B. I. Swanson, 1993, Phys. Rev. B **47**, 11107, and references therein.
Lunkenheimer, P., and A. Loidl, 2003, Phys. Rev. Lett. **91**, 207601.
Lupi, S., P. Maselli, H. Capizzi, P. Calvani, P. Giura, and P. Roy, 1999, Phys. Rev. Lett. **83**, 4852.
Lupi, S., D. Nicoletti, O. Limaj, L. Baldassarre, M. Ortolani, S. Ono, Y. Ando, and P. Calvani, 2009, Phys. Rev. Lett. **102**, 206409.
Mackenzie, A. P., and Y. Maeno, 2003, Rev. Mod. Phys. **75**, 657.
Mahan, G. D., 2000, *Many-Particle Physics* (Kluwer Adcademic/Plenum Press, New York), 3rd ed.
Maier, T., M. Jarrell, T. Pruschke, and M. H. Hettler, 2005, Rev. Mod. Phys. **77**, 1027.
Maier, T., D. Poilblanc, and D. Scalapino, 2008, Phys. Rev. Lett. **100**, 237001.
Mak, K. F., C. H. Lui, J. Shan, and T. F. Heinz, 2009, Preprint.
Mak, K. F., M. Y. Sfeir, Y. Wu, C. H. Lui, J. A. Misewich, and T. F. Heinz, 2008, Phys. Rev. Lett. **101**, 196405.
Maksimov, E. G., I. I. Mazin, S. N. Rashkeev, and Y. A. Uspenski, 1988, J. Phys. F **18**, 833.
Maksimov, E. G., S. N. Rashkeev, S. Y. Savrasov, and Y. A. Uspenskii, 1989, Phys. Rev. Lett. **63**, 1880.
Maldague, P. F., 1977, Phys. Rev. B **16**, 2437.
Mandrus, D., J. R. Thompson, R. Gaal, L. Forro, J. C. Bryan, B. C. Chakoumakos, L. M. Woods, B. C. Sales, R. S. Fishman, and V. Keppens, 2001, Phys. Rev. B **63**, 195104.
Mannella, N., W. L. Yang, X. J. Zhou, H. Zheng, J. F. Mitchell, J. Zaanen, T. P. Devereaux, N. Nagaosa, Z. Hussain, and Z.-X. Shen, 2005, Nature (London) **438**, 474.
Manyala, N., J. F. DiTusa, G. Aeppli, and A. P. Ramirez, 2008, Nature (London) **454**, 976.
Marezio, M., D. B. McWhan, J. P. Remeika, and P. D. Dernier, 1972, Phys. Rev. B **5**, 2541.
Marsiglio, F., 2006, Phys. Rev. B **73**, 064507.
Marsiglio, F., T. Startseva, and J. Carbotte, 1998, Phys. Lett. A **245**, 172.
Matsubara, M., Y. Okimoto, T. Ogasawara, Y. Tomioka, H. Okamoto, and Y. Tokura, 2007, Phys. Rev. Lett. **99**, 207401.
Matsuda, M., K. Katsumata, T. Osafune, N. Motoyama, H. Eisaki, S. Uchida, T. Yokoo, S. M. Shapiro, G. Shirane, and J. L. Zarestky, 1997, Phys. Rev. B **56**, 14 499.
Matsuda, Y., M. B. Gaifullin, K. Kumagai, K. Kadowaki, and T. Mochiku, 1995, Phys. Rev. Lett. **75**, 4512.
Matsunami, M., H. Okamura, A. Ochiai, and T. Nanba, 2009, Phys. Rev. Lett. **103**, 237202.
Mattis, D. C., and J. Bardeen, 1958, Phys. Rev. **111**, 412.
Mazumdar, S., and R. T. Clay, 2008, Phys. Rev. B **77**, 180515.
Mazurenko, D. A., A. A. Nugroho, T. T. M. Palstra, and P. H. M. van Loosdrecht, 2008, Phys. Rev. Lett. **101**, 245702.
McGill, S., R. Miller, O. Torrens, A. Mamchik, I. Chen, and J. Kikkawa, 2004, Phys. Rev. Lett. **93**, 047402.
McMahan, A. K., J. F. Annett, and R. M. Martin, 1990, Phys. Rev. B **42**, 6268.
McWhan, D. B., J. P. Remeika, T. M. Rice, W. F. Brinkman, J. P. Maita, and A. Menth, 1971, Phys. Rev. Lett. **27**, 941.
McWhan, D. B., T. M. Rice, and J. P. Remeika, 1969, Phys. Rev. Lett. **23**, 1384.
Meevasana, W., *et al.*, 2006, Phys. Rev. Lett. **96**, 157003.
Mena, F. P., J. F. DiTusa, D. van der Marel, G. Aeppli, D. P. Young, A. Damascelli, and J. A. Mydosh, 2006, Phys. Rev. B **73**, 085205.
Mena, F. P., D. van der Marel, A. Damascelli, M. Fäth, A. A. Menovsky, and J. A. Mydosh, 2003, Phys. Rev. B **67**, 241101.
Mena, F. P., D. van der Marel, and J. L. Sarrao, 2005, Phys. Rev. B **72**, 045119.
Merino, J., M. Dumm, N. Drichko, M. Dressel, and R. H. McKenzie, 2008, Phys. Rev. Lett. **100**, 086404.
Merino, J., A. Greco, N. Drichko, and M. Dressel, 2006, Phys. Rev. Lett. **96**, 216402.
Merino, J., and R. H. McKenzie, 2000, Phys. Rev. B **61**, 7996.
Merino, J., and R. H. McKenzie, 2001, Phys. Rev. Lett. **87**, 237002.
Merlin, R., 1997, Solid State Commun. **102**, 207.
Mihály, L., D. Talbayev, L. F. Kiss, J. Zhou, T. Fehér, and A. Jánossy, 2004, Phys. Rev. B **69**, 024414.
Miller, B. I., and A. H. Dayem, 1967, Phys. Rev. Lett. **18**, 1000.
Millis, A. J., 1992, *Heavy Electron Metals and Insulators*, edited by E. Manousakis, P. Schlottman, P. Kumar, K. Bedell and F. M. Mueller, Physical Phenomena in High Magnetic Fields (Addison-Wesley, Redwood, CA), pp. 146–155.
Millis, A. J., 2004, *Optical Conductivity and Correlated Electron Physics*, edited by D. Baeriswyl and L. Degiorgi, Strong Interactions in Low Dimensions (Kluwer Academic Publishers, Dordrecht, The Netherlands), pp. 195–236.
Millis, A. J., and S. N. Coppersmith, 1990, Phys. Rev. B **42**, 10 807.
Millis, A. J., M. Lavagna, and P. A. Lee, 1987, Phys. Rev. B **36**, 864.
Millis, A. J., and P. A. Lee, 1987, Phys. Rev. B **35**, 3394.
Millis, A. J., P. B. Littlewood, and B. I. Shraiman, 1995, Phys. Rev. Lett. **74**, 5144.

Millis, A. J., H. Monien, and D. Pines, 1990, Phys. Rev. B **42**, 167.
Millis, A. J., and M. R. Norman, 2007, Phys. Rev. B **76**, 220503.
Millis, A. J., B. I. Shraiman, and R. Mueller, 1996, Phys. Rev. Lett. **77**, 175.
Millis, A. J., A. Zimmers, R. P. S. M. Lobo, N. Bontemps, and C. C. Homes, 2005, Phys. Rev. B **72**, 224517.
Minakata, M., and Y. Maeno, 2001, Phys. Rev. B **63**, 180504.
Mishchenko, A. S., N. Nagaosa, Z.-X. Shen, G. D. Filippis, V. Cataudella, T. P. Devereaux, C. Bernhard, K. W. Kim, and J. Zaanen, 2008, Phys. Rev. Lett. **100**, 166401.
Misochko, O. V., 2001, J. Exp. Theor. Phys. **92**, 246.
Miyashita, S., and K. Yonemitsu, 2008, J. Phys. Soc. Jpn. **77**, 094712.
Mizuno, Y., and S. Koide, 1964, Phys. Condens. Matter **2**, 166.
Mo, S.-K., *et al.*, 2003, Phys. Rev. Lett. **90**, 186403.
Moca, C. P., B. L. Sheu, N. Samarth, P. Schiffer, B. Janko, and G. Zarand, 2009, Phys. Rev. Lett. **102**, 137203.
Molegraaf, H., C. Presura, D. van der Marel, P. Kes, and M. Li, 2002, Science **295**, 2239.
Monthoux, P., D. Pines, and G. G. Lonzarich, 2007, Nature (London) **450**, 1177.
Moon, S. J., *et al.*, 2008, Phys. Rev. Lett. **101**, 226402.
Morales, F., and R. Escudero, 2009, J. Low Temp. Phys. **154**, 68.
Moreo, A., and E. Dagotto, 1990, Phys. Rev. B **42**, 4786.
Mori, H., S. Tanaka, and T. Mori, 1998, Phys. Rev. B **57**, 12023.
Mori, H., S. Tanaka, T. Mori, and H. Kobayashi, 1998, Bull. Chem. Soc. Jpn. **71**, 789.
Mori, H., S. Tanaka, T. Mori, and H. Maruyama, 1995, Bull. Chem. Soc. Jpn. **68**, 1136.
Mori, T., 1998, Bull. Chem. Soc. Jpn. **71**, 2509.
Mori, T., 1999, Bull. Chem. Soc. Jpn. **72**, 2011.
Mori, T., 2000, Bull. Chem. Soc. Jpn. **73**, 2243.
Mori, T., H. Mori, and S. Tanaka, 1999, Bull. Chem. Soc. Jpn. **72**, 179.
Morin, F. J., 1959, Phys. Rev. Lett. **3**, 34.
Moriya, Z., 1960, Phys. Rev. Lett. **4**, 228.
Moser, J., M. Gabay, P. Auban-Senzier, D. Jérome, K. Bechgaard, and J. M. Fabre, 1998, Eur. Phys. J. B **1**, 39.
Mostovoy, M. V., D. I. Khomskii, and J. Knoester, 2002, Phys. Rev. B **65**, 064412.
Mott, N., 1990, *Metal-Insulator Transitions* (Taylor & Francis, London), 2 ed.
Mott, N., and R. Peierls, 1937, Proc. Phys. Soc. London **49** (Part 1), 72.
Müller, M., and B. I. Shklovskii, 2009, Phys. Rev. B **79**, 134504.
Munzar, D., C. Bernhard, and M. Cardona, 1999, Physica (Amsterdam) **312C**, 121.
Musfeldt, J. L., R. Świetlik, I. Olejniczak, J. E. Eldridge, and U. Geiser, 2005, Phys. Rev. B **72**, 014516.
Mutou, T., and H. Kontani, 2006, Phys. Rev. B **74**, 115107.
Myasnikova, A. E., and E. N. Myasnikov, 2008, Phys. Rev. B **77**, 165136.
Nagai, Y., T. Kunimoto, K. Nagasaka, H. Nojiri, M. Motokawa, F. Matsukura, T. Dietl, and H. Ohno, 2001, Jpn. J. Appl. Phys. **40**, 6231.
Nagamatsu, J., N. Nakagawa, T. Muranaka, Y. Zenitani, and J. Akimitsu, 2001, Nature (London) **410**, 63.
Nair, R. R., P. Blake, A. N. Grigorenko, K. S. Novoselov, T. J. Booth, T. Stauber, N. M. R. Peres, and A. K. Geim, 2008, Science **320**, 1308.
Nakajima, M., N. Takubo, Z. Hiroi, Y. Ueda, and T. Suemoto, 2008, Appl. Phys. Lett. **92**, 011907.
Nanba, T., H. Otha, M. Motokawa, S. Kimura, S. Kunii, and T. Kasuya, 1993, Physica (Amsterdam) **186B–188B**, 440.
Nasu, K., 2004, *Photoinduced Phase Transition* (World Scientific, Singapore).
Neto, A. H. C., and F. Guinea, 2007, Phys. Rev. B **75**, 045404.
Neto, A. H. C., F. Guinea, N. M. R. Peres, K. S. Novoselov, and A. K. Geim, 2009, Rev. Mod. Phys. **81**, 109.
Newman, R., and R. M. Chrenko, 1959, Phys. Rev. **114**, 1507.
Ng, H. K., T. Timusk, and K. Bechgaard, 1984, Phys. Rev. B **30**, 5842.
Ng, H. K., T. Timusk, D. Jérome, and K. Bechgaard, 1985, Phys. Rev. B **32**, 8041.
Nishi, T., S. ichi Kimura, T. Takahashi, H. Im, Y. seung Kwon, T. Ito, K. Miyagawa, H. Taniguchi, A. Kawamoto, and K. Kanoda, 2007, Phys. Rev. B **75**, 014525.
Norman, M. R., and A. V. Chubukov, 2006, Phys. Rev. B **73**, 140501.
Norman, M. R., A. V. Chubukov, E. van Heumen, A. B. Kuzmenko, and D. van der Marel, 2007, Phys. Rev. B **76**, 220509.
Norman, M. R., and C. Pépin, 2002, Phys. Rev. B **66**, 100506.
Nucara, A., P. Maselli, P. Calvani, R. Sopracase, M. Ortolani, G. Gruener, M. C. Guidi, U. Schade, and J. García, 2008, Phys. Rev. Lett. **101**, 066407.
Nunner, T. S., P. Brune, T. Kopp, M. Windt, and M. Grüninger, 2002, Phys. Rev. B **66**, 180404.
Ogasawara, T., T. Kimura, T. Ishikawa, M. Kuwata-Gonokami, and Y. Tokura, 2001, Phys. Rev. B **63**, 113105.
Ogasawara, T., M. Matsubara, Y. Tomioka, M. Kuwata-Gonokami, H. Okamoto, and Y. Tokura, 2003, Phys. Rev. B **68**, 180407.
Ohno, H., and T. Dietl, 2008, J. Magn. Magn. Mater. **320**, 1293.
Ohno, H., A. Shen, F. Matsukura, A. Oiwa, A. Endo, S. Katsumoto, and Y. Iye, 1996, Appl. Phys. Lett. **69**, 363.
Ohtomo, A., D. Muller, J. Grazul, and H. Hwang, 2002, Nature (London) **419**, 378.
Okamoto, H., K. Ikegami, T. Wakabayashi, Y. Ishige, J. Togo, H. Kishida, and H. Matsuzaki, 2006, Phys. Rev. Lett. **96**, 037405.
Okamoto, H., H. Matsuzaki, T. Wakabayashi, Y. Takahashi, and T. Hasegawa, 2007, Phys. Rev. Lett. **98**, 037401.
Okamoto, H., T. Mitani, K. Toriumi, and M. Yamashita, 1992, Phys. Rev. Lett. **69**, 2248.
Okamoto, H., and M. Yamashita, 1998, Bull. Chem. Soc. Jpn. **71**, 2023.
Okamura, H., S. Kimura, H. Shinozaki, T. Nanba, F. Iga, N. Shimizu, and T. Takabatake, 1998, Phys. Rev. B **58**, R7496.
Okamura, H., M. Matsunami, T. Inaoka, T. Nanba, S. Kimura, F. Iga, S. Hiura, J. Klijn, and T. Takabatake, 2000, Phys. Rev. B **62**, R13265.
Okamura, H., T. Michizawa, T. Nanba, and T. Ebihara, 2004, J. Phys. Soc. Jpn. **73**, 2045.
Okamura, H., T. Michizawa, T. Nanba, S. ichi Kimura, F. Iga, and T. Takabatake, 2005, J. Phys. Soc. Jpn. **74**, 1954.
Okamura, H., *et al.*, 2007, J. Phys. Soc. Jpn. **76**, 023703.
Okazaki, K., S. Sugai, Y. Muraoka, and Z. Hiroi, 2006, Phys. Rev. B **73**, 165116.
Okimoto, Y., T. Katsufuji, T. Ishikawa, T. Arima, and Y. Tokura, 1997, Phys. Rev. B **55**, 4206.
Okimoto, Y., T. Katsufuji, Y. Okada, T. Arima, and Y. Tokura, 1995, Phys. Rev. B **51**, 9581.
Okimoto, Y., R. Kumai, E. Saitoh, M. Izumi, S. Horiuchi, and Y. Tokura, 2004, Phys. Rev. B **70**, 115104.
Okimoto, Y., and Y. Tokura, 2000a, J. Supercond. **13**, 271.
Okimoto, Y., and Y. Tokura, 2000b, J. Supercond. Novel Magnetism **13**, 271.

Onida, G., L. Reining, and A. Rubio, 2002, Rev. Mod. Phys. **74**, 601.
Ono, M., K. Miura, A. Maeda, H. Matsuzaki, H. Kishida, Y. Taguchi, Y. Tokura, M. Yamashita, and H. Okamoto, 2004, Phys. Rev. B **70**, 085101.
Onose, Y., Y. Taguchi, K. Ishizaka, and Y. Tokura, 2001, Phys. Rev. Lett. **87**, 217001.
Orenstein, J., G. A. Thomas, A. J. Millis, S. L. Cooper, D. H. Rapkine, T. Timusk, L. F. Schneemeyer, and J. V. Waszczak, 1990, Phys. Rev. B **42**, 6342.
Ormeno, R. J., M. A. Hein, T. L. Barraclough, A. Sibley, C. E. Gough, Z. Q. Mao, S. Nishizaki, and Y. Maeno, 2006, Phys. Rev. B **74**, 092504.
Ortolani, M., P. Calvani, and S. Lupi, 2005, Phys. Rev. Lett. **94**, 067002.
Osafune, T., N. Motoyama, H. Eisaki, and S. Uchida, 1997, Phys. Rev. Lett. **78**, 1980.
Osafune, T., N. Motoyama, H. Eisaki, S. Uchida, and S. Tajima, 1999, Phys. Rev. Lett. **82**, 1313.
Oudovenko, V. S., G. Pálsson, S. Y. Savrasov, K. Haule, and G. Kotliar, 2004, Phys. Rev. B **70**, 125112.
Padilla, W. J., D. N. Basov, and D. R. Smith, 2006, Material Today **9**, 28.
Padilla, W. J., M. Dumm, S. Komiya, Y. Ando, and D. N. Basov, 2005, Phys. Rev. B **72**, 205101.
Padilla, W. J., Y. S. Lee, M. Dumm, G. Blumberg, S. Ono, K. Segawa, S. Komiya, Y. Ando, and D. N. Basov, 2005, Phys. Rev. B **72**, 060511.
Padilla, W. J., D. Mandrus, and D. N. Basov, 2002, Phys. Rev. B **66**, 035120.
Parcollet, O., G. Biroli, and G. Kotliar, 2004, Phys. Rev. Lett. **92**, 226402.
Park, H., K. Haule, and G. Kotliar, 2008, Phys. Rev. Lett. **101**, 186403.
Park, S. K., T. Ishikawa, and Y. Tokura, 1998, Phys. Rev. B **58**, 3717.
Parks, B., S. Spielman, and J. Orenstein, 1997, Phys. Rev. B **56**, 115.
Paschen, S., E. Felder, M. A. Chernikov, L. Degiorgi, H. Schwer, H. R. Ott, D. P. Young, J. L. Sarrao, and Z. Fisk, 1997, Phys. Rev. B **56**, 12 916.
Pashkin, A., M. Dressel, M. Hanfland, and C. A. Kuntscher, 2010, Phys. Rev. B **81**, 125109.
Pashkin, A., M. Dressel, and C. A. Kuntscher, 2006, Phys. Rev. B **74**, 165118.
Pereira, V., J. LopesdosSantos, E. Castro, and A. Castro Neto, 2004, Phys. Rev. Lett. **93**, 147202.
Peres, N. M. R., F. Guinea, and A. H. C. Neto, 2006, Phys. Rev. B **73**, 125411.
Perfetti, L., P. A. Loukakos, M. Lisowski, U. Bovensiepen, H. Berger, S. Biermann, P. S. Cornaglia, A. Georges, and M. Wolf, 2006, Phys. Rev. Lett. **97**, 067402.
Perkins, J. D., J. M. Graybeal, M. A. Kastner, R. J. Birgeneau, J. P. Falck, and M. Greven, 1993, Phys. Rev. Lett. **71**, 1621.
Perucchi, A., L. Baldassarre, P. Postorino, and S. Lupi, 2009, J. Phys. Condens. Matter **21**, 323202.
Perucchi, A., G. Caimi, H. R. Ott, L. Degiorgi, A. D. Bianchi, and Z. Fisk, 2004, Phys. Rev. Lett. **92**, 067401.
Peters, R., and T. Pruschke, 2009, Phys. Rev. B **79**, 045108.
Petukhov, K., and M. Dressel, 2005, Phys. Rev. B **71**, 073101.
Philipp, H. R., and H. Ehrenreich, 1963, Phys. Rev. **131**, 2016.
Phillips, P., 2006, Ann. Phys. (N.Y.) **321**, 1634.
Phillips, P., and C. Chamon, 2005, Phys. Rev. Lett. **95**, 107002.
Pickett, W. E., 1989, Rev. Mod. Phys. **61**, 433.
Pignon, B., G. Gruener, V. T. Phuoc, F. Gervais, C. Marin, and L. Ammor, 2008, J. Phys. Condens. Matter **20**, 075230.
Pimenov, A., A. Loidl, K. Gehrke, V. Moshnyaga, and K. Samwer, 2007, Phys. Rev. Lett. **98**, 197401.
Pimenov, A., A. Loidl, and S. I. Krasnosvobodtsev, 2002, Phys. Rev. B **65**, 172502.
Pimenov, A., A. Loidl, P. Przyslupski, and B. Dabrowski, 2005, Phys. Rev. Lett. **95**, 247009.
Pimenov, A., A. Mukhin, V. Ivanov, V. Travkin, A. Balbashov, and A. Loidl, 2006, Nature Phys. **2**, 97.
Pimenov, A., T. Rudolf, F. Mayr, A. Loidl, A. A. Mukhin, and A. M. Balbashov, 2006, Phys. Rev. B **74**, 100403.
Pimenov, A., A. Shuvaev, A. Loidl, F. Schrettle, A. A. Mukhin, V. D. Travkin, V. Y. Ivanov, and A. M. Balbashov, 2009, Phys. Rev. Lett. **102**, 107203.
Pines, D., and P. Nozières, 1966, *The Theory of Quantum Liquids* (Addison-Wesley, Reading, MA), Vol. I.
Pittini, R., M. Ikezawa, A. Ochiai, and T. Suzuki, 1998, Physica (Amsterdam) **246B–247B**, 584.
Plochocka, P., C. Faugeras, M. Orlita, M. L. Sadowski, G. Martinez, M. Potemski, M. O. Goerbig, J.-N. Fuchs, C. Berger, and W. A. de Heer, 2008, Phys. Rev. Lett. **100**, 087401.
Polini, M., R. Asgari, Y. Barlas, T. Pereg-Barnea, and A. MacDonald, 2007, Solid State Commun. **143**, 58.
Polli, D., M. Rini, S. Wall, R. W. Schoenlein, Y. Tomioka, Y. Tokura, G. Cerullo, and A. Cavalleri, 2007, Nature Mater. **6**, 643.
Popova, M., A. Sushkov, A. Vasilev, M. Isobe, and Y. Ueda, 1997, JETP Lett. **65**, 743.
Powell, B. J., and R. H. McKenzie, 2005, Phys. Rev. Lett. **94**, 047004.
Powell, B. J., and R. H. McKenzie, 2007, Phys. Rev. Lett. **98**, 027005.
Prasankumar, R. P., H. Okamura, H. Imai, Y. Shimakawa, Y. Kubo, S. A. Trugman, A. J. Taylor, and R. D. Averitt, 2005, Phys. Rev. Lett. **95**, 267404.
Prasankumar, R. P., S. Zvyagin, K. V. Kamenev, G. Balakrishnan, D. Mck. Paul, A. J. Taylor, and R. D. Averitt, 2007, Phys. Rev. B **76**, 020402.
Pratt, F. L., and S. J. Blundell, 2005, Phys. Rev. Lett. **94**, 097006.
Presura, C., M. Popinciuc, P. H. M. van Loosdrecht, D. van der Marel, M. Mostovoy, T. Yamauchi, and Y. Ueda, 2003, Phys. Rev. Lett. **90**, 026402.
Pronin, A. V., A. Pimenov, A. Loidl, and S. I. Krasnosvobodtsev, 2001, Phys. Rev. Lett. **87**, 097003.
Pucher, K., A. Loidl, N. Kikugawa, and Y. Maeno, 2003, Phys. Rev. B **68**, 214502.
Puchkov, A. V., D. Basov, and T. Timusk, 1996, J. Phys. Condens. Matter **8**, 10 049.
Puchkov, A. V., P. Fournier, D. N. Basov, T. Timusk, A. Kapitulnik, and N. N. Kolesnikov, 1996, Phys. Rev. Lett. **77**, 3212.
Puchkov, A. V., T. Timusk, M. Karlow, S. Cooper, P. Han, and D. Payne, 1995, Phys. Rev. B **52**, R9855.
Qazilbash, M. M., K. S. Burch, D. Whisler, D. Shrekenhamer, B. G. Chae, H. T. Kim, and D. N. Basov, 2006, Phys. Rev. B **74**, 205118.
Qazilbash, M. M., J. J. Hamlin, R. E. Baumbach, L. Zhang, D. J. Singh, M. B. Maple, and D. N. Basov, 2009a, Nature Phys. **5**, 647.
Qazilbash, M. M., Z. Q. Li, V. Podzorov, M. Brehm, F. Keilmann, B. G. Chae, H. T. Kim, and D. N. Basov, 2008, Appl. Phys. Lett. **92**, 241906.
Qazilbash, M. M., A. A. Schafgans, K. S. Burch, S. J. Yun, B. G. Chae, B. J. Kim, H. T. Kim, and D. N. Basov, 2008, Phys. Rev. B **77**, 115121.
Qazilbash, M. M., *et al.*, 2009b, Phys. Rev. B **79**, 075107.
Qazilbash, M. M., *et al.*, 2007, Science **318**, 1750.
Qin, Y., C. L. Vicente, and J. Yoon, 2006, Phys. Rev. B **73**, 100505.

Quijada, M., J. Cerne, J. R. Simpson, H. D. Drew, K. H. Ahn, A. J. Millis, R. Shreekala, R. Ramesh, M. Rajeswari, and T. Venkatesan, 1998, Phys. Rev. B **58**, 16 093.
Ramirez, A. P., 1997, J. Phys. Condens. Matter **9**, 8171.
Randall, J. J., and R. Ward, 1959, J. Am. Chem. Soc. **81**, 2629.
Rao, G. V. S., M. Reedyk, N. Kikugawa, and Y. Maeno, 2006, Phys. Rev. B **73**, 052507.
Ren, Y. H., M. Ebrahim, H. B. Zhao, G. Lupke, Z. A. Xu, V. Adyam, and Q. Li, 2008, Phys. Rev. B **78**, 014408.
Ren, Z.-A., *et al.*, 2008, Chin. Phys. Lett. **25**, 2215.
Rice, T. M., H. Launois, and J. P. Pouget, 1994, Phys. Rev. Lett. **73**, 3042.
Rigal, L. B., D. C. Schmadel, H. D. Drew, B. Maiorov, E. Osquiguil, J. S. Preston, R. Hughes, and G. D. Gu, 2004, Phys. Rev. Lett. **93**, 137002.
Rini, M., *et al.*, 2008, Appl. Phys. Lett. **92**, 181904.
Rini, M., R. Tobey, N. Dean, J. Itatani, Y. Tomioka, Y. Tokura, R. W. Schoenlein, and A. Cavalleri, 2007, Nature (London) **449**, 72.
Riseborough, P. S., 2000, Adv. Phys. **49**, 257.
Riseborough, P. S., 2003, Phys. Rev. B **68**, 235213.
Ritz, E., and M. Dressel, 2008a, J. Appl. Phys. **103**, 084902.
Ritz, E., and M. Dressel, 2008b, Phys. Status Solidi C **5**, 703.
Rodolakis, F., *et al.*, 2010, Phys. Rev. Lett. **104**, 047401.
Romijn, I. G., H. J. Hupkes, H. C. F. Martens, H. B. Brom, A. K. Mukherjee, and R. Menon, 2003, Phys. Rev. Lett. **90**, 176602.
Ronnow, H. M., C. Renner, G. Aeppli, T. Kimura, and Y. Tokura, 2006, Nature (London) **440**, 1025.
Rõõm, T., D. Hüvonen, U. Nagel, J. Hwang, T. Timusk, and H. Kageyama, 2004a, Phys. Rev. B **70**, 144417.
Rõõm, T., D. Hüvonen, U. Nagel, Y. J. Wang, and R. K. Kremer, 2004b, Phys. Rev. B **69**, 144410.
Rosch, A., 2006, Ann. Phys. (Leipzig) **15**, 526.
Rosch, A., and P. C. Howell, 2005, Phys. Rev. B **72**, 104510.
Rothwarf, A., and M. Cohen, 1963, Phys. Rev. **130**, 1401.
Rothwarf, A., and B. N. Taylor, 1967, Phys. Rev. Lett. **19**, 27.
Rotter, L. D., *et al.*, 1991, Phys. Rev. Lett. **67**, 2741.
Rotter, M., M. Tegel, I. Schellenberg, F. M. Schappacher, R. Pottgen, J. Deisenhofer, A. Gunther, F. Schrettle, A. Loidl, and D. Johrendt, 2009, New J. Phys. **11**, 025014.
Rozenberg, M. J., G. Kotliar, and H. Kajueter, 1996, Phys. Rev. B **54**, 8452.
Rozenberg, M. J., G. Kotliar, H. Kajueter, G. A. Thomas, D. H. Rapkine, J. M. Honig, and P. Metcalf, 1995a, Phys. Rev. Lett. **75**, 105.
Rozenberg, M. J., G. Kotliar, H. Kajueter, G. A. Thomas, D. H. Rapkine, J. M. Honig, and P. Metcalf, 1995b, Phys. Rev. Lett. **75**, 105.
Rübhausen, M., A. Gozar, M. V. Klein, P. Guptasarma, and D. G. Hinks, 2001, Phys. Rev. B **63**, 224514.
Rusydi, A., *et al.*, 2008, Phys. Rev. B **78**, 125110.
Ruzicka, B., L. Degiorgi, H. Berger, R. Gaál, and L. Forró, 2001, Phys. Rev. Lett. **86**, 4136.
Sacépé, B., C. Chapelier, T. I. Baturina, V. M. Vinokur, M. R. Baklanov, and M. Sanquer, 2008, Phys. Rev. Lett. **101**, 157006.
Sachdev, S., 1999, *Quantum Phase Transitions* (Cambridge University Press, Cambridge, UK).
Sadowski, M. L., G. Martinez, M. Potemski, C. Berger, and W. A. de Heer, 2006, Phys. Rev. Lett. **97**, 266405.
Salamon, M. B., and M. Jaime, 2001, Rev. Mod. Phys. **73**, 583.
Sambandamurthy, G., L. W. Engel, A. Johansson, E. Peled, and D. Shahar, 2005, Phys. Rev. Lett. **94**, 017003.
Sambandamurthy, G., L. W. Engel, A. Johansson, and D. Shahar, 2004, Phys. Rev. Lett. **92**, 107005.
Sambandamurthy, G., A. Johansson, E. Peled, D. Shahar, P. G. Bjornsson, and K. A. Moler, 2006, Europhys. Lett. **75**, 611.
Santander-Syro, A. F., R. P. S. M. Lobo, N. Bontemps, W. Lopera, D. Giratá, Z. Konstantinovic, Z. Z. Li, and H. Raffy, 2004, Phys. Rev. B **70**, 134504.
Sarma, S. D., E. H. Hwang, and W.-K. Tse, 2007, Phys. Rev. B **75**, 121406.
Sasaki, T., H. Oizumi, N. Yoneyama, N. Kobayashi, and N. Toyota, 2007, J. Phys. Soc. Jpn. **76**, 123701.
Sasaki, T., N. Yoneyama, N. Kobayashi, Y. Ikemoto, and H. Kimura, 2004, Phys. Rev. Lett. **92**, 227001.
Sasaki, T., N. Yoneyama, Y. Nakamura, N. Kobayashi, Y. Ikemoto, T. Moriwaki, and H. Kimura, 2008, Phys. Rev. Lett. **101**, 206403.
Saso, T., 2004, J. Phys. Soc. Jpn. **73**, 2894.
Sawatzky, G. A., and J. W. Allen, 1984, Phys. Rev. Lett. **53**, 2339.
Saxena, A., Z. Shuai, J. L. Brédas, and A. R. Bishop, 1997, Synth. Met. **86**, 2231.
Scalapino, D. J., E. Loh, and J. E. Hirsch, 1986, Phys. Rev. B **34**, 8190.
Schabel, M. C., C.-H. Park, A. Matsuura, Z.-X. Shen, D. A. Bonn, R. Liang, and W. N. Hardy, 1998, Phys. Rev. B **57**, 6107.
Schachinger, E., D. Neuber, and J. Carbotte, 2006, Phys. Rev. B **73**, 184507.
Schafgans, A. A., A. D. LaForge, S. V. Dordevic, M. M. Qazilbash, W. J. Padilla, K. S. Burch, Z. Q. Li, S. Komiya, Y. Ando, and D. N. Basov, 2010, Phys. Rev. Lett. **104**, 157002.
Scheffler, M., M. Dressel, and M. Jordan, 2009, J. Phys. Conf. Ser. **150**, 042174.
Scheffler, M., M. Dressel, and M. Jourdan, 2010, Eur. Phys. J. B **74**, 331.
Scheffler, M., M. Dressel, M. Jourdan, and H. Adrian, 2005, Nature (London) **438**, 1135.
Scheffler, M., M. Dressel, M. Jourdan, and H. Adrian, 2006, Physica (Amsterdam) **378B–380B**, 993.
Schlesinger, Z., R. T. Collins, F. Holtzberg, C. Feild, S. H. Blanton, U. Welp, G. W. Crabtree, Y. Fang, and J. Z. Liu, 1990, Phys. Rev. Lett. **65**, 801.
Schlesinger, Z., Z. Fisk, H.-T. Zhang, M. B. Maple, J. DiTusa, and G. Aeppli, 1993, Phys. Rev. Lett. **71**, 1748.
Schneider, M., *et al.*, 2002, Europhys. Lett. **60**, 460.
Schuller, I., and K. E. Gray, 1976, Phys. Rev. Lett. **36**, 429.
Schuster, H. G. 1975, Ed., *One-Dimensional Conductors: GPS Summer School Proceedings*, Lecture Notes in Physics (Springer-Verlag, Berlin), Vol 34.
Schwartz, A., M. Dressel, G. Grüner, V. Vescoli, L. Degiorgi, and T. Giamarchi, 1998, Phys. Rev. B **58**, 1261.
Schwoerer, M., and H. C. Wolf, 2007, *Organic Molecular Solids* (Wiley-VCH, Weinheim).
Sebastian, S. E., N. Harrison, E. Palm, T. P. Murphy, C. H. Mielke, R. Liang, D. A. Bonn, W. N. Hardy, and G. G. Lonzarich, 2008, Nature (London) **454**, 200.
Sega, I., and P. Prelovšek, 1990, Phys. Rev. B **42**, 892.
Segre, G. P., N. Gedik, and J. Orenstein, 2002, Phys. Rev. Lett. **88**, 137001.
Seo, H., C. Hotta, and H. Fukuyama, 2004, Chem. Rev. **104**, 5005.
Seo, H., J. Merino, H. Yoshioka, and M. Ogata, 2006, J. Phys. Soc. Jpn. **75**, 051009.
Seo, S. S. A., M. W. Kim, Y. S. Lee, T. W. Noh, Y. D. Park, G. T. Thaler, M. E. Overberg, C. R. Abernathy, and S. J. Pearton, 2003, Appl. Phys. Lett. **82**, 4749.
Shah, J., 1999, *Ultrafast Spectroscopy of Semiconductors and Semiconductor Nanostructures* (Springer-Verlag, Berlin).
Shalaev, V. M., 2007, Nat. Photon. **1**, 41.

Shibauchi, T., H. Kitano, K. Uchinokura, A. Maeda, T. Kimura, and K. Kishio, 1994, Phys. Rev. Lett. **72**, 2263.
Shim, J. H., K. Haule, and G. Kotliar, 2007, Science **318**, 1615.
Shimakawa, Y., Y. Kubo, and T. Manako, 1996, Nature (London) **379**, 53.
Shklovskii, B. I., and A. L. Efros, 1984, *Electronic Properties of Doped Semiconductors*, Springer Series in Solid State Sciences (Springer-Verlag, Berlin), Vol 45.
Shulga, S. V., O. V. Dolgov, and E. G. Maksimov, 1991, Physica (Amsterdam) **178C**, 266.
Si, Q., 2009, Nature Phys. **5**, 629.
Silvera, I., and J. Halley, 1966, Phys. Rev. **149**, 415.
Simpson, J. R., H. D. Drew, V. N. Smolyaninova, R. L. Greene, M. C. Robson, A. Biswas, and M. Rajeswari, 1999, Phys. Rev. B **60**, R16263.
Singh, D. J., 1995, Phys. Rev. B **52**, 1358.
Singh, D. J., P. Blaha, K. Schwarz, and J. O. Sofo, 2002, Phys. Rev. B **65**, 155109.
Singley, E. J., D. N. Basov, E. D. Bauer, and M. B. Maple, 2002, Phys. Rev. B **65**, 161101.
Singley, E. J., K. S. Burch, R. Kawakami, J. Stephens, D. D. Awschalom, and D. N. Basov, 2003, Phys. Rev. B **68**, 165204.
Singley, E. J., R. Kawakami, D. D. Awschalom, and D. N. Basov, 2002, Phys. Rev. Lett. **89**, 097203.
Sinova, J., T. Jungwirth, S.-R. E. Yang, J. Kučera, and A. H. MacDonald, 2002, Phys. Rev. B **66**, 041202(R).
Slater, J. C., 1929, Phys. Rev. **34**, 1293.
Slater, J. C., 1951, Phys. Rev. **82**, 538.
Sluchanko, N. E., *et al.*, 2000, Phys. Rev. B **61**, 9906.
Snoke, D. W., J. P. Wolfe, and A. Mysyrowicz, 1990, Phys. Rev. Lett. **64**, 2543.
Sommerfeld, A., 1928, Z. Elektrochem. Angew. Phys. Chem. **34**, 426.
Sondhi, S. L., S. M. Girvin, J. P. Carini, and D. Shahar, 1997, Rev. Mod. Phys. **69**, 315.
Spivak, B., P. Oreto, and S. A. Kivelson, 2008, Phys. Rev. B **77**, 214523.
Stahn, J., *et al.*, 2005, Phys. Rev. B **71**, 140509.
Stanescu, T. D., V. Galitski, and H. D. Drew, 2008, Phys. Rev. Lett. **101**, 066405.
Stauber, T., N. M. R. Peres, and A. H. C. Neto, 2008, Phys. Rev. B **78**, 085418.
Steinberg, K., M. Scheffler, and M. Dressel, 2008, Phys. Rev. B **77**, 214517.
Steiner, M. A., N. P. Breznay, and A. Kapitulnik, 2008, Phys. Rev. B **77**, 212501.
Stephan, W., and P. Horsch, 1990, Phys. Rev. B **42**, 8736.
Stevens, C. J., D. Smith, C. Chen, J. F. Ryan, B. Podobnik, D. Mihailovic, G. A. Wagner, and J. E. Evetts, 1997, Phys. Rev. Lett. **78**, 2212.
Stewart, G. R., 2001, Rev. Mod. Phys. **73**, 797.
Stewart, G. R., 2006, Rev. Mod. Phys. **78**, 743.
Struzhkin, V. V., A. F. Goncharov, H. K. Mao, R. J. Hemley, S. W. Moore, J. M. Graybeal, J. Sarrao, and Z. Fisk, 2000, Phys. Rev. B **62**, 3895.
Sudhakar Rao, G. V., S. Ocadlik, M. Reedyk, and C. Petrovic, 2009, Phys. Rev. B **80**, 064512.
Suemoto, T., and S. Tomimoto, 2002, Phase Transit. **75**, 787.
Sugita, A., T. Saito, H. Kano, M. Yamashita, and T. Kobayashi, 2001, Phys. Rev. Lett. **86**, 2158.
Sun, C. K., F. Vallee, L. Acioli, E. P. Ippen, and J. G. Fujimoto, 1993, Phys. Rev. B **48**, 12 365.
Sun, Z., J. F. Douglas, A. V. Fedorov, Y.-D. Chuang, H. Zheng, J. F. Mitchell, and D. S. Dessau, 2007, Nature Phys. **3**, 248.
Sun, Z., *et al.*, 2006, Phys. Rev. Lett. **97**, 056401.
Sushkov, A. B., R. V. Aguilar, S. Park, S.-W. Cheong, and H. D. Drew, 2007, Phys. Rev. Lett. **98**, 027202.
Sushkov, A. B., M. Mostovoy, R. V. Aguilar, S.-W. Cheong, and H. D. Drew, 2008, J. Phys. Condens. Matter **20**, 434210.
Suzuura, H., H. Yasuhara, A. Furusaki, N. Nagaosa, and Y. Tokura, 1996, Phys. Rev. Lett. **76**, 2579.
Tajima, H., S. Kyoden, H. Mori, and S. Tanaka, 2000, Phys. Rev. B **62**, 9378.
Tajima, N., J. ichi Fujisawa, N. Naka, T. Ishihara, R. Kato, Y. Nishio, and K. Kajita, 2005, J. Phys. Soc. Jpn. **74**, 511.
Tajima, S., J. Schützmann, S. Miyamoto, I. Terasaki, Y. Sato, and R. Hauff, 1997, Phys. Rev. B **55**, 6051.
Tajima, S., N. L. Wang, N. Ichikawa, H. Eisaki, S. Uchida, H. Kitano, T. Hanaguri, and A. Maeda, 1999, Europhys. Lett. **47**, 715.
Takahashi, A., H. Gomi, and M. Aihara, 2002, Phys. Rev. Lett. **89**, 206402.
Takahashi, K., M. Kawasaki, and Y. Tokura, 2001, Appl. Phys. Lett. **79**, 1324.
Takaishi, S., and M. Yamishita, 2008, Chem. Lett. **37**, 382.
Takeda, Y., *et al.*, 2004, Physica (Amsterdam) **351B**, 286.
Takenaka, K., Y. Sawaki, R. Shiozaki, and S. Sugai, 2000, Phys. Rev. B **62**, 13 864.
Takenaka, K., Y. Sawaki, and S. Sugai, 1999, Phys. Rev. B **60**, 13 011.
Takenaka, K., R. Shiozaki, S. Okuyama, J. Nohara, A. Osuka, Y. Takayanagi, and S. Sugai, 2002, Phys. Rev. B **65**, 092405.
Takenaka, K., M. Tamura, N. Tajima, H. Takagi, J. Nohara, and S. Sugai, 2005, Phys. Rev. Lett. **95**, 227801.
Talbayev, D., A. D. LaForge, S. A. Trugman, N. Hur, A. J. Taylor, R. D. Averitt, and D. N. Basov, 2008, Phys. Rev. Lett. **101**, 247601.
Talbayev, D., S. A. Trugman, A. V. Balatsky, T. Kimura, A. J. Taylor, and R. D. Averitt, 2008, Phys. Rev. Lett. **101**, 097603.
Talbayev, D., H. Zhao, G. Lupke, L. Chen, and Q. Li, 2005, Appl. Phys. Lett. **86**, 182501.
Tanabe, Y., T. Moriya, and S. Sugano, 1965, Phys. Rev. Lett. **15**, 1023.
Tanaka, K., *et al.*, 2006, Science **314**, 1910.
Tanaka, M., S. Kurita, T. Kojima, and Y. Yamada, 1984, Chem. Phys. **91**, 257.
Tanaka, Y., and K. Yonemitsu, 2007, J. Phys. Soc. Jpn. **76**, 053708.
Tanaka, Y., and K. Yonemitsu, 2008, J. Phys. Soc. Jpn. **77**, 034708.
Tanaka, Y., and K. Yonemitsu, 2009, J. Phys. Soc. Jpn. **78**, 018002.
Tanino, H., and K. Kobayashi, 1983, J. Phys. Soc. Jpn. **52**, 1446.
Tanner, D., G. Doll, A. Rao, P. Eklund, G. Arbuckle, and A. MacDiarmid, 2004, Synth. Met. **141**, 75.
Tanner, D. B., K. D. Cummings, and C. S. Jacobsen, 1981, Phys. Rev. Lett. **47**, 597.
Tanner, D. B., C. S. Jacobsen, A. F. Garito, and A. J. Heeger, 1974, Phys. Rev. Lett. **32**, 1301.
Tanner, D. B., C. S. Jacobsen, A. F. Garito, and A. J. Heeger, 1976, Phys. Rev. B **13**, 3381.
Tempere, J., and J. T. Devreese, 2001, Phys. Rev. B **64**, 104504.
Thirunavukkuarasu, K., F. Lichtenberg, and C. A. Kuntscher, 2006, J. Phys. Condens. Matter **18**, 9173.
Thomas, G., D. Rapkine, S. Carter, T. Rosenbaum, P. Metcalf, and D. Honig, 1994, J. Low Temp. Phys. **95**, 33.
Thoms, J., 2004, Ph.D. thesis (Universität Stuttgart).
Thomsen, C., H. T. Grahn, H. J. Maris, and J. Tauc, 1986, Phys. Rev. B **34**, 4129.
Timm, C., 2003, J. Phys. Condens. Matter **15**, R1865.
Timusk, T., and B. Statt, 1999, Rep. Prog. Phys. **62**, 61.

Tinkham, M., 1996, *Introduction to Superconductivity*, International Series in Pure and Applied Physics (McGraw-Hill, New York), 2nd ed.
Tobe, K., T. Kimura, Y. Okimoto, and Y. Tokura, 2001, Phys. Rev. B **64**, 184421.
Tohyama, T., 2006, J. Phys. Chem. Solids **67**, 2210.
Tohyama, T., S. Nagai, Y. Shibata, and S. Maekawa, 1999, Phys. Rev. Lett. **82**, 4910.
Tokura, Y., 2000, Ed., *Colossal Magnetoresistive Oxides* (Gordon and Breach, Amsterdam).
Tokura, Y., 2006, J. Phys. Soc. Jpn. **75**, 011001.
Tomczak, J., and S. Biermann, 2009, Europhys. Lett. **86**, 37 004.
Tomimoto, S., S. Miyasaka, T. Ogasawara, H. Okamoto, and Y. Tokura, 2003, Phys. Rev. B **68**, 035106.
Tomimoto, S., S. Saito, T. Suemoto, J. Takeda, and S. Kurita, 2002, Phys. Rev. B **66**, 155112.
Toschi, A., M. Capone, M. Ortolani, P. Calvani, S. Lupi, and C. Castellani, 2005, Phys. Rev. Lett. **95**, 097002.
Toyota, N., M. Lang, and J. Müller, 2007, *Low-Dimensional Molecular Metals*, Springer Series in Solid State Sciences, Vol. 154 (Springer-Verlag, Berlin).
Tran, P., S. Donovan, and G. Grüner, 2002, Phys. Rev. B **65**, 205102.
Tranquada, J. M., D. N. Basov, A. D. LaForge, and A. A. Schafgans, 2010, Phys. Rev. B **81**, 060506.
Travaglini, G., and P. Wachter, 1984, Phys. Rev. B **29**, 893.
Tsuboi, T., and W. Kleemann, 1994, J. Phys. Condens. Matter **6**, 8625.
Tsui, D., 1978, Surf. Sci. **73**, 419.
Uchida, S., T. Ido, H. Takagi, T. Arima, Y. Tokura, and S. Tajima, 1991, Phys. Rev. B **43**, 7942.
Uehara, M., T. Nagata, J. Akimitsu, H. Takahashi, N. Môri, and K. Kinoshita, 1996, J. Phys. Soc. Jpn. **65**, 2764.
Uemura, H., H. Matsuzaki, Y. Takahashi, T. Hasegawa, and H. Okamoto, 2010, Physica (Amsterdam) **405B**, S357.
Uemura, Y. J., 2003, Solid State Commun. **126**, 23.
Uemura, Y. J., *et al.*, 1991, Phys. Rev. Lett. **66**, 2665.
Ugawa, A., and D. Tanner, 2000, Physica (Amsterdam) **341C–348C**, 2201.
Uhrig, G. S., 1997, Phys. Rev. Lett. **79**, 163.
Unterhinninghofen, J., D. Manske, and A. Knorr, 2008, Phys. Rev. B **77**, 180509(R).
Uspenski, Y. A., E. G. Maksimov, S. N. Rashkeev, and I. I. Mazin, 1983, Z. Phys. B **53**, 263.
van der Eb, J. W., A. B. Kuz'menko, and D. van der Marel, 2001, Phys. Rev. Lett. **86**, 3407.
van der Marel, D., 1999, Phys. Rev. B **60**, R765.
van der Marel, D., F. Carbone, A. B. Kuzmenko, and E. Giannini, 2006, Ann. Phys. (N.Y.) **321**, 1716.
van der Marel, D., A. Damascelli, K. Schulte, and A. A. Menovsky, 1998, Physica (Amsterdam) **244B**, 138.
van der Marel, D., H. Molegraaf, J. Zaanen, Z. Nussinov, F. Carbone, A. Damascelli, H. Eisaki, M. Greven, P. Kes, and M. Li, 2003, Nature (London) **425**, 271.
Van Harlingen, D. J., 1995, Rev. Mod. Phys. **67**, 515.
van Heumen, E., A. Kuzmenko, and D. van der Marel, 2009, J. Phys. Conf. Ser. **150**, 052278.
van Heumen, E., W. Meevasana, A. Kuzmenko, H. Eisaki, and D. van der Marel, 2009, New J. Phys. **11**, 055067.
van Heumen, E., E. Muhlethaler, A. B. Kuzmenko, H. Eisaki, W. Meevasana, M. Greven, and D. van der Marel, 2009, Phys. Rev. B **79**, 184512.
van Loosdrecht, P. H. M., S. Huant, G. Martinez, G. Dhalenne, and A. Revcolevschi, 1996, Phys. Rev. B **54**, R3730.
van Mechelen, J. L. M., D. van der Marel, C. Grimaldi, A. B. Kuzmenko, N. P. Armitage, N. Reyren, H. Hagemann, and I. I. Mazin, 2008, Phys. Rev. Lett. **100**, 226403.
van Schilfgaarde, M., T. Kotani, and S. Faleev, 2006, Phys. Rev. Lett. **96**, 226402.
Varma, C., 1985a, Phys. Rev. Lett. **55**, 2723.
Varma, C. M., 1985b, in *Theory of Heavy Fermions and Valence Fluctuatings: Proceedings of the 8th Taniguchi Symposium*, Springer Series in Solid State Science, Vol 62 edited by T. Kasuya and T. Saso (Springer-Verlag, Berlin), p. 343.
Varma, C. M., P. B. Littlewood, S. Schmitt-Rink, E. Abrahams, and A. E. Ruckenstein, 1989, Phys. Rev. Lett. **63**, 1996.
Varma, C. M., Z. Nussinov, and W. van Saarloos, 2002, Phys. Rep. **361**, 267.
Vescoli, V., L. Degiorgi, M. Dressel, A. Schwartz, W. Henderson, B. Alavi, G. Grüner, J. Brinckmann, and A. Virosztek, 1999, Phys. Rev. B **60**, 8019.
Vescoli, V., L. Degiorgi, W. Henderson, G. Grüner, K. P. Starkey, and L. K. Montgomery, 1998, Science **281**, 1181.
Vinokur, V. M., T. I. Baturina, M. V. Fistul, A. Y. Mironov, M. R. Baklanov, and C. Strunk, 2008, Nature (London) **452**, 613.
Vollhardt, D., and P. Wölfle, 1980a, Phys. Rev. Lett. **45**, 842.
Vollhardt, D., and P. Wölfle, 1980b, Phys. Rev. B **22**, 4666.
von Löhneysen, H., A. Rosch, M. Vojta, and P. Wölfle, 2007, Rev. Mod. Phys. **79**, 1015.
Vuletić, T., T. Ivek, B. Korin-Hamzić, S. Tomić, B. Gorshunov, P. Haas, M. Dressel, J. Akimitsu, T. Sasaki, and T. Nagata, 2005, Phys. Rev. B **71**, 012508.
Vuletić, T., B. Korin-Hamzić, T. Ivek, S. Tomić, B. Gorshunov, M. Dressel, and J. Akimitsu, 2006, Phys. Rep. **428**, 169.
Vuletić, T., B. Korin-Hamzić, S. Tomić, B. Gorshunov, P. Haas, T. Rõom, M. Dressel, J. Akimitsu, T. Sasaki, and T. Nagata, 2003, Phys. Rev. Lett. **90**, 257002.
Wachter, P., 1994, in *Intermediate Valence in Heavy Fermions*, edited by K. A. Gschneidner, Jr., L. Eyring, G. H. Lander, and G. R. Choppin, Handbook on the Physics and Chemistry of Rare Earths, Vol 19 (North-Holland, Amsterdam), p. 177.
Wall, S., *et al.*, 2009 (to be published).
Wang, F., Y. Zhang, C. Tian, C. Girit, A. Zettl, M. Crommie, and Y. R. Shen, 2008, Science **320**, 206.
Wang, Y., L. Li, and N. P. Ong, 2006, Phys. Rev. B **73**, 024510.
Watanabe, H., and M. Ogata, 2005, J. Phys. Soc. Jpn. **74**, 2901.
Watanabe, H., and M. Ogata, 2006, J. Phys. Soc. Jpn. **75**, 063702.
Watanabe, T., H. Yokoyama, Y. Tanaka, and J. ichiro Inoue, 2006, J. Phys. Soc. Jpn. **75**, 074707.
Weber, H., and M. Vojta, 2008, Phys. Rev. B **77**, 125118.
Weber-Milbrodt, S. M., J. T. Gammel, A. R. Bishop, and E. Y. Loh, 1992, Phys. Rev. B **45**, 6435.
Weiss, P., 1907, J. Phys. Theor. Appl. (Paris) **6**, 661.
Wentzcovitch, R. M., W. W. Schulz, and P. B. Allen, 1994, Phys. Rev. Lett. **72**, 3389.
Werner, P., E. Gull, O. Parcollet, and A. J. Millis, 2009, Phys. Rev. B **80**, 045120.
Windt, M., *et al.*, 2001, Phys. Rev. Lett. **87**, 127002.
Wojciechowski, R., K. Yamamoto, K. Yakushi, M. Inokuchi, and A. Kawamoto, 2003, Phys. Rev. B **67**, 224105.
Wu, D., *et al.*, 2009, Phys. Rev. B **79**, 155103.
Wu, D., *et al.*, 2010a, Physica (Amsterdam) **470C**, S399.
Wu, D., *et al.*, 2010b, Phys. Rev. B **81**, 100512(R).
Wu, J., Q. Gu, B. S. Guiton, N. P. de Leon, L. Ouyang, and H. Park, 2006, Nano Lett. **6**, 2313.
Wu, Z. C., *et al.*, 2004, Science **305**, 1273.
Xu, Z. A., N. P. Ong, Y. Wang, T. Kakeshita, and S. Uchida, 2000, Nature (London) **406**, 486.

Yamamoto, K., K. Yakushi, K. Miyagawa, K. Kanoda, and A. Kawamoto, 2002, Phys. Rev. B **65**, 085110.
Yamamoto, S., and J. Ohara, 2007, Phys. Rev. B **76**, 235116.
Yan, J., Y. Zhang, P. Kim, and A. Pinczuk, 2007, Phys. Rev. Lett. **98**, 166802.
Yang, J., D. Hüvonen, U. Nagel, T. Rõõm, N. Ni, P. C. Canfield, S. L. Bud'ko, J. P. Carbotte, and T. Timusk, 2009, Phys. Rev. Lett. **102**, 187003.
Yang, J., J. Hwang, E. Schachinger, J. P. Carbotte, R. P. S. M. Lobo, D. Colson, A. Forget, and T. Timusk, 2009, Phys. Rev. Lett. **102**, 027003.
Yang, J., J. Hwang, T. Timusk, A. S. Sefat, and J. E. Greedan, 2006, Phys. Rev. B **73**, 195125.
Yasin, S., 2008, Ph.D. thesis (Universität Stuttgart).
Yelland, E. A., J. Singleton, C. H. Mielke, N. Harrison, F. F. Balakirev, B. Dabrowski, and J. R. Cooper, 2008, Phys. Rev. Lett. **100**, 047003.
Yen, T., W. Padilla, N. Fang, D. Vier, D. Smith, J. Pendry, D. Basov, and X. Zhang, 2004, Science **303**, 1494.
Yonemitsu, K., and K. Nasu, 2008, Phys. Rep. **465**, 1.
Yuen, J. D., R. Menon, N. E. Coates, E. B. Namdas, S. Cho, S. T. Hannahs, D. Moses, and A. J. Heeger, 2009, Nature Mater. **8**, 572.
Yunoki, S., A. Moreo, E. Dagotto, S. Okamoto, S. S. Kancharla, and A. Fujimori, 2007, Phys. Rev. B **76**, 064532.
Zaanen, J., 2004, Nature (London) **430**, 512.
Zaanen, J., G. A. Sawatzky, and J. W. Allen, 1985, Phys. Rev. Lett. **55**, 418.
Zasadzinski, J. F., L. Ozyuzer, N. Miyakawa, K. E. Gray, D. G. Hinks, and C. Kendziora, 2001, Phys. Rev. Lett. **87**, 067005.
Zemljic, M. M., and P. Prelovšek, 2005, Phys. Rev. B **72**, 075108.
Zhan, H., V. Astley, M. Hvasta, J. A. Deibel, D. M. Mittleman, and Y.-S. Lim, 2007, Appl. Phys. Lett. **91**, 162110.
Zhang, G. P., W. Hubner, G. Lefkidis, Y. Bai, and T. George, 2009, Nature Phys. **5**, 499.
Zhang, L. M., Z. Q. Li, D. N. Basov, M. M. Fogler, Z. Hao, and M. C. Martin, 2008, Phys. Rev. B **78**, 235408.
Zhang, T., E. Zhukova, B. Gorshunov, D. Wu, A. S. Prokhorov, V. I. Torgashev, E. G. Maksimov, and M. Dressel, 2010, Phys. Rev. B **81**, 125132.
Zhang, Y., T.-T. Tang, C. Girit, Z. Hao, M. C. Martin, A. Zettl, M. F. Crommie, Y. R. Shen, and F. Wang, 2009, Nature (London) **459**, 820.
Zhukova, E., B. Gorshunov, T. Zhang, D. Wu, A. S. Prokhorov, V. I. Torgashev, E. G. Maksimov, and M. Dressel, 2010, Europhys. Lett. **90**, 17 005.
Zimmers, A., J. Tomczak, R. Lobo, N. Bontemps, C. P. Hill, M. Barr, Y. Dagan, R. Greene, A. J. Millis, and C. C. Homes, 2005, Europhys. Lett. **70**, 225.
Zur, D., D. Menzel, I. Jursic, J. Schoenes, L. Patthey, M. Neef, K. Doll, and G. Zwicknagl, 2007, Phys. Rev. B **75**, 165103.
Žutić, I., J. Fabian, and S. Das Sarma, 2004, Rev. Mod. Phys. **76**, 323.
Zvezdin, A., and V. Kotov, 1997, *Modern Magnetooptics and Magnetoooptical Materials* (IOP Publishing, Bristol and Philadelphia).
Zylbersztejn, A., and N. F. Mott, 1975, Phys. Rev. B **11**, 4383.